SENESCENCE AS A STEPPINGSTONE FOR CANCER TREATMENT

If you stop, you might fall

Fleur Jochems

Senescence as a steppingstone for cancer treatment

If you stop, you might fall

Fleur Jochems

About the cover:

The cover portrays a seascape bathed in the warm hues of a setting sun. In the foreground, the surface of the water reveals a collection of steppingstones forming a pathway that stretches across the sea. These steppingstones embody a metaphorical representation of the research journey presented in this thesis, delving into the concept of senescence as a steppingstone in cancer treatment. This thesis explores a unique 'one-two punch' approach to cancer treatment, where senescence induction serves as the initial step, followed by the elimination of senescent cancer cells as the second step. This strategy halts the proliferation of cancer cells, rendering them vulnerable to therapies designed to specifically target these senescent cells. The subtitle 'if you stop, you might fall' alludes to the proliferative nature of cancer cells, which is halted upon senescence induction, leaving them susceptible to treatment. The metaphorical sun symbolizes the 'fallen' senescent cancer cells submerging beneath the surface, representing their vulnerability and eventual elimination. By intertwining these elements, the cover visually communicates the essence of the thesis and conveys the author's research journey.

Senescence as a steppingstone for cancer treatment
If you stop, you might fall

Senescentie als de eerste stap voor de behandeling van kanker

(met een samenvatting in het Nederlands)

Proefschrift

ter verkrijging van de graad van doctor aan de
Universiteit Utrecht
op gezag van de
rector magnificus, prof.dr. H.R.B.M. Kummeling,
ingevolge het besluit van het college voor promoties
in het openbaar te verdedigen op

donderdag 26 oktober 2023 des middags te 12.15 uur

door

Fleur Jochems

geboren op 16 december 1991
te Haarlem

Promotor:
Prof. dr. R. Bernards

Beoordelingscommissie:
Dr. L. Akkari
Prof. dr. J.G. Borst
Prof. dr. T.R. Brummelkamp
Prof. dr. ir. B.M.T. Burgering
Prof. dr. E.E. Voest (voorzitter)

Table of contents

Abbreviations

AKT	RAC (Rho family)-alpha serine/threonine-protein kinase
APAF1	apoptotic protease-activating factor 1
ATM	ataxia-telangiectasia mutated
ATR	ATM-and Rad3-Related
BAD	BCL-2-associated agonist of cell death
BAK	BCL-2 antagonist/killer
BAX	BCL-2-associated X protein
BCL-2	B-cell lymphoma 2
BCL-W	B cell lymphoma W
BCL-XL	B cell lymphoma extra large
BET	bromodomain and extraterminal domain
BFL-1	BCL-2-related protein A1
BFL-1	BCL-2 related isolated from fetal liver 1
BH domain	BCL-2 homology domain
BID	BH3-interacting domain death agonist
BIK	BCL-2-interacting killer
BIM	BCL-2-interacting mediator of cell death
BMF	BCL-2-modifying factor
BOK	BCL-2 related ovarian killer
BRAF	v-raf murine sarcoma viral oncogene homolog B1
BrdU	bromodeoxyuridine
c-FLIP	cellular FLICE-inhibitory protein
C/EBPß	CCAAT/enhancer-binding protein beta
C12FDG	5-dodecanoylaminofluorescein di-ß-D-galactopyranoside
Cas9	CRISPR-associated protein 9
Caspase	cysteine-aspartic proteases
CD95	cluster of differentiation 95
CDC7	cell division cycle 7
CDK	cyclin-dependent kinase
cGAS	cyclic guanosine monophosphate-adenosine monophosphate synthase
Chk1/2	checkpoint kinase 1/2
CRISPR	clustered regularly interspaced short palindromic repeats
DAPI	4',6-diamidino-2-phenylindole
DDR	DNA damage response
DIABLO	direct inhibitor of apoptosis-binding protein with low pI
DISC	death-inducing signaling complex
DNase2	deoxyribonuclease 2

DP	dimerization protein
DR	death receptor
DR4	death receptor 4
DR5	death receptor 5
DR6	death receptor 6
DREAM	dimerization partner, RB-like, E2F and multi-vulval class B
E2F	E2 promoter binding factor
EdU	5-ethynyl-2'-deoxyuridine
FADD	fas-associated death domain protein
Fas	fas cell surface death receptor
FOXO4	forkhead box protein O4
GATA4	GATA binding protein 4
gRNA	guide ribonucleic acid
H3K9me	methylated lysine 9 of histone H3
HMGA	high-mobility group A
HMGB1	high mobility group box 1 protein
HP1	heterochromatin protein 1
HRK	activator of apoptosis hara-kiri
HTRA2	high-temperature requirement protein A2
IL-6	interleukin-6
IRAK1	interleukin-1 receptor associated kinase
JAK2	janus kinase 2
KRAS	kirsten rat sarcoma virus
LINE-1	long interspersed element-1
MCL1	myeloid cell leukaemia 1
MDM2	murine double minute 2
miR-146a	microRNA-146a
MMP	matrix metalloproteinases
MMP-3	matrix metalloproteinase-3
MOMP	Mitochondrial membrane permeabilization
mTOR	mammalian target of rapamycin
mTOR	mammalian target of rapamycin
NF-κB	nuclear factor kappa light chain enhancer of activated B
NOXA	PMA-induced protein 1
OIS	oncogene-induced senescence
p38MAPK	p38 mitogen-activated protein kinase
PAI2	plasminogen activator inhibitor 2
PCNA	proliferating cell nuclear antigen
PI3K	phosphatidylinositol-3 kinase
PROTAC	proteolysis-targeting chimera

PTEN	phosphatase and tensin homolog deleted on chromosome 10
PUMA	p53-upregulated modulator of apoptosis
PUMA	p53 upregulated modulator of apoptosis
RB	retinoblastoma protein
SA-ß-gal	senescence-associated beta-galactosidase
SAHF	senescence-associated heterochromatin foci
SASP	Senescence-Associated Secretory Phenotype
SMAC	second mitochondria-derived activator of caspases
SMAC	second mitochondria-derived activator of caspases
SMS	Senescence Messaging Secretome
SRC	SRC Proto-Oncogene, Non-Receptor Tyrosine Kinase
STAT3	signal transducer and activator of transcription 3
STING	stimulator of interferon genes
STING	ER-resident protein stimulator of interferon (IFN) genes
TGF-ß	transforming growth factor-beta
TIS	therapy-induced senescence
TNFR	Tumor Necrosis Factor Receptor
TNFR1	tumor necrosis factor receptor 1
TP53	tumor protein p53 gene
TRAIL	tumor necrosis factor-related apoptosis-inducing ligand
TRAIL-R1	tumor necrosis factor-related apoptosis-inducing ligand receptor 1
TRAIL-R2	tumor necrosis factor-related apoptosis-inducing ligand receptor 2
TRAMP	receptor-related apoptosis-mediating protein
TREX1	three prime repair exonuclease 1
ULK1	unc-51 like autophagy activating kinase
VEGF	vascular endothelial growth factor
X-gal	5-bromo-4chloro-3-indooyl-ß-D-galactopyranoside
XIAP	X-linked inhibitor of apoptosis protein
XIAP	X-linked inhibitor of apoptosis protein

CHAPTER | 1

General Introduction and thesis outline

The human body encompasses roughly 10^{13} cells that form a highly controlled system pivotal for the proper functioning of an individual (Bianconi et al., 2013). Healthy cells can divide upon mitogenic growth signals received from their environment and when circumstances are favorable. During a lifetime, cells are continuously challenged by a myriad of intracellular and extracellular stresses. Examples of stresses are nutrient depletion, mechanical damage, toxins, excessive signaling, DNA replication errors, and irradiation. A plethora of stresses results in DNA damage, which jeopardizes the integrity of the genome and results in DNA mutations if not resolved correctly. Cells have adopted sensor and repair machineries that act as guardians against genetic transformation and aberrant behavior of cells. Nevertheless, when severe damage and stress responses sustain, cells can either activate various forms of programmed cell death or survive through the induction of senescence, a dormant state characterized by a stable proliferation arrest and impaired tissue functioning. The latter is also an underlying cause of organismal aging. When sensor and repair machineries are impaired, DNA mutations can occur that allow cells to survive and divide without the need for external growth factors. These cells are considered oncogenic and can form tumors.

This thesis introduction outlines how senescence is related to cancer, what the typical features of senescent cells are, how they resist apoptosis, what the consequence of their presence is in a tumor context, and how we can eliminate senescent cells. Finally, we describe how we can exploit senescence in the context of cancer and provide a summary of the thesis chapters.

An intertwined history: from senescence to cancer and back

Cellular senescence was discovered in 1961 by Hayflick and Moorhead through the observation that normal human diploid fibroblasts undergo a stable growth arrest after serial cultivation *in vitro*. This growth arrested state was accompanied by enlarged and flattened cell morphology. In this seminal study, the authors conjectured the visionary idea that cellular senescence was linked to organismal aging (Hayflick and Moorhead, 1961), which led to the finding that fibroblasts undergo senescence after 50 cell divisions, coined as 'the Hayflick limit' (Hayflick, 1965). Two decades later, it was found that this state was triggered by the loss of telomeric DNA (Harley et al., 1990), which formed the basis for the concept of 'replicative senescence' and organismal aging.

In the same period, the opposite scenario was discovered in cancer cells. It was revealed that HeLa cells acquire the capacity to divide indefinitely through the activation of telomerase (Morin, 1989), an enzyme that elongates telomeres and counteracts accrual telomeric DNA loss (Greider and Blackburn, 1985). This led

to the hypothesis that senescence could act as a mechanism against oncogenic transformation. Later research showed indeed that expressing oncogenic RAS in primary cells triggers senescence (Serrano et al., 1997), dubbed 'oncogene-induced senescence (OIS)'. Further corroboration of OIS was later seen in various studies showing that premalignant lesions harbor characteristics of senescence, while progressive cancers are associated with a bypass of the senescence fate. This was shown in human melanocytes that express *BRAF^V600E* (Michaloglou et al., 2005), *K-ras^V12* in mouse premalignant lung adenomas (Collado et al., 2005), *N-RAS* in premalignant T-cell lymphomas (Braig et al., 2005), and *PTEN*-deficient premalignant prostate cancer (Chen et al., 2005). Consequently, senescence-induction was considered a fail-safe mechanism against neoplastic transformation.

To escape the induction of senescence and apoptosis, cancer cells carry inactivating mutations in these pathways. An important gene is *TP53*, which encodes P53 and is essential for halting the cell cycle upon cell stress to induce senescence, as well as its role in activating apoptosis when damage could not be resolved. *TP53* is considered a tumor suppressor gene because inactivating mutations are frequently present in tumors, enhancing tumorigenesis. Restoring endogenous *Trp53* in murine liver carcinoma, sarcoma, and lymphomas resulted in senescence-induction, tumor regression and clearance, depending on tumor type and activation of innate immune response (Ventura et al., 2007; Xue et al., 2007). The observation that restoring the senescence-inducing capacity in tumors could have benefits in anti-cancer treatment also led to the search for pharmacological ways to reactivate senescence in tumor.

Hallmarks of cellular senescence

One important challenge in finding ways to induce senescence in tumors is the lack of unique markers of the senescent state. Cellular senescence has been described as a highly heterogeneous phenotype. This can be attributed to the numerous senescence triggers, the evolving phenotype overtime, single-cell variation, and the various cell types in which senescence has been studied (Basisty et al., 2020; Hernandez-Segura et al., 2017; Martínez-Zamudio et al., 2020; Wiley et al., 2017). As no markers are exclusive for the senescent state, the reliable detection of senescence is challenging *in vivo* as well as *in vitro*. For this reason, a constellation of markers is required to detect senescence (Gorgoulis et al., 2019). Below, we will discuss how senescence can be induced, what the hallmarks of senescent cells are, and how these features contribute to the senescent phenotype.

Senescence triggers

Senescence can be triggered by a myriad of stressors. Besides replicative senescence and OIS discussed above, other triggers can establish different forms of senescence (Gorgoulis et al., 2019; Hernandez-Segura et al., 2018). DNA damage is a shared feature of various forms of senescence because many damage-inflicting senescence triggers result in DNA damage. Examples of triggers are: oxidative stress (Moiseeva et al., 2009), through oxidative agents or by-products of the cell metabolism; mitochondria dysfunction (Wiley et al., 2016); therapy-induced senescence (TIS), for instance through chemotherapy, cyclin-dependent kinase inhibitors or epigenetic modifiers (Ewald et al., 2010; Gorgoulis et al., 2019); paracrine signaling derived from neighboring senescent cells (Acosta et al., 2013); and, various pathogens (Humphreys et al., 2020), including coronavirus (Lee et al., 2021b). It is generally considered that the degree of damage resulting from these triggers is an important indicator for the decision between apoptosis versus senescence, but the underlying mechanism that determines the cell fate is not fully uncovered yet (Childs et al., 2014).

Cell cycle arrest

When a senescence response is activated, cells undergo a cell cycle arrest. In proliferating conditions, members of the retinoblastoma (RB) family (pRB, p107, and p130) are phosphorylated by various cyclin-dependent kinases (CDKs; CDK2, CDK4, CDK6) which disrupts the suppressive binding of RB members with E2F and DP transcription factors. This allows the transcription of E2F/DP target genes that are involved in cell cycle progression and DNA replication (Bracken et al., 2004). In senescence however, CDKs are inhibited by one or more CDK inhibitor proteins: p16^{INK4a}, p15^{INK4b}, and p21^{CIP}. This results in dephosphorylated RB proteins, forming the DREAM complex that represses the transcription of E2F and mitotic genes, leading to the induction of senescence (Litovchick et al., 2011). These proteins can be activated through various upstream pathways that are highly interconnected and contain multiple side branches (Kumari and Jat, 2021).

An important axis that results in RB hypophosphorylation is the activation of the DNA damage response (DDR), in which ATM and ATR are recruited to DNA damage lesions and can stabilize p53 through direct and indirect phosphorylation via Chk1/Chk2 (Maréchal and Zou, 2013; Ryan et al., 2001; Shieh et al., 2000). Subsequently, p53 enhances the transcriptional expression of p21^{CIP}, leading to CDK inhibition (Di Leonardo et al., 1994). While the p21^{CIP}/p53 axis is often activated in DDR-induced senescence, another axis frequently activated in senescent cells is the p16^{INK4a}/pRB pathway, known to be upregulated in epigenetically-induced senescence (Petrova et al., 2016). In this pathway, p16^{INK4a} blocks the complex assembly of cyclin D with CDK4/6, therefore preventing the phosphorylation of RB (Serrano et al., 1993).

The upregulation of p16^{INK4a}, p15^{INK4b}, and p21^{CIP} are often used as markers of

senescence (Gorgoulis et al., 2019). Other senescence markers related to cell cycle arrest are the increase in p27[Kip1], absence of proliferation marker Ki67, lack of incorporation of nucleoside analogs -like EdU or BrdU -, or cell cycle indicators like PCNA (González-Gualda et al., 2021; Gorgoulis et al., 2019). Nevertheless, lack of proliferation is not an exclusive feature of senescent cells, as quiescent, terminal differentiated, dormant, and drug-tolerant persister cells also withdraw from the cell cycle (Buttitta and Edgar, 2007; De Conti et al., 2021; Recasens and Munoz, 2019).

Lysosomal markers of cellular senescence
Besides a cell cycle arrest and morphology change, a widely used biomarker of the senescent state is the increased activity of senescence-associated beta-galactosidase (SA-ß-gal) (Dimri et al., 1995). SA-ß-gal is an enzyme with hydrolase and transgalactosylase activity (Huber et al., 1976) that resides in lysosomes (Kurz et al., 2000). Increased abundance of SA-ß-gal marker reflects the enlarged lysosomal compartment of senescent cells (Kurz et al., 2000). SA-ß-gal is encoded by the *GLB1* gene and is not required for the induction nor the maintenance of the senescent state (Lee et al., 2006).

The activity of SA-ß-gal can be measured using the chromogenic substrate X-gal, a colorless soluble compound that upon cleavage by SA-ß-gal dimerizes into an insoluble, blue product (Juers et al., 2012). As this assay is performed at pH 6.0, which is a suboptimal pH for SA-ß-gal activity, senescent cells will be preferentially stained blue because of their elevated levels of SA-ß-gal activity (Lee et al., 2006). Limitations of this staining are that it can only be used on fresh tissue and that certain non-senescent cells stain positive as well (de Mera-Rodríguez et al., 2021). Examples of (seemingly) non-senescent cells that stained positive for SA-ß-gal are macrophages and osteoclasts (Hall et al., 2017; Kopp et al., 2007); neurons (Piechota et al., 2016); tissues from middle aged mice derived from the intestine, heart muscle, pancreas (Raffaele et al., 2020); and serum starved or confluent *in vitro* cultures (Severino et al., 2000; Yang and Hu, 2005).

Another method to detect SA-ß-gal is based on the hydrolysis of fluorogenic substrates that contain an incorporated galactose that upon cleavage result in fluorescence. Substrates are added to live cells after alkalinization of the lysosomes, and SA-ß-gal positive cells can be measured through flow cytometry (González-Gualda et al., 2021). Examples of substrates are $C_{12}FDG$ (Debacq-Chainiaux et al., 2009), SPiDER- ß-gal (Doura et al., 2016), and DDAOG (Tung et al., 2004).

Besides SA-ß-gal, lipofuscin accumulation is another senescence marker that indicates increased lysosomal content (Zglinicki et al., 1995). Lipofuscin consists of a mixture of non-degradable oxidation products from proteins and lipids (Gray and Woulfe, 2005), and can be detected through Sudan Black-B or GL13 staining (Ea et al., 2013; Evangelou et al., 2017). The advantage of these assays is that they can be used on

fixed material. Nevertheless, the jury is still out on how specific and sensitive these are compared to SA-ß-gal staining.

Nuclear markers of cellular senescence

Senescence associated macromolecular changes not only occur in the lysosomes but also in the nucleus. The first observed nuclear feature of senescent cells is the shortening of telomeres in replicative senescence (Harley et al., 1990), which can be measured by Q-PCR or FISH. In addition, senescent cells exhibit a global change in gene expression that is accompanied with the presence of heterochromatin structures, so-called Senescence-Associated Heterochromatin Foci (SAHF). These structures contribute to the transcriptional repression of proliferation genes and can be formed through the p16-pRB pathway (Narita et al., 2003). SAHF have a dense structure that can be determined through confocal microscopy of DAPI-stained DNA (Aird and Zhang, 2013). Moreover, SAHF recruit proteins involved in heterochromatin formation, like HP1, histone H2A variant macroH2A, methylated H3K9, and HMGA proteins (Narita et al., 2003, 2006; Zhang et al., 2005). Even though SAHF and associated proteins can serve as senescent markers in certain human senescent cells, robust SAHF has not been identified in murine cells so far.

Another high mobility group associated with senescence is HMGB1 (Davalos et al., 2013). This non-histone protein is involved in the bending of DNA to provide access to transcription factors like p53 (Jayaraman et al., 1998). Another feature of HMGB1 is that it functions as an Alarmin family member, which is rapidly released from the cell upon nonprogrammed cell death to provoke an innate immune response (Bianchi, 2007, 2009). One of the effects of secreted HMGB1 is the interaction with toll-like receptors, leading to the expression of NF-κB and inflammatory cytokines (Park et al., 2006). In senescence, nuclear HMGB1 is lost through secretion upon entering senescence, which optimizes the subsequent secretion of IL-6 and MMP-3 (Davalos et al., 2013). Furthermore, HMGB1 has been suggested to regulate the decision to enter senescence instead of apoptosis after genotoxic stress in fibroblasts and melanoma cells (Lee et al., 2019). Moreover, HMGB1 is involved in the activation of STING, which positively regulates the orchestration of secreted cytokines and chemokines of senescent cells (Lee et al., 2021a).

Another senescence-associated biomarker that is linked to the activation of STING is lamin B1. Nuclear lamina are structural proteins that contribute to the stability and shape of the nuclear envelope but also have scaffolding properties that anchor the chromatin and influence transcription (Gerace and Huber, 2012). Lamin B1 is found to be a senescence marker that is reduced in SAHF regions enriched for H3K9 trimethylation (Freund et al., 2012; Sadaie et al., 2013). Even though some studies reported that lamin B1 silencing could induce senescence and change chromatin structure (Shah et al., 2013; Shimi et al., 2011), other studies question whether this

causal relationship is generally true (Dreesen et al., 2013). The reduction of lamin B1 has been suggested to result from elevated autophagy in senescent cells, which degrades lamin B1 through the lysosomes (Dou et al., 2015). This degradation can result in the loss of nuclear envelope integrity (Adams et al., 2013), subsequent cytosolic chromatin fragments, and activation of cGAS-STING signaling (Glück et al., 2017).

Senescence-associated secretory phenotype (SASP)

Another key hallmark of senescent cells is the secretion of a myriad of factors called the Senescence-Associated Secretory Phenotype (SASP) (Coppé et al., 2008) or senescence messaging secretome (SMS) (Kuilman and Peeper, 2009). Typical SASP components are interleukins, chemokines, inflammatory molecules, growth modulators, proteases, bioactive lipids, receptors, extracellular matrix components, matrix metalloproteinases (MMP), and other non-protein molecules and insoluble factors (Coppé et al., 2010; Gorgoulis et al., 2019). The most conserved and commonly expressed SASP cytokines are IL-6 and IL-8 (Acosta et al., 2013; Coppé et al., 2010; Freund et al., 2010). The quantitative and qualitative expression of SASP varies amongst different cell lines, but also differs strongly between senescence triggers and is dynamic over time (Basisty et al., 2020; Coppé et al., 2008; Hernandez-Segura et al., 2017; Wiley et al., 2016). Furthermore, high SASP expression by only a few cells in the population is thought to account for changes seen at the population level (Wiley et al., 2017). Nevertheless, the full spectrum of secreted SASP factors in senescent (cancer) cells is still elusive.

SASP expression is predominantly driven by the DDR through direct activation as well as epigenetic modulation (Takahashi et al., 2012). Examples of pathways activated by DDR that are involved in SASP are p38MAPK (Freund et al., 2011), PI3K/mTOR (Bent et al., 2016; Herranz et al., 2015; Laberge et al., 2015), GATA4/p62-mediated autophagy (Kang et al., 2015), JAK2/STAT3 (Hubackova et al., 2012; Xu et al., 2015), and macroH2A1 and ATM (Chen et al., 2015). Most of these pathways converge on the activation of NF-kB and C/EBPβ transcription factors. These transcription factors regulate the expression of various SASP factors, like IL-1A, IL-6, IL-8, TGF-β family members, and VEGF. This creates a positive feedback loop that increases NF-kB and C/EBPβ activity even further (Acosta et al., 2008; Kuilman et al., 2008). Especially IL-1β is a master regulator of the SASP, as it can orchestrate the production of IL-1β, IL-6, IL-8, and CCL2 (Acosta et al., 2013; Orjalo et al., 2009). The activity of the SASP can also be dampened through negative feedback loops, one of which is the expression of miR-146a and miR-146b, activated through NF-kB and C/EBPβ signaling. These microRNAs inhibit NF-kB activity through a negative feedback loop (Bhaumik et al., 2009; Freund et al., 2010; Kang et al., 2015). As senescent cells with a fully established SASP express miR-146a, the expression of this microRNA is also considered a marker

of senescence (Kang et al., 2015; Olivieri et al., 2013).

Besides DDR signaling, cGAS is another player involved in the activation of the SASP. cGAS is a DNA sensor that plays an important role in the defense against pathogens by recognizing cytosolic DNA from bacteria (Li et al., 2013). Upon recognition of cytosolic DNA, cGAS can bind and activate STING, which mediates the activation of pathways involved in the antimicrobial response: activation of autophagosome formation and the expression of interferons and other cytokines and chemokines (Gui et al., 2019; Sun et al., 2013). In senescent cells, lamin B1 is downregulated, which compromises the nuclear architecture, leading to cytosolic DNA that activates cGAS-STING and SASP expression (Glück et al., 2017). In addition, a decrease in DNases TREX1 and DNase2 further contributes to the accumulation of cytosolic DNA (Takahashi et al., 2018). Particularly, LINE-1 was found to be retrotranscribed into cDNA and activate cGAS-STING in the cytosol of senescent cells (De Cecco et al., 2019; Simon et al., 2019).

Overall, to confidently detect the senescent state, the International Association of Cellular Senescence has postulated that multiple hallmarks of senescent cells **(Figure 1)** have to be assessed (Gorgoulis et al., 2019): markers indicating a cell cycle arrest (phospho-RB, p21, p16, p15, p53), lysosomal markers (SA-ß-gal, lipofuscin), nuclear markers (SAHFs, lamin B1, HMGB1), and indicators of SASP (IL-6, IL-8, IL1A, etc). Additional indicators of the SASP are the expression of NF-kB and C/EBPβ, as well as the expression of miR-146a and miR-146b. It is important to note that most studies have been performed in normal cells, while the hallmarks of senescent tumor cells have been studied less intensively.
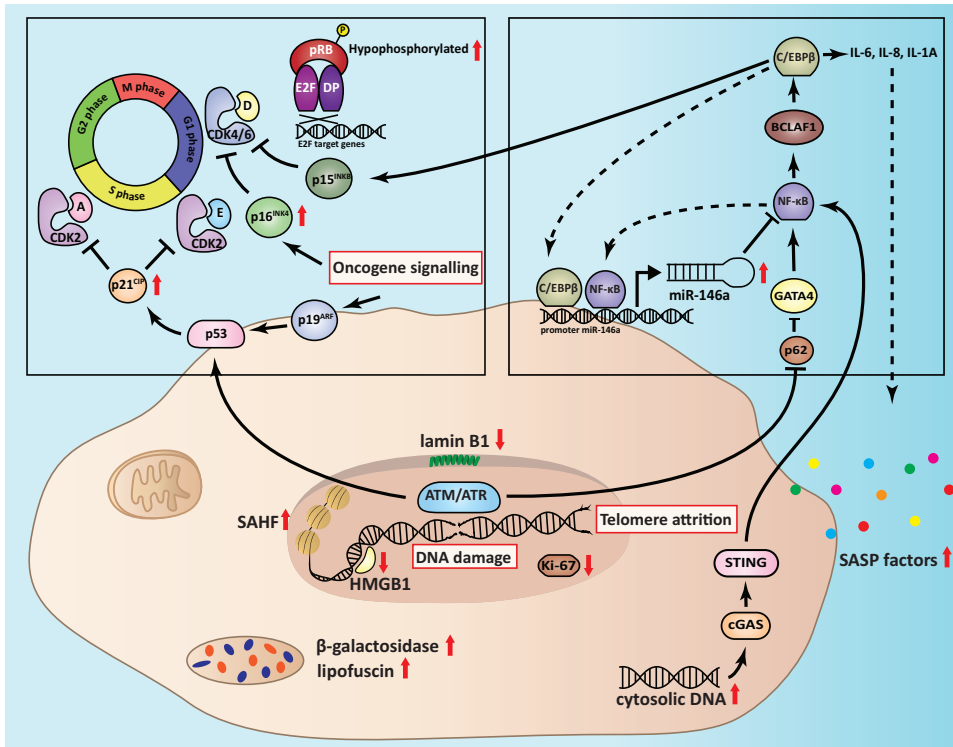
Figure 1. Cellular senescence hallmarks and pathways. Cellular senescence can be triggered by various stresses, like oncogene signaling, DNA damage, and telomere attrition. Most stresses cause DNA damage, which activates two axes: (i) the p53/RB axis, where p53 is stabilized by ATM/ATR and activates p21^{CIP}. This protein subsequently inhibits CDK2, which leads to hypophosphorylation of RB and transcriptional repression of E2F/DP target genes. (ii) the NF-κB/C/EBPß axis, in which ATM/ATR inhibit p62, which prevents the autophagic degradation of GATA4. GATA4 can then activate NF-κB, BCLAF1, and C/EBPß, leading to the expression of cytokines like IL-6, IL-8, and IL-1A. Another stimulator of this pathway is cytosolic DNA, that triggers cGAS-STING. This pathway also contains a negative feedback loop in which NF-κB and C/EBPß elevate miR-146a expression, which negatively regulates NF-κB. Once the senescence phenotype is established, various nuclear (decrease of lamin B1 and HMGB1, increase of SAHF), lysosomal (increase of ß-galactosidase and lipofuscin), cell cycle (upregulation of p21^{CIP}, p16^{INK4A}, and hypophosphorylated RB, decrease of Ki-67), and morphological (enlarged, flattened) markers can be detected.

Surviving the death sentence: senescent cells resist apoptosis

In addition to the hallmarks described above, another feature of senescent cells is their ability to adopt survival strategies to prevent apoptosis. The apoptosis pathway can be divided into the intrinsic and extrinsic pathway **(Figure 2)**, which converge downstream in the activation of cysteine-aspartic proteases (caspases) and subsequent demolition and phagocytosis of the cell (Elmore, 2007). Understanding these pathways is essential for understanding how senescent cells balance the act between senescence and apoptosis.
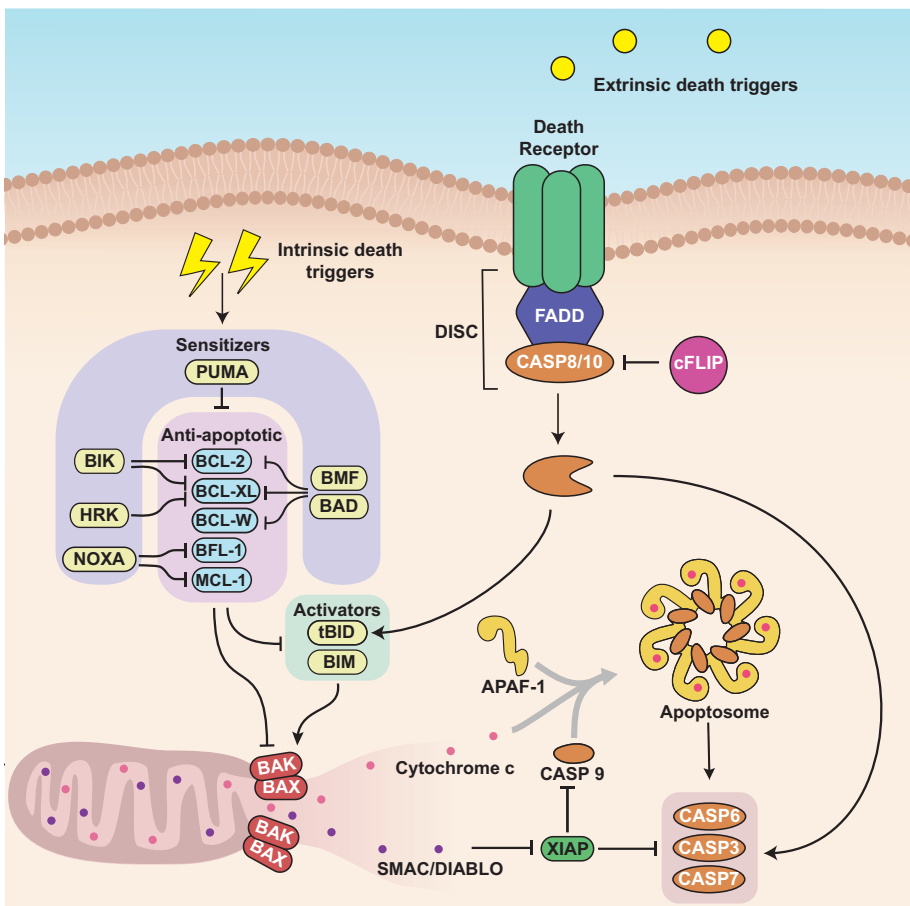

Figure 2. Intrinsic and extrinsic apoptosis pathways. Intrinsic apoptosis is triggered by a myriad of intrinsic death triggers, like DNA damage and oxidative stress. This activates BH3-only sensitizer proteins (PUMA, BIK, HRK, BMF, BAD, NOXA) to inhibit anti-apoptotic proteins (BCL-2, BCL-XL, BCL-W, BFL-1, MCL-1). This inhibition leads to the release of BH3-only activator proteins tBID and BIM from anti-apoptotic protein suppression. After that, effector proteins BAK and BAX are also released from anti-apoptotic inhibition and can be activated by the activator proteins. This leads

to the (hetero)dimerization of BAK and BAX, which induces pores in the outer mitochondrial membrane. In this way, cytochrome c, OMI/HTRA2 and SMAC/DIABLO are released to the cytosol. Cytochrome c can form a holoenzyme with APAF-1, autocatalytically cleaving CASP9 in the apoptosome. Activated CASP9 subsequently cleaves CASP3/7, leading to the demolition of the cell. However, degradation of caspases can be induced by XIAP, which is prevented by OMI and SMAC/ DIABLO. Besides the intrinsic apoptosis pathway, cells can also respond to external death signals through death receptor signaling. Upon binding of the death receptor ligands to death receptors, FADD and CASP8/10 are recruited to form DISC. Here, CASP8/10 are autocatalytically cleaved, which enables them to active caspases, while CASP8 can also create active tBID. CASP8/10 activation can be suppressed by cFLIP.

Intrinsic apoptosis

The intrinsic apoptosis pathway, also known as the mitochondrial pathway, is triggered via a myriad of intracellular death stimuli. Examples are radiation, hypoxia, hyperthermia, viral infections, toxins and free radicals. This induction can also be suppressed by other stimuli, like growth factors, hormones and cytokines (Elmore, 2007). The overall balance between pro- and anti-apoptotic signals determines not only the initial trigger, but also the final execution of the intrinsic apoptosis pathway.

Key players in intrinsic apoptosis are BCL-2 family proteins. These proteins harbor BCL-2 homology (BH) domains, BH1-4. Pro-apoptotic family members only contain the BH3 domain, referred to as BH3-only proteins. In contrast, anti-apoptotic proteins (BCL-XL, BCL-2, BCL-W, MCL-1, BFL-1) contain all BH domains, which allows them to bind and sequester BH3-only proteins. BH3-only proteins consist of sensitizer proteins (PUMA, NOXA, HRK, BAD, BIK, BMF) that inhibit anti-apoptotic proteins, and activator proteins (BIM, truncated (t)BID) that can activate the pore-forming effector proteins (BAK, BAX, BOK) (Czabotar et al., 2014; Letai et al., 2002).

Whether or not the outcome of BCL-2 protein interactions leads to mitochondrial outer membrane permeabilization (MOMP) depends on interrelated factors (Kale et al., 2017): (i) abundance, especially local concentrations of BCL-2 proteins can change their affinity; (ii) affinity, as BCL2 proteins have multiple binding partners and these proteins have various binding affinities to one or multiple partners; (iii) localization, BCL-2 proteins can be located at the mitochondrial membrane, cytoplasm, ER, nuclear envelope, and at the Golgi network. For instance, upon apoptotic stimuli, the recruitment of BCL-2 proteins to the mitochondrial membrane induces conformational changes that influences their affinity for other proteins; (iv) post-translational modification, which can alter the activity, abundance, stability and localization of the protein. These factors complicate the prediction of cell fate, which goes beyond the sum of individual components (Kale et al., 2017).

When the actions of pro-apoptotic players overrule anti-apoptotic proteins, MOMP can be induced. When pores are formed in the mitochondrial outer membrane, cytochrome c, SMAC (also known as DIABLO), and OMI (also called

HtrA2) are released from the mitochondrial intermembrane space (Hegde et al., 2002; Liu et al., 1996; Verhagen et al., 2000). Subsequently, cytochrome c forms together with APAF-1 the apoptosome, which activates a cleaving cascade of caspase-9, caspase-3, and caspase-7 (Taylor et al., 2008). SMAC and OMI inhibit XIAP, an anti-apoptotic protein that can prevent the catalytic activity of caspase-9, -3, and -7 by ubiquitinating active caspases for proteasomal degradation (Eckelman et al., 2006). Caspases cleave components of the cytoskeleton, nuclear envelope, chromatin, extracellular matrix, and organelles. This allows the engulfment by phagocytic cells and prevents the induction of an inflammatory response (Elmore, 2007; Taylor et al., 2008).

Extrinsic apoptosis
The extrinsic apoptosis pathway senses external death triggers and relies on the activation of transmembrane receptor-mediated interactions. These transmembrane receptors consist of six death receptors (DRs) from the Tumor Necrosis Factor Receptor (TNFR) superfamily, including FAS/APO-1/CD95, TNFR1/CD120a, TRAMP, TRAIL-R1/DR4, TRAIL-R2/DR5, and DR6 (Daniel et al., 2001; Green and Llambi, 2015). The cognate DR ligands TNF, FAS ligand, and TRAIL are predominantly expressed by activated immune cells - like NK cells, macrophages, and cytotoxic T-lymphocytes - to activate apoptosis in target cells. In addition, TRAIL is also expressed in various other cell types.

In the absence of ligands, DRs are present as monomers or inactive dimers and trimers at the cellular membrane. Upon binding, DRs undergo a conformational change that recruits the adapter protein FADD and pro-caspase-8/10 for the formation of the death-inducing signaling complex (DISC). Through this complex, these initiator caspases are auto-catalytically activated and can cleave BID, caspase 3, 6, and 7. These caspases are only active when BID induces MOMP through BAX, which leads to the release of SMAC and OMI, which inhibit XIAP (Kalkavan and Green, 2017; Reilly et al., 2016). Besides XIAP, another anti-apoptotic protein is c-FLIP, which prevents the activation of pro-caspase-8 and -10 by FADD (Safa and Author, 2012).

Senescent cells have adopted strategies to tip the balance of apoptotic members towards survival. Examples of this regulation is through the upregulation of anti-apoptotic BCL-2 family proteins (Chang et al., 2016; Ryu et al., 2007; Zhu et al., 2016), or through epigenetic downregulation of pro-apoptotic proteins like BAX (Sanders et al., 2013). Various upstream networks are involved in survival signaling. Examples of pathways involved in the survival of senescent cells are ephrins, SRC, PI3K, PAI2, p21, p53, FOXO4, and autophagy (Baar et al., 2017; Soto-gamez et al., 2019; Zhu et al., 2015).

Senescent cells in a tumor context: the bright and the dark side

The consequence of senescent cells in the tumor environment has been heavily debated **(Figure 3)** (Coppé et al., 2010; Faget et al., 2019; Sun et al., 2018; Takasugi et al., 2022). On the one hand, the induction of senescence in tumor cells halts their proliferative character, slowing down the progression of disease and enhancing treatment outcome (Althubiti et al., 2014; Haugstetter et al., 2010; Schmitt et al., 2002; Xue et al., 2007). Moreover, the SASP can attract immune cells to the tumor site that clear senescent cells, and it can induce angiogenesis that can improve the delivery of immune cells and anti-cancer drugs (Krizhanovsky et al., 2008; Munoz-Espin and Serrano, 2014; Ruscetti et al., 2018, 2020). Secreted SASP factors can reinforce and induce senescence in an autocrine and paracrine fashion (Acosta et al., 2008; Coppé et al., 2010; Kuilman et al., 2008).
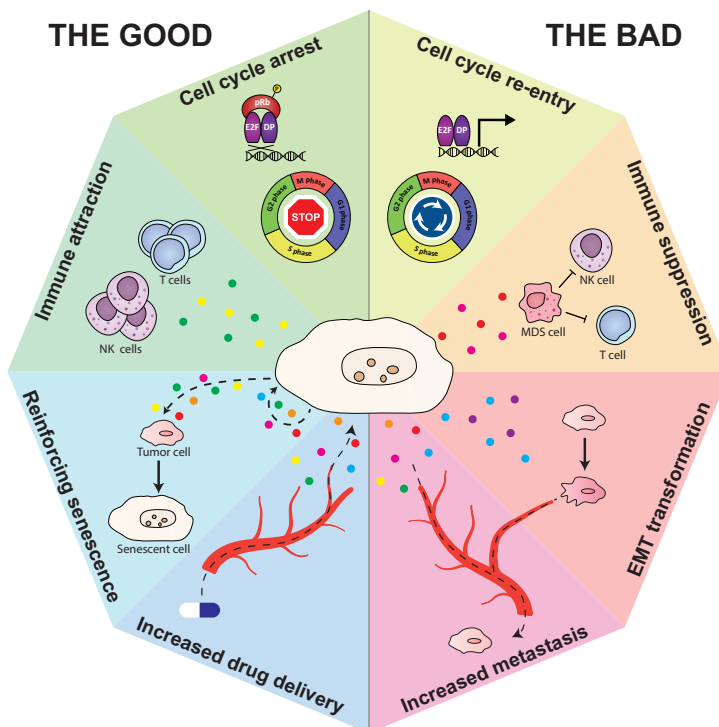

Figure 3. The good and the bad side of senescent tumor cells. There are good and bad consequences of having senescent tumor cells in the tumor microenvironment. On the one hand, senescence halts tumor proliferation, attracts immune cells, reinforces senescence through autocrine and paracrine signaling, and tumor vascularization increases drug uptake. On the other hand, senescent tumor cells can re-renter the cell cycle, attract MDSCs that suppress immune cells, induce EMT transformation of tumor cells, and enhance metastasis through the angiogenic effects of the SASP.

On the other hand, evidence has been increasing that senescent cells can start proliferating again and even have a more aggressive phenotype after re-entering the cell cycle (Dirac and Bernards, 2003; Milanovic et al., 2018; Roberson et al., 2005). For instance, senescent cells in which p53 was deleted started cycling again, but maintained SASP expression (Coppé et al., 2008). Furthermore, persistent secretion leads to chronic inflammation that can forestall immune clearance (Franceschi and Campisi, 2014). In addition, the SASP can recruit immune-suppressive myeloid cells to tumor sites (Eggert et al., 2016; Mitri et al., 2015). Moreover, the SASP can stimulate tumorigenesis by driving epithelial-mesenchymal transition, angiogenesis, and metastasis (Coppé et al., 2010; Laberge et al., 2012).

Taken together, the short-term anti-proliferation and immunogenic effects of senescent tumor cells can be considered beneficial, while the long-term reawakening and inflammatory effects are undesirable. This has increased the interest in removing cancer and non-cancer cells from the tumor environment to reduce the risk of tumor relapse and adverse effects of cancer treatments.

Elimination of senescent cells with senolytic agents

Senescent cells undergo changes that allow them to resist apoptosis, which makes them vulnerable to agents that target these apoptosis resistance mechanisms, so-called 'senolytics'. Senolytics have originally been developed to attenuate the effect of senescent cells in age-related diseases.

One of these agents is ABT-263, also known as navitoclax, which targets the anti-apoptotic proteins BCL-2, BCL-W, and BCL-XL (Chang et al., 2016; Zhu et al., 2016). This BH3 mimetic is effective in multiple senescent cells: from various cell types, induced by different triggers, both in normal as well as in cancer cells (Chang et al., 2016; Cristina et al., 2019; Demaria et al., 2017; Pan et al., 2017; Sugihara et al., 2020; Wang et al., 2017). ABT-263 reduces age-related symptoms in preclinical models (Chang et al., 2016; Cristina et al., 2019; Sugihara et al., 2020), and attenuates adverse effects from chemo or irradiation therapy (Chang et al., 2016; Demaria et al., 2017; Pan et al., 2017). Interestingly, this senolytic showed enhanced tumor cell killing in a two-step treatment in which cancer cells were first induced to senescence before being eliminated with ABT-263 (Saleh et al., 2020; Wang et al., 2017). In the clinic, ABT-263 therapy is accompanied with thrombocytopenia and neutropenia (Kaefer et al., 2014), but showed a safe toxicity profile in phase II clinical studies (clinicaltrials.gov; Brachet et al., 2022; de Vos et al., 2021). Nevertheless, alternative treatments for ABT-263 are under development that circumvent this toxicity. For instance, PROTACs PZ15227 and DT2216 target BCL-XL in the presence of cereblon or Von Hippel-Lindau E3 ligase activity, which is absent in platelets (He et al., 2020; Khan et al., 2019). In

addition, nanoparticles that release ABT-263 upon cleavage by SA-ß-galactosidase target only senescent cells (González-Gualda et al., 2020).

Other agents with senolytic efficacy are: ABT-737, an analog of ABT-263 targeting BCL-XL, BCL-2, and BCL-W (Yosef et al., 2016); BCL-XL inhibitors A1331852 and A1155463 (Zhu et al., 2017); BET family inhibitors, through downregulation of non-homologous end joining and activation of autophagy (Lu et al., 2015; Wakita et al., 2020); Dasatinib, a multi-tyrosine kinase inhibitor, in combination with Quercetin, a natural flavonoid (Zhu et al., 2015). Even though the exact mechanism remains elusive and these compounds target many pathways, it is thought to act through inhibition of SRC kinase and PI3K-AKT signaling nodes; Fisetin is another flavonoid with senolytic activity, probably with similar mechanism of action as quercetin (Yousefzadeh et al., 2018; Zhu et al., 2017); Piperlongumine is a senolytic small molecule with an unclear mechanism (Wang et al., 2016); FOXO4-DRI peptide, which disrupts the p53-FOXO4 interaction (Baar et al., 2017); UBX0101 prevents the interaction of p53 and MDM2 (Jeon et al., 2017); Cardiac glycosides digoxin and ouabain alter the Na$^+$/K$^+$ transport, and senescent cells are vulnerable to the depolarization and acidification of the plasma membrane caused by cardiac glycosides (Guerrero et al., 2019; Triana-Martínez et al., 2019); mTOR inhibitor AZD8055 has shown to be senolytic in *TP53* mutant liver cancer cells that were induced to senescence through CDC7 inhibition (Wang et al., 2019).

Overall, the vulnerabilities of senescent cells can be exploited in cancer therapy. As many current cancer treatments mostly induce apoptosis but can leave senescent cells behind, a senolytic treatment can be beneficial to remove the remaining cells to prevent long-term detrimental effects.

Thesis rationale and outline

As described in this introduction, the discovery that cancer cells can enter the senescent state and harbor vulnerabilities that can be exploited makes them an attractive phenotype to an 'one-two punch' therapy **(Figure 4)**. In this sequential therapy, cells are first induced to senescence by a senescence-inducing treatment or standard of care anti-cancer therapy, while the second treatment ablates the (remaining) senescent cancer cells. The major focus of this thesis is to identify ways to induce senescence in cancer cells and finding universal vulnerabilities of these senescent cancer cells to eliminate them.

In **chapter 2,** a customized CRISPR-Cas9 genetic screen has been developed that allows screening for genes that upon knock-out induce senescence in non-small lung cancer cells. This customized screen entails a suicide-switch system that depletes non-proliferating cells based on Ki-67 expression and enriches for miR-146a

expressing cells through fluorescence-activated cell sorting. This genetic screen identifies multiple genes that upon knock-out inhibited macroautophagy, which is involved in the degradation of (dysfunctional) cellular components. Various hit genes are involved in the ULK1 complex, and knock-down of these hit genes result in senescence-induction in lung cancer cells. This leads to the discovery that ULK1-inhibitors SBI02169565 and MRT68921 not only induce senescence in lung, but also in liver, colon, and pancreas cancer cells. Furthermore, these senescent cancer cells undergo apoptosis after treatment with ABT-263, a drug that antagonizes anti-apoptotic proteins. Thus, this study presents a novel genetic screening approach that identifies that the inhibition of autophagy can induce senescence in tumor cells and that these senescent cancer cells can be killed using ABT-263.
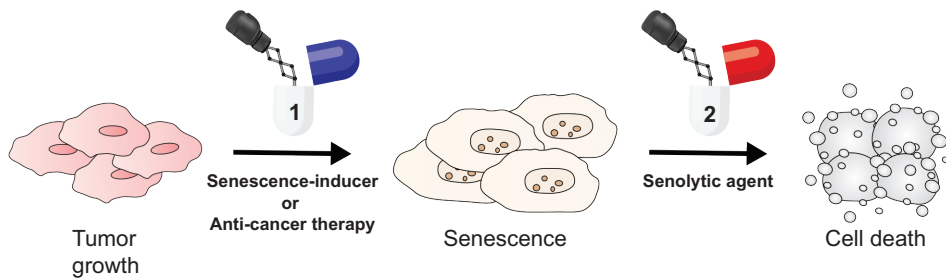

Figure 4. One-two punch approach. The one-two punch approach consists of two sequential treatments. Firstly, tumor cells are induced to senescence by a senescence-inducer or anti-cancer therapy. Secondly, the senescent tumor cells are targeted with a senolytic agent.

In **chapter 3** is sought for common features of senescent cancer cells that would identify universal vulnerabilities and allow unambiguous detection of senescent cancer cells. It appeared that cell lines derived from breast, colon, liver, and lung cancer are heterogeneous in their response to ABT-263, their transcriptome, and the SASP factors they express. This variability was mostly dictated by the nature of the cell line rather than the senescence-inducer. Moreover, the cancer type and the cell intrinsic properties of the parental cells form a blueprint for the SASP and the gene expression of their senescent counterparts. Because of this variability, this study highlights that the pro- or anti-tumor effects of senescent cells in a tumorous context will presumably be cancer-type and patient specific. To find shared expression patterns between the heterogeneous expression patterns of senescent cancer cells, artificial intelligence is used to build the 'SENCAN classifier model'. This algorithm can predict the probability that cells are senescent using transcriptome data. In

addition, a web tool is built that makes the SENCAN classifier easily accessible for other researchers to analyze transcriptome data. Moreover, this website also contains an interface to query the gene expression of single genes.

In **chapter 4,** the main focus is to find the underlying mechanisms that explain the variability of response to senolytic ABT-263. As ABT-263 acts as an inhibitor of anti-apoptotic proteins, the apoptosis pathway is investigated with BH3 profiling. This technique enables to measure the balance between pro- and anti-apoptotic proteins and the 'apoptotic priming' of cells (how close cells are to cell death). BH3 profiling is applied on parental as well as senescent cells and elucidates that cell lines with a high senolytic response to ABT-263 are more primed to apoptosis, not only in senescent but already in their parental state. Moreover, it becomes clear that during treatment with ABT-263, MCL-1 increases in abundance in cells with a low response to ABT-263. Even though the combined inhibition of MCL-1 and ABT-263 could efficiently kill senescent cancer cells, it is also expected to result in considerable toxicity. Overall, this study shows that senolytic sensitivity is already determined in the parental state, possibly providing a predictive biomarker for the response to senotherapies.

In the study described in **chapter 5**, the aim was to identify possible resistance mechanisms to senolytic killing with ABT-263. Where CRISPR/Cas9 resistance screens in proliferating cells rely on the outgrowth of resistant colonies to amplify their gRNA signal, a resistance screen in non-proliferating senescent cells comes with specific adaptations. In this chapter, recommendations are provided on how to perform resistance screens in senescent cells for senolytics. A resistance screen for ABT-263 in non-small lung cancer cells identifies various pathways: (i) proteins that negatively regulate the PI3K/AKT/mTOR pathway, (ii) proteins that negatively regulate anti-apoptotic proteins BFL-1 and MCL-1, and (iii) proteins not related to apoptosis. In addition, multiple hits genes are related to the increase of MCL-1, which corroborates with the findings in chapter 4. Further studies are required to validate these hit genes and elucidate whether a novel drug combination can be found that prevents the upregulation of MCL-1 targeting its upstream pathways, potentially providing a better therapeutic window.

In **chapter 6**, the research focus is to find a senolytic treatment strategy superior to ABT-263 to kill senescent cancer cells. From a genetic screen, cFLIP is identified as a gene that upon loss causes senolysis of cancer cells, indicating that senescent cancer cells rely on the effect of cFLIP - which inhibits extrinsic apoptosis - or their survival. Moreover, senescent cancer cells are also more sensitive to the stimulation of extrinsic apoptosis with TRAIL or DR5 agonist. This increased sensitivity is explained through the upregulation of NF-κB, resulting in increased expression of both c-FLIP as well as DR5. Moreover, a bystander effect seems to enhance the killing of non-senescent tumor cells with DR5 agonists. In mouse models for liver and

lung cancer, a pro-senescence treatment combined with a DR5 agonistic antibody shows efficient tumor killing. Forthcoming studies will determine whether this therapeutic method will enhance the treatment of cancer patients.

In **chapter 7**, the findings of this thesis are discussed in light of recent studies. The overall conclusion is that the heterogeneity of senescent cancer cells provides a challenge for the clinical development of the one-two punch strategy, but that various studies also describe various immune-enhancing effects of senescent tumor cells that stimulate tumor killing. Overall, senescence is expected to remain an interesting cancer research area in the coming decades.

References

Acosta, J.C., O'Loghlen, A., Banito, A., Guijarro, M. V., Augert, A., Raguz, S., Fumagalli, M., Da Costa, M., Brown, C., Popov, N., et al. (2008). Chemokine Signaling via the CXCR2 Receptor Reinforces Senescence. Cell https://doi.org/10.1016/j.cell.2008.03.038.

Acosta, J.C., Banito, A., Wuestefeld, T., Georgilis, A., Janich, P., Morton, J.P., Athineos, D., Kang, T.W., Lasitschka, F., Andrulis, M., et al. (2013). A complex secretory program orchestrated by the inflammasome controls paracrine senescence. Nat. Cell Biol. *15*, 978–990. https://doi.org/10.1038/ncb2784.

Adams, P.D., Ivanov, A., Pawlikowski, J., Manoharan, I., Tuyn, J. Van, Nelson, D.M., Singh Rai, T., Shah, P.P., Hewitt, G., Korolchuk, V.I., et al. (2013). Lysosome-mediated processing of chromatin in senescence. J. Cell Biol. *202*, 129–143. https://doi.org/10.1083/jcb.201212110.

Aird, K.M., and Zhang, R. (2013). Detection of senescence-associated heterochromatin foci (SAHF). Methods Mol. Biol. *965*, 185–196. https://doi.org/10.1007/978-1-62703-239-1_12.

Althubiti, M., Lezina, L., Carrera, S., Jukes-Jones, R., Giblett, S.M., Antonov, A., Barlev, N., Saldanha, G.S., Pritchard, C.A., Cain, K., et al. (2014). Characterization of novel markers of senescence and their prognostic potential in cancer. Cell Death Dis. https://doi.org/10.1038/cddis.2014.489.

Baar, M.P., Brandt, R.M.C., Putavet, D.A., Klein, J.D.D., Derks, K.W.J., Bourgeois, B.R.M., Stryeck, S., Rijksen, Y., van Willigenburg, H., Feijtel, D.A., et al. (2017). Targeted Apoptosis of Senescent Cells Restores Tissue Homeostasis in Response to Chemotoxicity and Aging. Cell *169*, 132–147. https://doi.org/10.1016/j.cell.2017.02.031.

Basisty, N., Kale, A., Jeon, O.H., Kuehnemann, C., Payne, T., Rao, C., Holtz, A., Shah, S., Sharma, V., Ferrucci, L., et al. (2020). A proteomic atlas of senescence-associated secretomes for aging biomarker development. PLoS Biol. *18*, e3000599. https://doi.org/10.1371/journal.pbio.3000599.

Bent, E.H., Gilbert, L.A., and Hemann, M.T. (2016). A senescence secretory switch mediated by PI3K/AKT/mTOR activation controls chemoprotective endothelial secretory responses. Genes Dev. *30*, 1811–1821. https://doi.org/10.1101/gad.284851.116.

Bhaumik, D., Scott, G.K., Schokrpur, S., Patil, C.K., Orjalo, A. V., Rodier, F., Lithgow, G.J., and Campisi, J. (2009). MicroRNAs miR-146a/b negatively modulate the senescence-associated inflammatory mediators IL-6 and IL-8. Aging (Albany. NY). *1*, 402–411. https://doi.org/10.1016/j.virol.2011.01.029.The.

Bianchi, M.E. (2007). DAMPs, PAMPs and alarmins: all we need to know about danger. J. Leukoc. Biol. *81*, 1–5. https://doi.org/10.1189/jlb.0306164.

Bianchi, M.E. (2009). HMGB1 loves company. J. Leukoc. Biol. *86*, 573–576. https://doi.org/10.1189/jlb.1008585.

Bianconi, E., Piovesan, A., Facchin, F., Beraudi, A., Casadei, R., Frabetti, F., Vitale, L., Pelleri, M.C., Tassani, S., Piva, F., et al. (2013). An estimation of the number of cells in the human body. Ann. Hum. Biol. *40*, 463–471. https://doi.org/10.3109/03014460.2013.807878.

Brachet, P.E., Fabbro, M., Leary, A., Medioni, J., Follana, P., Lesoin, A., Frenel, J.-S., Abadie Lacourtoisie, S., Floquet, A., Gladieff, L., et al. (2022). A GINECO phase II study of Navitoclax (ABT 263) in women with platinum resistant/refractory recurrent ovarian cancer (ROC). Gynecol. Oncol. *165*, 30–39. https://doi.org/https://doi.org/10.1016/j.ygyno.2022.01.021.

Bracken, A.P., Ciro, M., Cocito, A., and Helin, K. (2004). E2F target genes: Unraveling the biology. Trends Biochem. Sci. *29*, 409–417. https://doi.org/10.1016/j.tibs.2004.06.006.

Braig, M., Lee, S., Loddenkemper, C., Rudolph, C., Peters, A.H.F.M., Schlegelberger, B., Stein, H., Dörken, B., Jenuwein, T., and Schmitt, C.A. (2005). Oncogene-induced senescence as an initial barrier in lymphoma development. Nature https://doi.org/10.1038/nature03841.

Buttitta, L.A., and Edgar, B.A. (2007). Mechanisms controlling cell cycle exit upon terminal differentiation. Curr. Opin. Cell Biol. *19*, 697–704. https://doi.org/10.4324/9780203813805-28.

De Cecco, M., Ito, T., Petrashen, A.P., Elias, A.E., Skvir, N.J., Criscione, S.W., Caligiana, A., Brocculi, G., Adney, E.M., Boeke, J.D., et al. (2019). L1 drives IFN in senescent cells and promotes age-associated inflammation. Nature *566*, 73–78. https://doi.org/10.1038/s41586-018-0784-9.

Chang, J., Wang, Y., Shao, L., Laberge, R.-M., Demaria, M., Campisi, J., Janakiraman, K., Sharpless, N.E., Ding, S., Feng, W., et al. (2016). Clearance of senescent cells by ABT-263 rejuvenates aged hematopoietic stem cells in mice. Nat. Med. *22*, 78–83. https://doi.org/10.1097/CCM.0b013e31823da96d.Hydrogen.

Chen, H., Ruiz, P.D., McKimpson, W.M., Novikov, L., Kitsis, R.N., and Gamble, M.J. (2015). MacroH2A1

1

and ATM Play Opposing Roles in Paracrine Senescence and the Senescence-Associated Secretory Phenotype. Mol. Cell *59*, 719–731. https://doi.org/10.1016/j.molcel.2015.07.011.

Chen, Z., Trotman, L.C., Shaffer, D., Lin, H.K., Dotan, Z.A., Niki, M., Koutcher, J.A., Scher, H.I., Ludwig, T., Gerald, W., et al. (2005). Crucial role of p53-dependent cellular senescence in suppression of Pten-deficient tumorigenesis. Nature https://doi.org/10.1038/nature03918.

Childs, B.G., Baker, D.J., Kirkland, J.L., Campisi, J., and Deursen, J.M. (2014). Senescence and apoptosis: dueling or complementary cell fates? EMBO Rep. *15*, 1139–1153. https://doi.org/10.15252/embr.201439245.

Collado, M., Gil, J., Efeyan, A., Guerra, C., Schuhmacher, A.J., Barradas, M., Benguría, A., Zaballos, A., Flores, J.M., Barbacid, M., et al. (2005). Senescence in premalignant tumours. Nature https://doi.org/10.1038/436642a.

De Conti, G., Dias, M.H., and Bernards, R. (2021). Fighting drug resistance through the targeting of drug-tolerant persister cells. Cancers (Basel). *13*, 1–15. https://doi.org/10.3390/cancers13051118.

Coppé, J.-P., Desprez, P.-Y., Krtolica, A., and Campisi, J. (2010). The senescence-associated secretory phenotype: the dark side of tumor suppression. Annu. Rev. Pathol. *5*, 99–118. https://doi.org/10.1146/annurev-pathol-121808-102144.

Coppé, J.P., Patil, C.K., Rodier, F., Sun, Y., Muñoz, D.P., Goldstein, J., Nelson, P.S., Desprez, P.Y., and Campisi, J. (2008). Senescence-associated secretory phenotypes reveal cell-nonautonomous functions of oncogenic RAS and the p53 tumor suppressor. PLoS Biol. *6*, 2853–2868. https://doi.org/10.1371/journal.pbio.0060301.

Cristina, A.-M., Joshua, A., Lee Jr, T.B., Ayush, M., Talemal, L., Chipashvilli, V., Hollister-Lock, J., Van deursen, J., Weir, G., and Bonner-Weir, S. (2019). Acceleration of β-cell aging determines diabetes and senolysis improves disease outcomes. *30*, 129–142. https://doi.org/10.1016/j.cmet.2019.05.006.Acceleration.

Czabotar, P.E., Lessene, G., Strasser, A., and Adams, J.M. (2014). Control of apoptosis by the BCL-2 protein family: Implications for physiology and therapy. Nat. Rev. Mol. Cell Biol. *15*, 49–63. https://doi.org/10.1038/nrm3722.

Daniel, P.T., Wieder, T., Sturm, I., and Schulze-Osthoff, K. (2001). The kiss of death: Promises and failures of death receptors and ligands in cancer therapy. Leukemia *15*, 1022–1032. https://doi.org/10.1038/sj.leu.2402169.

Davalos, A.R., Kawahara, M., Malhotra, G.K., Schaum, N., Huang, J., Ved, U., Beausejour, C.M., Coppe,

J.P., Rodoer, F., and Campisi, J. (2013). p53-dependent release of Alarmin HMGB1 is a central mediator of senescent phenotypes. J. Cell Biol. *201*, 613–629. https://doi.org/10.1083/jcb.201206006.

Debacq-Chainiaux, F., Erusalimsky, J.D., Campisi, J., and Toussaint, O. (2009). Protocols to detect senescence-associated beta-galactosidase (SA-βgal) activity, a biomarker of senescent cells in culture and in vivo. Nat. Protoc. *4*, 1798–1806. https://doi.org/10.1038/nprot.2009.191.

Demaria, M., O'Leary, M.N., Chang, J., Shao, L., Liu, S., Alimirah, F., Koenig, K., Le, C., Mitin, N., Deal, A.M., et al. (2017). Cellular Senescence Promotes Adverse Effects of Chemotherapy and Cancer Relapse. Cancer Discov. *7*, 165–176. https://doi.org/10.1158/2159-8290.CD-16-0241.

Dimri, G.P., Lee, X., Basile, G., Acosta, M., Scott, G., Roskelley, C., Medrano, E.E., Linskens, M., Rubelj, I., Pereira-Smith, O., et al. (1995). A biomarker that identifies senescent human cells in culture and in aging skin in vivo. Proc. Natl. Acad. Sci. U. S. A. *92*, 9363–9367. https://doi.org/10.1073/pnas.92.20.9363.

Dirac, A.M.G., and Bernards, R. (2003). Reversal of senescence in mouse fibroblasts through lentiviral suppression of p53. J. Biol. Chem. *278*, 11731–11734. https://doi.org/10.1074/jbc.C300023200.

Dou, Z., Xu, C., Donahue, G., Shimi, T., Pan, J.A., Zhu, J., Ivanov, A., Capell, B.C., Drake, A.M., Shah, P.P., et al. (2015). Autophagy mediates degradation of nuclear lamina. Nature *527*, 105–109. https://doi.org/10.1038/nature15548.

Doura, T., Kamiya, M., Obata, F., Yamaguchi, Y., Hiyama, T.Y., Matsuda, T., Fukamizu, A., Noda, M., Miura, M., and Urano, Y. (2016). Detection of LacZ-Positive Cells in Living Tissue with Single-Cell Resolution. Angew. Chemie - Int. Ed. *55*, 9620–9624. https://doi.org/10.1002/anie.201603328.

Dreesen, O., Ong, P.F., Chojnowski, A., and Colman, A. (2013). The contrasting roles of lamin B1 in cellular aging and human disease. Nucleus *4*, 283–290. https://doi.org/10.4161/nucl.25808.

Ea, G., K, T.K.E., Pj, F.M., and Zoumpourlis, V. (2013). Specific lipofuscin staining as a novel biomarker to detect replicative and stress-induced senescence. A method applicable in cryo-preserved and archival tissues. Aging (Albany. NY). *5*, 37–50. .

Eckelman, B.P., Salvesen, G.S., and Scott, F.L. (2006). Human inhibitor of apoptosis proteins: Why XIAP is the black sheep of the family. EMBO Rep. *7*, 988–994. https://doi.org/10.1038/sj.embor.7400795.

Eggert, T., Wolter, K., Ji, J., Ma, C., Yevsa, T., Klotz, S., Medina-Echeverz, J., Longerich, T., Forgues, M., Reisinger, F., et al. (2016). Distinct Functions of Senescence-Associated Immune Responses in Liver Tumor Surveillance and Tumor Progression. Cancer Cell https://doi.org/10.1016/j.ccell.2016.09.003.

Elmore, S. (2007). Apoptosis: A review of programmed cell death. Toxicol Pathol 23, 495–516. https://doi.org/10.1080/01926230701320337.

Evangelou, K., Lougiakis, N., Rizou, S. V., Kotsinas, A., Kletsas, D., Muñoz-Espín, D., Kastrinakis, N.G., Pouli, N., Marakos, P., Townsend, P., et al. (2017). Robust, universal biomarker assay to detect senescent cells in biological specimens. Aging Cell 16, 192–197. https://doi.org/10.1111/acel.12545.

Ewald, J.A., Desotelle, J.A., Wilding, G., and Jarrard, D.F. (2010). Therapy-induced senescence in cancer. J. Natl. Cancer Inst. 102, 1536–1546. https://doi.org/10.1093/jnci/djq364.

Faget, D. V., Ren, Q., and Stewart, S.A. (2019). Unmasking senescence: context-dependent effects of SASP in cancer. Nat. Rev. Cancer 19, 439–453. https://doi.org/10.1038/s41568-019-0156-2.

Franceschi, C., and Campisi, J. (2014). Chronic inflammation (Inflammaging) and its potential contribution to age-associated diseases. Journals Gerontol. - Ser. A Biol. Sci. Med. Sci. 69, S4–S9. https://doi.org/10.1093/gerona/glu057.

Freund, A., Orjalo, A. V., Desprez, P.Y., and Campisi, J. (2010). Inflammatory networks during cellular senescence: causes and consequences. Trends Mol. Med. 16, 238–246. https://doi.org/10.1016/j.molmed.2010.03.003.

Freund, A., Patil, C.K., and Campisi, J. (2011). P38MAPK is a novel DNA damage response-independent regulator of the senescence-associated secretory phenotype. EMBO J. 30, 1536–1548. https://doi.org/10.1038/emboj.2011.69.

Freund, A., Laberge, R.M., Demaria, M., and Campisi, J. (2012). Lamin B1 loss is a senescence-associated biomarker. Mol. Biol. Cell 23, 2066–2075. https://doi.org/10.1091/mbc.E11-10-0884.

Gerace, L., and Huber, M.D. (2012). Nuclear lamina at the crossroads of the cytoplasm and nucleus. J. Struct. Biol. 177, 24–31. https://doi.org/10.1016/j.jsb.2011.11.007.Nuclear.

Glück, S., Guey, B., Gulen, M.F., Wolter, K., Schmacke, N.A., Bridgeman, A., Rehwinkel, J., Zender, L., and Ablasser, A. (2017). Innate immune sensing of cytosolic chromatin fragments through cGAS promotes senescence. Nat Cell Biol 19, 1061–1070. https://doi.org/10.1038/ncb3586.Innate.

González-Gualda, E., Pàez-Ribes, M., Lozano-Torres, B., Macias, D., Wilson, J.R., González-López, C., Ou, H.L., Mirón-Barroso, S., Zhang, Z., Lérida-Viso, A., et al. (2020). Galacto-conjugation of Navitoclax as an efficient strategy to increase senolytic specificity and reduce platelet toxicity. Aging Cell 1–19. https://doi.org/10.1111/acel.13142.

González-Gualda, E., Baker, A.G., Fruk, L., and Muñoz-Espín, D. (2021). A guide to assessing cellular senescence in vitro and in vivo. FEBS J. 288, 56–80. https://doi.org/10.1111/febs.15570.

Gorgoulis, V., Adams, P.D., Alimonti, A., Bennett, D.C., Bischof, O., Bishop, C., Campisi, J., Collado, M., Evangelou, K., Ferbeyre, G., et al. (2019). Cellular Senescence: Defining a Path Forward. Cell 179, 813–827. https://doi.org/10.1016/j.cell.2019.10.005.

Gray, D.A., and Woulfe, J. (2005). Lipofuscin and aging: a matter of toxic waste. Sci. Aging Knowledge Environ. 2005, 1–6. https://doi.org/10.1126/sageke.2005.5.re1.

Green, D.R., and Llambi, F. (2015). Cell death signaling. Cold Spring Harb. Perspect. Biol. 7, 1–24. https://doi.org/10.1101/cshperspect.a006080.

Greider, C.W., and Blackburn, E.H. (1985). Identification of a specific telomere terminal transferase activity in tetrahymena extracts. Cell 43, 405–413. https://doi.org/10.1016/0092-8674(85)90170-9.

Guerrero, A., Herranz, N., Sun, B., Wagner, V., Gallage, S., Guiho, R., Wolter, K., Pombo, J., Irvine, E.E., Andrew, J., et al. (2019). Cardiac glycosides are broad-spectrum senolytics. Nat. Metab. 1, 1074–1088. https://doi.org/10.1038/s42255-019-0122-z.Cardiac.

Gui, X., Yang, H., Li, T., Tan, X., Shi, P., Li, M., Du, F., and Chen, Z.J. (2019). Autophagy induction via STING trafficking is a primordial function of the cGAS pathway. Nature 567, 262–266. https://doi.org/10.1038/s41586-019-1006-9.

Hall, B.M., Balan, V., Gleiberman, A.S., Strom, E., Krasnov, P., Virtuoso, L.P., Rydkina, E., Vujcic, S., Balan, K., Gitlin, I.I., et al. (2017). p16(Ink4a) and senescence-associated β-galactosidase can be induced in macrophages as part of a reversible response to physiological stimuli. Aging (Albany. NY). https://doi.org/10.18632/aging.101268.

Harley, C.B., Futcher, A.B., and Greider, C.W. (1990). Telomeres shorten during ageing of human fibroblasts. Nature 345, 458–460. https://doi.org/10.1038/345458a0.

Haugstetter, A.M., Loddenkemper, C., Lenze, D., Gröne, J., Standfuss, C., Petersen, I., Dörken, B., and Schmitt, C.A. (2010). Cellular senescence predicts treatment outcome in metastasised colorectal cancer. Br. J. Cancer 103, 505–509. https://doi.org/10.1038/sj.bjc.6605784.

Hayflick, L. (1965). The limited in vitro lifetime of human diploid cell strains. Exp. Cell Res. 37, 614–636. https://doi.org/10.1016/0014-4827(65)90211-9.

Hayflick, L., and Moorhead, P.S. (1961). The serial cultivation of human diploid cell strains. Exp. Cell Res. https://doi.org/10.1016/0014-4827(61)90192-6.

He, Y., Zhang, X., Chang, J., Kim, H.N., Zhang, P., Wang, Y., Khan, S., Liu, X., Zhang, X., Lv, D., et al. (2020). Using proteolysis-targeting chimera technology to reduce navitoclax platelet toxicity and improve its senolytic activity. Nat. Commun. 11. https://doi.org/10.1038/s41467-020-15838-0.

Hegde, R., Srinivasula, S.M., Zhang, Z., Wassell, R., Mukattash, R., Cilenti, L., Dubois, G., Lazebnik, Y., Zervos, A.S., Fernandes-Alnemri, T., et al. (2002). Identification of Omi/HtrA2 as a mitochondrial apoptotic serine protease that disrupts inhibitor of apoptosis protein-caspase interaction. J. Biol. Chem. 277, 432–438. https://doi.org/10.1074/jbc.M109721200.

Hernandez-Segura, A., de Jong, T. V., Melov, S., Guryev, V., Campisi, J., and Demaria, M. (2017). Unmasking Transcriptional Heterogeneity in Senescent Cells. Curr. Biol. 27, 2652–2660. https://doi.org/10.1016/j.cub.2017.07.033.

Hernandez-Segura, A., Nehme, J., and Demaria, M. (2018). Hallmarks of Cellular Senescence. Trends Cell Biol. 28, 436–453. https://doi.org/10.1016/j.tcb.2018.02.001.

Herranz, N., Gallage, S., Mellone, M., Wuestefeld, T., Klotz, S., Hanley, C.J., Raguz, S., Acosta, J.C., Innes, A.J., Banito, A., et al. (2015). mTOR regulates MAPKAPK2 translation to control the senescence-associated secretory phenotype. Nat. Cell Biol. https://doi.org/10.1038/ncb3225.

Hubackova, S., Krejcikova, K., Bartek, J., and Hodny, Z. (2012). IL1-and TGFβ-Nox4 signaling, oxidative stress and DNA damage response are shared features of replicative, oncogene-induced, and drug-induced paracrine "Bystander senescence." Aging (Albany. NY). 4, 932–951. https://doi.org/10.18632/aging.100520.

Huber, R.E., Kurz, G., and Wallenfels, K. (1976). A quantitation of the factors which affect the hydrolase and transgalactosylase activities of beta-galactosidase (E. coli) on lactose. Biochemistry 15, 1994–2001. https://doi.org/10.1021/bi00654a029.

Humphreys, D., ElGhazaly, M., and Frisan, T. (2020). Senescence and Host-Pathogen Interactions. Cells 9, 1–17. https://doi.org/10.3390/cells9071747.

Jayaraman, L., Moorthy, N.C., Murthy, K.G.K., Manley, J.L., Bustin, M., and Prives, C. (1998). High mobility group protein-1 (HMG-1) is a unique activator of p53. Genes Dev. 12, 462–472. https://doi.org/10.1101/gad.12.4.462.

Jeon, O.H., Kim, C., Laberge, R.M., Demaria, M., Rathod, S., Vasserot, A.P., Chung, J.W., Kim, D.H., Poon, Y., David, N., et al. (2017). Local clearance of senescent cells attenuates the development of post-traumatic osteoarthritis and creates a pro-regenerative environment. Nat. Med. https://doi.org/10.1038/nm.4324.

Juers, D.H., Matthews, B.W., and Huber, R.E. (2012). LacZ β-galactosidase: Structure and function of an enzyme of historical and molecular biological importance. Protein Sci. 21, 1792–1807. https://doi.org/10.1002/pro.2165.

Kaefer, A., Yang, J., Noertersheuser, P., Mensing, S., Humerickhouse, R., Awni, W., and Xiong, H. (2014). Mechanism-based pharmacokinetic/pharmacodynamic meta-analysis of navitoclax (ABT-263) induced thrombocytopenia. Cancer Chemother. Pharmacol. 74, 593–602. https://doi.org/10.1007/s00280-014-2530-9.

Kale, J., Osterlund, E.J., and Andrews, D.W. (2017). BCL-2 family proteins: changing partners in the dance towards death. Cell Death Differ. 25, 65–80. https://doi.org/10.1038/cdd.2017.186.

Kalkavan, H., and Green, D.R. (2017). MOMP, cell suicide as a BCL-2 family business. Cell Death Differ. 25, 46–55. https://doi.org/10.1038/cdd.2017.179.

Kang, C., Xu, Q., Martin, T.D., Li, M.Z., Demaria, M., Aron, L., Lu, T., Yankner, B.A., Campisi, J., and Elledge, S.J. (2015). The DNA damage response induces inflammation and senescence by inhibiting autophagy of GATA4. Science 349, aaa5612. https://doi.org/10.1126/science.aaa5612.

Khan, S., Zhang, X., Lv, D., Zhang, Q., He, Y., Zhang, P., Liu, X., Thummuri, D., Yuan, Y., Wiegand, J.S., et al. (2019). A selective BCL-XL PROTAC degrader achieves safe and potent antitumor activity. Nat. Med. 25, 1938–1947. https://doi.org/10.1038/s41591-019-0668-z.

Kopp, H.G., Hooper, A.T., Shmelkov, S. V., and Rafii, S. (2007). β-galactosidase staining on bone marrow. The osteoclast pitfall. Histol. Histopathol. https://doi.org/10.14670/HH-22.971.

Krizhanovsky, V., Yon, M., Dickins, R.A., Hearn, S., Simon, J., Miething, C., Yee, H., Zender, L., and Lowe, S.W. (2008). Senescence of Activated Stellate Cells Limits Liver Fibrosis. Cell https://doi.org/10.1016/j.cell.2008.06.049.

Kuilman, T., and Peeper, D.S. (2009). Senescence-messaging secretome: SMS-ing cellular stress. Nat. Rev. Cancer 9, 81–94. https://doi.org/10.1038/nrc2560.

Kuilman, T., Michaloglou, C., Vredeveld, L.C.W.,

Douma, S., van Doorn, R., Desmet, C.J., Aarden, L.A., Mooi, W.J., and Peeper, D.S. (2008). Oncogene-Induced Senescence Relayed by an Interleukin-Dependent Inflammatory Network. Cell *133*, 1019–1031. https://doi.org/10.1016/j.cell.2008.03.039.

Kumari, R., and Jat, P. (2021). Mechanisms of Cellular Senescence: Cell Cycle Arrest and Senescence Associated Secretory Phenotype. Front. Cell Dev. Biol. *9*, 1–24. https://doi.org/10.3389/fcell.2021.645593.

Kurz, D.J., Decary, S., Hong, Y., and Erusalimsky, J.D. (2000). Senescence-associated β-galactosidase reflects an increase in lysosomal mass during replicative ageing of human endothelial cells. J. Cell Sci. *113*, 3613–3622. https://doi.org/10.1242/jcs.113.20.3613.

Laberge, R.M., Awad, P., Campisi, J., and Desprez, P.Y. (2012). Epithelial-mesenchymal transition induced by senescent fibroblasts. Cancer Microenviron. *5*, 39–44. https://doi.org/10.1007/s12307-011-0069-4.

Laberge, R.M., Sun, Y., Orjalo, A. V., Patil, C.K., Freund, A., Zhou, L., Curran, S.C., Davalos, A.R., Wilson-Edell, K.A., Liu, S., et al. (2015). MTOR regulates the pro-tumorigenic senescence-associated secretory phenotype by promoting IL1A translation. Nat. Cell Biol. https://doi.org/10.1038/ncb3195.

Lee, B.Y., Han, J.A., Im, J.S., Morrone, A., Johung, K., Goodwin, E.C., Kleijer, W.J., DiMaio, D., and Hwang, E.S. (2006). Senescence-associated β-galactosidase is lysosomal β-galactosidase. Aging Cell *5*, 187–195. https://doi.org/10.1111/j.1474-9726.2006.00199.x.

Lee, J.J., Park, I.H., Rhee, W.J., Kim, H.S., and Shin, J.S. (2019). HMGB1 modulates the balance between senescence and apoptosis in response to genotoxic stress. FASEB J. *33*, 10942–10953. https://doi.org/10.1096/fj.201900288R.

Lee, J.J., Park, I.H., Kwak, M.S., Rhee, W.J., Kim, S.H., and Shin, J.S. (2021a). HMGB1 orchestrates STING-mediated senescence via TRIM30α modulation in cancer cells. Cell Death Discov. *7*. https://doi.org/10.1038/s41420-021-00409-z.

Lee, S., Yu, Y., Trimpert, J., Benthani, F., Mairhofer, M., Richter-Pechanska, P., Wyler, E., Belenki, D., Kaltenbrunner, S., Pammer, M., et al. (2021b). Virus-induced senescence is driver and therapeutic target in COVID-19. Nature *599*, 283–289. https://doi.org/10.1038/s41586-021-03995-1.

Di Leonardo, A., Linke, S.P., Clarkin, K., and Wahl, G.M. (1994). DNA damage triggers a prolonged p53-dependent G1 arrest and long-term induction of Cip1 in normal human fibroblasts. Genes Dev. *8*, 2540–2551. https://doi.org/10.1101/gad.8.21.2540.

Letai, A., Bassik, M.C., Walensky, L.D., Sorcinelli, M.D., Weiler, S., and Korsmeyer, S.J. (2002). Distinct BH3 domains either sensitize or activate mitochondrial apoptosis, serving as prototype cancer therapeutics. Cancer Cell *2*, 183–192. https://doi.org/10.1016/S1535-6108(02)00127-7.

Li, X.-D., Wu, J., Gao, D., Wang, H., Sun, L., and Chen, Z.J. (2013). Pivotal Roles of cGAS-cGAMP Signaling in Antiviral Defense and Immune Adjuvant Effects. Science (80-.). *341*, 1390–1394. .

Litovchick, L., Florens, L.A., Swanson, S.K., Washburn, M.P., and Decaprio, J.A. (2011). DYRK1A protein kinase promotes quiescence and senescence through DREAM complex assembly. Genes Dev. *25*, 801–813. https://doi.org/10.1101/gad.2034211.

Liu, X., Kim, C.N., Yang, J., Jemmerson, R., and Wang, X. (1996). Induction of apoptotic program in cell-free extracts: Requirement for dATP and cytochrome c. Cell *86*, 147–157. https://doi.org/10.1016/S0092-8674(00)80085-9.

Lu, J., Qian, Y., Altieri, M., Dong, H., Wang, J., Raina, K., Hines, J., Winkler, J.D., Crew, A.P., Coleman, K., et al. (2015). Hijacking the E3 Ubiquitin Ligase Cereblon to Efficiently Target BRD4. Chem. Biol. https://doi.org/10.1016/j.chembiol.2015.05.009.

Maréchal, A., and Zou, L. (2013). DNA damage sensing by the ATM and ATR kinases. Cold Spring Harb. Perspect. Biol. *5*, 1–17. https://doi.org/10.1101/cshperspect.a012716.

Martínez-Zamudio, R.I., Roux, P.F., de Freitas, J.A.N.L.F., Robinson, L., Doré, G., Sun, B., Belenki, D., Milanovic, M., Herbig, U., Schmitt, C.A., et al. (2020). AP-1 imprints a reversible transcriptional programme of senescent cells. Nat. Cell Biol. *22*, 842–855. https://doi.org/10.1038/s41556-020-0529-5.

de Mera-Rodríguez, J.A., Álvarez-Hernán, G., Gañán, Y., Martín-Partido, G., Rodríguez-León, J., and Francisco-Morcillo, J. (2021). Is Senescence-Associated β-Galactosidase a Reliable in vivo Marker of Cellular Senescence During Embryonic Development? Front. Cell Dev. Biol. *9*, 1–12. https://doi.org/10.3389/fcell.2021.623175.

Michaloglou, C., Vredeveld, L.C.W., Soengas, M.S., Denoyelle, C., Kuilman, T., Van Der Horst, C.M.A.M., Majoor, D.M., Shay, J.W., Mooi, W.J., and Peeper, D.S. (2005). BRAFE600-associated senescence-like cell cycle arrest of human naevi. Nature *436*, 720–724. https://doi.org/10.1038/nature03890.

Milanovic, M., Fan, D.N.Y., Belenki, D., Däbritz, J.H.M., Zhao, Z., Yu, Y., Dörr, J.R., Dimitrova, L., Lenze, D., Monteiro Barbosa, I.A., et al. (2018). Senescence-associated reprogramming promotes cancer stemness. Nature *553*, 96–100. https://doi.

org/10.1038/nature25167.

Mitri, D. Di, Toso, A., and Alimonti, A. (2015). Tumor-infiltrating myeloid cells drive senescence evasion and chemoresistance in tumors. Oncoimmunology 4, 1–3. https://doi.org/10.4161/2162402X.2014.988473.

Moiseeva, O., Bourdeau, V., Roux, A., Deschênes-Simard, X., and Ferbeyre, G. (2009). Mitochondrial Dysfunction Contributes to Oncogene-Induced Senescence. Mol. Cell. Biol. https://doi.org/10.1128/mcb.01868-08.

Morin, G.B. (1989). The human telomere terminal transferase enzyme is a ribonucleoprotein that synthesizes TTAGGG repeats. Cell 59, 521–529. https://doi.org/10.1016/0092-8674(89)90035-4.

Munoz-Espin, D., and Serrano, M. (2014). Cellular senescence: from physiology to pathology. Nat. Rev. Mol. Cell Biol. 15, 482–496. https://doi.org/10.1038/nrm3823.

Narita, M., Nũnez, S., Heard, E., Narita, M., Lin, A.W., Hearn, S.A., Spector, D.L., Hannon, G.J., and Lowe, S.W. (2003). Rb-mediated heterochromatin formation and silencing of E2F target genes during cellular senescence. Cell 113, 703–716. https://doi.org/10.1016/S0092-8674(03)00401-X.

Narita, M., Narita, M., Krizhanovsky, V., Nuñez, S., Chicas, A., Hearn, S.A., Myers, M.P., and Lowe, S.W. (2006). A Novel Role for High-Mobility Group A Proteins in Cellular Senescence and Heterochromatin Formation. Cell 126, 503–514. https://doi.org/10.1016/j.cell.2006.05.052.

Olivieri, F., Lazzarini, R., Recchioni, R., Marcheselli, F., Rippo, M.R., Di Nuzzo, S., Albertini, M.C., Graciotti, L., Babini, L., Mariotti, S., et al. (2013). MiR-146a as marker of senescence-Associated pro-inflammatory status in cells involved in vascular remodelling. Age (Omaha). 35, 1157–1172. https://doi.org/10.1007/s11357-012-9440-8.

Orjalo, A. V., Bhaumik, D., Gengler, B.K., Scott, G.K., and Campisi, J. (2009). Cell surface-bound IL-1α is an upstream regulator of the senescence-associated IL-6/IL-8 cytokine network. Proc. Natl. Acad. Sci. U. S. A. https://doi.org/10.1073/pnas.0905299106.

Pan, J., Li, D., Xu, Y., Zhang, J., Wang, Y., Chen, M., Lin, S., Huang, L., Chung, E.J., Citrin, D., et al. (2017). Inhibition of BCL-2/xl with ABT-263 Selectively Kills Senescent Type II Pneumocytes and Reverses Persistent Pulmonary Fibrosis Induced by Ionizing Radiation in Mice. Int. J. Radiat. Oncol. Biol. Phys. 99, 353–361. https://doi.org/10.1016/j.ijrobp.2017.02.216.Inhibition.

Park, J.S., Gamboni-Robertson, F., He, Q., Svetkauskaite, D., Kim, J.Y., Strassheim, D., Sohn, J.W., Yamada, S., Maruyama, I., Banerjee, A., et al. (2006). High mobility group box 1 protein interacts with multiple Toll-like receptors. Am. J. Physiol. - Cell Physiol. 290, 917–924. https://doi.org/10.1152/ajpcell.00401.2005.

Petrova, N. V., Velichko, A.K., Razin, S. V., and Kantidze, O.L. (2016). Small molecule compounds that induce cellular senescence. Aging Cell 15, 999–1017. https://doi.org/10.1111/acel.12518.

Piechota, M., Sunderland, P., Wysocka, A., Nalberczak, M., Sliwinska, M.A., Radwanska, K., and Sikora, E. (2016). Is senescence-associated β-galactosidase a marker of neuronal senescence? Oncotarget 7, 81099–81109. https://doi.org/10.18632/oncotarget.12752.

Raffaele, M., Kovacovicova, K., Bonomini, F., Rezzani, R., Frohlich, J., and Vinciguerra, M. (2020). Senescence-like phenotype in post-mitotic cells of mice entering middle age. Aging (Albany. NY). 12, 13979–13990. .

Recasens, A., and Munoz, L. (2019). Targeting Cancer Cell Dormancy. Trends Pharmacol. Sci. 40, 128–141. https://doi.org/10.1016/j.tips.2018.12.004.

Reilly, E.O., Tirincsi, A., Logue, S.E., and Szegezdi, E. (2016). The janus face of death receptor signaling during tumor immunoediting. Front. Immunol. 7, 1–14. https://doi.org/10.3389/fimmu.2016.00446.

Roberson, R.S., Kussick, S.J., Vallieres, E., Chen, S.Y.J., and Wu, D.Y. (2005). Escape from therapy-induced accelerated cellular senescence in p53-null lung cancer cells and in human lung cancers. Cancer Res. 65, 2795–2803. https://doi.org/10.1158/0008-5472.CAN-04-1270.

Ruscetti, M., Leibold, J., Bott, M.J., Fennell, M., Kulick, A., Salgado, N.R., Chen, C.C., Ho, Y. jui, Sanchez-Rivera, F.J., Feucht, J., et al. (2018). NK cell–mediated cytotoxicity contributes to tumor control by a cytostatic drug combination. Science (80-.). https://doi.org/10.1126/science.aas9090.

Ruscetti, M., Iv, J.P.M., Mezzadra, R., Russell, J., Romesser, P.B., Simon, J., Kulick, A., Ho, Y., Fennell, M., Li, J., et al. (2020). Senescence-Induced Vascular Remodeling Creates Therapeutic Vulnerabilities in Pancreas Cancer. 181, 424–441. https://doi.org/10.1016/j.cell.2020.03.008.Senescence-Induced.

Ryan, K.M., Phillips, A.C., and Vousden, K.H. (2001). Regulation and function of the p53 tumor suppressor protein. Curr. Opin. Cell Biol. 13, 332–337. https://doi.org/10.1016/S0955-0674(00)00216-7.

Ryu, S.J., Oh, Y.S., and Park, S.C. (2007). Failure of stress-induced downregulation of Bcl-2 contributes to apoptosis resistance in senescent human diploid fibroblasts. Cell Death Differ. https://doi.org/10.1038/sj.cdd.4402091.

Sadaie, M., Salama, R., Carroll, T., Tomimatsu, K., Chandra, T., Young, A.R.J., Narita, M., Pérez-Mancera, P.A., Bennett, D.C., Chong, H., et al. (2013). Redistribution of the Lamin B1 genomic binding profile affects rearrangement of heterochromatic domains and SAHF formation during senescence. Genes Dev. 27, 1800–1808. https://doi.org/10.1101/gad.217281.113.

Safa, A.R., and Author, E.O. (2012). c-FLIP, A MASTER ANTI-APOPTOTIC REGULATOR. Exp Oncol 34, 176–184. .

Saleh, T., Carpenter, V.J., Tyutyunyk-Massey, L., Murray, G., Leverson, J.D., Souers, A.J., Alotaibi, M.R., Faber, A.C., Reed, J., Harada, H., et al. (2020). Clearance of therapy-induced senescent tumor cells by the senolytic ABT-263 via interference with BCL-XL–BAX interaction. Mol. Oncol. 14, 2504–2519. https://doi.org/10.1002/1878-0261.12761.

Sanders, Y.Y., Liu, H., Zhang, X., Hecker, L., Bernard, K., Desai, L., Liu, G., and Thannickal, V.J. (2013). Histone modifications in senescence-associated resistance to apoptosis by oxidative stress. Redox Biol. https://doi.org/10.1016/j.redox.2012.11.004.

Schmitt, C.A., Fridman, J.S., Yang, M., Lee, S., Baranov, E., Hoffman, R.M., and Lowe, S.W. (2002). A senescence program controlled by p53 and p16INK4a contributes to the outcome of cancer therapy. Cell 109, 335–346. https://doi.org/10.1016/S0092-8674(02)00734-1.

Serrano, M., Hannon, G.J., and Beach, D. (1993). A new regulatory motif in cell-cycle control causing specific inhibition of cyclin D/CDK4. Nature 366, 704–707. https://doi.org/10.1038/366704a0.

Serrano, M., Lin, A.W., McCurrach, M.E., Beach, D., and Lowe, S.W. (1997). Oncogenic ras provokes premature cell senescence associated with accumulation of p53 and p16(INK4a). Cell 88, 593–602. https://doi.org/10.1016/S0092-8674(00)81902-9.

Severino, J., Allen, R.G., Balin, S., Balin, A., and Cristofalo, V.J. (2000). Is β-galactosidase staining a marker of senescence in vitro and in vivo? Exp. Cell Res. 257, 162–171. https://doi.org/10.1006/excr.2000.4875.

Shah, P.P., Donahue, G., Otte, G.L., Capell, B.C., Nelson, D.M., Cao, K., Aggarwala, V., Cruickshanks, H.A., Rai, T.S., McBryan, T., et al. (2013). Lamin B1 depletion in senescent cells triggers large-scale changes in gene expression and the chromatin landscape. Genes Dev. 27, 1787–1799. https://doi.org/10.1101/gad.223834.113.

Shieh, S.Y., Ahn, J., Tamai, K., Taya, Y., and Prives, C. (2000). The human homologs of checkpoint kinases Chk1 and Cds1 (Chk2) phosphorylate, p53 at multiple DNA damage-inducible sites. Genes Dev. 14, 289–300. https://doi.org/10.1101/gad.14.3.289.

Shimi, T., Butin-Israeli, V., Adam, S.A., Hamanaka, R.B., Goldman, A.E., Lucas, C.A., Shumaker, D.K., Kosak, S.T., Chandel, N.S., and Goldman, R.D. (2011). The role of nuclear lamin B1 in cell proliferation and senescence. Genes Dev. 25, 2579–2593. https://doi.org/10.1101/gad.179515.111.

Simon, M., Van Meter, M., Ablaeva, J., Ke, Z., Gonzalez, R.S., Taguchi, T., De Cecco, M., Leonova, K.I., Kogan, V., Helfand, S.L., et al. (2019). LINE1 Derepression in Aged Wild-Type and SIRT6-Deficient Mice Drives Inflammation. Cell Metab. 29, 871-885.e5. https://doi.org/10.1016/j.cmet.2019.02.014.

Soto-gamez, A., Quax, W.J., and Demaria, M. (2019). Regulation of Survival Networks in Senescent Cells: From Mechanisms to Interventions. J. Mol. Biol. 431, 2629–2643. https://doi.org/10.1016/j.jmb.2019.05.036.

Sugihara, H., Teramoto, N., Nakamura, K., Shiga, T., Shirakawa, T., Matsuo, M., Ogasawara, M., Nishino, I., Matsuwaki, T., Nishihara, M., et al. (2020). Cellular senescence-mediated exacerbation of Duchenne muscular dystrophy. Sci. Rep. 10, 1–17. https://doi.org/10.1038/s41598-020-73315-6.

Sun, L., Wu, J., Du, F., Chen, X., and Chen, Z.J. (2013). Cyclic GMP–AMP synthase is a cytosolic DNA sensor that activates the type I interferon pathway. Science (80-.). 339, 786–791. .

Sun, Y., Coppé, J.-P., and Lam, E.W.-F. (2018). Cellular Senescence: The Sought or the Unwanted? Trends Mol. Med. xx, 1–15. https://doi.org/10.1016/j.molmed.2018.08.002.

Takahashi, A., Imai, Y., Yamakoshi, K., Kuninaka, S., Ohtani, N., Yoshimoto, S., Hori, S., Tachibana, M., Anderton, E., Takeuchi, T., et al. (2012). DNA damage signaling triggers degradation of histone methyltransferases through APC/C Cdh1 in senescent cells. Mol. Cell 45, 123–131. https://doi.org/10.1016/j.molcel.2011.10.018.

Takahashi, A., Loo, T.M., Okada, R., Kamachi, F., Watanabe, Y., Wakita, M., Watanabe, S., Kawamoto, S., Miyata, K., Barber, G.N., et al. (2018). Downregulation of cytoplasmic DNases is implicated in cytoplasmic DNA accumulation and SASP in senescent cells. Nat. Commun. 9, 1–12. https://doi.org/10.1038/s41467-018-03555-8.

Takasugi, M., Yoshida, Y., Hara, E., and Ohtani, N. (2022). The role of cellular senescence and SASP in tumour microenvironment. FEBS J. 1–14. https://doi.org/10.1111/febs.16381.

Taylor, R.C., Cullen, S.P., and Martin, S.J. (2008).

Apoptosis: Controlled demolition at the cellular level. Nat. Rev. Mol. Cell Biol. *9*, 231–241. https://doi.org/10.1038/nrm2312.

Triana-Martínez, F., Picallos-Rabina, P., Da Silva-Álvarez, S., Pietrocola, F., Llanos, S., Rodilla, V., Soprano, E., Pedrosa, P., Ferreirós, A., Barradas, M., et al. (2019). Identification and characterization of Cardiac Glycosides as senolytic compounds. Nat. Commun. *10*, 1–12. https://doi.org/10.1038/s41467-019-12888-x.

Tung, C.H., Zeng, Q., Shah, K., Kim, D.E., Schellingerhout, D., and Weissleder, R. (2004). In Vivo Imaging of β-Galactosidase Activity Using Far Red Fluorescent Switch. Cancer Res. *64*, 1579–1583. https://doi.org/10.1158/0008-5472.CAN-03-3226.

Ventura, A., Kirsch, D.G., McLaughlin, M.E., Tuveson, D.A., Grimm, J., Lintault, L., Newman, J., Reczek, E.E., Weissleder, R., and Jacks, T. (2007). Restoration of p53 function leads to tumour regression in vivo. Nature *445*, 661–665. https://doi.org/10.1038/nature05541.

Verhagen, A.M., Ekert, P.G., Pakusch, M., Silke, J., Connolly, L.M., Reid, G.E., Moritz, R.L., Simpson, R.J., and Vaux, D.L. (2000). Identification of DIABLO, a mammalian protein that promotes apoptosis by binding to and antagonizing IAP proteins. Cell *102*, 43–53. https://doi.org/10.1016/S0092-8674(00)00009-X.

de Vos, S., Leonard, J.P., Friedberg, J.W., Zain, J., Dunleavy, K., Humerickhouse, R., Hayslip, J., Pesko, J., and Wilson, W.H. (2021). Safety and efficacy of navitoclax, a BCL-2 and BCL-XL inhibitor, in patients with relapsed or refractory lymphoid malignancies: results from a phase 2a study. Leuk. Lymphoma *62*, 810–818. https://doi.org/10.1080/10428194.2020.1845332.

Wakita, M., Takahashi, A., Sano, O., Loo, T.M., Imai, Y., Narukawa, M., Iwata, H., Matsudaira, T., Kawamoto, S., Ohtani, N., et al. (2020). A BET family protein degrader provokes senolysis by targeting NHEJ and autophagy in senescent cells. Nat. Commun. *11*, 1–13. https://doi.org/10.1038/s41467-020-15719-6.

Wang, C., Vegna, S., Jin, H., Benedict, B., Lieftink, C., Ramirez, C., de Oliveira, R.L., Morris, B., Gadiot, J., Wang, W., et al. (2019). Inducing and exploiting vulnerabilities for the treatment of liver cancer. Nature *574*, 268–272. https://doi.org/10.1038/s41586-019-1607-3.

Wang, L., Leite de Oliveira, R., Wang, C., Fernandes Neto, J.M., Mainardi, S., Evers, B., Lieftink, C., Morris, B., Jochems, F., Willemsen, L., et al. (2017). High-Throughput Functional Genetic and Compound Screens Identify Targets for Senescence Induction in Cancer.

Cell Rep. *21*, 773–783. https://doi.org/10.1016/j.celrep.2017.09.085.

Wang, Y., Chang, J., Liu, X., Zhang, X., Zhang, S., Zhang, X., Zhou, D., and Zheng, G. (2016). Discovery of piperlongumine as a potential novel lead for the development of senolytic agents. Aging (Albany. NY). *8*, 2915–2926. https://doi.org/10.18632/aging.101100.

Wiley, C.D., Velarde, M.C., Lecot, P., Liu, S., Sarnoski, E.A., Freund, A., Shirakawa, K., Lim, H.W., Davis, S.S., Ramanathan, A., et al. (2016). Mitochondrial dysfunction induces senescence with a distinct secretory phenotype. Cell Metab. *23*, 303–314. https://doi.org/10.1016/j.cmet.2015.11.011.

Wiley, C.D., Flynn, J.M., Morrissey, C., Lebofsky, R., Shuga, J., Dong, X., Unger, M.A., Vijg, J., Melov, S., and Campisi, J. (2017). Analysis of individual cells identifies cell-to-cell variability following induction of cellular senescence. Aging Cell *16*, 1043–1050. https://doi.org/10.1111/acel.12632.

Xu, M., Tchkonia, T., Ding, H., Ogrodnik, M., Lubbers, E.R., Pirtskhalava, T., White, T.A., Johnson, K.O., Stout, M.B., Mezera, V., et al. (2015). JAK inhibition alleviates the cellular senescence-associated secretory phenotype and frailty in old age. Proc. Natl. Acad. Sci. U. S. A. *112*, E6301–E6310. https://doi.org/10.1073/pnas.1515386112.

Xue, W., Zender, L., Miething, C., Dickins, R.A., Hernando, E., Krizhanovsky, V., Cordon-Cardo, C., and Lowe, S.W. (2007). Senescence and tumour clearance is triggered by p53 restoration in murine liver carcinomas. Nature *445*, 656–660. https://doi.org/10.1038/nature05529.

Yang, N.C., and Hu, M.L. (2005). The limitations and validities of senescence associated-β-galactosidase activity as an aging marker for human foreskin fibroblast Hs68 cells. Exp. Gerontol. *40*, 813–819. https://doi.org/10.1016/j.exger.2005.07.011.

Yosef, R., Pilpel, N., Tokarsky-Amiel, R., Biran, A., Ovadya, Y., Cohen, S., Vadai, E., Dassa, L., Shahar, E., Condiotti, R., et al. (2016). Directed elimination of senescent cells by inhibition of BCL-W and BCL-XL. Nat. Commun. 7. https://doi.org/10.1038/ncomms11190.

Yousefzadeh, M.J., Zhu, Y., McGowan, S.J., Angelini, L., Fuhrmann-Stroissnigg, H., Xu, M., Ling, Y.Y., Melos, K.I., Pirtskhalava, T., Inman, C.L., et al. (2018). Fisetin is a senotherapeutic that extends health and lifespan. EBioMedicine *36*, 18–28. https://doi.org/10.1016/j.ebiom.2018.09.015.

Zglinicki, T. Von, Nilsson, E., Döcke, W.D., and Brunk, U.T. (1995). Lipofuscin accumulation and ageing of fibroblasts. Gerontology *41*, 95–108. .

Zhang, R., Poustovoitov, M. V., Ye, X., Santos, H.A., Chen, W., Daganzo, S.M., Erzberger,

J.P., Serebriiskii, I.G., Canutescu, A.A., Dunbrack, R.L., et al. (2005). Formation of macroH2A-containing senescence-associated heterochromatin foci and senescence driven by ASF1a and HIRA. Dev. Cell *8*, 19–30. https://doi.org/10.1016/j.devcel.2004.10.019.

Zhu, Y., Tchkonia, T., Pirtskhalava, T., Gower, A.C., Ding, H., Giorgadze, N., Palmer, A.K., Ikeno, Y., Hubbard, G.B., Lenburg, M., et al. (2015). The Achilles' heel of senescent cells: From transcriptome to senolytic drugs. Aging Cell 644–658. https://doi.org/10.1111/acel.12344.

Zhu, Y., Tchkonia, T., Fuhrmann-Stroissnigg, H., Dai, H.M., Ling, Y.Y., Stout, M.B., Pirtskhalava, T., Giorgadze, N., Johnson, K.O., Giles, C.B., et al. (2016). Identification of a novel senolytic agent, navitoclax, targeting the Bcl-2 family of anti-apoptotic factors. Aging Cell *15*, 428–435. https://doi.org/10.1111/acel.12445.

Zhu, Y., Doornebal, E.J., Pirtskhalava, T., Giorgadze, N., Wentworth, M., Fuhrmann-Stroissnigg, H., Niedernhofer, L.J., Robbins, P.D., Tchkonia, T., and Kirkland, J.L. (2017). New agents that target senescent cells: the flavone, fisetin, and the BCL-XL inhibitors, A1331852 and A1155463. Aging (Albany. NY). *9*, 1–9. https://doi.org/10.18632/aging.101202.

1

CHAPTER 2

Identification of autophagy-related genes as targets for senescence induction using a customizable CRISPR-based suicide switch screen

Arnout Schepers[1], Fleur Jochems[1], Cor Lieftink[1], Liqin Wang[1],
Ziva Pogacar[1], Rodrigo Leite de Oliveira[1], Giulia De Conti[1],
Roderick L. Beijersbergen[1], Rene Bernards[1]

[1]Division of Molecular Carcinogenesis, Oncode Institute, Netherlands Cancer Institute, Plesmanlaan 121, 1066 CX Amsterdam, The Netherlands

2

Abstract

Pro-senescence therapies are increasingly being considered for the treatment of cancer. Identifying additional targets to induce senescence in cancer cells could further enable such therapies. However, screening for targets whose suppression induces senescence on a genome-wide scale is challenging, as senescent cells become growth arrested, and senescence-associated features can take 1-2 weeks to develop. For a screen with a whole-genome CRISPR library, this would result in billions of undesirable proliferating cells by the time the senescent features emerge in the growth arrested cells. Here, we present a suicide switch system that allows genome-wide CRISPR screening in growth-arrested subpopulations by eliminating the proliferating cells during the screen through activation of a suicide switch in proliferating cells. Using this system, we identify in a genome-scale CRISPR screen several autophagy related proteins as targets for senescence induction. We show that inhibiting macroautophagy with a small molecule ULK1 inhibitor can induce senescence in cancer cell lines of different origin. Finally, we show that combining ULK1 inhibition with the senolytic drug ABT-263 leads to apoptosis in a panel of cancer cell lines.

Introduction

Cellular senescence is a state of stable cell cycle arrest that can be induced by several cellular stresses, like telomere shortening, oncogene activation, DNA damage and oxidative stress (Hernandez-Segura et al., 2018). Besides upregulating cell-cycle inhibitors, senescent cells usually develop several senescence-associated features, e.g. the formation of senescence-associated heterochromatin foci, elevated lysosomal activity, positive staining of senescence-associated β-galactosidase (SA-β-gal), and the adoption of a senescence-associated secretory phenotype (SASP). The SASP is characterized by elevated secretion of chemokines, cytokines and growth factors and can vary by cell type and stressor (Wang et al., 2020).

Senescence induction provides an important barrier against tumor development as it limits the proliferative potential of damaged cells. However, long-term presence of senescent cells in tissues may promote tumor invasion and metastasis (Coppé et al., 2010). The deleterious long term effects of senescence-inducing cancer therapy can be countered by combining it with a follow up therapy such as a senolytic agent (Leite de Oliveira and Bernards, 2018; Sieben et al., 2018). We have recently demonstrated the utility of cancer treatments consisting of a combination of a pro-senescence therapy and a treatment that selectively eliminates the senescent cancer cells (Wang et al., 2019, 2017). Moreover, pro-senescence therapies may be synergistic with checkpoint immunotherapies as the SASP can chemo-attract several immune cells (Kale et al., 2020), and senescence induction has been shown to cause vascular remodeling leading to enhanced drug delivery and T cell infiltration (Ruscetti et al., 2020).

Identifying additional targets to induce senescence in cancer cells could further enable such therapies. However, screening for such targets is challenging, as senescent cells become growth arrested, and senescent associated features can take 1-2 weeks to develop. For a screen with a whole-genome CRISPR library, this would result in billions of cells by the time the senescent features emerge. Here, we present a suicide switch system that allows genome-wide CRISPR screening in growth-arrested subpopulations and identify autophagy related proteins as targets for senescence induction.

Results

To enable genome-wide CRISPR screening for targets whose inhibition induces senescence, we aimed to remove proliferating cells during the screen. The most common way to eliminate proliferating cells is by cytotoxic drugs that inhibit cell division. Alternatively, there are inducible methods, e.g. based on BrdU

incorporation and visible light (Burmer and Norwood, 1980), or on expression of the Herpes Simplex Virus Thymidine Kinase gene in combination with treatment with ganciclovir (Tieng et al., 2016). However, the elimination of cells using these methods relies on cell cycle arrest caused by DNA damage, which by itself may induce senescence and lead to noise in a senescence focused genetic screen. To circumvent this problem, we utilized the inducible caspase 9 system (iCasp9) that was originally developed as a safety switch for T-cell therapy (Straathof et al., 2005). This construct contains the intracellular portion of the human caspase 9 protein, fused to a drug-binding domain derived from the human FK506-binding protein (FKBP) (Figure 1A). Addition of the chemical induction of dimerization (CID) drug AP20187 leads to dimerization of the caspase 9 homodimers, resulting in cellular apoptosis. In order to specifically induce apoptosis in proliferating cells, we needed a suitable gene promoter to drive the expression of the safety switch. Previous work from our laboratory has identified alisertib, an aurora kinase A inhibitor, as an inducer of senescence in non-small cell lung cancer A549 cells (Wang et al., 2017). We tested whether the widely-used marker of proliferation, Ki-67 (Menon et al., 2019), was reduced in expression in these cells upon induction of senescence with alisertib. Figure 1A shows that expression of mRNA for Ki-67 is strongly reduced in senescent A549 cells. We therefore generated a suicide construct that contains iCasp9 driven by the Ki-67 promoter. The resulting proliferation-driven suicide switch was combined with an IRES-RFP element to enable sorting of infected cells (Figure 1A).

To validate the suicide switch vector, proliferating A549 cells were infected with the suicide switch construct and RFP positive cells were sorted by FACS to generate single cell clones, which we named 'A549-CID' cells. Clones were selected in which addition of the CID drug rapidly induced apoptosis as judged by changes in morphology and an increase in the signal of the Caspase-3/7-activated green fluorescent dye (Figure 1B). Upon treatment with alisertib, the cells became growth-arrested with a flattened morphology characteristic of senescence. Addition of the CID drug to alisertib-treated senescent cells did not induce apoptosis, indicating that the iCasp9 homodimers of the suicide switch, under the control of Ki-67 promoter, are not expressed to sufficient levels to effectively induce apoptosis in these cells (Figure 1B).

In addition to eliminating proliferating cells, we aimed to distinguish senescent cells from other growth arrested populations. We have shown previously that a lentiviral vector with a miR-146a promoter driving expression of the green fluorescent mClover3 can be used to mark senescent cells (Wang et al., 2017). We inserted the miR-146a-mClover3 vector into the A549-CID cells, yielding A549-CID-mClover3 cells. To determine the optimal timing to develop sufficient green fluorescent reporter signal, parental cells and A549-CID-mClover3 cells were

treated with alisertib. Upon treatment, the cells increased in size as can be seen in the forward- and side scatter plots (FSC-A, SSC-A; Figures 1C, F). Although the enlargement of the senescent cells resulted in increased auto-fluorescence (Figures 1D, G), after ten days of treatment with alisertib, the mClover3 signal could readily be detected over background (Figures 1E, H).

To perform a genome-scale CRISPR screen for pro-senescence targets, we followed a strategy as outlined in Figure 1I. In short, we infected A549-CID-mClover3 cells with the Brunello CRISPR library with low multiplicity of infection as described (Doench et al., 2016). After infection, the cells were selected with puromycin for 48 hours. At day six post infection, the CID drug was added to eliminate the proliferating cells. At day 14, the remaining cells were sorted by FACS into a mClover3 positive and a negative fraction. DNA was isolated from cells after puromycin selection (t0) and from the flow-sorted fractions (t14pos and t14neg). Subsequently, sgRNAs were recovered by PCR and quantified by sequencing.

There was a small group of sgRNAs with very high abundance, which were mostly enriched in the mClover3 negative fraction (Figure S1). These sgRNAs targeted the suicide switch, either by knocking out FKBP or caspase-9, which are part of the switch, or caspase-3 and -7, which are the downstream effectors of the switch. The enrichment of these sgRNAs provided an additional control for proper functioning of the suicide switch. We focused on sgRNAs that were enriched in the mClover3 positive fraction, as these could target genes whose suppression induces senescence. Differentially expressed sgRNAs were analyzed by DESeq2 as described (Anders and Huber, 2010; Love et al., 2014), and the MAGeCK Robust Rank Algorithm (Li et al., 2014) was used to determine hit genes, shown in the volcano plot in Figure 2A. The four hit genes: ATG9A, RB1CC1, ATG101 and RAB14 are all associated with early autophagy and were selected for further validation. Validation of these hit genes was performed in A549 cells without the suicide switch to rule out potential artifacts of this system. shRNA knockdown of the 4 targets all induced a flattened morphology and an increase in the percentage of SA-□-gal positive cells (Figure 2B-D). In addition, we knocked out ATG9A, RB1CC1, ATG101 and RAB14 using CRISPR-Cas9 and analyzed senescence markers. We demonstrate a reduction of expression of LaminB1 and phospho-RB, and an increase in P21 expression in the knockout cells (Figure S2). To further certify the senescent nature of the cells, RNAseq was performed on mRNA isolated from cells with shRNA knockdown of the top hit, ATG9A, and parental controls. Gene set enrichment analysis showed an enrichment of the Fridman (Fridman and Tainsky, 2008) senescence gene signature in the ATG9A knockdown cells, confirming their senescent state (Figure 2E).
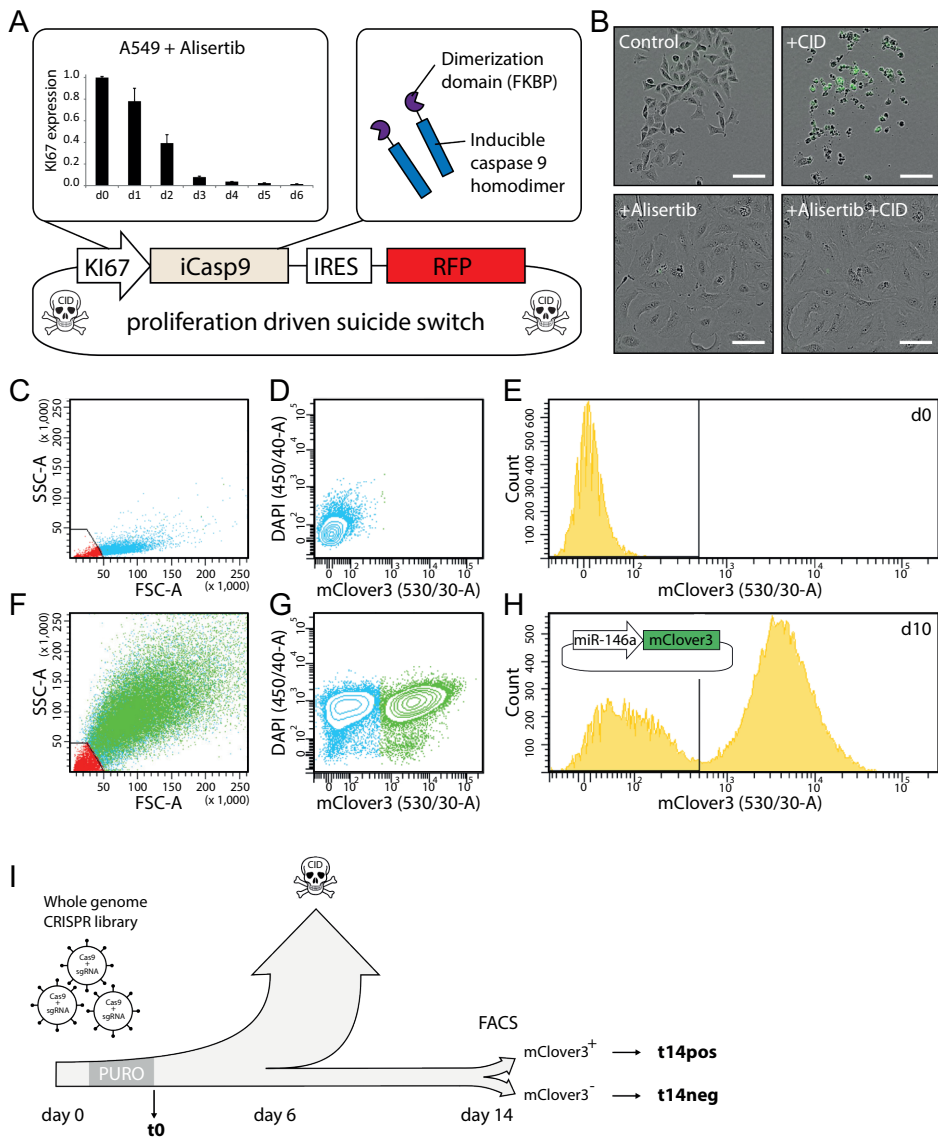
Figure 1. A proliferation driven suicide switch facilitates positive selection of growth-arrested populations. (A) Schematic representation of the proliferation driven suicide switch plasmid and the iCasp9 homodimers. Expression of Ki-67 mRNA in A549 cells was analyzed upon treatment with 0.5μM of the senescence inducer alisertib. Error bars represent SEM of three biological replicates. **(B)** A549-CID cells before and after 24hr CID treatment. Alisertib treated cells were treated for 4 days with alisertib before addition of CID. Scale bars represent 100μm. **(C-E)** Flow cytometry analysis of A549-CID-mClover3 cells representing the cell size **(C)**, autofluorescence **(D)** and signal of the miR-146a reporter **(E)**. **(F-H)** As in C-E, but for cells treated with alisertib for 10 days. **(I)** Schematic overview of the CRISPR screening setup.
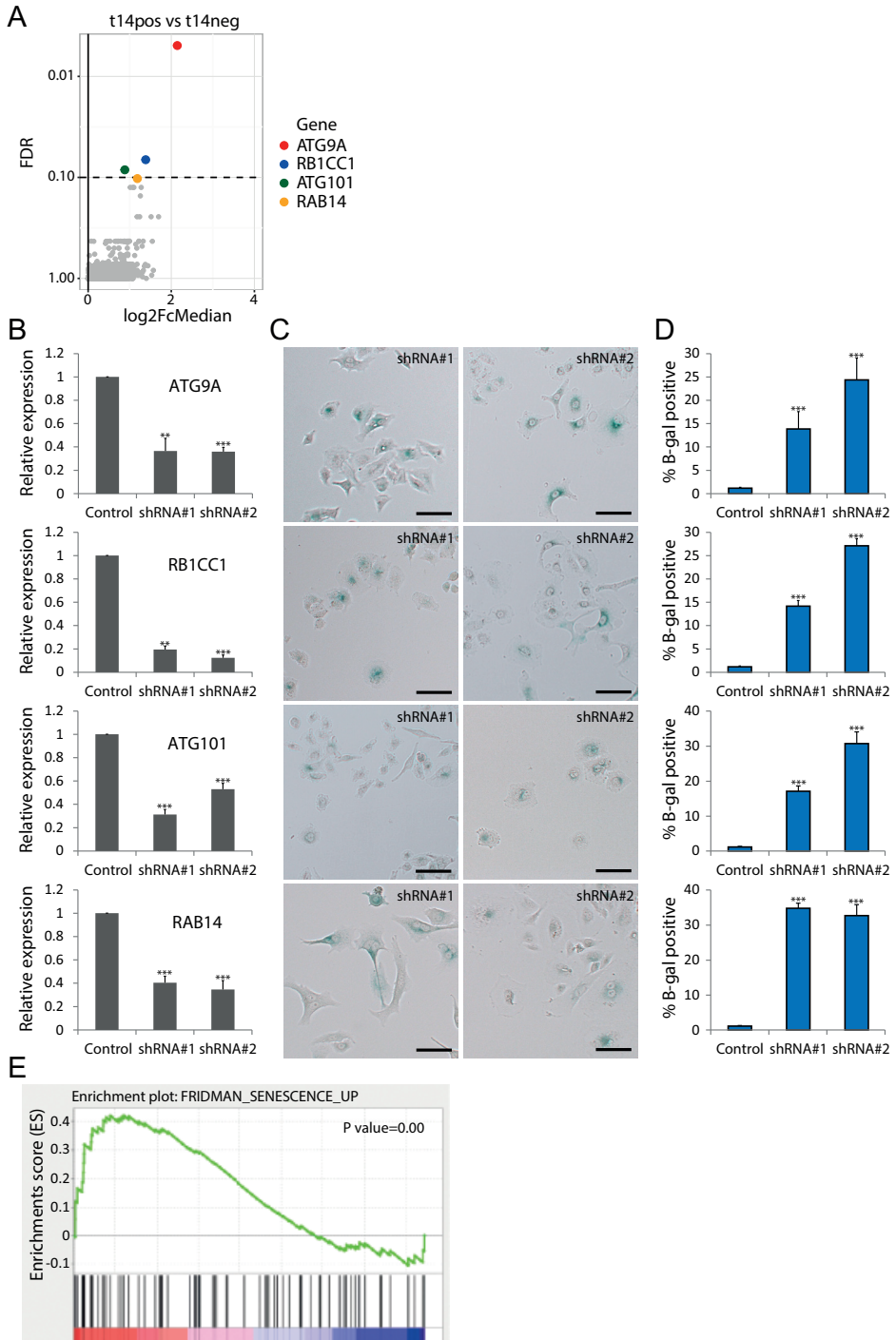
Figure 2. Identification and validation of autophagy-related genes as targets for senescence induction. (**A**) Volcano plot showing hit genes of the screen (FDR = False Discovery Rate). (**B-C**) shRNA knockdown of top hit genes in A549 cells (**B**) induces a flattened morphology and

increases the percentage of SA-β-gal positive cells (**C**). Scale bars in images represent 100µm. (**D**) Quantification of the percentage of SA-β-gal positive cells. Error bars represent SEM of three biological replicates. Asterisks represent significance as analyzed by t-test, ** = P < 0.01, *** = P < 0.001). (**E**) Gene set enrichment analysis of RNAseq data obtained from A549 cells infected with a vector with shRNA against ATG9A vs control shows enrichment of senescence associated genes. Samples were sequenced eight days after infection.

Autophagy is a tightly regulated intracellular degradation process that has an important role in cellular homeostasis (Mizushima, 2007). The main autophagy pathway, commonly referred to as macroautophagy, removes damaged, toxic or excess cellular components and also serves as a recycling pathway to maintain protein synthesis under nutrient starvation conditions. The process is initiated by the formation of isolation membranes, that eventually form double membrane-bound autophagosomes and fuse with lysosomes to degrade their contents (Hamasaki et al., 2013). ATG9A, RB1CC1 and ATG101 are directly involved in autophagosome formation (He and Klionsky, 2009). RB1CC1 and ATG101 are members of the ULK1 complex, fundamental for the early steps of autophagosome biogenesis, whereas ATG9A transiently interacts with the forming autophagosome (Figure 3A). In addition, RAB14 may be indirectly involved in early autophagy due to its role in intracellular membrane trafficking which is necessary for autophagosome growth, positioning and fusion (Junutula et al., 2004).

There are currently no small molecule inhibitors available to inhibit the function of any of these proteins. However, the main effector of the ULK1 complex, the kinase ULK1, can be inhibited by SBI0206965. A549 cells treated with SBI0206965 show a dose dependent reduction in proliferation (Figure 3B) and adopt a flattened morphology with strong SA-□-gal activity, indicative of senescent cells (Figure 3C). In addition, the comparison of mRNA expression of treated with untreated cells shows an enrichment of the Fridman senescence gene signature (Figure 3D). We observed similar effects on growth arrest, flattened morphology and the percentage of SA-□-gal positive cells in cancer cell lines derived from liver (Hep3B), pancreas (PANC1) and colon (RKO) (Figures 3E-J). In addition, we performed ULK-1 inhibition in MCF7, PC9, T47D and non-transformed BJ fibroblasts, and demonstrate that SBI0206965 can inhibit tumor growth and induce SA-□-gal activity in all three cancer cell lines, but does not induce senescence in BJ cells (Figure S3). Unfortunately, pharmacokinetic analysis in two different mouse strains showed rapid depletion of SBI0206965 from the blood plasma (Figure S4). Due to this unfavorable pharmacokinetic profile, we did not pursue further in vivo experimentation with this compound.
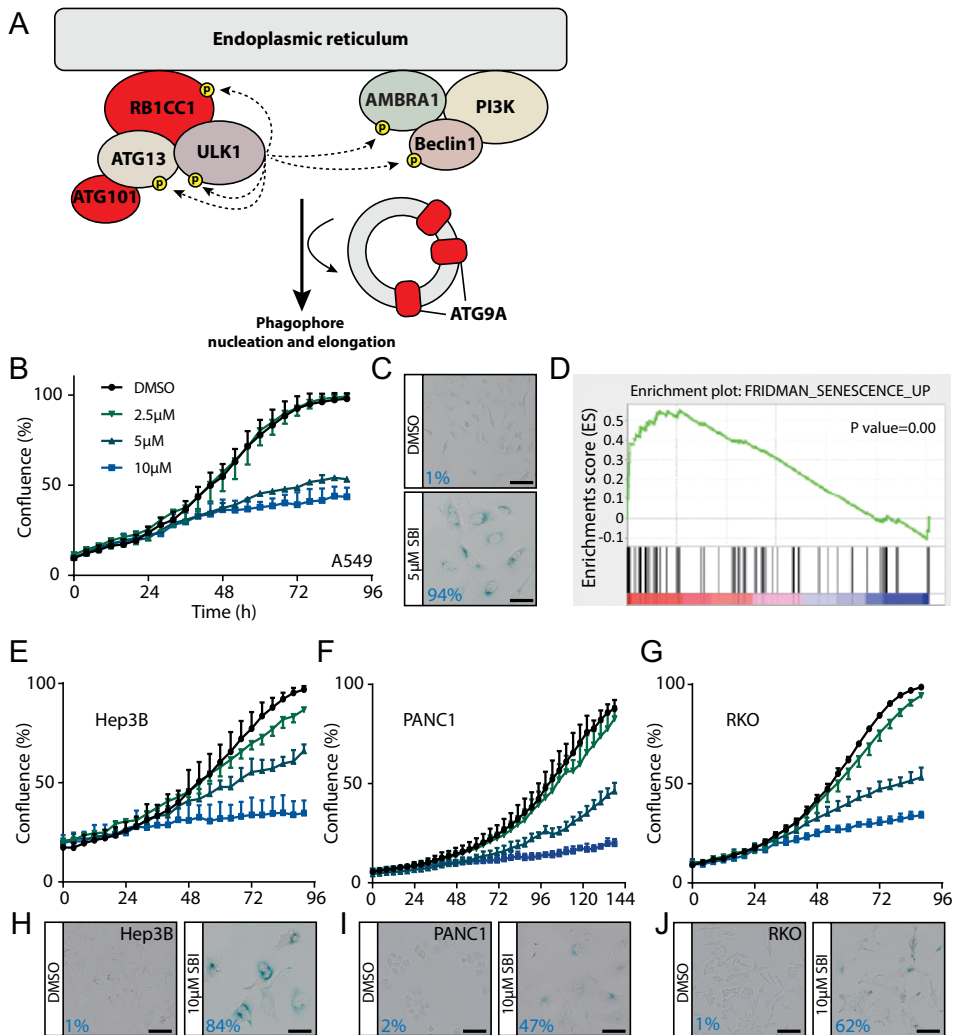
Figure 3. SBI0206965 treatment induces senescence. (**A**) Schematic overview of essential players in autophagophore nucleation and elongation. (**B**) IncuCyte proliferation assay of A549 cells treated with different doses of SBI0206965. (**C**) SA-β-gal staining of treated cells and untreated controls after 4 days of treatment. The number inset represents the percentage of SA-β-gal positive cells. Scale bars represent 100μm. (**D**) Gene set enrichment analysis of RNAseq data obtained from A549 cells treated with SBI0206965 vs control shows enrichment of the Fridman senescence signature. (**E-J**) As in B&C, but for Hep3B (**E, H**), PANC1 (**F, I**) and RKO (**G, J**). Scale bars represent 100μm.

To gain insight into how SBI0206965 induces senescence we looked at expression changes in A549 cells over time of proteins involved in autophagy and cellular stress (Figure 4A). LC3B plays a central role in the early stages of autophagosome formation and phagophore membrane elongation, and is eventually degraded in the autolysosomal lumen. Turnover of LC3B is often used as a marker to monitor autophagy and autophagy-related processes (Tanida et al., 2008). The accumulation of LC3B after several days of treatment with SBI0206965 indicates that autophagy is compromised and stalled in the early stage of autophagosome formation. In addition, after two days of treatment, we observed an increase in the levels of p53 and p21, which are pivotal for the establishment of senescence (Kastenhuber and Lowe, 2017). Furthermore, we observed a significant increase in the expression of the apoptosis inhibitory protein BCL2, commonly elevated in senescent cells (Yosef et al., 2016). BCL2 family members can be targeted with the BH3 mimetic ABT-263 (Zhu et al., 2016). Parental A549 were not affected by ABT-263, whereas cells pretreated with SBI0206965 were eliminated (Figure 4B). The same effect was observed in Hep3B, PANC1, and RKO cells. Combination of SBI0206965 with ABT-263 induced a significant increase in the percentage of apoptotic cells, assessed by fluorescence of the Caspase-3/7 Green Dye (Figure 4C). To validate that this effect was not due to potential off target effects of SBI02169565, we confirmed our findings using the ULK1 inhibitor MRT68921 (Figure 5). These data highlight the utility of a combination therapy consisting of a pro-senescence and a senolytic agent.
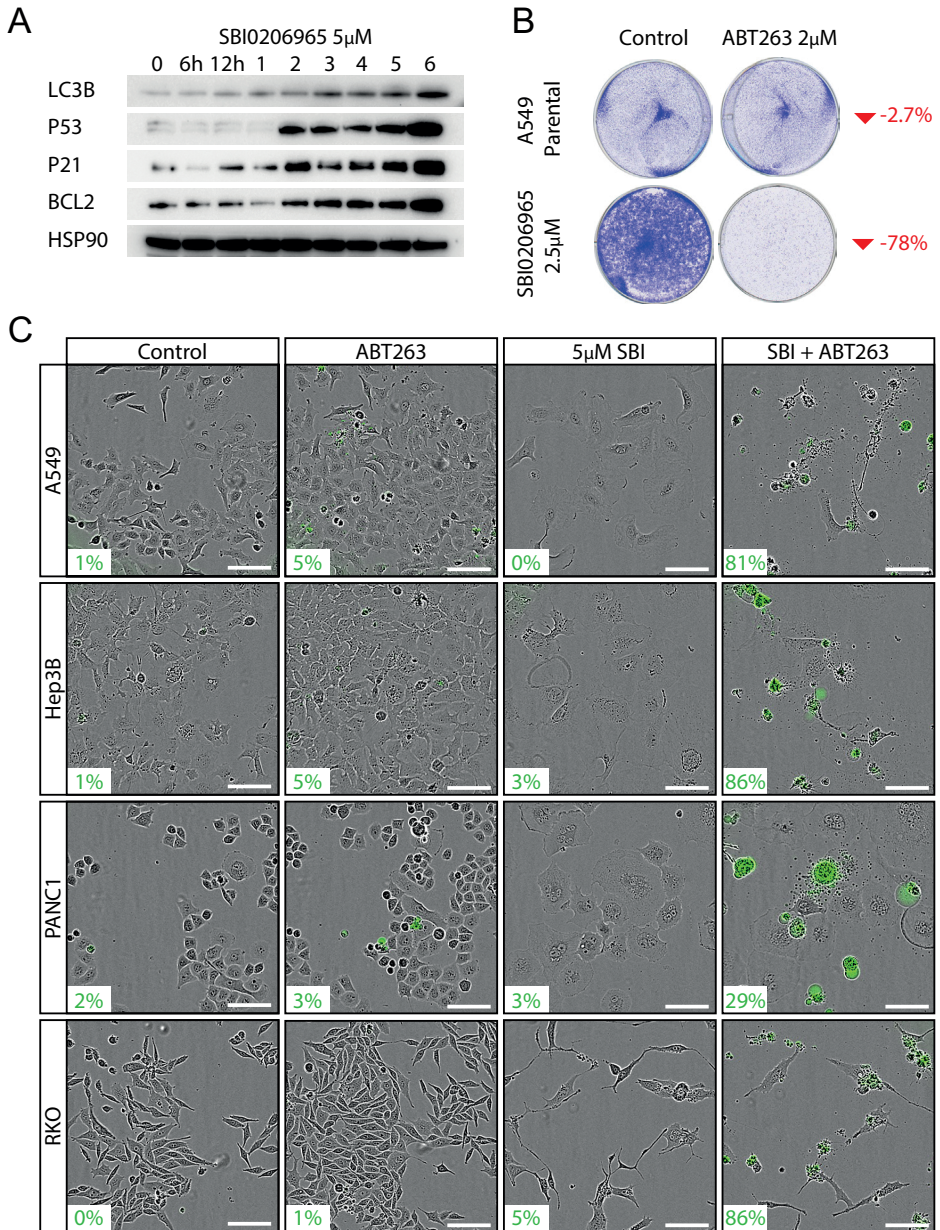
Figure 4. Treatment with SBI0206965 sensitizes cells to senolytic treatment. (A) Western blot analysis of A549 treated with 5μM SBI0206965 for different durations up to 6 days. **(B)** Crystal violet staining of parental A549 cells and cells treated with SBI0206965 for 4 days, with and without addition of ABT-263. The quantification of the elimination of cells, represented by the decrease in staining intensity, is shown in red. **(C)** Representative images for A549, Hep3B, PANC1 and RKO cell lines showing control cells and SBI0206965 pretreated cells, before and 24h after addition of ABT263. Apoptotic cells were determined by caspase-3/7 apoptosis assay. Scale bars represent 100μm.

Discussion

The suicide switch we describe here can be used to deplete proliferating cell populations, which is useful in performing screens for proliferation arrest by enriching the growth-arrested population. We used this concept to perform genome-wide screens with positive selection of senescent cells. This allowed discovery of targets for pro-senescence therapy on a genome-wide scale. Using the proliferation-driven suicide switch we could culture our cells of interest for two weeks without overgrowth of proliferating cells. This timing and the retention of growth-arrested cells was crucial to identify sufficient senescent cells to call hits using a genome-wide library. A whole-genome approach in pro-senescence CRISPR screens is desirable as senescence is involved in a variety of physiological and pathological processes and is regulated by manifold pathways. In addition, we did not want to limit ourselves to the usual established drug target classes, as recent developments like PROTACs (proteolysis targeting chimeras) and molecular glues are gradually increasing the playing field for targets with therapeutic potential (Churcher, 2018).

Our genome-wide approach led to the identification of several targets related to autophagy that when inhibited can induce senescence. Autophagy plays an important role in quality control of macromolecules and energy homeostasis and the connection between autophagy and senescence has been described extensively. However, the jury is still out on whether autophagy has a positive or negative impact on senescence, or both (Kang and Elledge, 2016). On the one hand, autophagy has been suggested to mediate the acquisition of the senescence phenotype (Young et al., 2009). The associated protein turnover and recycling of cellular material would be essential to facilitate the mass synthesis of secretory proteins. On the other hand, impairment of autophagy with siRNA or shRNA has been described to induce senescence (Kang et al., 2011). The senescence induction is potentially caused by accumulation of damaged macromolecules and an increase in cytotoxic stresses, as ROS scavenging or inhibition of p53 activation delayed its onset upon autophagy impairment. Small molecule inhibition of autophagy with SBI0206965 mimicked this effect, with senescence induction in combination with increased levels of p21 and p53.

Combination of SBI0206965 with the BH3 mimetic ABT-263 induced apoptosis in a panel of cancer cell lines in vitro. Further experiments will have to be done to determine whether autophagy inhibition can induce senescence in cancer cells in vivo and whether such therapy is effective when combined with a senolytic treatment. Nevertheless, the identification and validation of new targets and a small molecule to induce senescence in cancer cells underscores the potential of using a suicide switch in screens. This switch system can help to perform large scale gene knockout screens in a rapid and cost-effective manner. Furthermore, the concept

of the suicide switch could also be extrapolated from growth arrest to other traits depending on the nature of the promoter used to drive the inducible suicide switch.

Materials and methods

Cell Lines
The A549 lung cancer cell line, PANC1 pancreatic cancer cell line, RKO colon cancer cell line and 293T human embryonic kidney cell line were obtained from ATCC. The Hep3B liver cancer cell line was obtained from S. Huang (NKI, Amsterdam, the Netherlands). A549 and RKO were cultured in RPMI-based medium supplemented with 10% FBS and 1% penicillin/streptomycin. Hep3B and PANC1 were cultured in DMEM-based medium supplemented with 10% FBS and 1% penicillin/streptomycin. All cell lines were validated by STR profiling (Eurofins) and regularly tested for Mycoplasma spp using a PCR-based assay.

Plasmids
The suicide switch plasmid was constructed using the following plasmids: backbone: pLV-EF1a-IRES-Puro (addgene #85132), inducible caspase 9: pMSCV-F-del Casp9.IRES.GFP (addgene #15567), RFP: pMSCV-pBabeMCS-IRES-RFP (addgene #35395). The Ki-67 promoter was amplified from genomic DNA using KI67_promoter_fwd GGGAGCCAAGCTCCAAGGGTTGCTGG and KI67_promoter_rev ATCCGGCCCGCAAGGCCACTTGT. The miR-146a-EGFP plasmid was a gift from Stephen Elledge.

Lentiviral transduction
Viral particles were produced in 293T cells by co-transfection of the suicide switch plasmid with 2nd generation packaging plasmids as described in https://www.addgene.org/protocols/lentivirus-production. Destination cells were infected with lentiviral supernatants at a multiplicity of infection of 0.3 using and with 8 µg/mL polybrene. After 24 hours of incubation, the supernatant was replaced by medium containing 10 µg/mL BSD or 2 µg/mL puromycin.

FACS-Assisted Genetic Screen

A549-CID- mClover3 cells were infected in 3 independent biological replicates. 24h after infection, cells were selected with puromycin for 48hrs. At day 6 after infection, the suicide switch was activated by addition of 10nM CID. At day 8 after infection, remaining cells were reseeded and cultured for 6 more days in the presence of 10nM CID. At day 14 after infection, cells were sorted into a mClover3-positive and a mClover3-negative fraction. Genomic DNA was isolated using the DNasy Blood and Tissue Kit (#69506 QIAGEN) and sgRNA inserts were recovered from DNA by PCR amplification. Each PCR reaction consisted of 500 ng DNA, 10 µL GC buffer (5×), 1 µL forward primer (10 µM), 1 µL reverse primer (10 µM), 1 µL dNTPs (10 mM), 1.5 µL DMSO, and 0.5 µL polymerase in a total volume of 50 µl. Barcoded forward primers (Evers et al., 2016) were used to be able to deconvolute multiplexed samples after next-generation sequencing. PCR program consisted of initial denaturation at 98°C for 2 min, 16 cycles of 30s denaturation at 98°C, 30s of annealing at 60°C, and 30s elongation at 72°C, with a final extension at 72°C for 5 min. PCR product purification was performed using the High Pure PCR Product Purification Kit according to manufacturers' instructions (#11732676001, Roche). PCR products of each sample were pooled, and 2.5 µL was used for a second PCR reaction in technical duplicates. Primers in this reaction contained barcodes and an adaptor sequence for next-generation sequencing. Sample concentrations were measured on a BioAnalyzer and were pooled equimolarly. sgRNA sequences were identified by Illumina HiSeq 2500 genome analyzer at the Genomics Core Facility (NKI). For sequence depth normalization, a relative total size factor was calculated for each sample by dividing the total counts of each sample by the geometric_mean of all totals. After normalization, a differential test between the t14pos and t14neg for each sgRNA was performed using DESeq2 (Love et al., 2014). The output from the DESeq2 analysis contains the DESeq2 test statistic. Positive DESeq2 test statistic indicate positive log2FoldChange value, negative DESeq2 test statistic indicate negative log2FoldChange value. We sorted the output of DESeq2 on the test statistic in decreasing order, putting the most significant enriched sgRNA at the top. We then used the MAGeCK Robust Rank Algorithm (Li et al., 2014) to determine for each gene if its sgRNAs are enriched towards the top of the result list. The resulting enrichment p-values were corrected for multiple testing using the Benjamini-Hochberg correction, resulting in a FDR value. As hits we took the genes that had a FDR <= 0.1 and took along the borderline hit RAB14 which had a FDR of 0.102.

Incucyte cell proliferation assay and apoptosis assay

Cell lines were seeded into 384-well plates at a density of 500-2000 cells per well, depending on growth rate and the design of the experiment. Drugs were added at the indicated concentrations using the HP D300 Digital Dispenser (HP). Cells

were imaged every 4 h using the Incucyte ZOOM (Essen Bioscience). Phase-contrast images were analyzed to detect cell proliferation based on cell confluence. For the cell apoptosis assay, caspase-3/7 green apoptosis assay reagent (Essen Bioscience, #4440) was added to the culture medium and cell apoptosis was analyzed based on green fluorescent staining of apoptotic cells. The percentage of apoptotic cells was quantified based on images generated from biological triplicates.

Protein lysate preparation and western blots

Cells were washed with PBS and lysed in RIPA buffer supplemented with Complete Protease Inhibitor (Roche) and Phosphatase Inhibitor Cocktails II and III (Sigma). Protein quantification was performed with the BCA Protein Assay Kit (Pierce). All lysates were freshly prepared and processed with Novex NuPAGE Gel Electrophoresis Systems (Thermo Fisher Scientific) followed by western blotting.

qRT-PCR

Total RNA was extracted from cells using the Quick-RNA MiniPrep kit (Zymo Research). cDNA synthesis was performed using Maxima Universal First Strand cDNA Synthesis Kit (Thermo Scientific) according to the manufacturer's instructions. qPCR reactions were performed with FastStart Universal SYBR Green Master Rox (Roche). Sequences of the primers used for qRT-PCR analyses: KI67_fwd ATCAGCCGAAGTCAACATGA; KI67_rev GAGTTTGCGTGGCCTGTACT; ATG101_fwd TTCATCGACTTCACTTATGTGCG; ATG101_rev GATGCACTCGTCTGAGAATGG; ATG9A_ fwd CTGCCCTTCCGTATTGCAC; ATG9A_rev CTCACGTTTGTGGATGCAGAT; RAB14_ fwd TATGGCTGATTGTCCTCACACA; RAB14_rev CTGTCCTGCCGTATCCCAAAT; RB1CC1_fwd ATCGAAGAGTGTGTACCTACAGT; RB1CC1_rev GCAGGTGGACGATCACATAAGAT.

Staining for senescence associated β-galactosidase Activity

Senescence associated β-galactosidase activity in cells was detected using the Senescence Cells Histochemical Staining Kit (Sigma-Aldrich, CS0030), according to the manufacturer's instructions. The percentage of SA-β-gal staining positive cells was quantified by manual counting of positive and negative cells.

RNA sequencing

RNA (one sample per cell line / condition) was isolated using Trizol, and cDNA libraries were sequenced on an Illumina HiSeq2500 to obtain 65-bp single-end sequence reads. Reads were aligned to the GRCh38 human reference genome. Gene set enrichment analysis (GSEA) was performed using gene set enrichment analysis software as described previously (Subramanian et al., 2005). The FRIDMAN_ SENESCENCE_UP gene set was used to assess the enrichment of senescence-

associated genes (Fridman and Tainsky, 2008). Enrichment scores were corrected for gene-set size (normalized enrichment score). The P value estimates the statistical significance of the enrichment score for a single gene set as described previously (Subramanian et al., 2005). The exact P value is shown in the figures unless the P value < 0.001.

Compounds and antibodies

lisertib, ABT263 and SBI0206965 were purchased from MedKoo. The chemical inducer of dimerization CID/AP20187 was purchased from Takara Bio. Antibodies against HSP90 (sc-13119), p53 (sc-126), and p21 (sc-271610) were purchased from Santa Cruz Biotechnology. Antibodies against LC3B (#2775), and BCL2 (#2872) were purchased from Cell Signalling.

CRISPR-Cas9 knockout and TIDE analysis

A549 cells were infected with virus containing pLentiCRISPR with a guide RNA for the specified targets. One day after infection cells were selected with puromycin for two days. Nine days after infection cells were lysed for western blot and TIDE analysis (Brinkman et al., 2014) (https://tide.nki.nl/#about). Sequences used for knockout and TIDE analyses: ATG101_guide CACCTACTCCATTGGCACCG; ATG101_fwd ATTCTGACCTGGGCTCCTTT; ATG101_rev GGGAAAGGAAAAGTGGAAGC; ATG9A_guide CCGTTTCCAGAACTACATGG; ATG9A_fwd GCTCACAACCCCTGAATCTC; ATG9A_rev ATGGTGAGGGCAATAAGCAC; RAB14_guide AGCGATTTAGGGCTGTTACA; RAB14_fwd GGATTTTCCCCCTCTAGGC; RAB14_rev CAAACACCTTCAGATGCAAGC; RB1CC1_guide GACCAGATGATTGCTAGCTG; RB1CC1_fwd TTCCCATGCTTTTGCTTTTT; RB1CC1_rev TAGCCATTCCATCACCTTCC;

All mouse study protocols were approved by the NKI Animal Welfare Body.

References

Anders, S., and Huber, W. (2010). Differential Expression analysis for sequence count data. Nat. Preceedings *11*, R106.

Brinkman, E.K., Chen, T., Amendola, M., and Van Steensel, B. (2014). Easy quantitative assessment of genome editing by sequence trace decomposition. Nucleic Acids Res. *42*, e168.

Burmer, G.C., and Norwood, T.H. (1980). Selective elimination of proliferating cells in human diploid cell cultures by treatment with BrdU, 33258 Hoechst and visible light. Mech. Ageing Dev. *12*.

Churcher, I. (2018). Protac-Induced Protein Degradation in Drug Discovery: Breaking the Rules or Just Making New Ones? J. Med. Chem. *61*.

Coppé, J.-P., Desprez, P.-Y., Krtolica, A., and Campisi, J. (2010). The senescence-associated secretory phenotype: the dark side of tumor suppression. Annu. Rev. Pathol. *5*, 99–118.

Doench, J.G., Fusi, N., Sullender, M., Hegde, M., Vaimberg, E.W., Donovan, K.F., Smith, I., Tothova, Z., Wilen, C., Orchard, R., et al. (2016). Optimized sgRNA design to maximize activity and minimize off-target effects of CRISPR-Cas9. Nat. Biotechnol. *34*.

Evers, B., Jastrzebski, K., Heijmans, J.P.M., Grernrum, W., Beijersbergen, R.L., and Bernards, R. (2016). CRISPR knockout screening outperforms shRNA and CRISPRi in identifying essential genes. Nat. Biotechnol. *34*, 11–14.

Fridman, A.L., and Tainsky, M.A. (2008). Critical pathways in cellular senescence and immortalization revealed by gene expression profiling. Oncogene *27*, 5975–5987.

Hamasaki, M., Furuta, N., Matsuda, A., Nezu, A., Yamamoto, A., Fujita, N., Oomori, H., Noda, T., Haraguchi, T., Hiraoka, Y., et al. (2013). Autophagosomes form at ER-mitochondria contact sites. Nature *495*.

He, C., and Klionsky, D.J. (2009). Regulation mechanisms and signaling pathways of autophagy. Annu. Rev. Genet. *43*.

Hernandez-Segura, A., Nehme, J., and Demaria, M. (2018). Hallmarks of Cellular Senescence. Trends Cell Biol. *28*, 436–453.

Junutula, J.R., De Maziére, A.M., Peden, A.A., Ervin, K.E., Advani, R.J., Van Dijk, S.M., Klumperman, J., and Scheller, R.H. (2004). Rab14 Is Involved in Membrane Trafficking between the Golgi Complex and Endosomes. Mol. Biol. Cell *15*.

Kale, A., Sharma, A., Stolzing, A., Stolzing, A., Desprez, P.Y., Desprez, P.Y., Campisi, J., and Campisi, J. (2020). Role of immune cells in the removal of deleterious senescent cells. Immun. Ageing *17*.

Kang, C., and Elledge, S.J. (2016). How autophagy both activates and inhibits cellular senescence. Autophagy *12*.

Kang, H.T., Lee, K.B., Kim, S.Y., Choi, H.R., and Park, S.C. (2011). Autophagy impairment induces premature senescence in primary human fibroblasts. PLoS One *6*.

Kastenhuber, E.R., and Lowe, S.W. (2017). Putting p53 in Context. Cell *170*.

Leite de Oliveira, R., and Bernards, R. (2018). Anti-cancer therapy: senescence is the new black. EMBO J. *37*.

Li, W., Xu, H., Xiao, T., Cong, L., Love, M.I., Zhang, F., Irizarry, R.A., Liu, J.S., Brown, M., and Liu, X. (2014). MAGeCK enables robust identification of essential genes from genome-scale CRISPR/ Cas9 knockout screens. Genome Biol. *15*, 554.

Love, M.I., Huber, W., and Anders, S. (2014). Moderated estimation of fold change and dispersion for RNA-seq data with DESeq2. Genome Biol. *15*.

Menon, S.S., Guruvayoorappan, C., Sakthivel, K.M., and Rasmi, R.R. (2019). Ki-67 protein as a tumour proliferation marker. Clin. Chim. Acta *491*, 39–45.

Mizushima, N. (2007). Autophagy: Process and function. Genes Dev. *21*.

Ruscetti, M., Iv, J.P.M., Mezzadra, R., Russell, J., Romesser, P.B., Simon, J., Kulick, A., Ho, Y., Fennell, M., Li, J., et al. (2020). Senescence-Induced Vascular Remodeling Creates Therapeutic Vulnerabilities in Pancreas Cancer. *181*, 424–441.

Sieben, C.J., Sturmlechner, I., van de Sluis, B., and van Deursen, J.M. (2018). Two-Step Senescence-Focused Cancer Therapies. Trends Cell Biol. *28*, 723–737.

Straathof, K.C., Pulè, M.A., Yotnda, P., Dotti, G., Vanin, E.F., Brenner, M.K., Heslop, H.E., Spencer, D.M., and Rooney, C.M. (2005). An inducible caspase 9 safety switch for T-cell therapy. Blood *105*.

Subramanian, A., Tamayo, P., Mootha, V.K., Mukherjee, S., Ebert, B.L., Gillette, M.A., Paulovich, A., Pomeroy, S.L., Golub, T.R., Lander, E.S., et al. (2005). Gene set enrichment analysis: A knowledge-based approach for interpreting genome-wide expression profiles. Proc. Natl. Acad. Sci. U. S. A. *102*, 15545–15550.

Tanida, I., Ueno, T., and Kominami, E. (2008). LC3 and autophagy. Methods Mol. Biol. *445*.

Tieng, V., Cherpin, O., Gutzwiller, E., Zambon, A.C., Delgado, C., Salmon, P., Dubois-Dauphin,

2

M., and Krause, K.H. (2016). Elimination of proliferating cells from CNS grafts using a Ki67 promoter-driven thymidine kinase. Mol. Ther. - Methods Clin. Dev. 3.

Wang, B., Kohli, J., and Demaria, M. (2020). Senescent Cells in Cancer Therapy: Friends or Foes? Trends in Cancer.

Wang, C., Vegna, S., Jin, H., Benedict, B., Lieftink, C., Ramirez, C., Leite de Oliveira, R., Morris, B., Gadiot, J., Wang, W., et al. (2019). Inducing and exploiting vulnerabilities for the treatment of liver cancer. Nature 574, 268–272.

Wang, L., Leite de Oliveira, R., Wang, C., Fernandes Neto, J.M., Mainardi, S., Evers, B., Lieftink, C., Morris, B., Jochems, F., Willemsen, L., et al. (2017). High-Throughput Functional Genetic and Compound Screens Identify Targets for Senescence Induction in Cancer. Cell Rep. 21, 773–783.

Yosef, R., Pilpel, N., Tokarsky-Amiel, R., Biran, A., Ovadya, Y., Cohen, S., Vadai, E., Dassa, L., Shahar, E., Condiotti, R., et al. (2016). Directed elimination of senescent cells by inhibition of BCL-W and BCL-XL. Nat. Commun. 7.

Young, A.R.J., Narita, M., Ferreira, M., Kirschner, K., Sadaie, M., Darot, J.F.J., Tavaré, S., Arakawa, S., Shimizu, S., Watt, F.M., et al. (2009). Autophagy mediates the mitotic senescence transition. Genes Dev. 23.

Zhu, Y., Tchkonia, T., Fuhrmann-Stroissnigg, H., Dai, H.M., Ling, Y.Y., Stout, M.B., Pirtskhalava, T., Giorgadze, N., Johnson, K.O., Giles, C.B., et al. (2016). Identification of a novel senolytic agent, navitoclax, targeting the Bcl-2 family of anti-apoptotic factors. Aging Cell 15, 428–435.
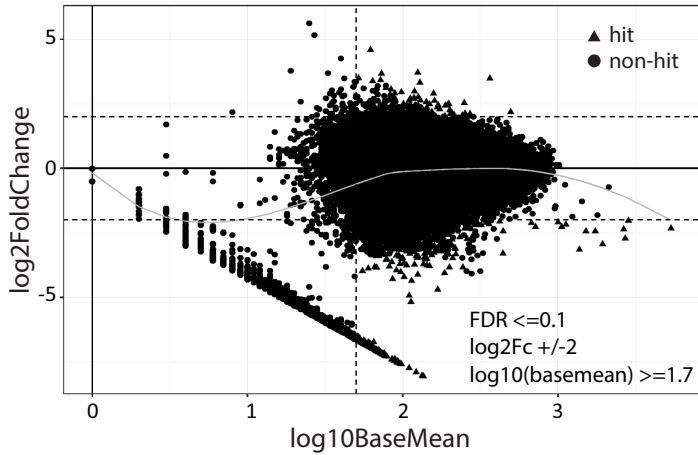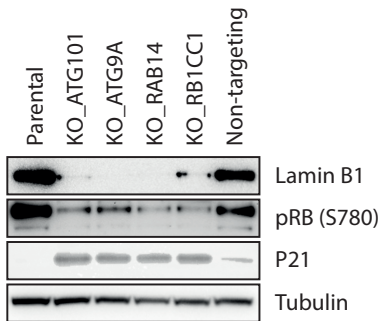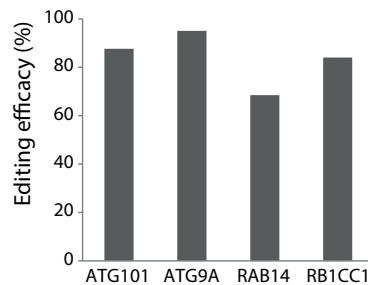
Supplementary

Figure S1. MA plot showing the representation of guides in the sorted mClover3 positive cells compared to the mClover3 negative fraction at t14. Each dot represents the average representation versus the fold enrichment for a sgRNA, hits are represented as triangles.
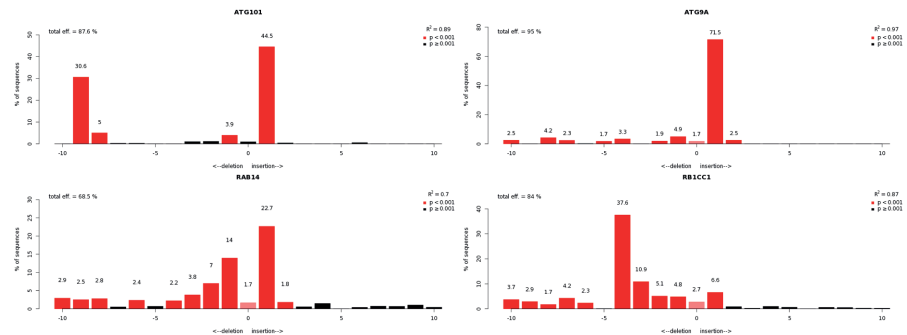

Figure S2. Target validation of hits from the screen using CRISPR-Cas9 knockout. (A) Western blot for senescence markers Lamin B1, phospho-RB and P21, comparing parental A549 cells and CRISPR-Cas9 knockout cells. **(B)** Editing efficiency in the CRISPR-Cas9 knockout cells, as analyzed by TIDE (https://tide.nki.nl/#about). **(C)** Identity and frequency of the indels detected by TIDE.
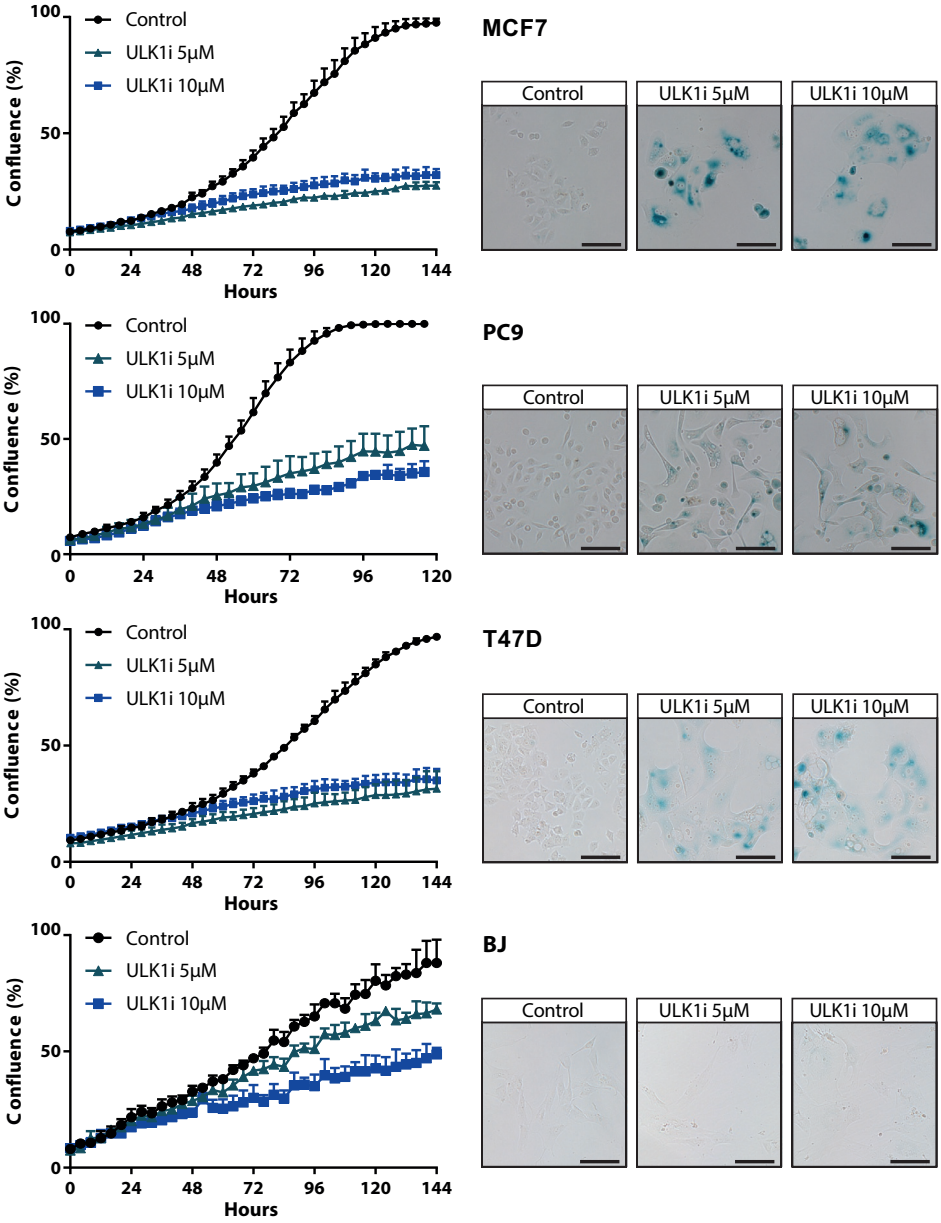
2

Figure S3. Senescence markers after treatment with ULK1 inhibitor. IncuCyte proliferation assay and SA-B-gal staining of cells (MCF7, PC9, T47D, BJ) treated with different doses of ULK1 inhibitor SBI0206965.
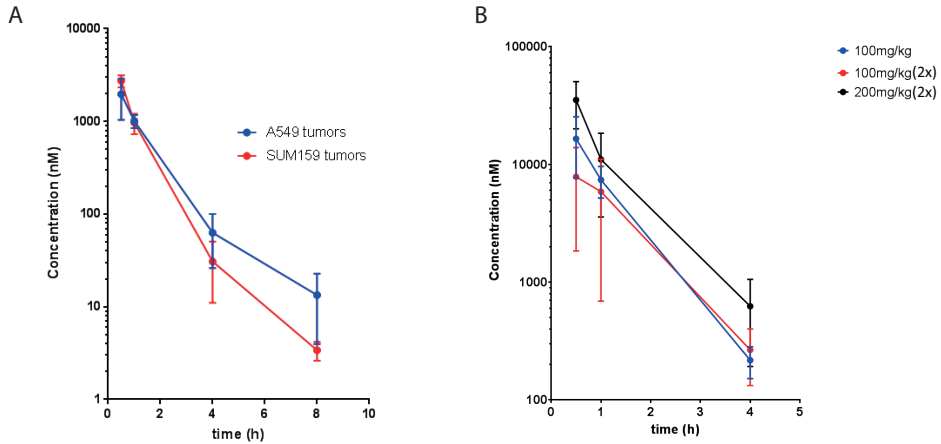
Figure S4. SBI0206965 pharmacokinetic profiles in mouse plasma. (A) NMRI mice with A549 xenografts or SUM159 xenografts, dosed with 50mg/kg SBI0206965 every other day. **(B)** Balb-C mice with A549 xenografts, dosed with 100mg/kg SBI0206965 every day, 100mg/kg twice per day, or 200mg/kg twice per day. Xenografts were generated by subcutaneous injection of 2M tumor cells (in a 1:1 mix of matrigel:PBS), in the flank of male or female mice. SBI0206965 was injected into the peritoneum in a vehicle solution of 3.5% DMSO, 6.5% Tween 80, 90% Saline.
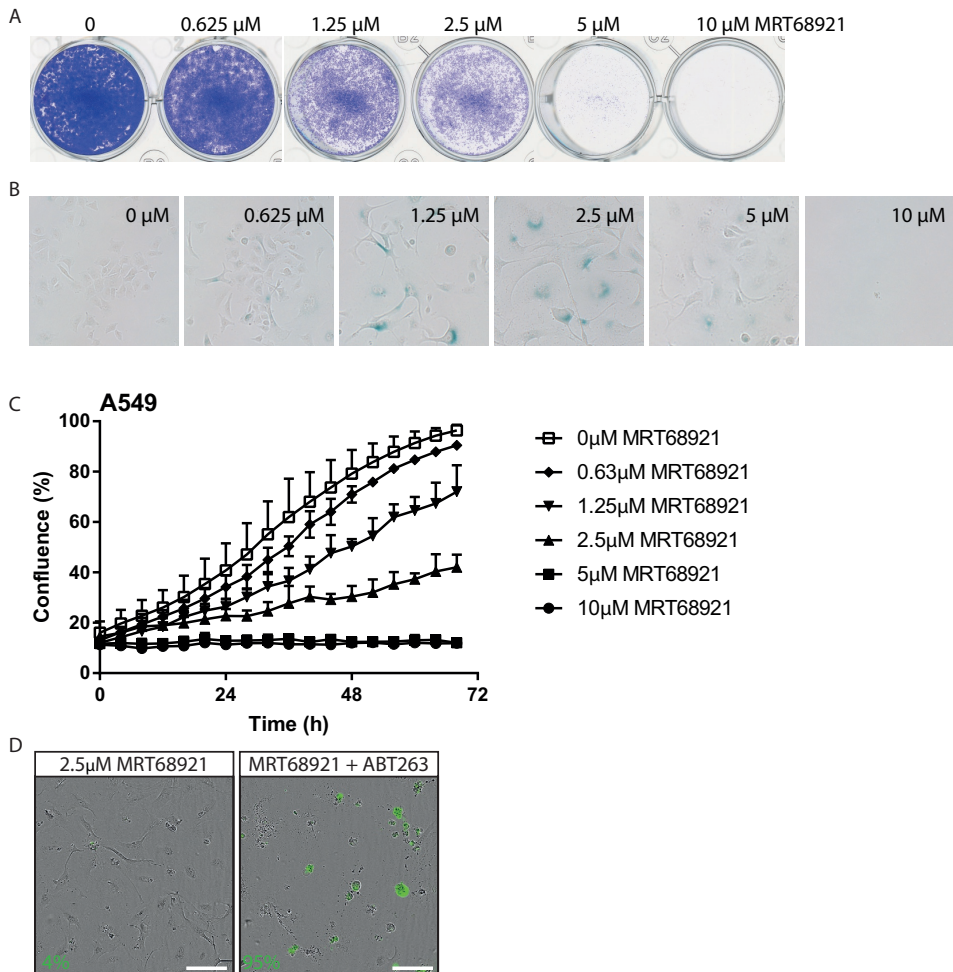
Figure S5. A549 cells treated with the ULK1 inhibitor MRT68921. (A) Crystal violet staining of cells treated with different concentrations of MRT68921 for six days. **(B)** SA-B-gal staining of cells after MRT68921 treatment for six days. **(C)** IncuCyte proliferation assay of A549 cells treated with different doses of MRT68921. **(D)** Representative images showing cells treated with 2.5μM MRT68921 for six days on the left, and cells treated for five days with MRT68921 and one day of 2.5μM MRT68921 + 1μM ABT263 on the right. Apoptotic cells were determined by caspase-3/7 apoptosis assay. Inset shows percentage of apoptotic cells. Scale bars represent 100μm.

CHAPTER 3

The cancer SENESCopedia – a delineation of cancer cell senescence

Fleur Jochems,[1,6] Bram Thijssen,[1,6] Giulia De Conti,[1,7]
Robin Jansen,[1,7] Ziva Pogacar,[1] Kelvin Groot,[1] Liqin Wang,[1]
Arnout Schepers,[1] Cun Wang,[1,3] Haojie Jin,[1]
Roderick L. Beijersbergen,[2] Rodrigo Leite de Oliveira,[1,4]
Lodewyk F.A. Wessels,[1,5,8,*] René Bernards[1,8,9]

[1]Division of Molecular Carcinogenesis, Oncode Institute, Netherlands Cancer Institute, Plesmanlaan 121, 1066 CX Amsterdam, The Netherlands
[2]Division of Molecular Carcinogenesis, The NKI Robotics and Screening Center, Netherlands Cancer Institute, Plesmanlaan 121, 1066 CX Amsterdam, The Netherlands
[3]Present address: State Key Laboratory of Oncogenes and Related Genes, Shanghai Cancer Institute, Renji Hospital, Shanghai Jiao Tong University School of Medicine, Shanghai, China.
[4]Present address: CRISPR Expertise Center, Cancer Center Amsterdam, Amsterdam UMC, Amsterdam, The Netherlands
[5]Faculty of EEMCS, Delft University of Technology, Delft, The Netherlands
[6]These authors contributed equally
[7]These authors contributed equally
[8]Senior author
[9]Lead contact

Abstract

Cellular senescence is characterized as a stable proliferation arrest that can be triggered by multiple stresses. Most knowledge about senescent cells is obtained from studies in primary cells. However, senescence features may be different in cancer cells, since the pathways that are involved in senescence induction are often deregulated in cancer. We report here a comprehensive analysis of the transcriptome and senolytic responses in a panel of 13 cancer cell lines rendered senescent by two distinct compounds. We show that in cancer cells the response to senolytic agents and the composition of the senescence-associated secretory phenotype are more influenced by the cell of origin, than by the senescence trigger. Using machine learning, we establish the SENCAN gene expression classifier for the detection of senescence in cancer cell samples. The expression profiles and senescence classifier are available as an interactive online Cancer SENESCopedia.

3
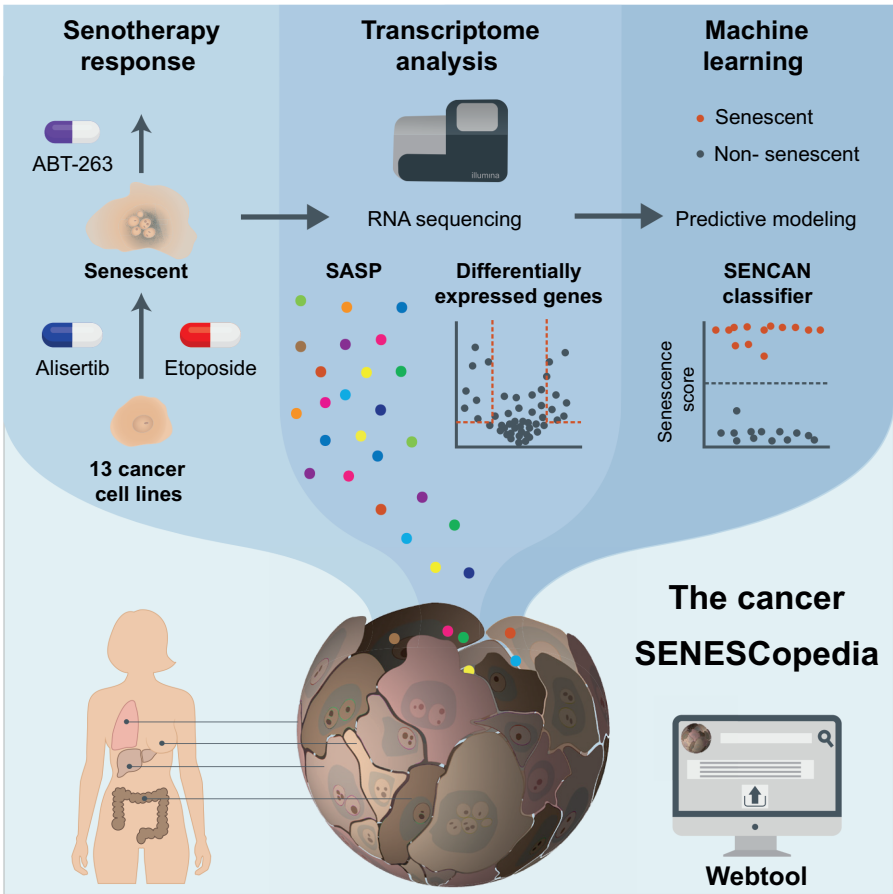
Introduction

Cellular senescence is a stable proliferation arrest evoked by a plethora of stress-inducing factors and is characterized by alterations in cell morphology, gene expression, heterochromatin formation, and metabolic activity (Fridman and Tainsky, 2008; Hayflick, 1965; Narita et al., 2003). An important feature of senescence is the secretion of a variety of cytokines and chemokines, referred to as the senescence associated secretory phenotype (SASP) (Coppé et al., 2008)**.** This phenotype is heterogeneous and dynamic and depends not only on the senescence trigger, but also on the cell of origin (Basisty et al., 2020; Hernandez-Segura et al., 2017; Wiley et al., 2017).

The current understanding of senescence has derived mainly from studies in non-transformed fibroblasts and primary epithelial cells. However, both normal and cancer cells can undergo senescence after treatment with chemotherapeutic agents, a phenomenon called 'therapy-induced senescence' (TIS) (Ewald et al., 2010). The consequence of TIS in the tumor environment is still highly controversial (Lee and Lee, 2014; Pérez-Mancera et al., 2014; Schosserer et al., 2017). On the one hand, TIS can halt tumor growth and the SASP can create an immunogenic environment (Greten and Eggert, 2017; Haugstetter et al., 2010; Schmitt et al., 2002). On the other hand, prolonged SASP signaling can jeopardize immune clearance and promote epithelial-to-mesenchymal transition and tumorigenesis in neighboring cells (Davalos et al., 2010; Demaria et al., 2016; Freund et al., 2010). Furthermore, there is increasing evidence that senescent cells can reenter the cell cycle, promote cancer stemness, and eventually contribute to tumor relapse (Dirac and Bernards, 2003; Milanovic et al., 2018; Roberson et al., 2005; Saleh et al., 2017). This evoked interest in the removal of senescent cancer cells by so-called 'senolytics' –agents that kill senescent cells– (Lozano-Torres et al., 2019), which have the potential to increase the efficacy of senescence-provoking cancer treatments and reduce potentially deleterious side-effects. A potent senolytic for multiple primary senescent cell types is ABT-263 (navitoclax), a BH3 family mimetic that inhibits the anti-apoptotic proteins BCL-2, BCL-W, and BCL-xL (Chang et al., 2016; Zhu et al., 2016).

A major difficulty in elucidating the role of senescence in cancer and in assessing the efficacy of senolytics is the lack of universal markers to detect cancer cell senescence *in vitro* and *in vivo*. Besides assessing Senescence-Associated ß-galactosidase (SA-ß-gal) activity, multiple markers have to be combined to define senescence in normal cells (Gorgoulis et al., 2019). Cancer cells often harbor mutations in pathways that are involved in the onset of senescence, such as mutations in *TP53* and *CDKN2A*, and frequently contain deficiencies in apoptotic pathways (Hanahan and Weinberg, 2011). We hypothesized that this may influence the appearance of conventional senescence markers as identified in non-cancer

cells, the composition of their SASP, and their response to senolytic agents.

In this study, we analyzed a large panel of cancer cells rendered senescent by different compounds, with the aim to find common vulnerabilities to induce cell death and shared features that would allow unambiguous identification of the senescent state in the context of a cancerous phenotype.

Results

Senescence-induction by alisertib or etoposide in a panel of 13 cancer cell lines
To characterize cancer cell senescence, we curated a panel of 13 cell lines from four cancer types rendered senescent with two clinically relevant triggers: (i) alisertib, an aurora kinase A inhibitor that was previously identified to be an effective senescence inducer (Wang et al., 2017), and (ii) etoposide, a topoisomerase II inhibitor used as a chemotherapeutic agent in a wide spectrum of human cancers (Baldwin and Osheroff, 2005).

To induce senescence, A549 and HCT116 cells were treated with increasing concentrations of alisertib and etoposide. This resulted in decreased confluency (Figure 1A), cell proliferation arrest (Figure 1B), and at specific concentrations cells obtained an enlarged, flattened morphology and increased SA-ß-gal activity (Figure 1C). Similarly, we determined the optimal senescence-inducing concentrations in 11 additional cell lines (Figure S1), which resulted in 80-100% SA-ß-gal positive populations (Figure 1D). Only for PC9 40-60% of cells were rendered positive. Next, we checked five protein markers of senescence (Retinoblastoma protein (RB) phosphorylation, laminB1, p53, p21, p16, and γ-H2AX), and detected at least two positive markers per condition (Figure 1SB). Remarkably, even when grouped on mutation status, these markers varied strongly between cell lines.

To further study the features of senescence in this cell line panel, we collected RNA-sequencing (RNA-seq) data from treated and untreated cells. We assessed the enrichment of four gene sets previously described as upregulated in non-cancer cell senescence (Table S1): hallmark gene signatures of Fridman and Tainsky (2008), and of Casella *et al.* (2019); and differentially expressed genes from Hernandez-Segura *et al.* (2017) and Purcell *et al.* (2014). There was virtually no overlap between these gene sets (Figure 1E). We analyzed the difference in single sample Gene Set Enrichment Analysis (ssGSEA) scores (Barbie et al., 2009) of treated samples compared to their untreated control (Figure 1F). For almost all cell lines, the ssGSEA scores were enriched in the expected direction. Only alisertib-treated Huh7 and Hep3B were enriched in the opposite direction for the Fridman and Purcell gene sets respectively. Overall, these data support the notion that alisertib or etoposide treatment results in a senescent phenotype in the cancer cells tested, and while SA-

ß-gal, changed morphology, and growth arrest were universally present, the other markers were not (Figure S1C).
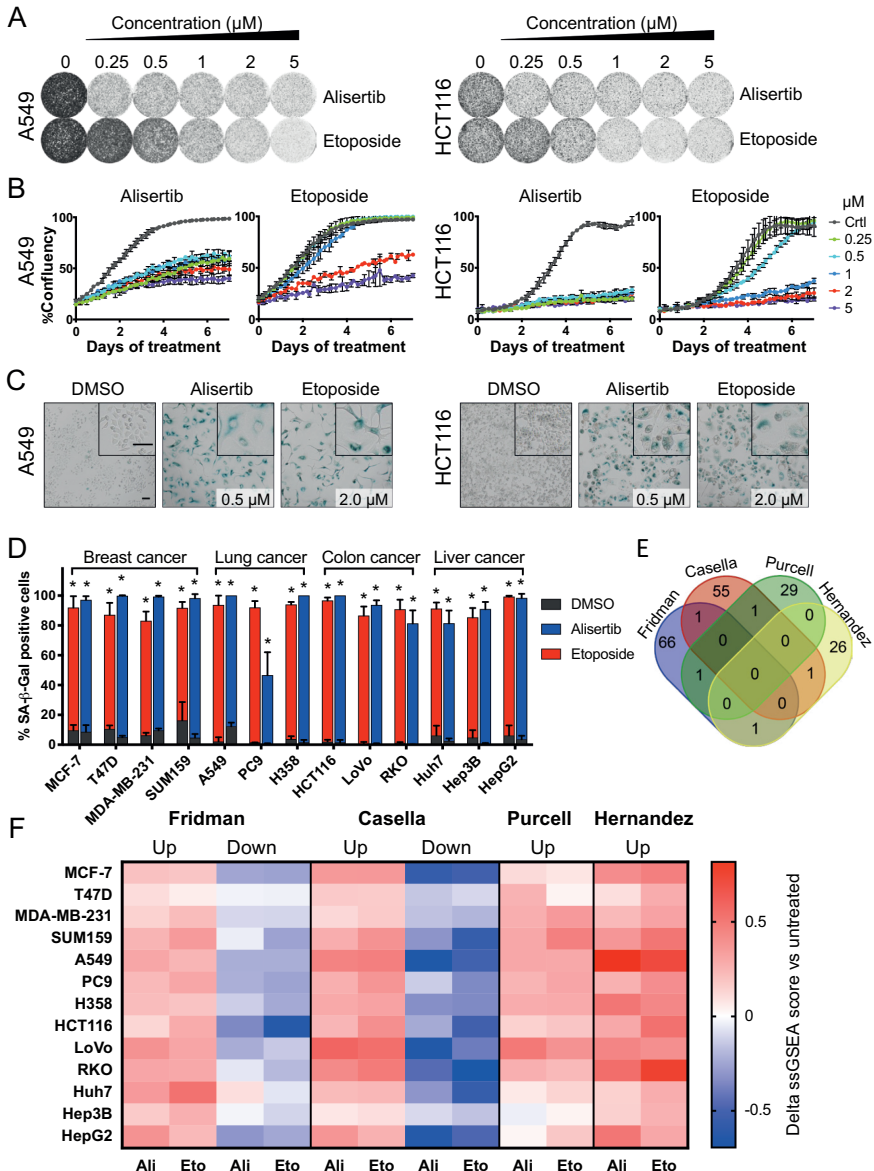
Figure 1. Senescence-induction by alisertib or etoposide in a panel of 13 cancer cell lines.
(A-C) A549 and HCT116 were cultured for 7 days with the indicated alisertib or etoposide concentrations. (A) colony formation assay and (B) cell proliferation curves (obtained with IncuCyte®). Data represent the mean ±SEM of triplicate wells and are representative of two independent experiments. (C) Representative images of SA-ß-gal staining from three independent

experiments (quantification in D). Scale bar = 100 µm. **(D)** Quantification of SA-ß-gal positive cells for cells treated for 7 days with DMSO, alisertib, or etoposide (images are shown in C and figure S1). Bars represent the mean ±SEM. Data is obtained in biological triplicate and analyzed with a two-sided Student's *t*-test. * *P* <0.01. **(E)** Venn diagram of gene sets from hallmark gene signatures for senescence (Fridman and Casella) and differentially expressed genes in senescence (Purcell and Hernandez). Up- and down-regulated genes are pooled for Fridman and Casella. **(F)** RNA sequencing was performed on 13 cell lines in parental and treated cells. Data were analyzed with single-sample Geneset Enrichment Analysis (ssGSEA) for four gene sets associated with senescence. Delta ssGSEA scores represent the difference between parental and senescent samples. Values were normalized per gene set. Ali = alisertib, Eto = etoposide.

Senescent cancer cells respond differently to senolytic ABT-263

In the search for common vulnerabilities, we asked whether senescent cancer cells are universally sensitive to the senolytic ABT-263. We performed dose-response assays in parental and senescent cells (Figure 2A), which showed responses ranging from strong sensitization with a senolytic index ($IC50_{SEN}$/ $IC50_{parental}$) of 220 in A549, to virtually no change in IC50 in senescent LoVo cells (Figure 2B). While the responses to ABT-263 were highly divergent for different cell lines (Figure 2C and S2A; *P* <0.001, two-way ANOVA), the influence of the senescence trigger was not significant (*P* = 0.11, two-way ANOVA) and the response of etoposide-induced senescent cells (SEN Eto) correlated with alisertib-induced senescent cells (SEN Ali) (Figure 2D).

To assess whether non-senescent cells were interfering with the ABT-263 sensitivity read-out, we performed SA-ß-gal staining of the remaining cells after treatment with 1µM ABT-263 (Figure 2E and S2B). For A549, the number of SA-ß-gal positive cells was decreased after ABT-263 treatment versus DMSO, while for LoVo, the number of SA-ß-gal positive cells was sustained after ABT-263 treatment (Figure 2E-F). This is consistent with the notion that senescent LoVo cells are insensitive to ABT-263. However, a substantial population of SA-ß-gal negative cells was present in SEN Eto LoVo after ABT-263 treatment, suggesting that non-senescent cells did proliferate during ABT-263 treatment. However, the reduction in SA-ß-gal positive cells (Figure S2B) correlated with the ABT-263 IC50 value of each cell line (Figure 2G), which suggest strongly that the behavior of senescent cells, rather than that of non-senescent cells, contributes to the variability in IC50 values.
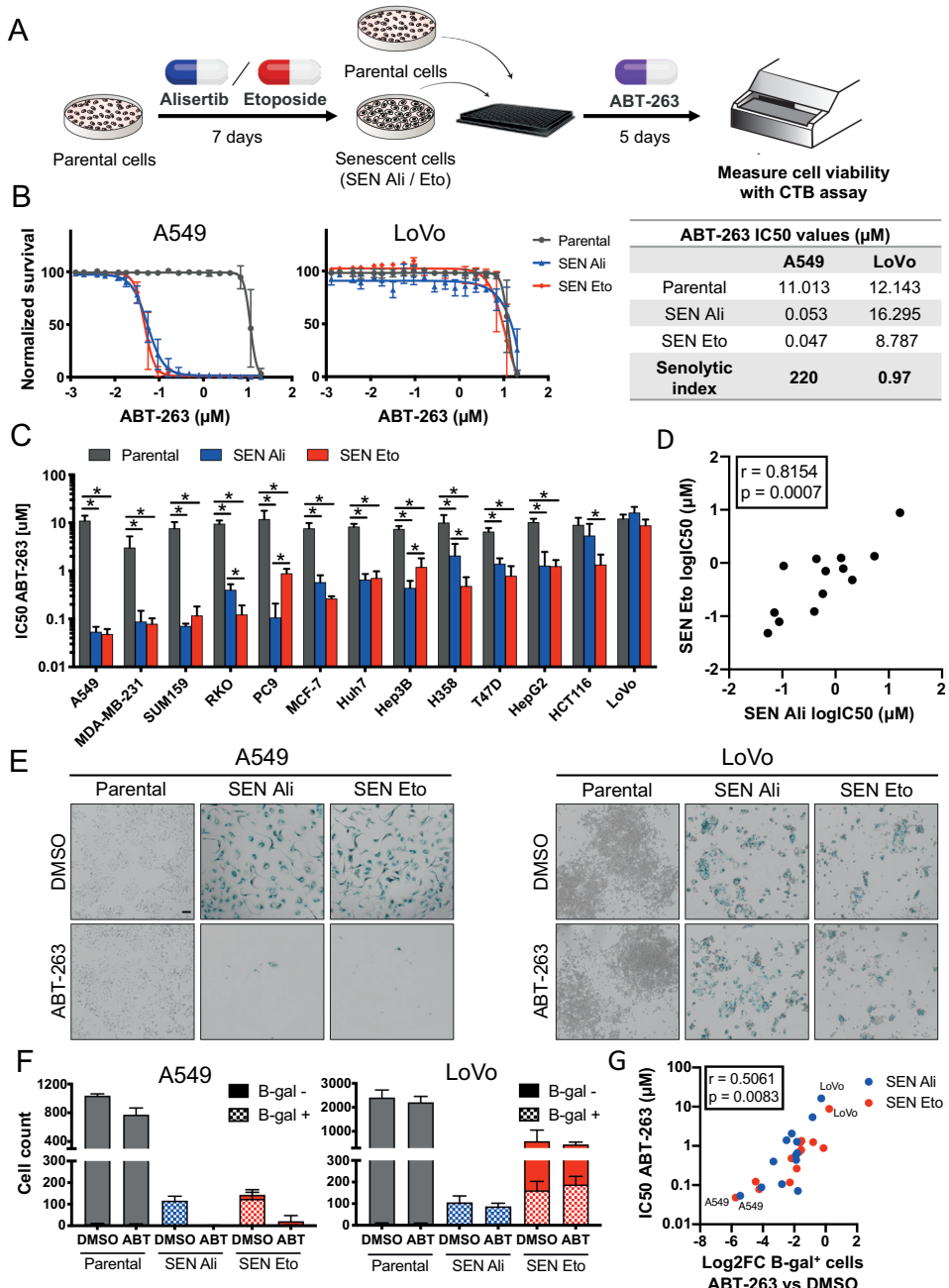
Figure 2. Senescent cancer cells respond differently to senolytic ABT-263. (A) Schematic outline of the experimental procedures used in B-D. Cells were treated with senescence-inducing concentrations of alisertib or etoposide for seven days. Senescent cells and parental cells were reseeded in 96-wells and cultured with increasing concentrations of ABT-263. After five days, cell viability was measured with Cell Titer Blue (CTB) assay. SEN Ali = alisertib-induced senescent, SEN Eto = etoposide-induced senescent. **(B)** Dose-response curves and senolytic indexes for ABT-263 of

a responsive and unresponsive cell line. Values represent the mean ±SEM of three independent biological experiments. **(C)** Bar graph of ABT-263 IC50 values extrapolated from dose-response curves presented in B and figure S3. Data were analyzed with two-way ANOVA and post-hoc Tukey test. * *P* adjusted <0.01. **(D)** Pearson correlation analysis for the ABT-263 logIC50 values of SEN Eto and SEN Ali. Each dot represents a cell line. r = Pearson correlation coefficient, p = *P*-value. **(E)** Representative images of SA-ß-gal staining from three technical replicates. Scale bar = 100 μm. **(F)** Quantification of SA-ß-gal positive and SA-ß-gal negative cells from SA-ß-gal staining as depicted in E. **(G)** Spearman rank correlation analysis for 13 cancer cell lines. Each dot represents a cell line with its corresponding foldchange of B-gal positive cells for ABT-263 versus DMSO (x-axis, counts are shown in F and figure S4) and ABT-263 IC50 value (y-axis). The names of the most responsive and unresponsive cell lines are presented. r = Spearman rank correlation coefficient, Log2FC = log2 foldchange.

Next, we asked whether the gene expression of specific pro- or anti-apoptotic proteins could explain the divergent response to ABT-263. We tested the correlation between the expression of 16 genes involved in apoptosis (Figure S3A) and the response to ABT-263 of SEN Eto and SEN Ali. Although none of the apoptotic proteins were significantly correlated (Figure S3B), the positive correlation for *BAD* was potentially interesting, since this pro-apoptotic sensitizer protein has the same targets as ABT-263, and high levels of *BAD* could result in sensitization to this drug. However, already in the parental state, *BAD* ranges from high to low expression (Figure S3C), and the correlation for senescent cells is not strong enough to solely explain the sensitivity to ABT-263. For *MCL1*, *BIK,* and *BID*, the difference in gene expression between ABT-263 unresponsive and responsive cells was small, or the correlation was in the opposite direction. In conclusion, the transcriptome of apoptosis-related genes could not explain the divergent response to ABT-263 of senescent cancer cells.

Gene expression in senescent cancer cells evolves over time and is independent of senescence trigger

The gene expression of normal senescent cells is influenced by the inducer, cell origin, and time (Hernandez-Segura et al., 2017; Wiley et al., 2017). Since this might complicate the search for a robust classifier in cancer, we asked how similar SEN Ali cells and SEN Eto cells are in transcriptome, and how SEN Ali cells change over-time. We used RNA-sequencing data from the 13 SEN Ali and SEN Eto cell lines, which were treated for 7 days (early senescent state), and included a late senescent state for 11 cell lines, where cells were treated with alisertib for 14 days (SEN Ali L). MCF-7 and RKO started to die after prolonged treatment with alisertib.

First, to assess the inducer effect, SEN Ali and SEN Eto were compared to their parental counterparts using a paired differential gene expression analysis (DGEA) across the 13 cell lines. This yielded 1,875 and 1,275 differentially expressed genes (DEGs), respectively (Figure 3A-B). Importantly, the majority of DEGs were overlapping between SEN Ali and SEN Eto, and when compared directly to each other, no DEGs were found between the two senescent states (Figure 3C). This

implies that alisertib and etoposide induce a similar senescence phenotype.

To assess the gene expression of cells at a later stage of senescence, SEN Ali and SEN Ali L were compared. DGEA identified more DEGs (2,936) between SEN Ali L and parental cells (Figure 3D) than DEGs detected between SEN Ali and parental cells (Figure 3B). SEN Ali L especially showed more genes that were downregulated. Furthermore, when SEN Ali and SEN Ali L were compared directly (Figure 3E), 69 DEGs were detected. This can be explained by gene expression evolving over time, where a large set of genes may start to change at an early time point but only becomes significantly different from parentals at a later time point.

To identify genes that are differentially expressed in various senescence conditions, we compared SEN Ali, SEN Ali L, and SEN Eto samples to their parental counterparts, as outlined in Figure 3F. From 37 senescent models, 245 genes were identified as most significantly different (adjusted P-value < $1x10^{-8}$) with at least a 2-fold change in gene expression (Figure 3F, Table S2). GSEA of 50 hallmark gene sets (Liberzon et al., 2016) revealed that gene sets involved in proliferation (MYC targets, G2M checkpoint, E2F targets) were negatively enriched, as well as oxidative phosphorylation, MTORC1 signaling, DNA repair, and unfolded protein response (Figure 3G). The negative enrichment of the MTORC1 signaling and DNA repair pathway gene sets may be the result of decreased proliferation since these gene sets contain many proliferation genes. Although not statistically significant, trends for positive enrichment were seen for gene sets involved in inflammatory responses (interferon-alpha, interferon-gamma, TNF-α signaling via NF-κB, IL-6/JAK/STAT3 signaling). Similarly, the top 20 overrepresented gene ontology terms included gene sets describing mitosis, RNA processing, and DNA damage responses (Figure 3H).

Although cellular senescence was originally characterized as a stable G1 phase cell cycle arrest, later studies challenged this idea and confirmed the existence of a G2 arrest and G2 exit, dependent on *TP53* and *RB1* status (reviewed in Gire and Dulic, 2015). We asked how cell cycle distribution changed upon senescence-induction in cancer cells, often mutated in *TP53*, *RB1,* and *CDKN2A*. Figure S4A shows that cell cycle gene sets have a decreased expression in senescence, consistent with the notion that senescent cells do not proliferate. Remarkably, the *TP53* mutant cells show a different expression pattern than *TP53* wild-type cells. For *TP53* wild-type cells, the expression of G1, M/G1, and G1/S phase gene sets decreased moderately, while the other phase gene sets decreased strongly, consistent with a G1 cell cycle arrest. On the other hand, *TP53* mutant cells were not arrested in a specific cell cycle phase. *RB1* mutant cells also lacked a phase-specific cell cycle arrest, in concordance with the observation that all *RB1* mutant cells in this cell panel also have a *TP53* mutation. The mutation status of other cell cycle genes (*CDKN1A, CDKN2A*) did not appear to relate to this G1 arrest pattern. This suggests that cell cycle arrest of senescent cancer cells is influenced by their *TP53* mutation status. Indeed, it has been shown that alisertib

induces a G1/4N arrest in *TP53*-wildtype HCT116 cells, after an initial G2/M arrest and subsequent mitotic slippage, while *TP53* knockout in these cells leads to further entry into S-phase (Marxer et al., 2014).

Taken together, these data indicate that SEN Ali and SEN Eto were similar in gene expression, while the expression of SEN Ali is dynamic over time and genes involved in proliferation were negatively enriched in senescent cancer cells.
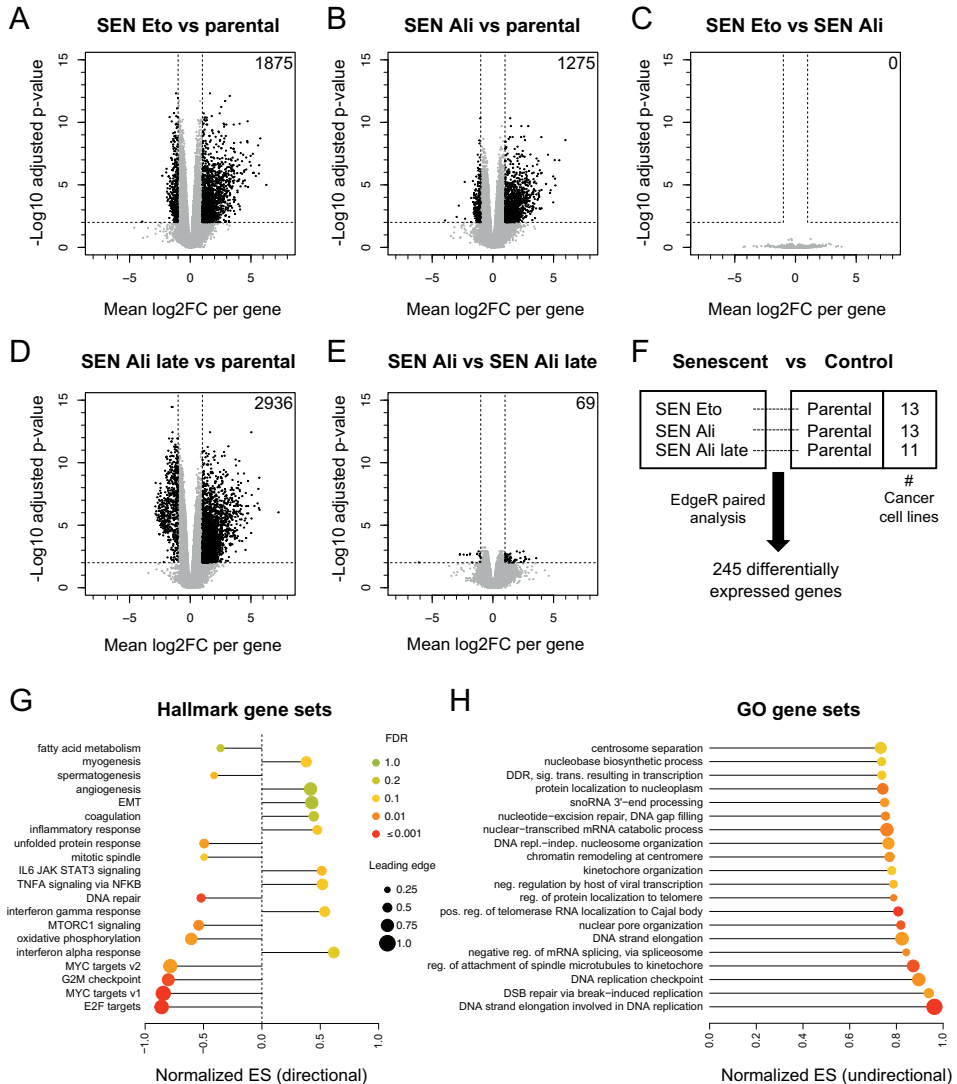

Figure 3. Gene expression in senescent cancer cells changes over time and is independent of alisertib or etoposide trigger. (A-E) Volcano plots exhibit the results from edgeR paired differential expression analyses. Each dot represents a gene with its corresponding mean log2 foldchange (x-axis) and multiple testing corrected *P*-value (-log10, y-axis). Log2FC = log2 foldchange.

Black dots illustrate differentially expressed genes, using a cut-off of $P < 0.01$ and Log2FC > 1 or < -1. **(F)** Outline of samples that were used in the differential gene expression analysis. The paired samples of SEN Eto, SEN Ali, and SEN Ali late contained 13, 13, and 9 cancer cell lines, respectively. **(G-H)** Results of gene set enrichment analyses (GSEAs) for senescent vs control samples (presented in **(F)**). Lollipop chart shows the normalized enrichment scores (ES) where dot color indicates significance level, and dot size represents the leading edge, a measure for the number of genes that contribute to the enrichment of the gene set. **(G)** Top 20 enriched GSEA hallmark gene sets ranked based on normalized ES. Direction of enrichment score indicates negative or positive enrichment in senescent samples. EMT = epithelial mesenchymal transition. **(H)** Top 20 overrepresented GSEA gene ontology gene sets, ranked based on normalized ES. Enrichment score is non-directional. Sig. trans. = Signal transduction, Repl.-indep. = replication independent. Reg. = regulation. Neg. = negative. Pos. = positive. DDR = DNA damage response.

SASP gene expression is heterogeneous among senescent cancer cells

SASP factors produced by senescent cells represent a collection of secreted signaling factors that are involved in inflammatory responses (Coppé et al., 2010). It was surprising that although inflammatory responses were among the top 20 enriched Hallmark gene sets, the enrichment was not significant (Figure 3G). This raised the question of which SASP factors were expressed in the individual senescence models. To assess the expression of genes that potentially contribute to the composition of the SASP, we focused on those that were differentially expressed in senescence and encode secreted proteins. Interestingly, the mean expression of most of these genes was upregulated (Figure S4B), but even for the most highly expressed genes, the expression was not consistently increased in the individual senescent models (Figure 4A). Instead, it seems that the gene expression in the parental state predicts the change in expression upon senescence-induction. For instance, *MMP1, IL6, SAA1,* and *SAA2* are highly expressed in senescent MDA-MB-231 and SUM159, but also show higher baseline levels in the parental state. Principal component analysis of the full transcriptome shows that cells cluster by cell line and cancer type rather than by treatment (Figure S4C). Thus, the baseline expression of parental cells seems to influence the gene expression in the senescent state and determine which SASP factors are expressed.

IL-6 (*IL6*) and IL-8 (*CXCL8*) have been described as classical SASP factors that are consistently upregulated in normal cell senescence and play a role in the maintenance and propagation of SASP expression (Coppé et al., 2010, 2008; Ortiz-Montero et al., 2017). Nonetheless, the baseline expression of *IL6* and *CXCL8* in cancer cells seems to be determined by the cancer tissue type of origin, and, especially for *CXCL8*, ranges from low to high expression (Figure 4B). Upon senescence induction, expression of *IL6* is mostly induced in lung and breast cancer cells with high baseline expression levels, while for *CXCL8,* expression increases for some cell lines but not for others. Overall, these data indicate that the SASP in senescent cancer cells is heterogeneous.

The senescence phenotype is more influenced by cell type than senescence trigger

Above we showed that SEN Ali cells and SEN Eto cells had a similar transcriptome profile (Figure 3C), SASP expression (Figure 4A), and response to ABT-263 (Figure 1C-D). This would suggest that the senescence phenotype is less dependent on the trigger and rather dependent on the cell line model. To expand on this, we asked whether the same trend in response to ABT-263 and SASP factors is seen for two other drugs described to induce senescence: (i) doxorubicin, a DNA intercalator and topoisomerase II inhibitor (Chang et al., 1999; Gewirtz, 1999), and (ii) cyclin dependent kinase (CDK) 2/4/6 inhibitor PF-06873600 (next referred to as PF) (Kumarasamy et al., 2021; Pandey et al., 2020). Four cell line models (A549, HCT116, MCF7, Huh7) were selected based on the cancer type (lung, colon, breast, and liver), response to ABT-263, and expression of IL6).

First, senescence was induced with doxorubicin or PF, as judged by a growth arrest and morphology change, an increase of SA-ß-gal positive cells (Figure 5A, S5A), and the presence of senescence protein markers (Figure 5B). The ABT-263 response of these doxorubicin and PF-induced senescent cells (SEN Dox and SEN PF) was compared to SEN Ali and SEN Eto and was highly similar (Figure 5C). Moreover, the IC_{50} values of the senescent cells were significantly different between cell lines (P < 0.001, two-way ANOVA), while the senescence-inducer only explained 1.84% of the total variation (P = 0.1668, two-way ANOVA). However, Tukey post-hoc test revealed that for MCF7, the response of SEN Ali and SEN Eto was different from SEN Dox and SEN PF (Figure 5D). Although a large SA-ß-gal negative population was detected for SEN PF after ABT-263/DSMO treatment, the SA-ß-gal positive cells still showed little response to ABT-263 (Figure S5B).

Next, we assessed whether expression of SASP genes *IL6, CXCL8, IL1A,* and *IL1B* changed upon different senescence triggers. Interestingly, the expression of *IL6* and *CXCL8* was induced in senescent A549 and Huh7, while HCT116 and MCF7 lacked expression, regardless of the trigger (Figure 5E-F). The difference in SASP expression for *IL6,* and *CXCL8* was significantly different between cell lines (P < 0.001, two-way ANOVA), while the senescence-inducer had no significant contribution (P = 0.103 and 0.08 respectively). The expression of *IL1A* and *IL1B* remained low in all samples, below the accurate detection limit of qPCR (not shown). On a cautionary note, MCF7 SEN PF did not show a decrease in *LMNB1*, while the other senescent MCF7 cells did, which indicates a less efficient senescence-induction (Figure S5C).

An explanation why *IL6* and *CXCL8* were not expressed in senescent HCT116 and MCF7 is that these cells are intrinsically incapable of activating these genes, for instance, due to a repressive chromatin state or a lack of NF-kB activation (Lopes-Paciencia et al., 2019). To test this, we transduced A549, HCT116, and MCF7 with a lentiviral NF-kB reporter (Wilson et al., 2013), and subsequent exposure to protein

kinase C activator phorbol myristate acetate (PMA) increased NF-kB activity in A549 and HCT116, but not in MCF7. In addition, exposure to tumor necrosis factor (TNF)-αincreased NF-kB activity in all cell lines (Figure 5G). Therefore, although NF-kB is less primed for activation in MCF7, it is still activatable. Next, we checked whether the activation of NF-kB would drive the expression of *IL6* and *CXCL8*. Interestingly, expression was strongly increased in A549, while expression remained absent in HCT116, similar as in senescence (Figure 5H). This suggests that *IL6* and *CXCL8* might be silenced in HCT116, but not in A549. However, MCF7 lacked expression of *IL6* but did show an increase in *CXCL8* upon stimulation with PMA and TNF-alpha (Figure 5H). Although it is known that unraveling the variability of SASP is highly complex and still poorly understood (Cuollo et al., 2020), collectively these results hint towards a cell line intrinsic inability to express certain cytokines. Overall, it becomes apparent that the senescence phenotype is influenced by the nature of the cell line, and to a lesser extent by the senescence-trigger.

SENCAN classifier for cancer cell senescence
Given the fluctuating and heterogeneous gene expression of senescent cells in general (Hernandez-Segura et al., 2017) and the apparent influence of parental cell characteristics, we studied whether a machine learning approach could be used to find a classifier that identifies senescent cancer cells based on gene expression measurements. Although the expression of genes in the existing senescence gene signatures change consistently between senescent cells and a reference control sample, there was no threshold at which samples would be accurately classified as senescent or not using singscore (Foroutan et al., 2018) or ssGSEA (Figure 6A and supplementary figure S6A). Therefore, we compared several classification methods (ridge regression, elastic net, random forest, support vector machines, and Gaussian processes) through "leave-all-samples-of-one-cell-line-out"-cross validation (see Methods for details). Among these, elastic net (Zou and Hastie, 2005) gave the best performance, and we continued the rest of the analysis with that method. To provide the classifier with additional examples of non-senescent cells, we also included 45 untreated samples from the Cancer Cell Line Encyclopedia (Table S3). The elastic net classifier was able to classify almost all samples correctly as either senescent or not (Figure 6B). The only sample that was classified incorrectly was Hep3B after 7-day alisertib treatment. The alisertib-treated PC9 sample received a score of 0.44, however, 7-day alisertib treatment indeed only induced about 40-60% senescent cells in this cell line (see Figure 1D).
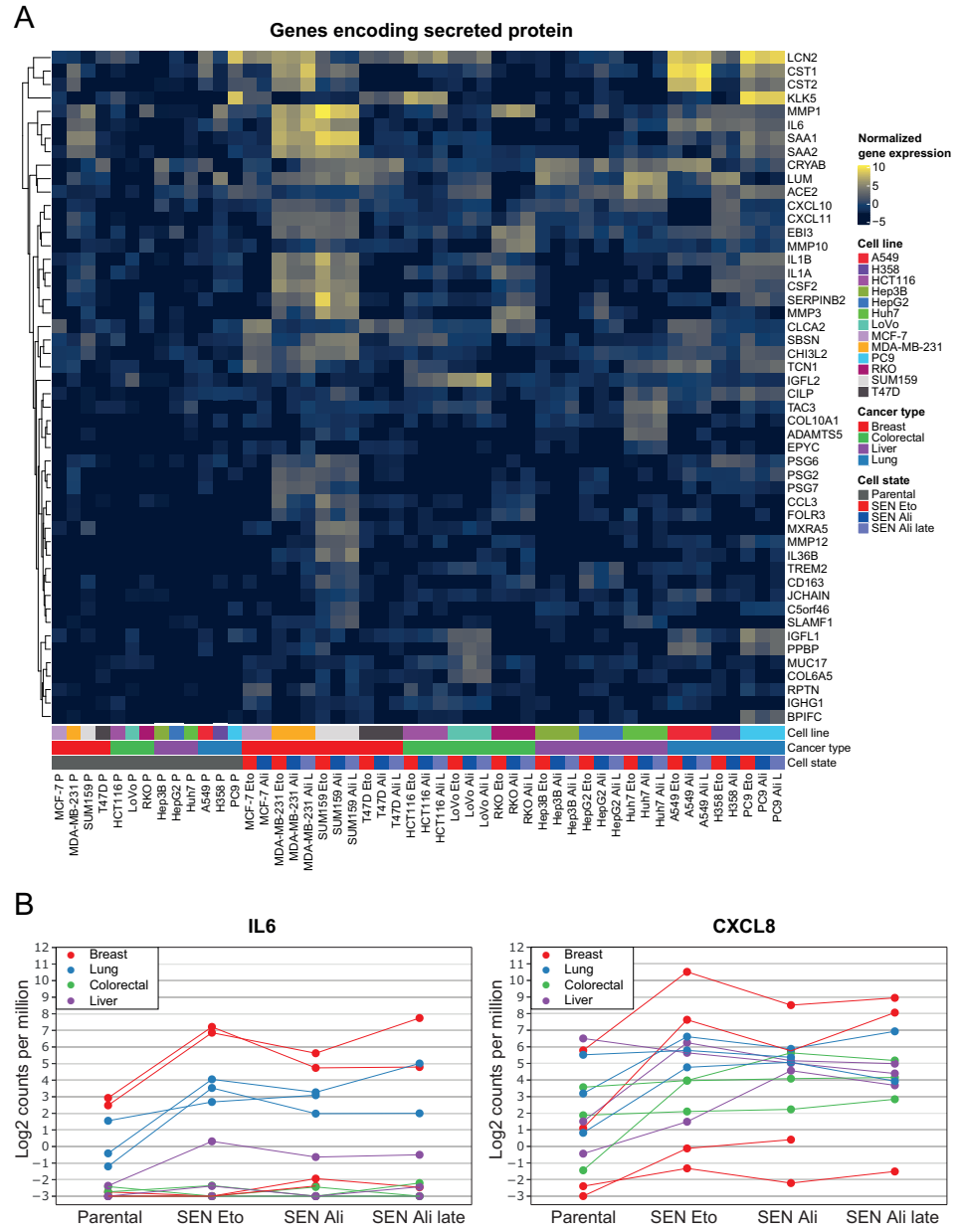
Figure 4. SASP gene expression is heterogeneous among senescent cancer cells. (A) Heatmap representing supervised hierarchical clustering of the gene expression of 62 differentially expressed genes encoding secreted protein. **(B)** Beeswarm plots for the gene expression of IL6 and CXCL8 genes. Each dot represents a cell line.

After the optimal parameter settings were determined in cross-validation, an elastic net was trained on all samples employing the optimal settings, yielding the SENCAN classifier for classifying senescence in cancer samples. The 137 genes selected by the SENCAN classifier (Table S4) include several well-known senescence-associated genes (*CDKN1A* and *HMGB1*), as well as genes involved in mRNA processing and splicing (like *SNRPA* and *SRSF2*), interferon response genes (like *IFIT2* and *ISG15*), histone variants (like *H4C8* and *H2AC20*), and the telomere regulator *RTEL1*. Apart from *CDKN1A*, no other genes clearly associated with proliferation were selected. Interestingly, the SENCAN classifier also comprised various long non-coding RNAs, novel transcripts, and antisense transcripts. Some of the novel transcripts aligned downstream and in close proximity to known protein-coding genes (such as AL512306.2, downstream of *MDM4*). It could be that AL512306.2 is specifically upregulated in senescence, however, the reads aligning to AL512306.2 may also be the result of transcriptional readthrough of *MDM4*. Transcriptional readthrough has been associated with senescence before (Muniz et al., 2017). In line with this, there were also more reads located between *MDM4* and AL512306.2 in senescent samples than in the parentals ($P < 0.001$ by *t*-test), while there are no transcripts annotated in that region. Altogether, it appears that the SENCAN classifier uses several different processes to identify senescent samples, including mRNA processing, interferon response, and a signal that may be derived from transcriptional readthrough.

To validate the SENCAN classifier, we searched the literature for RNA sequencing samples of senescent cancer cells and found five datasets where senescence was induced in other cell lines and/or by means other than alisertib and etoposide (Table S5). This included data from Nojima *et al.* (2018), Ávila-López *et al.* (2021), Kolesnichenko *et al.* (2019), and datasets from Wang C *et al.* (2019) and Wang L *et al.* (2017) derived from previous studies from our own laboratory. In these five external datasets, the SENCAN classifier was able to correctly distinguish senescent from non-senescent samples in 44 out of 49 samples (90% accuracy, Figure 6C; precision = 0.94, sensitivity = 0.8, specificity = 0.97). Three incorrectly classified samples were from Wang C *et al.* (2019): SK-Hep1 cells treated with XL413, which were described as non-senescent due to their wild-type *TP53* status, but scored as senescent by the classifier (score of 0.81), and PLC and Hep3B cells treated with XL413, which were defined as senescent, but received a non-senescent score (0.10 and 0.37 respectively). The H2A.Z knockdown samples from Ávila-López et al. (2021) were also not classified as senescent, but it should be noted that although these samples were described as senescent, they contained less than 50% of senescent cells (Ávila-López et al., 2021). This indicates that the classifier may only classify a sample as senescent if the majority of cells are senescent.

Although our aim was to build a classifier for senescent cancer cells, we asked how the classifier would behave on normal senescent cells. Therefore, we scored

3

samples from Casella *et al.* (2019), which included HAEC and HUVEC endothelial cells, and IMR-90 and WI-38 fibroblast cells made senescent via various triggers (Figure 6D). Notably, the SENCAN classifier correctly classified the fibroblast and HUVEC samples, but could not detect senescence in the irradiated endothelial HAEC samples. HAEC cells did not upregulate *CDKN1A* at the transcript level (Casella et al., 2019), so their type of senescence may indeed be different from that observed in cancer cells.

Next, to test if the classifier could distinguish senescent from quiescent cells, we attempted to obtain multiple proliferation-arrested cancer cells by serum starvation. Inducing stable quiescence only succeeded for A549, indicated by a proliferation arrest (Figure S6C), accumulation of cells in G0/G1, and increased Ki67 negative cells after serum starvation (Figure S6D). The SENCAN classifier scored both the quiescent population and control as non-senescent (scores of $3.5 \cdot 10^{-7}$ and 0.0016 respectively), suggesting that the SENCAN classifier is able to distinguish senescence from quiescence.

Finally, we wondered if the SENCAN classifier could be validated for detecting senescence in *in vivo* cancer samples. We were able to find only one publicly available dataset with RNA sequencing data of senescent human cancer cells *in vivo* (Mainardi et al., 2018); this study used patient-derived xenografts (PDXs) of non-small cell lung cancer in mice, which were treated with the SHP2-inhibitor SHP099. The PDX samples from which RNA sequencing was available ('PDX2') were not unambiguously senescent, since a minority of cancer cells stained SA-ß-gal positive (Mainardi et al., 2018). The SENCAN classifier classified all of these PDX samples as non-senescent (Figure S6E). This could indicate that the classifier is not able to detect senescence in *in vivo* samples, or that samples do not receive a high senescence score when only a minority of cells are senescent, similar to the *in vitro* samples of Ávila-López et al. (2021) described above. It is therefore unclear whether the classifier is accurate for use *in vivo*.

Taken together, the SENCAN classifier is able to accurately detect senescence in many cancer cells and fibroblasts (Figure 6E and S6B) *in vitro*, although a low senescence score does not completely rule out that cells are senescent, and a separate line of evidence is still necessary to unambiguously identify senescent cells.
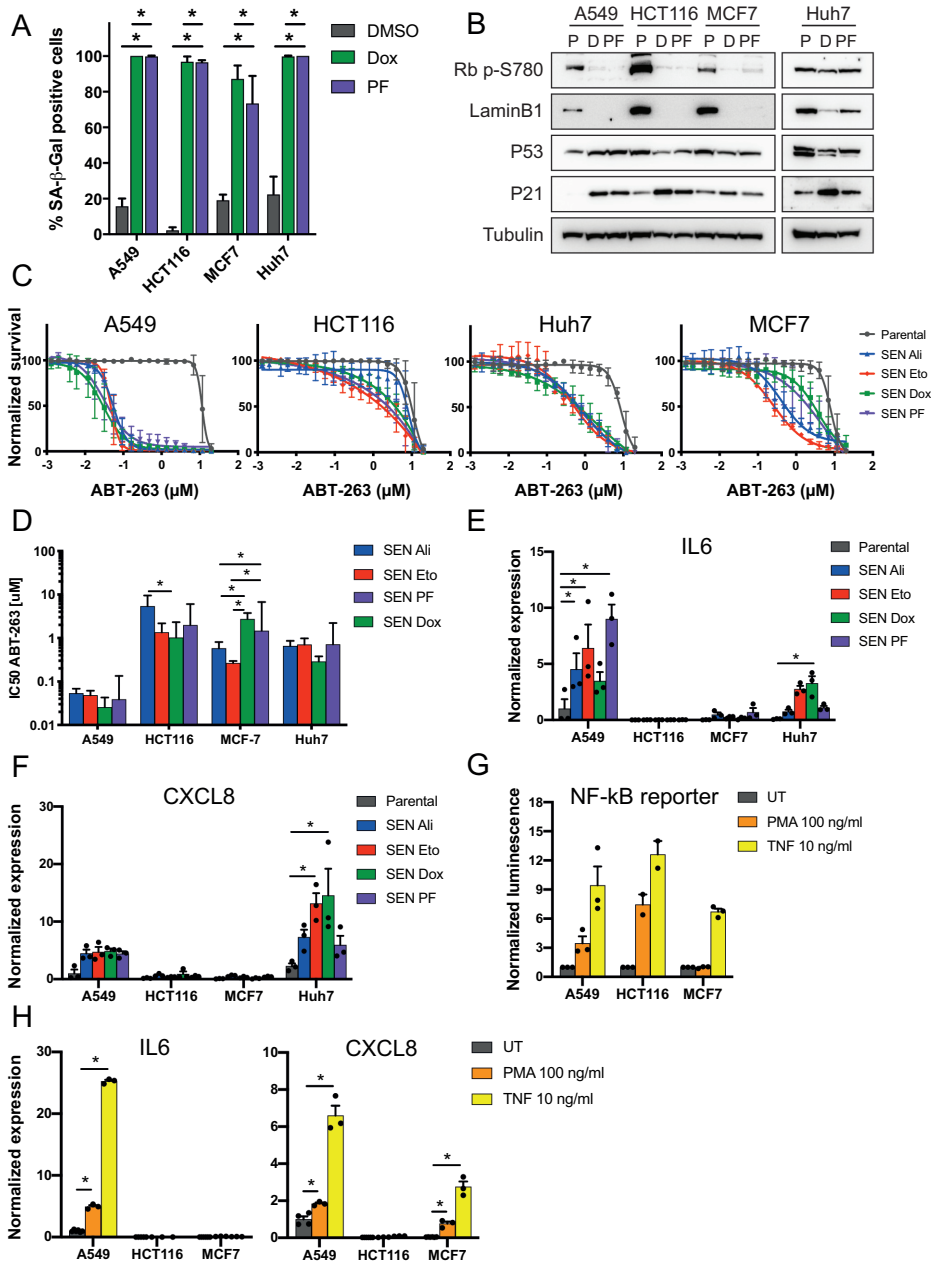
Figure 5. The senescence phenotype is more influenced by cell type than senescence trigger. (A) Quantification of SA-ß-gal positive cells for cells treated for 7 days with DMSO, doxorubicin, or PF = PF-06873600 (images are shown in Figure S5A). Bars represent the mean ±SEM. Data is obtained in triplicate and analyzed with a two-sided Student's *t*-test. *$P < 0.0001$. **(B)** Western blot for senescence markers for cells treated for 7 days. P = parental. D = doxorubicin. **(C-F)** SEN Ali = alisertib-induced senescent, SEN Eto = etoposide-induced senescent, SEN Dox = doxorubicin-induced senescent, SEN PF = PF-06873600-induced senescent. **(C)** Dose-response curves for ABT-263. Values represent the mean ±SEM of three independent experiments. **(D)** Bar graph of ABT-263 IC50 values extrapolated from dose-response curves presented in C. Data were analyzed with two-way ANOVA and post-hoc

Tukey test. * *p* adjusted <0.01. (**E-F**) Normalized mRNA expression determined by qPCR. Expression is relative to GAPDH and normalized to A549 parental. (**G**) Luciferase luminescence measurements derived from cells transduced with NF-KB reporter. (**H**) Normalized mRNA expression determined by qPCR. Expression is relative to GAPDH and normalized to A549 parental. (**D-H**) Values represent the mean ±SEM of three independent experiments. * *P* <0.01 Dots represent the mean of technical duplicates.
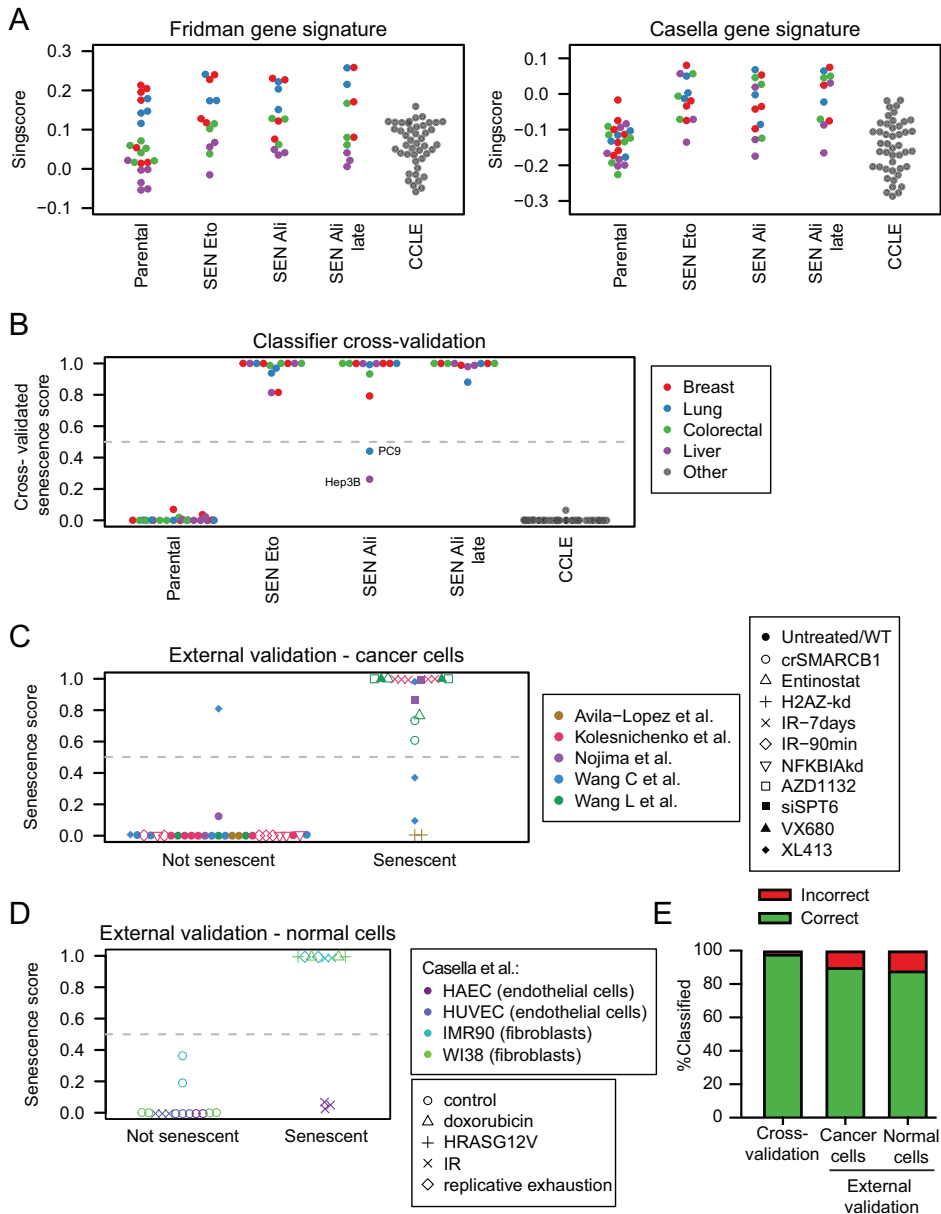

Figure 6. Validation of SENCAN elastic net classifier for cancer cell senescence. (**A**) Singscores for Fridman and Casella gene expression signatures. Each dot represents a cell line. CCLE = Cancer

Cell Line Encyclopedia. **(B)** SENCAN scores in cross-validation; all samples of one cell line were left out and the elastic net was trained on the remaining cell lines.
(C) SENCAN scores of external validation samples from senescent cancer cells (GSE110028; GSE129182; GSE121276; GSE102639, GSE158743). **(D)** Senescence scores of 25 normal cells of Casella et al. (2019) (GSE130727). **(E)** SENCAN classifier performance in cross-validation (in B) and external validation sets (in C and D).

Discussion

Here, we report a Cancer SENESCopedia, which encompasses transcriptome and senolytic response data from a panel of senescent cancer cells, with the aim to find universal weaknesses for senotherapy and ubiquitous markers of cancer cell senescence. Our data show that the senolytic response to ABT-263 is highly divergent among cell lines but remarkably similar for senescent cells induced with alisertib, etoposide, doxorubicin, and PF-06873600. Although ABT-263 has been described as a broad-spectrum senolytic and eliminated various senescent cells *in vivo* (Bussian et al., 2018; Chang et al., 2016; Childs et al., 2016; Demaria et al., 2016; Kim et al., 2017; Pan et al., 2017), a cell type-specificity has been reported before in senescent preadipocytes (Zhu et al. 2016) and doxorubicin-induced senescent breast cancer cells (Shahbandi et al., 2020). Since a (transient) DNA damage response (DDR) can be activated by the drugs we used to induce senescence (Montecucco et al., 2015; Niu et al., 2015; Tacar et al., 2013; Wang et al., 2020), and since the senescence transcriptome was similar between senescent cells triggered via different drugs, it might be possible that senescence is triggered via DDR and that a similar senescence phenotype is elicited in a given cell line, regardless of the DDR-inducer.

   Our results highlight that the therapeutic potential of senolytic approaches based on BCL-2 family inhibition in cancer treatment will be context-dependent. Although the clinical use of ABT-263 is partly hampered by its on-target platelet toxicity (Kaefer et al., 2014), others have recently developed modified versions of ABT-263 that spare platelets (González-Gualda et al., 2020; He et al., 2020; Khan et al., 2019). With these and potentially other ABT-263 based senotherapies on the horizon, it will be important to elucidate why certain senescent cells respond while others remain unresponsive. Mechanisms that are likely involved are the activity of anti-apoptotic proteins BFL-1 or MCL-1; effects of ABT-263 on the stability of MCL1 (Wang et al., 2014) or lacking activity of pro-apoptotic proteins in ABT-263 unresponsive cells. Indeed, the most unresponsive cell line LoVo contains biallelic frameshift mutations in *BAX*, and HCT116 carries a heterozygous mutation for this gene. This could explain their resistance to ABT-263. Moreover, overexpression of NOXA, which inhibits MCL-1, conferred sensitivity in doxorubicin-induced senescent breast cancer cells (Shahbandi et al., 2020). In future experiments, we plan to investigate

the pro- and anti-apoptotic signaling using BH3 profiling (Touzeau et al., 2016).

The consequences of senescent cells within a tumor micro-environment are attributed to their unique SASP mixture. Our data indicate that the expression levels of SASP genes vary strongly between various cancer types, which is in line with previous research that reported a significant heterogeneity in gene expression among senescent cells (Basisty et al., 2020; Hernandez-Segura et al., 2017), with even cell-to-cell variability (Wiley et al., 2017) and changes over time (Hernandez-Segura et al., 2017; Martínez-Zamudio et al., 2020). Our data show that even IL-6 and IL-8, often used as senescence markers, are expressed at variable levels at baseline and senescence-induction changes their expression diversely, mostly depending on the cell line and less on the trigger. Although it is still understood poorly what drives these differences, proposed mechanisms are the chromatin state of SASP genes, *TP53* mutation status, and the activity of NF-kB and C/EBP isoforms (Cuollo et al., 2020). Recently, it has been shown in pre-clinical models of pancreatic cancer that a combination of pro-senescence therapy and checkpoint blockade can be an efficient combination therapy (Ruscetti et al., 2020). Given the heterogeneous nature of the SASP produced in our senescent cancer cell line panel, it remains to be determined whether this treatment strategy has broad applicability. In this context, it is important to note that two recent papers have reported that IL-8 levels in plasma, tumor, and peripheral blood mononuclear cells are associated with reduced response to immune checkpoint inhibitors (Schalper et al., 2020; Yuen et al., 2020). It will therefore be critical to distinguish which type of cytokines and chemokines are secreted by senescent cells from different tumor origins.

The heterogeneity of the senescence phenotype makes it challenging to find markers that unequivocally detect senescence (Gorgoulis et al., 2019). Moreover, current gene expression signatures for senescence measure the enrichment of senescence genes compared to a reference sample, but we show that the ssGSEA or singscores for these gene sets were not effective to determine the senescent state in an individual sample. We present here the SENCAN classifier for cancer senescence that measures the probability that a sample is senescent based on RNA-seq data. It is interesting that the classifier did not select genes that were involved in proliferation, but rather in mRNA processing, interferon responses, and a signal that seems to result from transcriptional readthrough. This could explain why the classifier is more robust in detecting the senescent state in cancer compared to conventional hallmark gene signatures for senescence. Since the classifier includes long-non-coding RNA features, we advise to use the classifier on samples sequenced with poly-A capture and adhere to the analysis script (available as webtool). We also asked how the SENCAN classifier performed *in vivo,* but we were unable to unambiguously validate whether the classifier is suitable for in vivo use. However, most likely a large set of *in vivo* samples where high levels of senescence are induced

is necessary to train and validate an *in vivo* classifier.

This work underscores the context-dependency of the senescence cancer phenotype and compares the characteristics of senescent cancer cells in a sizeable number of senescence models. Our data also emphasize the need for a systematic approach to study the pleiotropic nature of senescence. Besides already existing (relational) databases, like SeneQuest (Gorgoulis et al., 2019), Human Ageing Genomic Resources (HAGR) (de Magalhães et al., 2005), and SASP Atlas (Basisty et al., 2020), multi-parametric testing will be pivotal to map senotherapy responses, SASP compositions and the various effects of senescent tumor cells. We share an interactive online Cancer SENESCopedia interface (available at https://ccb.nki.nl/publications/cancer-senescence/), which allows interrogation of the gene expression pattern of senescent cancer cells and provides the SENCAN classifier as a tool to classify whether cancer cells are senescent using transcriptome data as input. This will help to unify the validation and detection of cancer cell senescence in the path towards understanding and eliminating senescent cells in each cancerous context.

3

Acknowledgments

Methods

Cell lines

Liver cancer cell lines HepG2 (RRID:CVCL_0027), Huh7 (RRID:CVCL_0336), Hep3B (RRID:CVCL_0326), triple-negative breast cancer (TNBC) cell line MDA-MB-231 (RRID:CVCL_0062) were maintained in DMEM medium supplemented with 10% fetal bovine serum (FBS, Serana), 1% penicillin/streptomycin (P/S, Gibco) and 2mM L-glutamine (Gibco). Colon cancer cell lines HCT116 (RRID:CVCL_0291), RKO (RRID:CVCL_0504), LoVo (RRID:CVCL_0399) and lung cancer cell lines A549 (RRID:CVCL_0023), PC9 (RRID:CVCL_B260) and H358 (RRID:CVCL_1559) were cultured in RPMI medium (Gibco) supplemented with 10% FBS, 1% P/S and 2mM L-glutamine (Gibco). ER+ breast cancer cell lines MCF-7 (RRID:CVCL_0031) and T47D (RRID:CVCL_0553) were grown in RPMI (Gibco) supplemented with 10% FBS, 1% P/S and 10 µg/ml insulin (Sigma-Aldrich). TNBC cell line SUM159 (RRID:CVCL_5423) was maintained in DMEM/F12 (Gibco) medium supplemented with 10% FBS, 1% P/S and 5 µg/ml insulin and 1ug/ml hydrocortisone (Sigma-Aldrich).

HepG2 (RRID:CVCL_0027), Huh7 (RRID:CVCL_0336), and Hep3B (RRID:CVCL_0326) were provided by Erasmus University (Rotterdam, Netherlands), SUM159 was provided by Metello Innocenti (NKI, Amsterdam). Other cell lines were purchased from ATCC. All cell lines were regularly tested for mycoplasma contamination and their identity was validated via short tandem repeat analysis (by Eurofins Genomics). The STR profiles were analyzed with CLASTR (Robin et al., 2020). Cell lines derived from female: MCF7, T47D, MDA-MB-231, SUM159, RKO, Huh7, Hep3B, PC9. Cell lines derived from male: HCT116, LoVo, HepG2, A549, H358. Based on STR profiling, HCT116, LoVo, and HepG2 have lost their Y-chromosome.

Colony Formation Assay
Cells were grown for 7 days in 6-well until 80-90% confluency, 15k cells were seeded for A549 and 20k cells for HCT116. Alisertib (Medkoo Bioscience) and etoposide (Medkoo Bioscience) drugs were refreshed every 3-4 days. Colonies were fixed with 4% paraformaldehyde (v/v) and stained with 0.5% crystal violet (w/v) for visualization.

IncuCyte Assay
A549 cells (20k/well) and HCT116 cells (40k/well) were seeded in 96-well and cultured for 7 days. Confluency was measured by IncuCyte ® every 4 h.

Senescence-Associated β-Galactosidase Activity (SA-β-Gal) Staining
Cells were stained for SA-β-Gal activity with the Senescence Cells Histochemical Staining Kit (cat#: CS0030) from Sigma-Aldrich. The staining was performed according to manufacturer's instructions. To assess senescence-induction, SA-β-gal positive cells were determined from three independent experiments, and at least 100 cells were counted per condition.

For quantification of SA-β-gal cells after ABT-263 treatment, cells were seeded into a 6-well and treated with alisertib or etoposide for 7 days, and medium was subsequently replaced by medium supplemented with DMSO or 1μM ABT-263. Cells were cultured for another 5 days before SA-ß-gal staining was performed. The total number of cells were counted from 3 images from the same experiment. Images were taken at 100x magnification, 5 images per well.

Senescence-induction
Cells were seeded in 150 mm dishes at the following cell densities and treated with the following alisertib (Ali), etoposide (Eto), doxorubicin (Dox), or PF-06873600 (PF) concentrations: MCF7, 2.5×10^6 cells, 1 μM Ali, 2.5 μM Eto, 0.13 μM Dox, 1 μM PF; T47D, 2.5×10^6 cells, 3 μM Ali, 0.5 μM Eto; MDA-MB-231, 2.0×10^6 cells, 0.5 μM Ali, 1.25 μM Eto; SUM159, 7.5×10^5 cells, 0.5 μM Ali, 0.5 μM Eto; HCT116, 2.5×10^6 cells, 0.5 μM Ali, 3 μM Eto, 0.5 μM Dox, 0.38 μM PF; LoVo, 3.0×10^6 cells, 0.25 μM Ali, 1 μM Eto; RKO, 2.0×10^6

cells, 0.5 μM Ali, 2.0 μM Eto; Huh7, 5.0×10^5 cells, 0.25 μM Ali, 0.5 μM Eto, 0.13 μM Dox, 0.5 μM PF; Hep3B, 1.0×10^6 cells, 0.25 μM Ali, 0.321 μM Eto; HepG2, 1.0×10^6 cells, 0.5 μM Ali, 2.5 μM Eto. A549, 5.0×10^5 cells, 0.5 μM Ali, 1.25 μM Eto, 0.13 μM Dox, 0.5 μM PF; NCI-H358, 1.0×10^6 cells, 0.25 μM Ali, 1 μM Eto; PC9, 1.0×10^6 cells, 0.125 μM Ali, 4 μM Eto. 24h after seeding, cells were treated and drug was refreshed every 3 to 4 days. After 7 days of treatment, the cells reached about 70-90% confluency and were senescent. For downstream applications, senescent cells from one 150 mm dish were reseeded into a full 96-well plate (96 x 96-wells) or a full 6-well plate (6 x 6-wells).

Dose-response assay
After senescence-induction of 7 days (see senescence-induction method), cells were reseeded in 96-well and treated with a range of concentrations of ABT-263 using the HP D300 Digital Dispenser. Cell viability was assessed in a CellTiter-Blue assay with resazurin sodium salt (sigma-Aldrich, #R7017) and measured with EnVision 2104 Multilabel Reader (PerkinElmer). Half maximal inhibitory concentration (IC50) was estimated using the three-parameter logistic curve

$$y = a + \frac{(1-a)}{1+10^{h \cdot (x-IC_{50}) - log_{10}(\frac{1-a}{0.5}-1)}},$$

where y is the viability measurement normalized to the positive and negative controls, x is the drug concentration, a is the maximal inhibition, h is the steepness and IC_{50} is the log_{10}-transformed half maximal inhibitory concentration. This equation was fitted to the viability measurements with robust non-linear regression (M-estimator with iterative reweighted least squares). Phenylarsine oxide (Sigma-Aldrich, cat:#P3075) was used as a positive control and DMSO as a negative control. The senolytic index for ABT-263 represents the IC50 value for parental cells divided by the mean IC50 value of etoposide- and alisertib-induced senescent cells. Assays were run in technical triplicates, in three independent experiments.

Quantitative Real-time PCR (qPCR)
Total RNA was extracted using ISOLATE II RNA Mini kit (Bioline, cat#BIO-52073). RNA was retrotranscribed using SensiFAST cDNA Synthesis kit (Bioline, cat#BIO-65054). qPCR reactions were performed with SensiFAST SYBR Lo-ROX mix (Bioline, cat#BIO94020) and the following primers: GAPDH_Fw: AATCCCATCACCATCTTCCA, GAPDH_Rv: TGGACTCCACGACGTACTCA, IL6_Fw: ACTCACCTCTTCAGAACGAATTG, IL6_Rv: CCATCTTTGGAAGGTTCAGGTTG, IL8_Fw: TCCTGATTTCTGCAGCTCTGT, IL8_Rv: AAATTTGGGGTGGAAAGGTT, LMNB1_Fw: TTCTCGAAGCTTGATCTGGG, LMNB1_

Rev: GATCGAGCTGGGCAAGTG. All procedures were executed according to the manufacturer's instructions. Briefly, qPCR assays were run in 96-well on the 7500 Fast Real-Time PCR System (Applied Biosystems, Thermo Fisher Scientific) with the following thermal profile: 1 cycle at 95 °C for 20 min, 40 cycles at 95 °C for 3 s, 60 °C for 30 s, and 72 °C for 15 s. Melting curve analysis was performed ramping from 60 °C to 90 °C and rising by 0.5 °C every 2 s. Normalized mRNA expression was calculated using the $2^{-\Delta\Delta CT}$ method. GAPDH was used as the housekeeping gene, and A549 parental sample served as control in figure 5E, F and H, while parental T47D parental served as control sample in figure S5E. Assays were run in technical duplicates, in three independent experiments.

Western blot

Cells were seeded in 150-mm cell culture dishes and were treated with alisertib, etoposide for 7 days (See senescence-induction method), and 24h drug-washout. Then, cells were washed with cold PBS and lysed with RIPA buffer [25mM Tris-Cl (pH7.5), 1% NP40, 1% sodium deoxycholate, 0.1% SDS, and 150mM NaCl], supplemented with Halt™ Protease & Phosphatase Single-Use Inhibitor cocktail (Thermo Scientific, cat:#78442). After centrifugation for 30 min at 14.000 rpm at 4 °C, supernatant was collected. Protein concentrations were determined using Pierce™ BCA assay (Thermo Scientific, cat:# 23225), according to manufacturer's instructions. Samples were denatured with Bolt™ Sample Reducing Agent (Thermo Fisher, cat:#B0009) followed by 5 min incubation at 95 °C. After that, sampels were resolved on a 5-15% Bis-Tris gel (Thermo Fisher) and run (SDS-PAGE) for 30 min at 200V. Proteins were transferred to a polyvinylidene fluoride (PVDF) membrane at 340 mA for 120 min. Blocking, incubation of primary and secondary antibody was performed under conditions recommended by the manufacturer. Primary antibodies detected Phospho-S780 Rb (RRID: AB_10950972), Lamin B1 (RRID:AB_2650517), P53 (RRID:AB_331743), Phospho-S15 P53 (RRID: AB_331741), P21 (RRID:AB_2890611), P16 (RRID:AB_10858268), Phospho-Histone (gamma) H2A.X (Ser139) (RRID:AB_309864), Alpha-Tubulin (RRID: AB_477593). Membranes were incubated with a 1:10000 dilution of secondary HRP conjugated anti-mouse (RRID: AB_11125547) or anti-rabbit (RRID: AB_11125142) antibody for 1 hour in blocking solution. After washing, a chemiluminescence substrate (ECL, Bio-Rad) was added to visualize the protein signal on the ChemiDoc (Bio-Rad).

NF-kB activation experiments

To generate NF-kB reporter cell lines, cells were transduced with a lentiviral construct containing four tandem copies of the NF-kB consensus sequence upstream a minimal promoter controlling the firefly luciferase reporter gene (Wilson et al., 2013) (addgene #49343). Transduced cells have been FACS sorted by

using the constitutive expression of the GFP reporter gene present in the construct.

For the NF- kB stimulation experiments, reporter cells were plated in 96-wells for overnight stimulation with PMA 100 ng/ml or TNF 10 ng/ml. NF-kB activation level has been assessed by measuring luciferase signal with the Luciferase Assay System (Promega, cat:#E1500), according to manufacturer's protocol. Luciferase signal is shown as average of three biological replicates.

RNA-sequencing

Cells were seeded in 150-mm cell culture dishes and were treated with alisertib or etoposide for 7 days (See senescence-induction method). Senescent cells were cultured for 24 h without drug before total RNA was extracted with RNeasy mini kit (Qiagen, cat# 74106), including a column DNase digestion (Qiagen, cat#79254), according to manufacturer's instruction. Quality and quantity of total RNA was assessed by the 2100 Bioanalyzer using a Nano chip (Agilent, Santa Clara, CA). Total RNA samples having RIN>8 were subjected to library generation.

Strand-specific libraries were generated using the TruSeq Stranded mRNA samples preparation kit (illumine Inc., San Diego, RS-122-2101/2) according to manufacturer's instructions (Illumina, part #15031047 Rev.E). Briefly, polyadenylated RNA from intact total RNA was purified using oligo-dT beads. Following purification, the RNA was fragmented, random primed and reverse transcribed using SuperScript II Reverse Transcriptase (Invitrogen, part # 18064-014) with the addition of Actinomycin D. Second strand synthesis was performed using Polymerase I and RNaseH with replacement of dTTP for dUTP. The generated cDNA fragments were 3' end adenylated and ligated to Illumina Paired-end sequencing adapters and subsequently amplified by 12 cycles of PCR. The libraries were analyzed on a 2100 Bioanalyzer using a 7500 chip (Agilent, Santa Clara, CA), diluted and pooled equimolar into a multiplex sequencing pool. The libraries were sequenced with single-end 65bp reads on a HiSeq 2500 using V4 chemistry (Illumina inc., San Diego).

Transcript levels were quantified using kallisto (v0.46) and summed to gene level. As reference transcriptome, Gencode v34 was used, where we filtered out transcripts from genes annotated as unexpressed pseudogenes as well as transcripts with a transcript support level of 5, unless the transcript has a consensus coding sequence identifier. The gene expression levels were normalized between samples with edgeR (v3.26.8) using trimmed mean of M-values with singleton pairing. For differential gene expression analysis the estimated kallisto counts were used directly, and for other downstream analysis, log2-transformed counts per millions were used. Transformed gene expression values are available in Table S6.

Gene set enrichment analysis

For calculating single-sample gene set scores, we used single-sample gene set

enrichment analysis (ssGSEA) (Barbie et al., 2009), as implemented in the GSVA R package (Hänzelmann et al., 2013). Delta ssGSEA scores represent the difference between treated samples and their parental counterparts. The scores were adjusted for gene set size and normalized per gene set. Senescent gene sets are summarized in Table S1.

For differential gene set enrichment analysis, we used the flexgsea R package (Bismeijer and Kim, 2019) with the default weighted KS-like statistic (Subramanian et al., 2005). Significance was estimated by sample permutation. For gene sets without direction, absolute enrichment scores were used. As gene sets, we used the MSigDB Hallmark and Gene Ontology (GO) biological process sets (Liberzon et al., 2015). For the GO terms, REVIGO (Supek et al., 2011) was used on the enrichment scores with the "small" setting to obtain a summarized list.

Differential gene expression analysis

Differentially expressed genes were identified with edgeR using generalized linear models (GLMs) (McCarthy et al., 2012) and quasi-likelihood F-tests. First, the dispersion was estimated from the samples which were sequenced in duplicate, with a GLM with a factor for every condition. Using these dispersion estimates, a GLM was fitted with a factor for each cell line, and either a factor per treatment (for the treatment-specific DGEA), or a factor for senescence status (for the DGEA of all treatments together). P-values were adjusted for multiple testing by false discovery rate correction.

Cell cycle analysis

To estimate the change in cell cycle distribution from the gene expression values, we calculated the average expression of genes specific for each cell cycle phase in the untreated cells relative to the untreated cells. For this, we used the marker genes from Mizuno *et al.* (2009). First, we calculated the average expression for each cell cycle phase as follows, for every sample:

$$y_{i,j} = \frac{1}{N_i} \sum_{k=1}^{N_i} x_{j,k},$$

where i indicates a geneset of a specific cell cycle phase, j indicates a sample and k indices the genes in geneset i; x is the $\log_2$ counpts per million, and N_i is the amount of genes in geneset i, and $y_{i,j}$ is the resulting score. The scores shown in the heatmap in Supplementary Figure 4 were calculated by taking the difference in the score y for a sample and the corresponding untreated cell.

Senescence classifier

We used our cell line panel and CCLE samples as input to the classifier. We first selected CCLE samples corresponding to the same cell lines used in our panel and performed a DGEA to identify genes which were significantly different between our study and the CCLE samples – these genes reflect genes which are variable between sites and were excluded from the classifier (1,448 genes). We then selected 45 other CCLE samples (3 cell lines each for the 15 main cancer types in CCLE which were not included in our panel, Table S3). In the classifier, these CCLE samples were given a weight such that the total weight of untreated and senescent samples was equal. Log_2 counts per million for each gene were mean-centered and normalized by dividing by the weighted standard deviation over all samples. We further excluded genes for which the 95$^{\text{th}}$ percentile was below 1 count per million and filtered out all mitochondrial-encoded genes as the mitochondrial content is likely to differ significantly between sample preparations, leaving 17,405 genes as input for the elastic net. An elastic net with logistic link function was fitted with double-loop cross-validation (CV), with fixed mixing parameter α=0.7, using the glmnet R package (Friedman et al., 2010).The inner CV loop was used to selected the optimal , using the 1-standard error rule. The outer CV loop was used to estimate classification performance. In both CV loops, a cross-validation fold constituted of leaving out all samples from one cell line and training on the remaining set (resulting in two cell lines being left out in the inner loop). Several other classification methods were tried, but were found to give worse performance.

After this cross-validation, an elastic net was fitted on all samples with single-loop CV to optimize λ. Gene expression of external samples was re-quantified from the raw reads using the same procedure described above in the RNA-sequencing section, with the same reference transcriptome. Estimated read counts were adjusted to our gene expression data using edgeR with trimmed mean of M-values with singleton pairing against the reference sample in our dataset. To ensure that samples with a very high sequencing depth have comparable expression values, log2 counts per million values below the minimum value observed in our dataset were clamped to that minimum (-2.99). The gene expression values were centered and scaled with the mean and standard deviation of our dataset. A script for calculating senescence scores with this classifier is available at https://ccb.nki.nl/publications/cancer-senescence/.

For the validation analysis on normal senescent cells from Casella *et al.* (2019) included only the main set of 25 samples and excluded their second set of 12 samples, as the latter samples had a strong 3'UTR bias in the sequencing reads, indicative of RNA degradation, given that ribosome-depletion was used. Importantly, these 12 samples were also excluded from part of the analysis by Casella *et al.* (2019).

Quiescence-induction

A549 cells (0.5x10^6) were plated in 150-mm dishes in complete media (RPMI 10% FBS). After 24h, cells were starved in serum free media for 72h. Cells were collected, counted and fixed in 70% ethanol and incubated at -20C for 2h.

For cell cycle analysis, 10^6 cells were stained with anti-Ki67 PE-conjugated antibody (Clone B56, BD Pharmigen) for 30 min at RT. Finally, cells were re-suspended in PBS containing DAPI (5 ug/ml) and incubated at 4°C for 2h before acquisition. Samples were acquired with LSR Fortessa (BD) and analyzed using FlowJo software (v10).

For RNAseq analysis, after 72h of starvation, cells were washed with cold PBS and collected in RLT buffer (Qiagen) for RNA extraction.

Quantification and statistical analysis

Statistical details of experiments can be found in the figure legends and results. How significance was defined can be found in the legends and results. Data was analyzed using Graphpad Prism v8.4.3 and R statistical computing language (v3.6.0).

Additional resources

SENESCopedia webtool with processed RNA sequencing data of senescent and parental cells, and the SENCAN classifier: 'https://ccb.nki.nl/publications/cancer-senescence/'. The following tables are available at 'https://www.sciencedirect.com/science/article/pii/S2211124721008585?via%3Dihub': Table S2, entitled 'differentially expressed genes from EdgeR, related to figure 3; Table S4, entitled 'SENCAN classifier coefficients, related to figure 6'; Table S5, entitled 'External validation samples, related to figure 6; and Table S6, entitled 'RNAseq processed log2CPM, related to figure 3'.

References

Ávila-López, P.A., Guerrero, G., Nuñez-Martínez, H.N., Peralta-Alvarez, C.A., Hernández-Montes, G., Álvarez-Hilario, L.G., Herrera-Goepfert, R., Albores-Saavedra, J., Villegas-Sepúlveda, N., Cedillo-Barrón, L., et al. (2021). H2A.Z overexpression suppresses senescence and chemosensitivity in pancreatic ductal adenocarcinoma. Oncogene *40*, 2065–2080.

Baldwin, E.L., and Osheroff, N. (2005). Etoposide, topoisomerase II and cancer. Curr. Med. Chem. - Anti-Cancer Agents *5*, 363–372.

Barbie, D.A., Tamayo, P., Boehm, J.S., Kim, S.Y., Moody, S.E., Dunn, I.F., Schinzel, A.C., Sandy, P., Meylan, E., Scholl, C., et al. (2009). Systematic RNA interference reveals that oncogenic KRAS-driven cancers require TBK1. Nature *462*, 108–112.

Basisty, N., Kale, A., Jeon, O.H., Kuehnemann, C., Payne, T., Rao, C., Holtz, A., Shah, S., Sharma, V., Ferrucci, L., et al. (2020). A proteomic atlas of senescence-associated secretomes for aging biomarker development. PLoS Biol. *18*, e3000599.

Bismeijer, T., and Kim, Y. (2019). FlexGSEA: Flexible Gene Set Enrichment Analysis (Version v1.3). Zenodo http://doi.org/10.5281/zenodo.2616660.

Bussian, T.J., Aziz, A., Meyer, C.F., Swenson, B.L., van Deursen, J.M., and Baker, D.J. (2018). Clearance of senescent glial cells prevents tau-dependent pathology and cognitive decline. Nature *562*, 578–582.

Casella, G., Munk, R., Kim, K.M., Piao, Y., De, S., Abdelmohsen, K., and Gorospe, M. (2019). Transcriptome signature of cellular senescence. Nucleic Acids Res. *47*, 7294–7305.

Chang, B.D., Broude, E. V., Dokmanovic, M., Zhu, H., Ruth, A., Xuan, Y., Kandel, E.S., Lausch, E., Christov, K., and Roninson, I.B. (1999). A senescence-like phenotype distinguishes tumor cells that undergo terminal proliferation arrest after exposure to anticancer agents. Cancer Res. *59*, 3761–3767.

Chang, J., Wang, Y., Shao, L., Laberge, R.-M., Demaria, M., Campisi, J., Janakiraman, K., Sharpless, N.E., Ding, S., Feng, W., et al. (2016). Clearance of senescent cells by ABT-263 rejuvenates aged hematopoietic stem cells in mice. Nat. Med. *22*, 78–83.

Childs, B.G., Baker, D.J., Wijshake, T., Conover, C.A., Campisi, J., and Deursen, J.M. Van (2016). Senescent intimal foam cells are deleterious at all stages of atherosclerosis. Science (80-.). *354*, 472–477.

Coppé, J.-P., Desprez, P.-Y., Krtolica, A., and Campisi, J. (2010). The senescence-associated secretory phenotype: the dark side of tumor suppression. Annu. Rev. Pathol. *5*, 99–118.

Coppé, J.P., Patil, C.K., Rodier, F., Sun, Y., Muñoz, D.P., Goldstein, J., Nelson, P.S., Desprez, P.Y., and Campisi, J. (2008). Senescence-associated secretory phenotypes reveal cell-nonautonomous functions of oncogenic RAS and the p53 tumor suppressor. PLoS Biol. *6*, 2853–2868.

Cuollo, L., Antonangeli, F., Santoni, A., and Soriani, A. (2020). The Senescence-Associated Secretory Phenotype and Age-Related Diseases. *9*, 1–16.

Davalos, A.R., Coppe, J.P., Campisi, J., and Desprez, P.Y. (2010). Senescent cells as a source of inflammatory factors for tumor progression. Cancer Metastasis Rev. *29*, 273–283.

Demaria, M., O'Leary, M.N., Chang, J., Shao, L., Liu, S., Alimirah, F., Koenig, K., Le, C., Mitin, N., Deal, A.M., et al. (2016). Cellular Senescence Promotes Adverse Effects of Chemotherapy and Cancer Relapse. Cancer Discov. *7*, 165–176.

Dirac, A.M.G., and Bernards, R. (2003). Reversal of senescence in mouse fibroblasts through lentiviral suppression of p53. J. Biol. Chem. *278*, 11731–11734.

Ewald, J.A., Desotelle, J.A., Wilding, G., and Jarrard, D.F. (2010). Therapy-induced senescence in cancer. J. Natl. Cancer Inst. *102*, 1536–1546.

Foroutan, M., Bhuva, D.D., Lyu, R., Horan, K., Cursons, J., and Davis, M.J. (2018). Single sample scoring of molecular phenotypes. BMC Bioinformatics *19*, 1–10.

Freund, A., Orjalo, A. V., Desprez, P.Y., and Campisi, J. (2010). Inflammatory networks during cellular senescence: causes and consequences. Trends Mol. Med. *16*, 238–246.

Fridman, A.L., and Tainsky, M.A. (2008). Critical pathways in cellular senescence and immortalization revealed by gene expression profiling. Oncogene *27*, 5975–5987.

Friedman, J., Hastie, T., and Tibshirani, R. (2010). Regularization Paths for Generalized Linear Models via Coordinate Descent. J. Stat. Softw. *33*, 1–22.

Gewirtz, D.A. (1999). A critical evaluation of the mechanisms of action proposed for the antitumor effects of the anthracycline antibiotics adriamycin and daunorubicin. Biochem. Pharmacol. *57*, 727–741.

Gire, V., and Dulic, V. (2015). Senescence from G2 arrest, revisited. Cell Cycle *14*, 297–304.

González-Gualda, E., Pàez-Ribes, M., Lozano-Torres, B.,

3

Macias, D., Wilson, J.R., González-López, C., Ou, H.L., Mirón-Barroso, S., Zhang, Z., Lérida-Viso, A., et al. (2020). Galacto-conjugation of Navitoclax as an efficient strategy to increase senolytic specificity and reduce platelet toxicity. Aging Cell 1–19.

Gorgoulis, V., Adams, P.D., Alimonti, A., Bennett, D.C., Bischof, O., Bishop, C., Campisi, J., Collado, M., Evangelou, K., Ferbeyre, G., et al. (2019). Cellular Senescence: Defining a Path Forward. Cell 179, 813–827.

Greten, T.F., and Eggert, T. (2017). Cellular senescence associated immune responses in liver cancer. Hepatic Oncol. 4, 123–127.

Hanahan, D., and Weinberg, R.A. (2011). Hallmarks of cancer: The next generation. Cell 144, 646–674.

Hänzelmann, S., Castelo, R., and Guinney, J. (2013). GSVA: Gene set variation analysis for microarray and RNA-Seq data. BMC Bioinformatics 14.

Haugstetter, A.M., Loddenkemper, C., Lenze, D., Gröne, J., Standfuss, C., Petersen, I., Dörken, B., and Schmitt, C.A. (2010). Cellular senescence predicts treatment outcome in metastasised colorectal cancer. Br. J. Cancer 103, 505–509.

Hayflick, L. (1965). The limited in vitro lifetime of human diploid cell strains. Exp. Cell Res. 37, 614–636.

He, Y., Zhang, X., Chang, J., Kim, H.N., Zhang, P., Wang, Y., Khan, S., Liu, X., Zhang, X., Lv, D., et al. (2020). Using proteolysis-targeting chimera technology to reduce navitoclax platelet toxicity and improve its senolytic activity. Nat. Commun. 11.

Hernandez-Segura, A., de Jong, T. V., Melov, S., Guryev, V., Campisi, J., and Demaria, M. (2017). Unmasking Transcriptional Heterogeneity in Senescent Cells. Curr. Biol. 27, 2652–2660.

Kaefer, A., Yang, J., Noertersheuser, P., Mensing, S., Humerickhouse, R., Awni, W., and Xiong, H. (2014). Mechanism-based pharmacokinetic/pharmacodynamic meta-analysis of navitoclax (ABT-263) induced thrombocytopenia. Cancer Chemother. Pharmacol. 74, 593–602.

Khan, S., Zhang, X., Lv, D., Zhang, Q., He, Y., Zhang, P., Liu, X., Thummuri, D., Yuan, Y., Wiegand, J.S., et al. (2019). A selective BCL-XL PROTAC degrader achieves safe and potent antitumor activity. Nat. Med. 25, 1938–1947.

Kim, H.N., Chang, J., Shao, L., Han, L., Iyer, S., Manolagas, S.C., O'Brien, C.A., Jilka, R.L., Zhou, D., and Almeida, M. (2017). DNA damage and senescence in osteoprogenitors expressing Osx1 may cause their decrease with age. Aging Cell 16, 693–703.

Kolesnichenko, M., Mikuda, N., Höpken, U.E., Milanovic, M., Bugra Tufan, A., Uyar, B., Sun, W., Schleich, K., von Hoff, L., Willenbrock, M., et al. (2019). A novel IKK- and proteasome-independent mechanism of RelA activation triggers senescence associated secretome via transcriptional repression of NFKBIA. BioRxiv.

Kumarasamy, V., Vail, P., Nambiar, R., Witkiewicz, A.K., and Knudsen, E.S. (2021). Functional determinants of cell cycle plasticity and sensitivity to CDK4/6 inhibition. Cancer Res. 81, 1347–1360.

Lee, M., and Lee, J.S. (2014). Exploiting tumor cell senescence in anticancer therapy. BMB Rep. 47, 51–59.

Liberzon, A., Birger, C., Thorvaldsdóttir, H., Ghandi, M., Mesirov, J.P., and Tamayo, P. (2015). The Molecular Signatures Database Hallmark Gene Set Collection. Cell Syst. 1, 417–425.

Liberzon, A., Birger, C., Ghandi, M., Jill, P., Tamayo, P., Jolla, L., and Jolla, L. (2016). The Molecular Signatures Database (MSigDB) hallmark gene set collection. Cell Syst. 1, 417–425.

Lopes-Paciencia, S., Saint-Germain, E., Rowell, M.C., Ruiz, A.F., Kalegari, P., and Ferbeyre, G. (2019). The senescence-associated secretory phenotype and its regulation. Cytokine 117, 15–22.

Lozano-Torres, B., Estepa-Fernández, A., Rovira, M., Orzáez, M., Serrano, M., Martínez-Máñez, R., and Sancenón, F. (2019). The chemistry of senescence. Nat. Rev. Chem. 3, 426–441.

de Magalhães, J.P., Costa, J., and Toussaint, O. (2005). HAGR: The Human Ageing Genomic Resources. Nucleic Acids Res. 33, 537–543.

Mainardi, S., Mulero-Sánchez, A., Prahallad, A., Germano, G., Bosma, A., Krimpenfort, P., Lieftink, C., Steinberg, J.D., De Wit, N., Gonçalves-Ribeiro, S., et al. (2018). SHP2 is required for growth of KRAS-mutant non-small-cell lung cancer in vivo letter. Nat. Med. 24, 961–967.

Martínez-Zamudio, R.I., Roux, P.F., de Freitas, J.A.N.L.F., Robinson, L., Doré, G., Sun, B., Belenki, D., Milanovic, M., Herbig, U., Schmitt, C.A., et al. (2020). AP-1 imprints a reversible transcriptional programme of senescent cells. Nat. Cell Biol. 22, 842–855.

Marxer, M., Ma, H.T., Man, W.Y., and Poon, R.Y.C. (2014). P53 deficiency enhances mitotic arrest and slippage induced by pharmacological inhibition of Aurora kinases. Oncogene 33, 3550–3560.

McCarthy, D.J., Chen, Y., and Smyth, G.K. (2012). Differential expression analysis of multifactor RNA-Seq experiments with respect to biological variation. Nucleic Acids Res. 40, 4288–4297.

Milanovic, M., Fan, D.N.Y., Belenki, D., Däbritz, J.H.M., Zhao, Z., Yu, Y., Dörr, J.R., Dimitrova, L., Lenze, D.,

3

Monteiro Barbosa, I.A., et al. (2018). Senescence-associated reprogramming promotes cancer stemness. Nature *553*, 96–100.

Mizuno, H., Nakanishi, Y., Ishii, N., Sarai, A., and Kitada, K. (2009). A signature-based method for indexing cell cycle phase distribution from microarray profiles. BMC Genomics *10*, 1–10.

Montecucco, A., Zanetta, F., Biamonti, G., and Molecolare, G. (2015). Review article : MOLECULAR MECHANISMS OF ETOPOSIDE. 95–108.

Muniz, L., Deb, M.K., Aguirrebengoa, M., Lazorthes, S., Trouche, D., and Nicolas, E. (2017). Control of Gene Expression in Senescence through Transcriptional Read-Through of Convergent Protein-Coding Genes. Cell Rep. *21*, 2433–2446.

Narita, M., Nūnez, S., Heard, E., Narita, M., Lin, A.W., Hearn, S.A., Spector, D.L., Hannon, G.J., and Lowe, S.W. (2003). Rb-mediated heterochromatin formation and silencing of E2F target genes during cellular senescence. Cell *113*, 703–716.

Niu, H., Manfredi, M., and Ecsedy, J.A. (2015). Scientific rationale supporting the clinical development strategy for the investigational Aurora A kinase inhibitor alisertib in cancer. Front. Oncol. *5*, 1–9.

Nojima, T., Tellier, M., Foxwell, J., Ribeiro de Almeida, C., Tan-Wong, S.M., Dhir, S., Dujardin, G., Dhir, A., Murphy, S., and Proudfoot, N.J. (2018). Deregulated Expression of Mammalian lncRNA through Loss of SPT6 Induces R-Loop Formation, Replication Stress, and Cellular Senescence. Mol. Cell *72*, 970-984.e7.

Ortiz-Montero, P., Londoño-Vallejo, A., and Vernot, J.P. (2017). Senescence-associated IL-6 and IL-8 cytokines induce a self- and cross-reinforced senescence/inflammatory milieu strengthening tumorigenic capabilities in the MCF-7 breast cancer cell line. Cell Commun. Signal. *15*, 1–18.

Pan, J., Li, D., Xu, Y., Zhang, J., Wang, Y., Chen, M., Lin, S., Huang, L., Chung, E.J., Citrin, D.E., et al. (2017). Inhibition of Bcl-2/xl With ABT-263 Selectively Kills Senescent Type II Pneumocytes and Reverses Persistent Pulmonary Fibrosis Induced by Ionizing Radiation in Mice. Int. J. Radiat. Oncol. Biol. Phys. *99*, 353–361.

Pandey, K., Park, N., Park, K.S., Hur, J., Cho, Y. Bin, Kang, M., An, H.J., Kim, S., Hwang, S., and Moon, Y.W. (2020). Combined cdk2 and cdk4/6 inhibition overcomes palbociclib resistance in breast cancer by enhancing senescence. Cancers (Basel). *12*, 1–17.

Pérez-Mancera, P.A., Young, A.R.J., and Narita, M. (2014). Inside and out: the activities of senescence in cancer. Nat. Rev. Cancer *14*, 547–558.

Purcell, M., Kruger, A., Tainsky, M.A., Purcell, M., Kruger, A., Gene, M.A.T., Purcell, M., Kruger, A., and Tainsky, M.A. (2014). Gene expression profiling of replicative and induced senescence. Cell Cycle *13*, 3927–3937.

Roberson, R.S., Kussick, S.J., Vallieres, E., Chen, S.Y.J., and Wu, D.Y. (2005). Escape from therapy-induced accelerated cellular senescence in p53-null lung cancer cells and in human lung cancers. Cancer Res. *65*, 2795–2803.

Robin, T., Capes-Davis, A., and Bairoch, A. (2020). CLASTR: The Cellosaurus STR similarity search tool - A precious help for cell line authentication. Int. J. Cancer *146*, 1299–1306.

Ruscetti, M., Morris, J.P., Mezzadra, R., Russell, J., Leibold, J., Romesser, P.B., Simon, J., Kulick, A., Ho, Y. jui, Fennell, M., et al. (2020). Senescence-Induced Vascular Remodeling Creates Therapeutic Vulnerabilities in Pancreas Cancer. Cell *181*, 424-441.e21.

Saleh, T., Cudjoe, E.K., Kyte, S.L., Henderson, S.C., Elmore, L.W., and Gewirtz, D. (2017). Reversibility of chemotherapy-induced senescence is independent of autophagy and a potential model for tumor dormancy and cancer recurrence. BioRxiv 804–828.

Schalper, K.A., Carleton, M., Zhou, M., Chen, T., Feng, Y., Huang, S.P., Walsh, A.M., Baxi, V., Pandya, D., Baradet, T., et al. (2020). Elevated serum interleukin-8 is associated with enhanced intratumor neutrophils and reduced clinical benefit of immune-checkpoint inhibitors. Nat. Med. *26*, 688–692.

Schmitt, C.A., Fridman, J.S., Yang, M., Lee, S., Baranov, E., Hoffman, R.M., and Lowe, S.W. (2002). A senescence program controlled by p53 and p16INK4a contributes to the outcome of cancer therapy. Cell *109*, 335–346.

Schosserer, M., Grillari, J., and Breitenbach, M. (2017). The Dual Role of Cellular Senescence in Developing Tumors and Their Response to Cancer Therapy. Front. Oncol. *7*, 278.

Shahbandi, A., Rao, S.G., Anderson, A.Y., Frey, W.D., Olayiwola, J.O., Ungerleider, N.A., and Jackson, J.G. (2020). BH3 mimetics selectively eliminate chemotherapy-induced senescent cells and improve response in TP53 wild-type breast cancer. Cell Death Differ.

Subramanian, A., Tamayo, P., Mootha, V.K., Mukherjee, S., Ebert, B.L., Gillette, M.A., Paulovich, A., Pomeroy, S.L., Golub, T.R., Lander, E.S., et al. (2005). Gene set enrichment analysis: A knowledge-based approach for interpreting genome-wide expression profiles. Proc. Natl. Acad. Sci. U. S. A. *102*, 15545–15550.

Supek, F., Bošnjak, M., Škunca, N., and Šmuc, T. (2011).

Revigo summarizes and visualizes long lists of gene ontology terms. PLoS One 6.

Tacar, O., Sriamornsak, P., and Dass, C.R. (2013). Doxorubicin: An update on anticancer molecular action, toxicity and novel drug delivery systems. J. Pharm. Pharmacol. 65, 157–170.

Touzeau, C., Ryan, J., Guerriero, J.L., Moreau, P., Ni, T., Gouill, S. Le, Richardson, P., Anderson, K., Amiot, M., and Letai, A. (2016). BH3-profiling identifies heterogeneous dependency on Bcl-2 family members in Multiple Myeloma. Leukemia 30, 761–764.

Wang, B., Ni, Z., Dai, X., Qin, L., Li, X., Xu, L., Lian, J., and He, F. (2014). The Bcl-2/xL inhibitor ABT-263 increases the stability of Mcl-1 mRNA and protein in hepatocellular carcinoma cells. Mol. Cancer 13, 1–11.

Wang, L., Leite de Oliveira, R., Wang, C., Fernandes Neto, J.M., Mainardi, S., Evers, B., Lieftink, C., Morris, B., Jochems, F., Willemsen, L., et al. (2017). High-Throughput Functional Genetic and Compound Screens Identify Targets for Senescence Induction in Cancer. Cell Rep. 21, 773–783.

Wang, T.H., Chen, C.C., Leu, Y.L., Lee, Y.S., Lian, J.H., Hsieh, H.L., and Chen, C.Y. (2020). Palbociclib induces DNA damage and inhibits DNA repair to induce cellular senescence and apoptosis in oral squamous cell carcinoma. J. Formos. Med. Assoc. 1–11.

Wiley, C.D., Flynn, J.M., Morrissey, C., Lebofsky, R., Shuga, J., Dong, X., Unger, M.A., Vijg, J., Melov, S., and Campisi, J. (2017). Analysis of individual cells identifies cell-to-cell variability following induction of cellular senescence. Aging Cell 16, 1043–1050.

Wilson, A.A., Kwok, L.W., Porter, E.L., Payne, J.G., McElroy, G.S., Ohle, S.J., Greenhill, S.R., Blahna, M.T., Yamamoto, K., Jean, J.C., et al. (2013). Lentiviral delivery of RNAi for in vivo lineage-specific modulation of gene expression in mouse lung macrophages. Mol. Ther. 21, 825–833.

Yuen, K.C., Liu, L.F., Gupta, V., Madireddi, S., Keerthivasan, S., Li, C., Rishipathak, D., Williams, P., Kadel, E.E., Koeppen, H., et al. (2020). High systemic and tumor-associated IL-8 correlates with reduced clinical benefit of PD-L1 blockade. Nat. Med. 26, 693–698.

Zhu, Y., Tchkonia, T., Fuhrmann-Stroissnigg, H., Dai, H.M., Ling, Y.Y., Stout, M.B., Pirtskhalava, T., Giorgadze, N., Johnson, K.O., Giles, C.B., et al. (2016). Identification of a novel senolytic agent, navitoclax, targeting the Bcl-2 family of anti-apoptotic factors. Aging Cell 15, 428–435.

Zou, H., and Hastie, T. (2005). Regularization and variable selection via the elastic net. J. R. Stat. Soc. Ser. B Stat. Methodol. 67, 301–320.
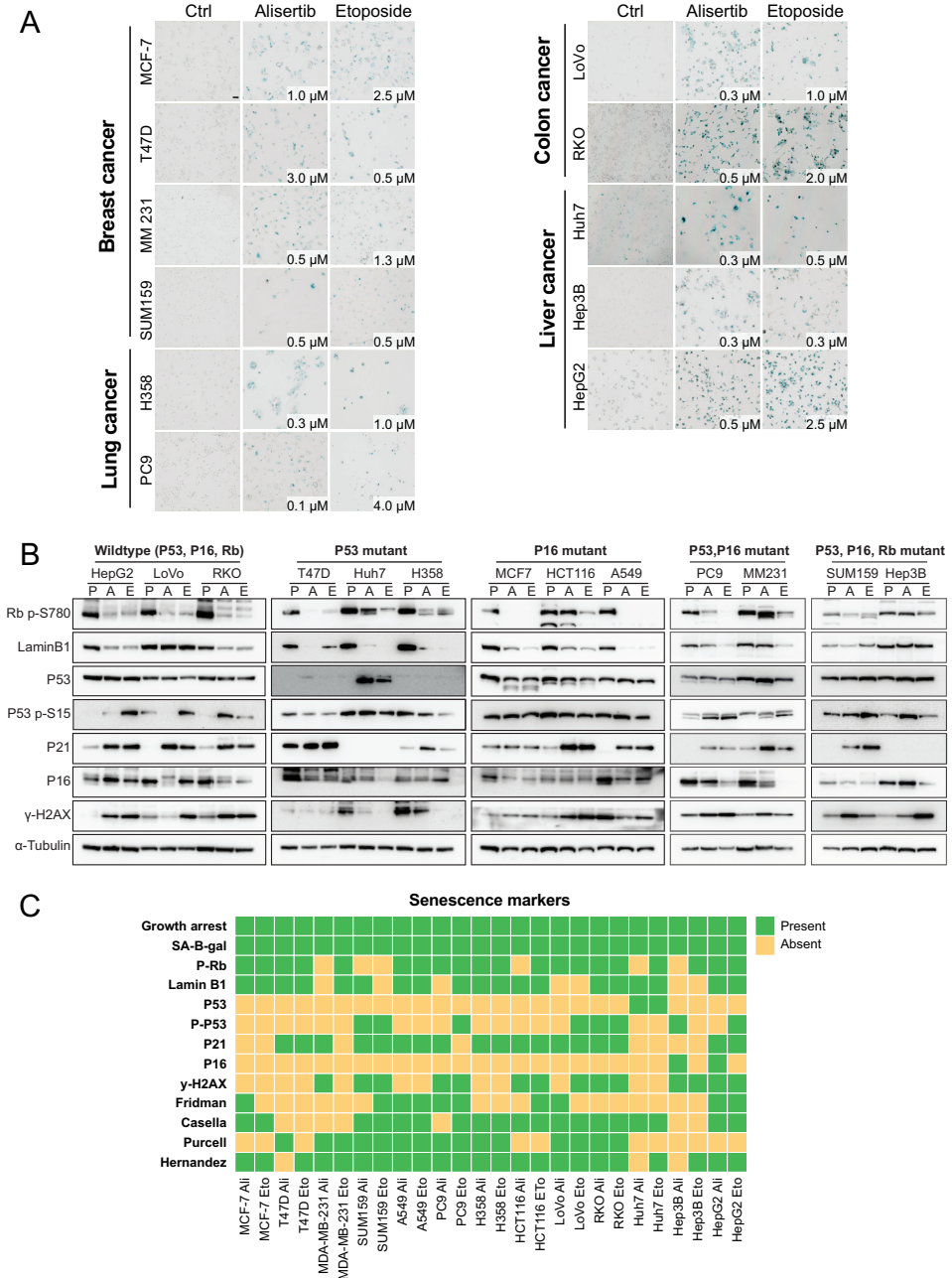
Supplementary Figures

A

B

C

Figure S1. Senescence markers are present in cells treated with alisertib or etoposide, related to figure 1. (A) Representative images of SA-ß-gal staining from three independent biological replicates for 11 cell lines (quantification in figure 1D). Cells were cultured for 7 days with the

indicated alisertib or etoposide concentrations. Scale bar = 100 µm. MM231 = MDA-MB-231 **(B)** Westernblot for senescence markers. Cells were lysed after a treatment for 7 days and 24h drug-washout. P = parental, E = etoposide-induced senescence, A = alisertib-induced senescence. MM231 = MDA-MB-231. **(C)** Overview of senescence markers for etoposide- and alisertib-induced senescent cells. Pospho-Rb (P-Rb) and LaminB1 are scored as present when decreased in senescence, while P53, Phospho-P53 (P-P53), P21, P16 and gamma-H2AX are present when increased upon senescence (from figure S1B). Fridman, Casella, Purcell and Hernandez are scored as absent when the Delta ssGSEA scores (from figure 1F) are between 0.2 and -0.2, higher or lower scores are scored as present. Fridman and Casella signatures score as present when both up and down signatures are present.
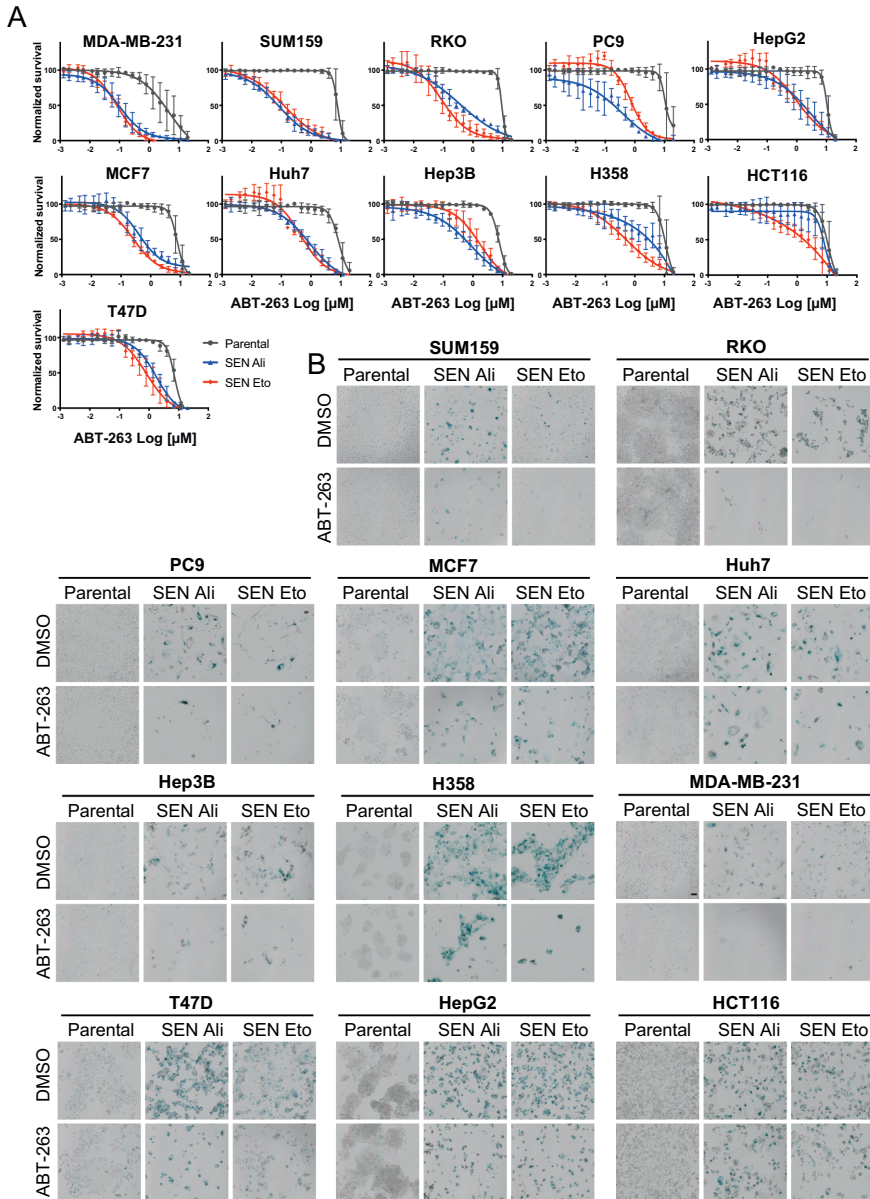
Figure S2. Drug response to ABT-263 differs between senescent cancer cells,
related to figure 2. (A) Dose-response curves for increasing concentrations of ABT-263 for 13
cell lines. Cells were treated with senescence-inducing concentrations of alisertib or etoposide
for seven days. Senescent cells and parental cells were reseeded in 96-wells and cultured with
increasing concentrations of ABT-263. After five days, cell viability was measured with Cell Titer
Blue (CTB) assay. SEN Ali = alisertib-induced senescent, SEN Eto = etoposide-induced senescent.
Values represent the mean ±SEM of three independent biological experiments. **(B)** Representative
images of SA-ß-gal staining from three technical replicates for 13 cell lines. Cells were seeded into a
6-well and treated with alisertib or etoposide for 7 days, and medium was subsequently replaced by
medium supplemented with DMSO or 1μM ABT-263. Cells were cultured for another 5 days before
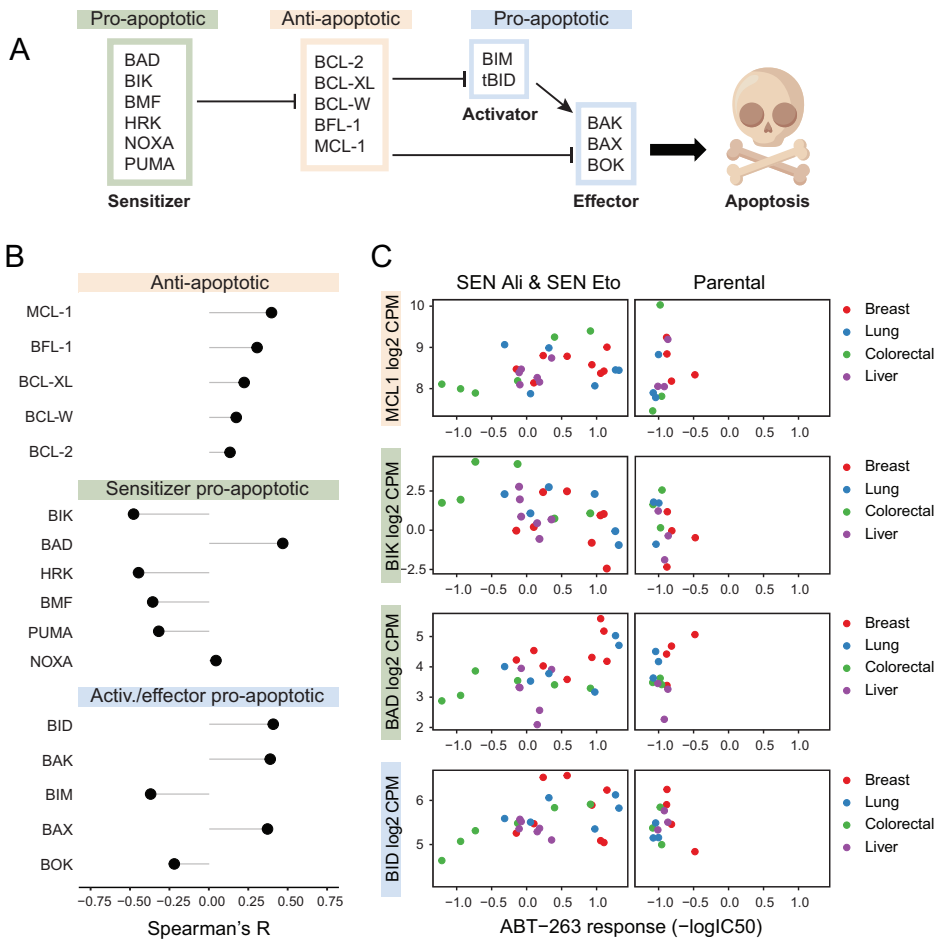SA-ß-gal staining was performed. Scale bar = 100 μm.

Figure S3. Gene expression of BAD correlates with response to ABT-263, related to figure 2. (A) Schematic outline of the actions of BCL-2 family proteins in apoptosis. tBID = truncated BID. **(B)** Lollipop chart shows the results from the Spearman rank correlation analysis in which the gene expression of 16 apoptotic proteins was compared to the ABT-263 response (-logIC50) in etoposide- and alisertib-induced senescent cells. All proteins scored higher than Benjamini-Hochberg (FDR) corrected p-value 0.05. Activ. = activator. **(C)** Scatter plots depict ABT-263 response (-logIC50) versus gene expression of BCL-2 family members that are significantly correlated based on Spearman rank correlation analysis (in B). In the left plots, each dot represents a cell line that was treated with alisertib or etoposide. On the right plots, each dot represents a cell line in parental state. CPM = counts per million. SEN Ali = alisertib-induced senescent cells. SEN Eto = etoposide-induced senescent cells.
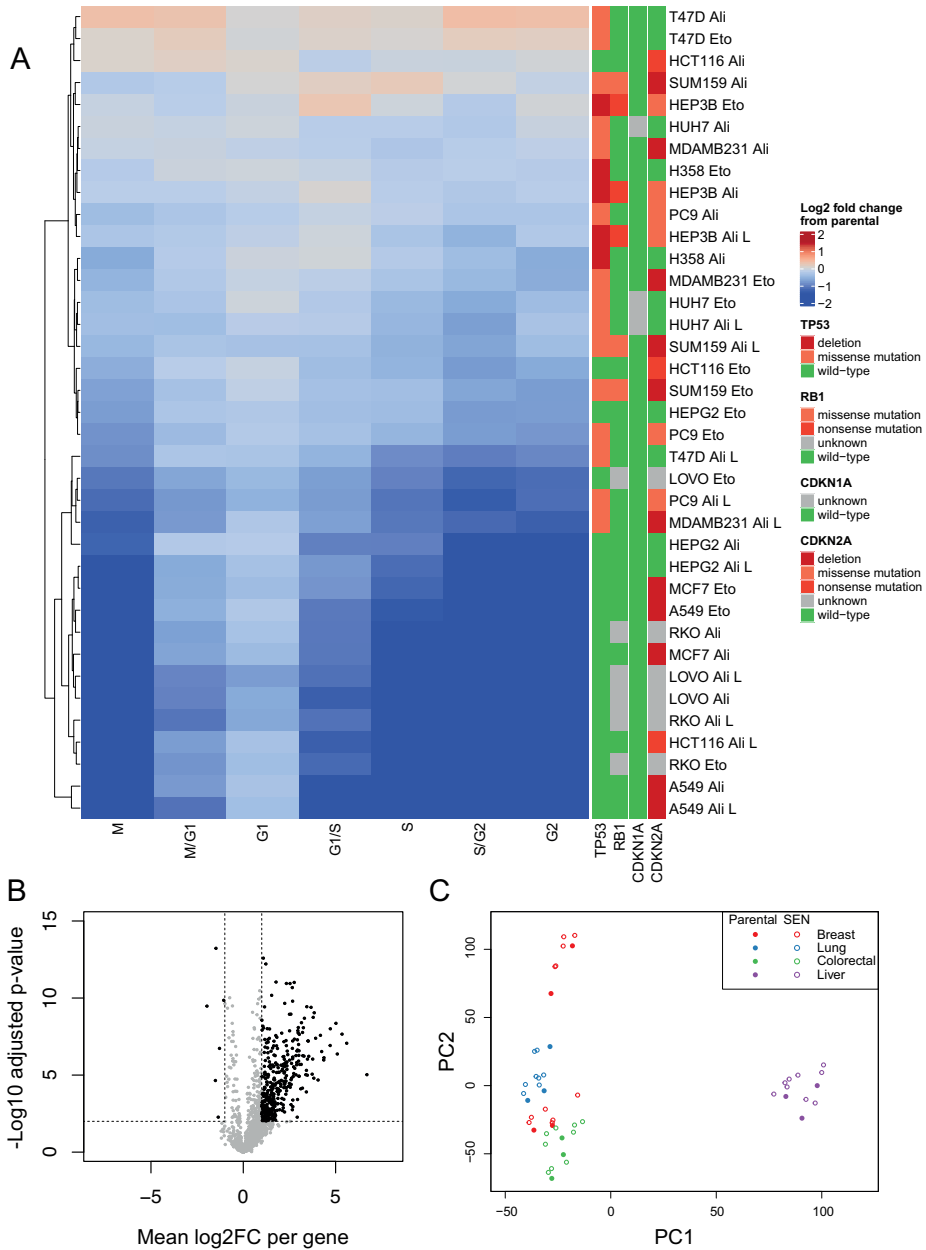
Figure S4. Gene expression pattern of senescent cancer cells is dictated by the parental state, related to figure 4. (A) Relative estimation of cell cycle phases, calculated by the difference in mean log expression of marker genes for each phase between treated and untreated samples. **(B)** Volcano plot exhibit the results from edgeR paired differential expression analyses, showing only the genes which have a secreted protein product. Each dot represents a gene with its corresponding mean log2 foldchange (x-axis) and multiple testing corrected p-value (-log10, yaxis). Black dots illustrate differentially expressed genes. Log2FC = log2 foldchange. **(C)** Principal component analysis for parental and senescent cells (SEN) covering the full transcriptome.
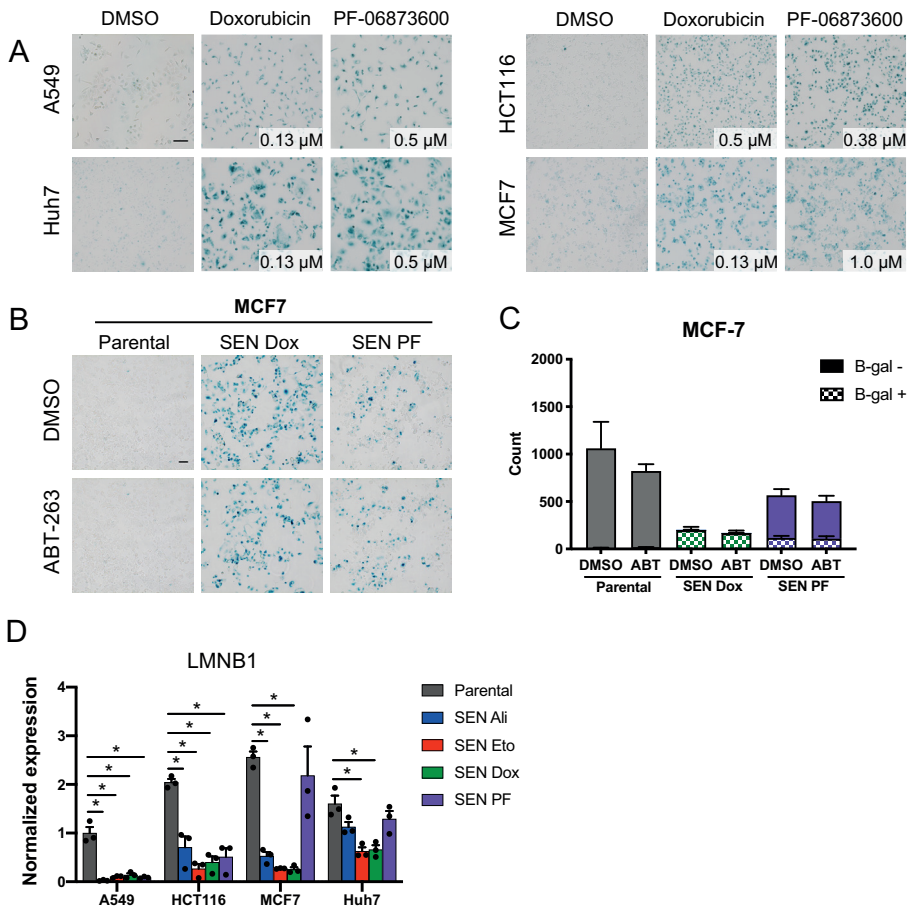
Figure S5. The senescence phenotype is more influenced by cell type than senescence trigger, related to figure 5. (A) Representative images of SA-ß-gal staining from three biological replicates. Cells were treated for 7 days. Scale bar =100 µm. **(B)** Representative images of SA-ß-gal staining from three technical replicates. Cells were
seeded into a 6-well and treated with alisertib or etoposide for 7 days, and medium was subsequently replaced by medium supplemented with DMSO or 1µM ABT-263. Cells were cultured for another 5 days before SA-ß-gal staining was performed. Scale bar = 100 µm. **(C)** Quantification of SA-ß-gal + and SA-ß-gal – cells for MCF7. Calculations were performed on images shown in B. **(D)** Normalized mRNA expression determined by qPCR. Expression is relative to GAPDH and normalized to T47D parental.
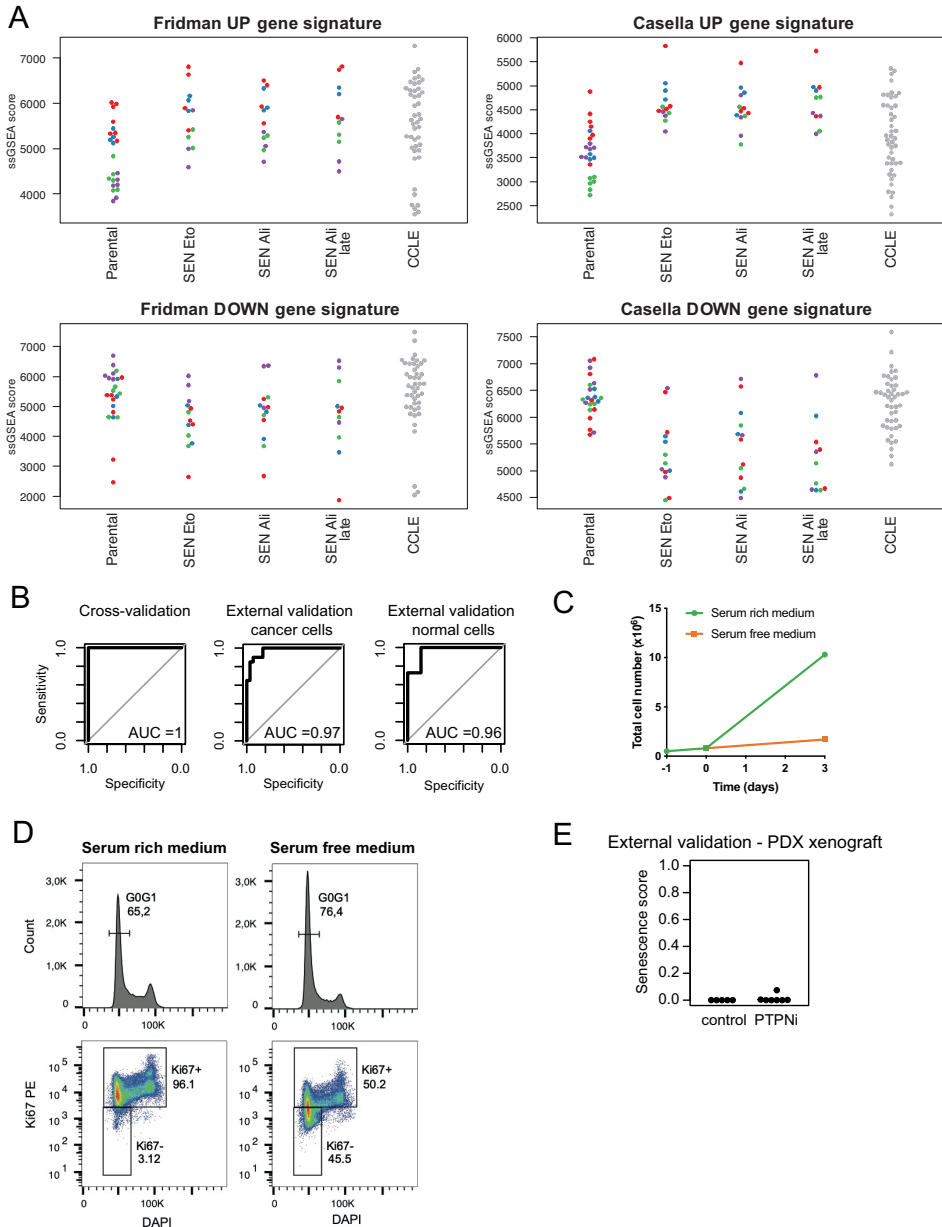
Figure S6. Signature performance and quiescence induction, related to figure 6.
(**A**) ssGSEA scores for Fridman and Casella gene expression signatures. (**B**) Receiver Operating Characteristic (ROC) curve of the SENCAN classifier for crossvalidation, and external validation in cancer and normal cells. (**C**) Cell counts of A549 cultured in serum rich and serum starved medium for 3 days. 500 k A549 cells were seeded at day -1. Medium was changed after one day to serum free or serum rich medium. (**D**) Cell cycle analysis of cells stained with DAPI and anti-KI67 PE-conjugated antibody. (**E**) SENCAN senescence scores for in vivo validation samples from PDX xenograft models treated with SHP2-inhibitor SHP099 (GSE109270).

Supplementary Tables

Table S1. Genes in senescence gene sets, related to figure 1 and STAR methods

Casella_UP	Casella_DOWN	Fridman	Fridman_down	Purcell	Hernandez
TMEM159	MCUB	CRYAB	ALDH1A1	OASL	FAM214B
CHPF2	FBL	IGFBP7	BMI1	APOL1	P4HA2
SLC9A7	NIBAN1	SERPINE1	CCN4	IFI27	CCND1
PLOD1	ANP32B	CDKN1A	CCNB1	COL17A1	DYNLT3
FAM234B	PARP1	MMP1	CDC25B	CD82	SCOC
DHRS7	LBR	ISG15	COL3A1	IL32	TAF13
SRPX	SSRP1	IGFBP6	E2F4	APOL3	TOLLIP
SRPX2	TMSB15A	MDM2	EGR1	C3	GBE1
TNFSF13B	CBS	IGFBP5	ID1	CTSS	CHMP5
PDLIM1	CDCA7L	IGFBP1	LAMA1	RSPO3	UFM1
ELMOD1	H1-4	OPTN	LDB2	HERC5	DGKA
CCND3	CBX2	FN1	MARCKS	PLAU	PLXNA3
TMEM30A	PTMA	CCND1		BIRC3	DDA1
STAT1	ITPRIPL1	PEA15		CLDN1	TMEM87B
RND3	AC074135.1	GSN		CD163L1	ZBTB7A
TMEM59		SMPD1		MYD88	RAI14
SARAF		NRG1		IL1B	TSPAN13
SLCO2B1		RRAS		TNFAIP3	ZNHIT1
ARRDC4		IGFBP4		BATF2	ACADVL
PAM		GUK1		GNG11	SLC10A3
WDR78		MAP1LC3B		PMAIP1	POFUT2
WDR63		RAB5B		MLKL	B4GALT7
NCSTN		SPARC		GCA	BCL2L2
SLC16A14		TNFAIP2		DUSP6	NOL3
GPR155		RAB13		ICAM1	KLC1
CLDN1		THBS1		ATF3	PLK3
JCAD		CD44		LGALS9	SLC16A3
BLCAP		IFI16		GMPR	ADPGK
FILIP1L		STAT1		ISG20	
TAP1		TNFAIP3		CXCL2	
TNFRSF10C		CREG1		TNFRSF18	
SAMD9L		CLTB			
SMCO3		S100A11			
POFUT2		CITED2			
KIAA1671		RAC1			
LRP10		HSPA2			
DIO2		VIM			
MAP4K3-DT		RABGGTA			
LINC02154		AOPEP			
TM4SF1-AS1		IRF5			
PTCHD4		TSPYL5			
H2AJ		MAP2K3			
PURPL		RBL2			
		HPS5			

Table S1. CONTINUED.

Casella_UP	Casella_DOWN	Fridman	Fridman_down	Purcell	Hernandez
		IGFBP3			
		RGL2			
		RAB31			
		TES			
		SOD1			
		TP53			
		HBS1L			
		ING1			
		TGFB1I1			
		IGFBP2			
		CCN2			
		F3			
		IRF7			
		HTATIP2			
		CDKN2D			
		EIF2S2			
		SMURF2			
		IGSF3			
		CYP1B1			
		TFAP2A			
		ALDH1A3			
		RHOB			
		CDKN1C			
		CDKN2B			
		CDKN2A			

3

Table S3. Validation samples from the Cancer Cell Line Encyclopedia (CCLE), related to figure 6

SRA_sample_id	CCLE_name	cell_line_name	tissue_type
SRR8615692	U2OS_BONE	U-2 OS	bone
SRR8616101	SAOS2_BONE	Saos-2	bone
SRR8616211	HOS_BONE	HOS	bone
SRR8615746	SF268_CENTRAL_NERVOUS_SYS-TEM	SF268	central_nervous_system
SRR8615748	SF539_CENTRAL_NERVOUS_SYS-TEM	SF539	central_nervous_system
SRR8615745	SF295_CENTRAL_NERVOUS_SYS-TEM	SF-295	central_nervous_system
SRR8615493	ISHIKAWAHERAKLIO02ER_ENDO-METRIUM	Ishikawa (Heraklio) 02 ER-	endometrium
SRR8615275	HEC1A_ENDOMETRIUM	HEC-1-A	endometrium
SRR8615907	KLE_ENDOMETRIUM	KLE	endometrium
SRR8616198	BV173	BV173	haematopoietic_and_lymphoid_tissue
SRR8615717	K562_HAEMATOPOIETIC_AND_LYMPHOID_TISSUE	K-562	haematopoietic_and_lymphoid_tissue
SRR8616133	HL60_HAEMATOPOIETIC_AND_LYMPHOID_TISSUE	HL-60	haematopoietic_and_lymphoid_tissue
SRR8616015	A498_KIDNEY	A-498	kidney
SRR8615272	CAKI1_KIDNEY	Caki-1	kidney
SRR8615333	UO31_KIDNEY	UO-31	kidney
SRR8615226	OE19_OESOPHAGUS	OE19	oesophagus
SRR8615228	OE33_OESOPHAGUS	OE33	oesophagus
SRR8615484	JHESOAD1_OESOPHAGUS	JH-EsoAd1	oesophagus
SRR8615505	SKOV3_OVARY	SK-OV-3	ovary
SRR8615844	IGROV1_OVARY	IGROV1	ovary
SRR8615870	OVCAR4_OVARY	OVCAR-4	ovary
SRR8615377	PANC1005	Panc10.05	pancreas
SRR8615519	MIAPACA2	MiaPaCa2	pancreas
SRR8615685	PANC1	Panc1	pancreas
SRR8615641	PC3_PROSTATE	PC-3	prostate
SRR8615547	LNCAPCLONEFGC_PROSTATE	LNCaP clone FGC	prostate
SRR8615300	DU145_PROSTATE	DU 145	prostate
SRR8616020	A375	A375	skin
SRR8615414	HS294T	Hs294T	skin
SRR8616054	SKMEL28	Sk-Mel-28	skin
SRR8615722	RH30	RH-30	soft_tissue
SRR8615595	RD_SOFT_TISSUE	RD	soft_tissue
SRR8615861	SKUT1_SOFT_TISSUE	SK-UT-1	soft_tissue
SRR8615362	KATOIII_STOMACH	KATO III	stomach
SRR8615495	NCIN87_STOMACH	NCI-N87	stomach
SRR8615934	SNU16_STOMACH	SNU-16	stomach
SRR8615869	FTC133_THYROID	FTC-133	thyroid
SRR8615773	BCPAP_THYROID	B-CPAP	thyroid
SRR8615644	8505C_THYROID	8505C	thyroid
SRR8615826	TCCSUP_URINARY_TRACT	TCCSUP	urinary_tract

3

Table S3. CONTINUED.

SRA_sample_id	CCLE_name	cell_line_name	tissue_type
SRR8616100	SCC15_UPPER_AERODIGESTIVE_TRACT	SCC-15	upper_aerodigestive_tract
SRR8616097	SCC25_UPPER_AERODIGESTIVE_TRACT	SCC-25	upper_aerodigestive_tract
SRR8615267	CAL27_UPPER_AERODIGESTIVE_TRACT	CAL 27	upper_aerodigestive_tract
SRR8616045	HT1197_URINARY_TRACT	HT-1197	urinary_tract
SRR8615858	T24_URINARY_TRACT	T24	urinary_tract
SRR8615826	TCCSUP_URINARY_TRACT	TCCSUP	urinary_tract

3

CHAPTER 4

Senolysis by ABT-263 is associated with increased apoptotic priming of cancer cells, already in the non-senescent state

Fleur Jochems[1], Chrysiida Baltira[3,5], Julie A. MacDonald[2,5], Veerle Daniels[2], Mark C. de Gooijer[3], Olaf van Tellingen[3], René Bernards[1,6,*], Anthony Letai[2,6,7]

[1]Division of Molecular Carcinogenesis, Oncode Institute, Netherlands Cancer Institute, Plesmanlaan 121, 1066 CX Amsterdam, The Netherlands
[2]Dana-Farber Cancer Institute, Boston, MA 02215, USA; Harvard Medical School, Boston, MA 02215, USA
[3]Division of Pharmacology, Netherlands Cancer Institute, Plesmanlaan 121, 1066 CX Amsterdam, The Netherlands
[4]Present address: Immuno-Oncology department, KU Leuven, Leuven, Belgium
[5]These authors contributed equally
[6]These authors contributed equally
[7]Lead contact

In preparation

Introduction

During their life-span, cells experience a plethora of endogenous and exogenous insults that result in cellular stress. Depending on the severity of cellular damage, cells undergo various forms of cell death or cellular senescence. This is a non-proliferative state accompanied by upregulation of survival signaling, Senescence-Associated ß-galactosidase (SA-ß-gal) activity and changes in cell morphology, metabolism, transcriptome, epigenome, and the secretion of various molecules known as the senescence-associated secretory phenotype (SASP) (Hayflick and Moorhead, 1961; Wang et al., 2022). Senescent cells accumulate as we age, and have been implicated in various age-related diseases like frailty, atherosclerosis, diabetes type two, and pulmonary fibrosis (Kaur and Farr, 2020). In addition to senescence in normal cells, senescence also occurs in the context of cancer. For instance, cellular senescence acts as a safeguard against oncogenic transformation, as seen in BRAF[V600E] mutated melanocytes (Michaloglou et al., 2005). In addition, cancer cells can undergo therapy-induced senescence (TIS) after treatment with chemotherapeutic agents (Ewald et al., 2010).

The removal of senescent cells has been considered beneficial to counteract age-related pathologies and extend life-span (Van Deursen, 2019), and the elimination of senescent cancer cells in anti-cancer therapies is considered important to prevent cancer reawakening and limit side-effects of chemotherapy (Demaria et al., 2017; Wang et al., 2022). This led to the identification of drugs that specifically kill senescent cells, referred to as senolytics. In order to survive, senescent fibroblast cells upregulate anti-apoptotic proteins BCL-2 and BCL-W, and BH3 mimetic ABT-263 (navitoclax) can act as a potent senolytic in senescent cells by activating intrinsic apoptosis targeting anti-apoptotic proteins BCL-2, BCL-W, and BCL-XL (Chang et al., 2016; Zhu et al., 2016). Moreover, BH3 mimetics ABT-199 (venetoclax; targeting BCL-2) and ABT-737 (targeting BCL-2, BCL-XL and BCL-W) also have senolytic potential (Lafontaine et al., 2021; Wang et al., 2022; Yosef et al., 2016).

In senescent cancer cells, we and others have shown that the response to ABT-263 of senescent cancer cells varied from highly sensitive to fully resistant (Jochems et al., 2021; Shahbandi et al., 2020). Even though the presence of NOXA was associated with ABT-263 response in certain breast cancer cell lines (Shahbandi et al., 2020), and BAX mutations could explain ABT-263 resistance in some colorectal cancer cell lines (Jochems et al., 2021), protein and RNA levels of pro- and anti-apoptotic proteins in parental and senescent cells could not explain the full range of variation in ABT-263 sensitivity. However, the dynamic interaction rather than the abundance of anti- and proapoptotic proteins are key determinants of response to BH3 mimetics (Sarosiek and Letai, 2016).

Intrinsic apoptosis is regulated by the interplay of BCL-2 family proteins: pro-

apoptotic BH3-only proteins (BIM, BID, NOXA, HRK, PUMA, BAD and BMF), anti-apoptotic proteins (BCL-XL, BCL-2, BCL-W, MCL-1, BFL-1) and pro-apoptotic effector proteins (BAK, BAX and BOK) (Kale et al., 2017). Activation of effector proteins leads to mitochondrial outer membrane permeabilization (MOMP) and subsequent release of cytochrome c. This activates a caspase reaction leading to cell disassembly (Taylor et al., 2008). BH3 profiling is a method that measures the mitochondrial apoptotic priming - also known as the 'readiness' to undergo apoptosis - by challenging mitochondria with BH3 mimetics and synthetic BH3 peptides encoding the active domains of pro-apoptotic BH3 proteins. When cells are more primed to apoptosis, exposure to these agents results in MOMP (Del Gaizo Moore and Letai, 2013). The reaction to various peptides can be measured with high-throughput flow cytometry detecting MOMP. This is dubbed 'iBH3 profiling' (Ryan et al., 2016). As drug treatments can also alter the mitochondrial priming, dynamic BH3 profiling (DBP) can be used to measure the change of drug-treated versus untreated cells (Montero et al., 2015).

In the present study, we aim to elucidate the mechanistic underpinning of the variability in response to ABT-263 in a panel of 12 senescent cancer cells, using iBH3 profiling. Our findings provide new insights into the differential sensitivity of senescent cancer cells to the BH3 mimetic ABT-263.

Results

Curation of cell line panel covering a range of senolytic responses to ABT-263
As eliminating senescent cancer cells is considered beneficial for the treatment of cancer, we aimed to understand the (un)responsiveness to senolytic ABT-263 therapy by studying its target proteins and other members of the apoptosis pathway (Figure 1A). Our former study shows a diverse senolytic response to ABT-263 in a panel of cancer cell lines derived from breast, lung, liver, and colon cancer. Furthermore, it was shown that this difference in sensitivity could not readily be explained based on RNA levels and protein levels of members of the apoptosis pathway in the parental and senescent state (Jochems et al., 2021). This differential response could potentially be attributed to post-translational modification and regulation, in which signaling is modulated by protein-binding kinetics and binding partner competition (Kale et al., 2017). To study the apoptosis pathway on a functional level with BH3 profiling, we curated a panel of cell lines that, in the senescent state, cover a range response to ABT-263. Therefore, we included the ABT-263 resistant cell line SK-Mel-28, in which senescence was induced with a 7-day treatment with 1μM of aurora kinase A inhibitor alisertib. Senescence was confirmed by a stable proliferation arrest (Figure 1B), morphology change and >90% SA-ß-galactosidase

positive cells (Figure 1C-D), increased p27[Kip1] protein, and decrease of Lamin B1 and Ser-780 phosphorylation of Retinoblastoma protein (RB) (Figure 1E). Moreover, the ABT-263 IC_{50} value of senescent and parental SK-Mel-28 was 8-10 µM, indicating drug resistance (Figure 1F). Combining this resistant cell line and cell lines described in Jochems et al., 2021, we curated a panel of 12 cell lines exhibiting a variable senolytic sensitivity to ABT-263 (Figure 1G). The final panel included lung, colon, liver, breast and skin cancer cell lines that were sensitive (A549, MDA-MB-231, SUM159), moderately sensitive (RKO, Huh7, Hep3B, H358, HepG2, T47D) or resistant (HCT116, SK-Mel-28 and LoVo) to senolytic ABT-263 killing. Senescence was induced by Aurora kinase inhibitor alisertib (SEN Ali) or chemotherapeutic agent etoposide (SEN Eto). An overview of the ABT-263 IC_{50} values for the final panel is presented in (Figure 1G). It is important to note that the parental cells were resistant to ABT-263 as their IC50 values were around 10 µM (equivalent with -1 -log(IC_{50})), and that SEN Ali and SEN Eto cells exhibit similar responses to ABT-263. This indicated that the response was more strongly influenced by the nature of the cell line rather than the senescence trigger.

Overall priming to apoptosis is lower in senescent cells compared to their parental counterparts

iBH3 profiling is a technique in which BH3 profiling is performed using a flow cytometry-based readout (Ryan et al., 2016). In this procedure, cells are permeabilized with digitonin and exposed to BH3 peptides or BH3 mimetics that will trigger the release of cytochrome c depending on the apoptotic priming of cells. Cytochrome c can be measured by fluorophore-conjugated antibody staining and subsequent flow cytometry (Figure S1A).

In a first attempt to BH3 profile senescent cells, we exposed A549, the cell line with the highest ABT-263 sensitivity, to alamethicin, a positive control for cytochrome c release as this antibiotic permeabilizes the cellular and mitochondrial membrane, and high dose (100 µM) of BIM peptide, which activates the pro-apoptotic effectors (Figure 1A) and measures the overall apoptotic priming of cells. Surprisingly, exposure to these agents resulted in an incomplete cytochrome c release in the senescent state, judged by the minimal shift in cytochrome c levels in senescent cells (Figure S1B). More specifically, alamethicin and BIM only triggered cytochrome c release in 60% and 20% of the cell population, respectively, while parental cells released cytochrome c in >90% of cell population (Figure S1C). As responses to alamethicin and BIM (in primed cell lines) are considered a proxy for adequate technical performance, we asked if we could further optimize BH3 profiling of senescent cells.
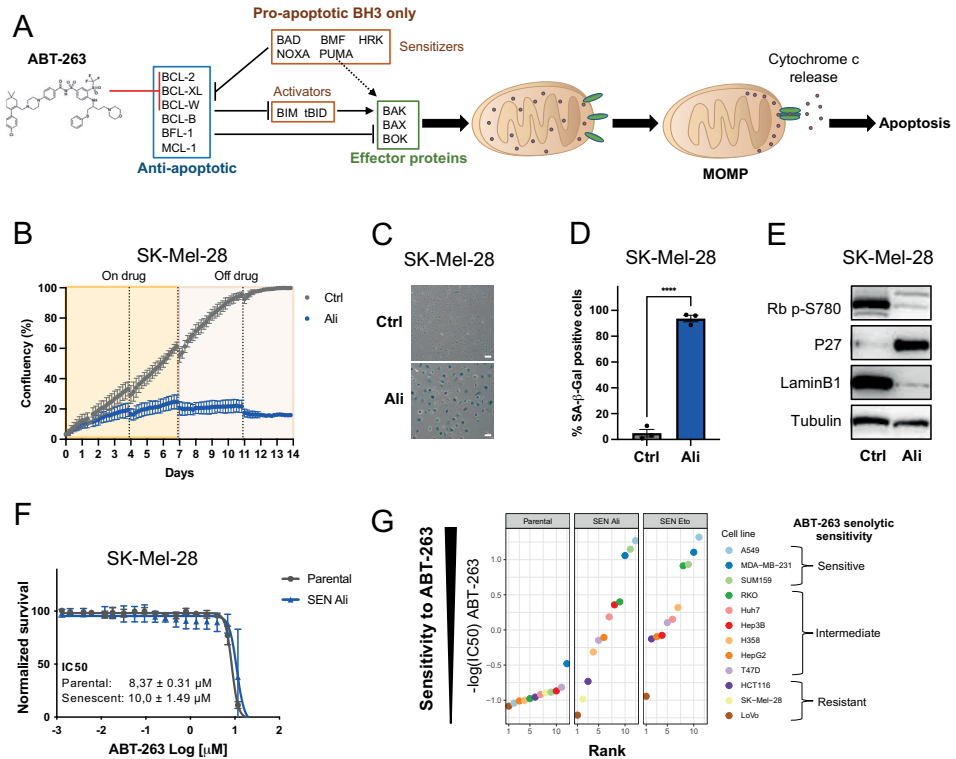
Figure 1: Curation of cell line panel covering a range of senolytic responses to ABT-263
(A) Outline of apoptosis pathway and targets of ABT-263. Two classes of pro-apoptotic BH3 only proteins exist that can activate apoptosis: the sensitizer proteins, which inhibit anti-apoptotic proteins, and activator proteins, which stimulate the pore-forming activity of effector proteins BAK and BAX. This results in mitochondrial outer membrane permeabilization and subsequent release of cytochrome c into the cytosol. This triggers the apoptosis cascade. MOMP., mitochondrial outer membrane permeabilization. (B) Growth curve of SK-Mel-28 with and without exposure to alisertib. $1x10^3$ cells were seeded into 96-well and were cultured in the presence or absence of 0.5 µM alisertib for 7 days. After that, cells were cultured for seven days without drug. Values represent the mean ±SEM of three biological replicates. (C-D) SK-Mel-28 cells were maintained in the presence or absence of 0.5 µM alisertib for one week before analysis. Ali., alisertib. (C) Representative image of SA-β-galactosidase staining. Scale bar represents 100 µm. (D) Quantification of SA-β-galactosidase positive cells (as represented in C). Data represents the mean ±SEM of three biological replicates. Data were analyzed with a two-sided Student's t test. ****$p < 0.0001$. (E) Westernblot for senescence markers. RB., Retinoblastoma protein. (F) Dose-response curve for SK-Mel-28 senescent and parental cells. Senescent and parental cells were treated with ABT-263 in 96-well for 5 days. Cell viability was determined with Cell Titer Blue (CTB) assay. Values represent the mean of three independent replicates ±SEM. SEN Ali., alisertib-induced senescent cells. (G) Rank dot plot for ABT-263 sensitivity (-logIC$_{50}$) in parental, SEN Ali and SEN Eto cells. SEN Eto., etoposide-induced senescent cells. Cell line legend order was ranked based on the mean ABT-263 sensitivity of SEN Ali and SEN Eto cells.

A possible explanation for a lack of cytochrome c shift is the presence of apoptotic cells before starting the assay. For that reason, we gate for permeabilized cells that are DAPI positive, which did not undergo nuclear degradation as a result of late apoptosis. Gating of negative controls (treated with DMSO) showed no significant increase in senescent cells that were apoptotic before the start of the assay (Figure S1D). Besides A549, other cell lines showed similar responses to alamethicin and BIM, except for HCT116, which showed an adequate response to alamethicin (Figure S1E).

It has been observed before that changes in cellular content can influence the assay (Fraser et al., 2019). Since senescent cells were clearly increased in size (FSC-A values), as well as in cytochrome c signal (Figure S1D), we hypothesized that increased cellular and mitochondrial mass would result in a lower BH3 agent to mitochondrial mass ratio, affecting the assay. Accordingly, we examined an heterogenous (2-7 fold) increase in mitochondrial mass upon senescence induction across the 12 cell lines (Figure S2A). We noticed that cells with the highest ABT-263 sensitivity (MDA-MB-231, A549, SUM159) had the highest increase in mitochondrial content, while cells with low sensitivity (LoVo, Hep3B, T47D) had only a small increase in mitochondria. Nevertheless, the correlation between ABT-263 sensitivity and the increase in mitochondrial content was close to, but not significant (P= 0.056, ρ = 0.573). Next, we asked if we could correct the mitochondrial mass:BH3 agent ratio by lowering the cell number input of senescent cells. Indeed, for MDA-MB-231, the cell line with the highest increase in mitochondrial content (7-fold), we observed a better separation of cytochrome c signal between the DMSO and alamethicin at low cell density compared to high cell density (Figure S2B). At 8 x 10^3 cells per well, DMSO and alamethicin curves overlap. Surprisingly, this overlap was mainly attributed to a low cytochrome c signal for the DMSO control at high cell density. To exclude the possibility that the cytochrome c antibody (which was used in excess) staining was compromised due to inefficient permeabilization of the plasma membrane, we increased the digitonin concentration with 7-fold. Nevertheless, this increase did not enhance the separation between controls at a cell density of 4 x 10^3 (Figure S2C). Notably, the cell density corrected for mitochondrial content (1,5 x 10^3 cells per well) was similar to the cell density at which the positive and negative controls separated properly (1-2 x 10^3 cells per well) (Figure S2D), while acquiring enough cells (>500) for accurate analysis (Figure S2E). Therefore, it seems that correcting the mitochondria:BH3 agent ratio restored the functionality of the BH3 profiling assay in senescent cells.

Subsequently, we corrected the cell numbers for the senescent cells such that the mitochondrial input was equivalent to their parental counterparts, and performed BH3 profiling using BH3 peptides and BH3 mimetics with various targets (Figure 2A). This improved the response to alamethicin and high dose of BIM for most cell lines (Figure 2B). Overall, the % cytochrome release in response to BIM or alamethicin was

>60%, which we considered sufficient for a properly working BH3 profiling assay. Subsequently, we asked if there were any general differences in apoptotic priming between the parental and senescent state across cell lines. When testing the pairwise difference in response to BH3 agents in senescent versus parental cells, we identified that the response to BIM was significantly lower in the senescent state, while the response to other peptides was non-significant (Figure 2C-D). This means that the overall apoptotic priming of senescent cells is lower than that of the parental cells.

The senolytic sensitivity to ABT-263 correlates to the apoptotic priming of senescent as well as parental cells

After we explored the overall changes in apoptotic priming in senescent cells, we asked if we could find changes in mitochondrial state that could explain the variation in ABT-263 sensitivity across cell lines. First of all, even though the parental cells are largely insensitive to ABT-263, some variation in IC_{50} values can be observed between different cell lines (Figure 1G). For this reason, we utilized the mitochondrial responses of the parental cell lines to various BH3 agents – represented in Figure 2B as % cytochrome c release – and asked if these responses correlate to the cellular sensitivity of ABT-263 of parental cells – represented in Figure 1G as ABT-263 -$logIC_{50}$ values – for individual BH3 agents. We found that the cellular sensitivity of the parental cells significantly correlated to their mitochondrial response to BAD peptide (*P= 0.016,* ρ= 0.670), which targets the same anti-apoptotic proteins as ABT-263 (Figure 3A). This rank-based correlation showed indeed the highest mitochondrial BAD response for cell lines with higher ABT-263 sensitivity (Figure 3B). In addition, ABT-263 ranked after BAD, but the correlation was not significant (*P=* 0.168, ρ=0.427). This essentially confirms that the BH3 profiling assay is working, and that sensitivity to ABT-263 in the parental cells was associated with mitochondrial response to antagonism of the targets of ABT-263: BCL-XL, BCL-2, and BCL-W.
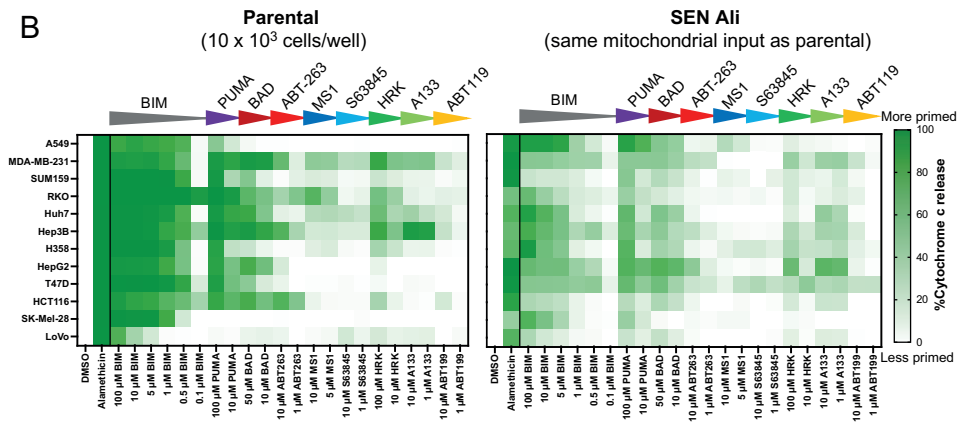
After this, we assessed the cellular sensitivity to ABT-263 of senescent cells in relation to the mitochondrial response to BH3 agents of senescent cells. We found significant correlations for PUMA and BIM peptides (Figure 3C). This indicates that senescent cells with higher cellular sensitivity to ABT-263 (-$logIC_{50}$ values) exhibits higher mitochondrial responses to PUMA and BIM peptides (Figure 3D). BIM peptide measures the overall apoptotic priming, while PUMA peptide measures how dependent cells are on the overall anti-apoptotic signaling. This is because PUMA peptide acts as a pro-apoptotic sensitizer that interacts with all the anti-apoptotic proteins (Figure 2A). As senescent cell lines with high cellular sensitivity to ABT-263 have a higher response to PUMA and BIM peptides than cells with a low sensitivity, we can conclude that ABT-263 sensitive cells are highly primed to apoptosis and depend on anti-apoptotic proteins for their survival, while ABT-263 resistant cells do not. Nevertheless, it was unexpected that the mitochondrial response to ABT-263/

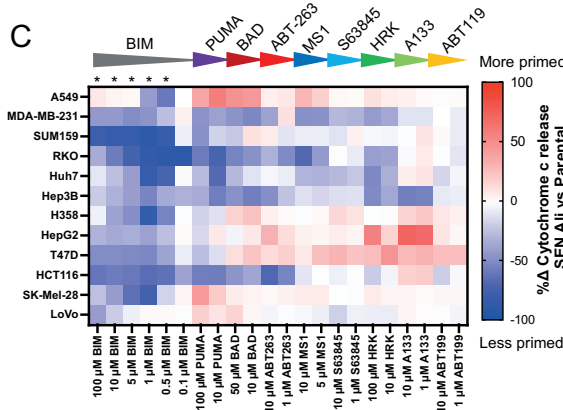BAD peptide and the cellular sensitivity to ABT-263 of the senescent cells was not correlated.
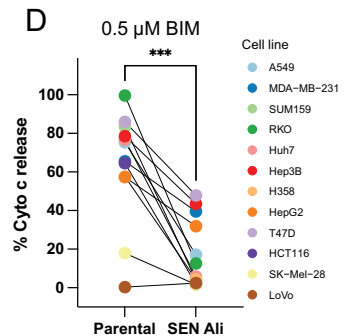

Figure 2: Overall priming to apoptosis is lower in senescent cells compared to their parental counterparts

(**A**) Table of BH3 peptides and BH3 mimetics and their respective targets. A133., A1331852. (**B**) Heatmap showing mitochondrial priming state of parental and SEN Ali cells. Values represent the mean of triplicates and are representative of at least two independent experiments. (**C**) Heatmap of difference in mitochondrial priming in SEN Ali compared to parental cells as presented in B.

Data was analyzed with two-way ANOVA repeated measures and Šidák's post-hoc test. *p < 0.001. **(D)** Before-after graph of the mitochondrial response to 0.5μM BIM. Data was analyzed with a paired two-sided Student's t-test. ***p< 0.001. **(B-D)** Cell line order was based on ABT-263 sensitivity.

Next, we asked if the sensitivity of the senescent cells to ABT-263 could already be discerned using the mitochondrial peptide responses in the parental state. We correlated the mitochondrial responses of the parental cells to peptides (from Figure 2B) to the cellular ABT-263 sensitivity of their senescent counterparts (from Figure 1G). Surprisingly, the response to BIM and PUMA peptide of the parental cells correlated significantly with the ABT-263 cellular sensitivity after these same cell lines had entered senescence (Figure 3E). Senescent cells with high sensitivity to ABT-263 showed a higher response to PUMA and BIM, already in their parental state (Figure 3F). This indicates that the overall apoptotic priming and the dependency on anti-apoptotic proteins is already different in cell lines with ABT-263 senolytic responsiveness compared to cell lines that remain refractory.

In conclusion, the response to BIM and PUMA peptides indicates that senescent cells with greater sensitivity to ABT-263 are more primed and rely more heavily on the activity of anti-apoptotic members. Cells with a high response to both BIM and PUMA are considered highly primed, since they are capable of activating MOMP upon the inhibition of anti-apoptotic proteins and already have high activity of activator proteins BIM and tBID. Therefore, the combined response to BIM and PUMA seems to determine their degree of senolytic sensitivity to ABT-263, not only in senescence but also in the non-senescent state.

ABT-263 sensitive cells show increased sensitivity to MCL-1 inhibition upon ABT-263 treatment

As the signaling of cells can change upon drug exposure, we asked if we could identify changes in apoptotic priming of senescent cells upon a three-hour treatment with ABT-263, using dynamic BH3 profiling. Our first observation was a significant change in response to the MCL-1 antagonist MS1 in treated versus untreated cells (Figure 4A). This suggests a greater MCL-1 dependency in cells treated with ABT-263. Response to other peptides was variable across cell lines. Predominantly, the change in cytochrome c release upon MS1 exposure showed an increased sensitivity of cells that were more sensitive to ABT-263 in senescent state, with A549 as the highest responder. For SUM159, Hep3B, H358, Huh7, and HepG2, the cytochrome c release was below 20% in the untreated setting and increased to 20-40% upon ABT-263 treatment (Figure 4B).
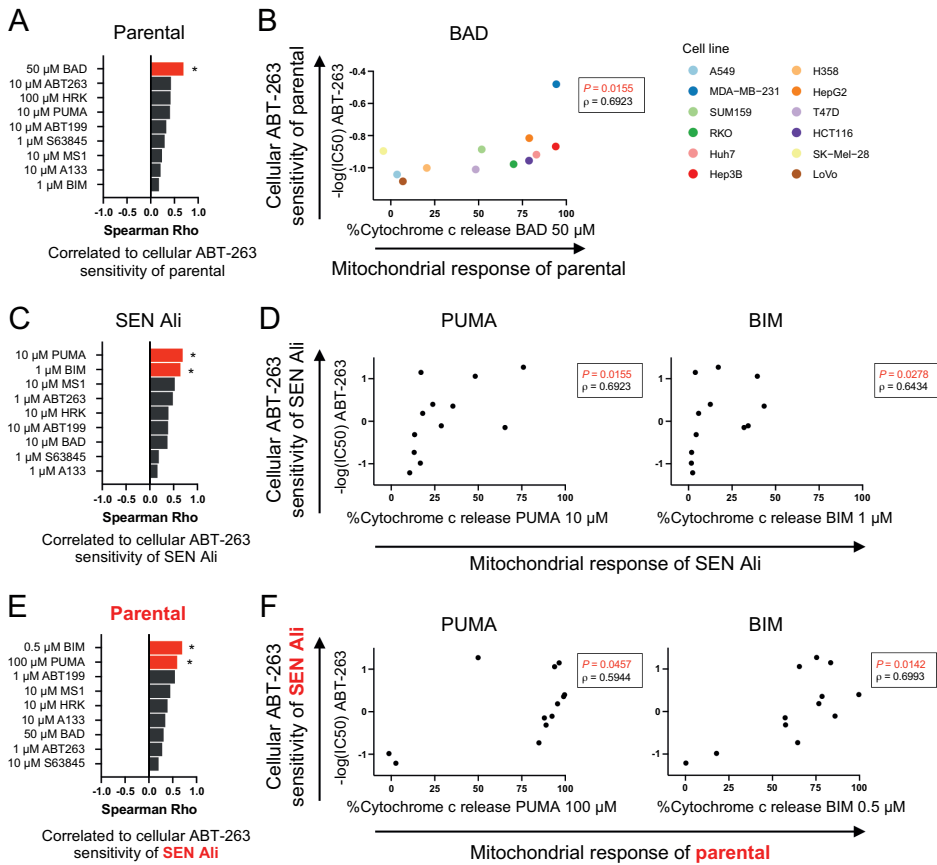
Figure 3: The senolytic sensitivity to ABT-263 correlates to the apoptotic priming of senescent as well as parental cells

(**A**) Bar graph of the results from Spearman rank correlation analysis in which the cellular ABT-263 sensitivity (-logIC$_{50}$) of parental cell lines were correlated to their mitochondrial response to BH3 agents. (**B**) Scatterplot of the cellular ABT-263 sensitivity (-logIC$_{50}$) of parental cells versus the mitochondrial response to 50 µM BIM peptide of parental cells. Each dot indicates a cell line. (**C**) Bar graphs of the results from Spearman rank correlation analysis. The cellular ABT-263 sensitivity of SEN Ali cells for various cell lines were correlated to their mitochondrial response to BH3 agents. (**D**) Scatterplots of the cellular ABT-263 sensitivity of SEN Ali cells versus the mitochondrial response to PUMA and BIM peptide of SEN Ali cells. Each dot indicates a cell line. (**E**) Bar graphs of the results from Spearman rank correlation analysis. The cellular ABT-263 sensitivity of SEN Ali cells was correlated to the mitochondrial response to BH3 agents of their parental counterparts. (**F**) Scatterplots of the cellular ABT-263 sensitivity of SEN Ali cells versus the mitochondrial response to PUMA and BIM peptide of their parental counterparts. (**A-F**) Data was analyzed with Spearman rank correlation analysis. *p<0.05. For each peptide, the most significant concentration is displayed.

To test whether the increased MCL-1 dependency was indeed associated with ABT-263 response, we tested whether the difference in cytochrome c release of ABT-263 treated versus untreated cells correlated to their ABT-263 sensitivity. This revealed a correlation for two antagonists of MCL1: MS1 peptide and BH3 mimetic S63845 (Figure 4C). This means that ABT-263 responsive cells become more sensitive to MCL-1 inhibition upon ABT-263 treatment (Figure 4D), indicating a higher MCL-1 dependency during treatment with ABT-263. On the contrary, resistant/ intermediate low cells were less sensitive to MCL-1 inhibition during treatment. This could be explained by a lack of MCL-1 dependence, or increased abundance of MCL-1, which renders cells less sensitive to its antagonism.

The abundance of MCL-1 is regulated via proteasomal degradation through NOXA (Gomex-Bougie et al., 2011) and via stabilization through BIM binding, which prevents NOXA-induced degradation (Czabotar et al., 2007). For that reason, we analyzed the levels of MCL-1, NOXA, and BIM of parental and SEN Ali cells treated with 1µM ABT-263 for 3 hours (Figure 4E). The three sensitive cell lines A549, MDA-MB-231, and SUM159 seem to have low MCL-1 levels (below detection limit) in the senescent state. Interestingly, MCL-1 levels seem to be informative in cell lines with intermediate sensitivity/ resistance to ABT-263 (Huh7, H358, T47D, HepG2, and HCT116). These followed a specific pattern: MCL-1 abundance was high in parental state, reduced in senescence, but subsequently increased upon ABT-263 treatment. This could explain why these cell lines have a lower response to MCL-1 antagonism and lower sensitivity to ABT-263 compared to sensitive cell lines. Nevertheless, MCL-1 abundance does not explain the sensitivity of every cell line, and the resistant cells SK-Mel-28 and LoVo did not show this pattern. Moreover, NOXA and BIM levels were not associated with the abundance of MCL-1, and ABT-263 treatment does not affect MCL-1 levels in parental cells.

Overall, BH3 profiling of senescent cells showed a correlation between the response to MCL-1 inhibition and ABT-263 sensitivity. This can be partly explained by upregulation of MCL-1 in resistant cells during ABT-263 treatment.
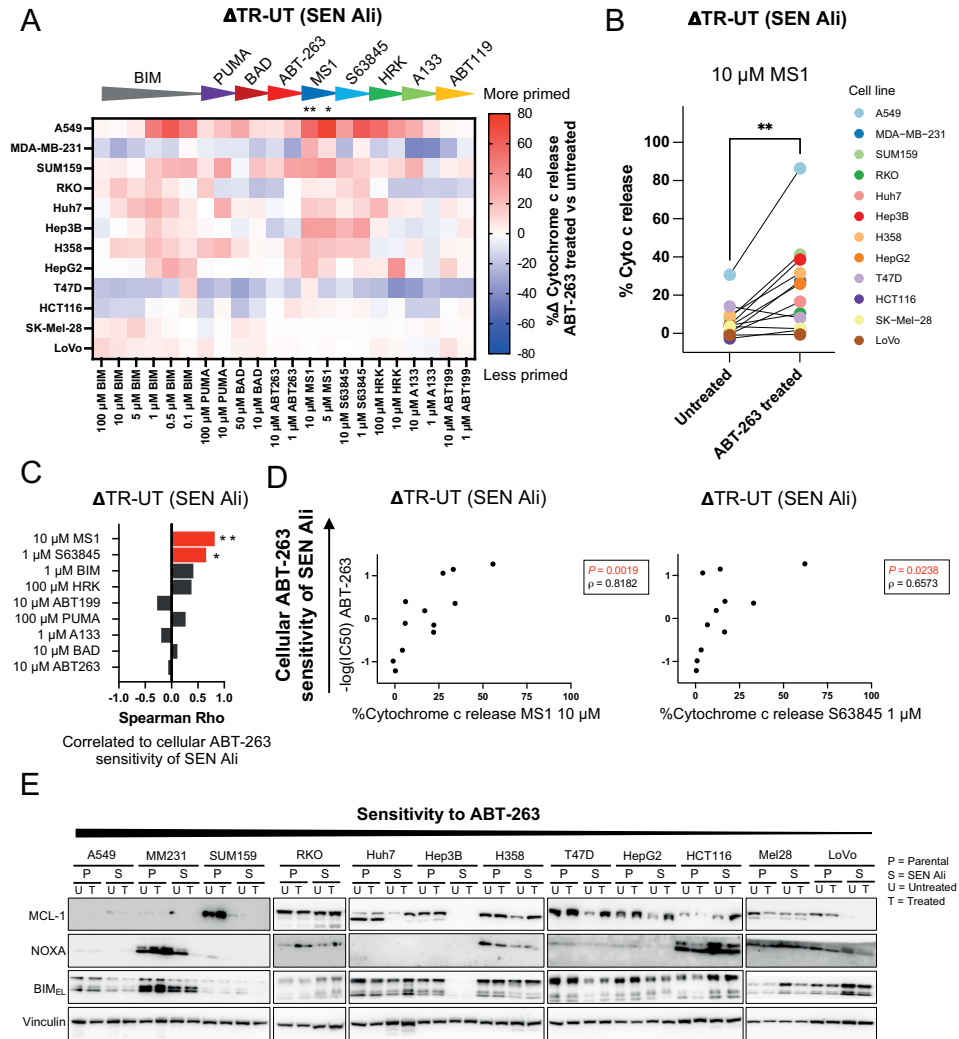
4

Figure 4: ABT-263 sensitive cells show increased sensitivity to MCL-1 inhibition upon ABT-263 treatment

(A-D) Before iBH3 profiling, SEN Ali were cultured in the presence and absence of 1 µM ABT-263 for 3 hours. ΔTR-UT., difference between ABT-263 treated and untreated cells. Cell line order was based on ABT-263 sensitivity. (A) Heatmap of difference in mitochondrial priming in ABT-263 treated versus untreated SEN Ali cells. Data was analyzed with two-way ANOVA repeated measures and Šidák's post-hoc test. *$p < 0.05$; **$p < 0.01$. (B) Before-after graph of the mitochondrial response to 10 µM MS1. Data was analyzed with a paired two-sided Student's t-test. **$p < 0.01$. (C) Bar graph of the results from Spearman rank correlation analysis in which the cellular ABT-263 sensitivity ($-logIC_{50}$) of SEN Ali cells is correlated to the difference in mitochondrial response to BH3 peptides and BH mimetics of SEN Ali ABT-263 treated versus untreated cells. (D) Scatterplots of the cellular ABT-263 sensitivity of SEN Ali cells versus the difference in mitochondrial response to MS1 and S63845 of SEN Ali ABT-263 treated versus untreated cells. (C-D) Data was analyzed with Spearman rank correlation analysis. *$p < 0.05$; **$p < 0.01$. For each peptide, the most significant concentration is displayed. (E) Western blot of cells in parental and SEN Ali state cultured in the presence or absence of 1µM ABT-263. U., untreated control; T., treated for 3 hours with ABT-263; MM231., MDA-MB-231; Mel28., SK-Mel-28.

Discussion

The long-term presence of senescent cancer cells is considered harmful and a source of cancer recurrence, and senolytic treatment has the potential to reduce these detrimental effects (Demaria et al., 2017; Wang et al., 2022). We and others have shown before that senescent cancer cells have a variable sensitivity to senolytic agent ABT-263 (Jochems et al., 2021; Shahbandi et al., 2020). In the current study, we applied BH3 profiling to elucidate how the response to ABT-263 relates to the apoptotic priming and anti-apoptotic dependency of parental and senescent cells. We found that in general, the overall apoptotic priming (measured by BIM peptide) is lower in the senescent cells compared to their parental counterparts, and that the senolytic sensitivity to ABT-263 was associated with the mitochondrial response to BIM and PUMA peptides. It even appeared that the degree of priming in the non-senescent state could predict the ABT-263 response after senescence-induction. Moreover, dynamic BH3 profiling of senescent cells treated with ABT-263 identified that response to MCL-1 antagonists (MS1 and S63845) was higher in ABT-263 sensitive cells compared to moderately sensitive or resistant cells. For some cell lines, this could be explained by the upregulation of MCL-1 upon ABT-263 treatment. Overall, these findings are summarized in Figure 5.
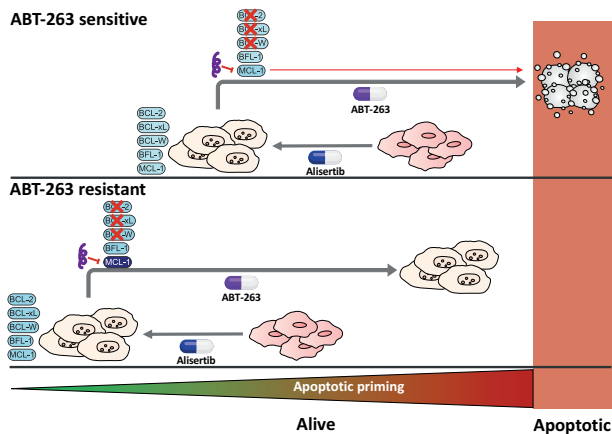
4

Figure 5: Model of mitochondrial priming state of ABT-263 sensitive and ABT-263 resistant cells.
Senescent cells are lower in apoptotic priming (measured by BIM) than parental cells, but ABT-263 sensitive cell lines are higher primed for apoptosis compared to ABT-263 resistant cells, both in parental as well as in the senescent state. The dependency on anti-apoptotic proteins (measured by PUMA) is lower in SEN Ali cells that resist ABT-263 treatment compared to those that are sensitive. More specifically, when ABT-263 sensitive SEN Ali cells are exposed to a short treatment of ABT-263, they more highly depend on MCL-1 for their survival compared to ABT-263 resistant cells.

To optimally perform BH3 profiling of senescent cells, we recommend to adjust the assay input such that the mitochondrial content of senescent and parental cells is equivalent. As senescent cells increase in size, their cellular and mitochondrial content is also increased. We show that this increase varies between 2-7 fold, which is in line with multiple studies in normal senescent cells (Martini and Passos, 2022). Without adjusting for mitochondrial input, we observed either insufficient cytochrome c staining (e.g. in MDA-MB-231) or incomplete response to alamethicin (e.g. in A549). The efficiency of cytochrome c staining can be influenced by the permeabilization of the cellular membrane by digitonin. This detergent induces pores in the cellular membrane through its interaction with cholesterol (Fan and Heerklotz, 2017). As the total cholesterol of fibroblast cells is decreased in replicative senescence (Nakamura et al., 2003), digitonin permeabilization could be impaired in senescent cells. Indeed, an increase in digitonin did not affect cytochrome c staining or response to alamethicin, however, a decrease in cell input enhanced the antibody staining and cytochrome c release upon alamethicin treatment. From this, it seems that not only the permeabilization agents but all the BH3 assay components were limiting in the senescent setting, most likely caused by the increased cellular and mitochondrial content. Nevertheless, reducing the cell numbers such that the mitochondrial input is the same between parental and senescent cells enhanced assay sensitivity restored the balance between BH3 (re)agents and mitochondrial load.

With the optimized assay, we observed that senescent cells scored lower in mitochondrial apoptotic priming (measured by BIM). On the one hand, this result was surprising to us because other studies have shown that cells responsive to BH3 mimetics are generally more primed to apoptosis than cells that do not respond to these agents (Deng et al., 2007; Letai, 2022). As cells only respond to ABT-263 after the induction of senescence, we expected higher priming in senescent compared to parental cells for cell lines that were ABT-263 sensitive. On the other hand, even though we cannot exclude the possibility that comparing parental versus senescent cells is technically challenging, there are reasons to think that we might have stumbled upon something different. The lower priming is in line with a recognized hallmark of senescent cells: they are resistant to intrinsic and extrinsic pro-apoptotic triggers (Hernandez-Segura et al., 2018; Hu et al., 2022). The reduced response to BIM indicates a reduced ability to activate BAK/BAX and subsequent MOMP in senescent cells. An obsolete dogma is that cytochrome c release from a single mitochondrion presents a 'point of no return', engaging a feedforward activation of MOMP in all mitochondria (Goldstein et al., 2000). Later, incomplete MOMP (iMOMP) was described, in which cells can survive various death stimuli through repopulation of mitochondria, leading to treatment resistance. Interestingly, treatment with ABT-737, an analog of ABT-263, could still induce apoptosis in these cells (Tait et al., 2010).

Furthermore, as we observed a small rather than complete shift in cytochrome c signal after challenging cells with alamethicin, it might be possible that senescent cells have a buffering mechanism that allows iMOMP to occur but does not induce cytochrome c release in all mitochondria. A recent study in ABT-737- and S63845-drug-tolerant persister cells described that iMOMP activates a survival response through heme-regulated inhibitor kinase (HRI) and integrated stress response (ISR) (Kalkavan et al., 2022). In addition, increase of mitochondrial mass, hyperfusion and elongation of mitochondria has been observed before in various models of senescence, and can contribute to drug resistance (Martini and Passos, 2022). Future studies will be required to determine if iMOMP could explain the low response to BIM and how the mitochondrial phenotype contributes to cell survival.

We observed that ABT-263 resistant cells showed a low response to BIM and/or PUMA. This can be due to a lack of functional activators BIM and BID or effectors BAK and BAX. Indeed, LoVo carries biallelic frameshift mutations in *BAX*, and HCT116 carries a heterozygous mutation in this gene (Rampino et al., 1997), which seem to impair but not completely prevent the activation of MOMP based on the BH3 profiling result. In both the parental as well as in the senescent state, BIM and PUMA responses were lower in these cell lines compared to the rest of the panel. Nine out of twelve cell lines showed more than 20% cytochrome c release upon BIM and PUMA peptides, meaning that cells were primed to apoptosis, while depending on anti-apoptotic signaling. In these cells, the response to BIM and PUMA correlated with senolytic sensitivity to ABT-263. This corroborates the work of others showing that the mitochondrial state measured by BH3 profiling can predict the (pre)clinical response to chemotherapy (Montero et al., 2015), NK-cell killing (Pan et al., 2022), and BH3 mimetics (Bhatt et al., 2020). Moreover, the finding that the response to ABT-263 after the induction of senescence is predetermined by its mitochondrial state is in line with our previous work, showing that the parental state dictates the behavior and characteristics of the senescent phenotype. The cell line rather than the senescence trigger strongly determines the transcriptome, SASP expression and response to ABT-263 (Jochems et al., 2021).

Moreover, we observed that ABT-263 sensitive cells have low MCL-1 levels and are more sensitive to the inhibition of this apoptotic protein during ABT-263 treatment compared to resistant cells. This indicates that the combination of ABT-263 and an MCL-1 inhibitor could enhance the apoptosis-inducing capacity in senescent cells. In fact, this combination is effective in senescent breast cancer cells and senescent melanocytes that are resistant to ABT-263. The absence of NOXA results in MCL-1 stabilization in senescent breast cancer cells (Shahbandi et al., 2020), whereas senescent melanocytes increase translation of MCL-1 through mTORC1 (Kohli et al., 2022). This indicates that different upstream processes can convert into a common mechanism of resistance, and interfering downstream of

these events might provide a treatment that can be applied for various senescent contexts. Nevertheless, clinical development of MCL-1 inhibitors is more difficult because of on-target cardiac toxicity (Bolomsky et al., 2020). Recently, a phase I trial of S64315 and Venetoclax had to be terminated (NCT03672695). Overall, it still has to be investigated whether the combination of MCL-1 inhibitors with platelet sparing ABT-263-based therapies (González-Gualda et al., 2020; He et al., 2020; Khan et al., 2019) will provide a therapeutic window.

In conclusion, this works shows that the mitochondrial precondition of the parental cell line can predict the sensitivity to ABT-263 of the same cells rendered senescent. It has been shown that BH3 profiling can be a valuable tool for *ex vivo* functional testing of liquid and solid tumors for their response to chemotherapies and BH3 mimetics (Bhatt et al., 2020; Del Gaizo Moore and Letai, 2013; Potter et al., 2021; Vo et al., 2012). The duration of this assay requires typically a few hours instead of prolonged *ex vivo* culture. BH3 profiling could be especially useful to predict the responses in a 'one-two punch' approach in which tumor cells are first induced to senesce before being treated with a senolytic. This is because the median survival of *ex vivo* primary human cancer tissues is typically 8 days (Hughes et al., 2021). As the senescence phenotype takes around a week to fully develop upon treatment, this limits the time for senolytic functional testing. Our data shows that BH3 profiling of parental cells before treatment could already be informative whether or not these cells will respond to a senolytic. This opens opportunities in which BH3 profiling could serve as a predictive index for senolytics in cancer therapy, and might provide guidance in clinical decision making.

Methods

Cell lines

Lung cancer cell lines A549 (RRID:CVCL_0023), and H358 (RRID:CVCL_1559), colon cancer cell lines RKO (RRID:CVCL_0504), HCT116 (RRID:CVCL_0291), and LoVo (RRID:CVCL_0399), were grown in RPMI medium (Gibco) supplemented with 10% FBS, 1% P/S and 2mM L-glutamine (Gibco). Triple-negative breast cancer cell line MDA-MB-231 (RRID:CVCL_0062), melanoma cell line SK-Mel-28 (RRID:CVCL_0526) and liver cancer cell lines Hep3B (RRID:CVCL_0326), HepG2 (RRID:CVCL_0027), and Huh7 (RRID:CVCL_0336), were cultured in DMEM medium supplemented with 10% fetal bovine serum (FBS, Serana), 1% penicillin/streptomycin (P/S, Gibco) and 2mM L-glutamine (Gibco). Estrogen receptor positive breast cancer cell lines T47D (RRID:CVCL_0553) was maintained in RPMI (Gibco) supplemented with 10% FBS, 1% P/S and 10 µg/ml insulin (Sigma-Aldrich). TNBC cell line SUM159 (RRID:CVCL_5423) was cultured in DMEM/F12 (Gibco) medium supplemented with 10% FBS, 1% P/S and

5 µg/ml insulin and 1ug/ml hydrocortisone (Sigma-Aldrich).

Huh7, Hep3B, and HepG2, were a gift from the Erasmus University (Rotterdam, Netherlands), and SUM159 was provided by Metello Innocenti (NKI, Amsterdam). The rest of the cell lines were obtained from ATCC, and each cell line was regularly tested for contamination with mycoplasma and their identity was validated via short tandem repeat analysis (by Eurofins Genomics). The STR profiles were analyzed with CLASTR (Robin et al., 2020). Female cell lines: T47D, MDA-MB-231, SUM159, RKO, Huh7, Hep3B. Male cell lines: HCT116, LoVo, HepG2, A549, H358, SK-Mel-28. STR profiling identified that HCT116, LoVo, and HepG2 have lost their Y-chromosome.

Compounds and peptides

Alisertib (#201931), etoposide (#100330) and ABT-263 (Navitoclax; #201970) were obtained from MedKoo Bioscience. ABT-199 (Navitoclax; #HY-15531), S63845 (#HY-100741), A-1331852 (#HY-19741) were purchased from MedChemExpress. Alamethicin (#BML-A150-0005) was obtained from Enzo Life Sciences.

The following BH3 peptide sequences were synthesized by New England Peptide: hBIM, Acetyl-MRPEIWIAQELRRIGDEFNA-Amide; mBAD, Acetyl -LWAAQRYGREL-RRMSDEFEGSFKGL- Amide; Puma, Acetyl -EQWAREIGAQLRRMADDLNA- Amide; HRK-y, Acetyl -SSAAQLTAARLKALGDELHQY- Amide; MS1, Acetyl-RPEIWMTQGLRRL-GDEINAYYAR-Amide.

IncuCyte assay

SK-Mel-28 cells (1x10^3 cells per well) were grown in 96-wells and cultured for 14 days in the presence and absence of drugs. Confluency was measured every 4 hours by IncuCyte.

Senescence-induction

The following cell numbers were seeded in 150 mm dishes and treated with the indicated alisertib (Ali) concentration: T47D, 2.5x10^6 cells, 3 µM Ali; MDA-MB-231, 2.0x10^6 cells, 0.5 µM Ali; SUM159, 7.5x10^5 cells, 0.5 µM Ali; HCT116, 2.5x10^6 cells, 0.5 µM Ali; LoVo, 3.0x10^6 cells, 0.25 µM Ali; RKO, 2.0x10^6 cells, 0.5 µM Ali; Huh7, 5.0x10^5 cells, 0.25 µM Ali; Hep3B, 1.0x10^6 cells, 0.25 µM Ali; HepG2, 1.0x10^6 cells, 0.5 µM Ali. A549, 5.0x10^5 cells, 0.5 µM Ali; NCI-H358, 1.0x10^6 cells, 0.25 µM Ali; SK-Mel-28, 1.0x10^6 cells, 0.5 µM. 24h after seeding, cells were treated and drug was refreshed every 3 to 4 days. After 7 days of treatment, the cells reached around 70-90% confluency and were senescent.

BH3 profiling by intracellular staining (iBH3)

iBH3 profiling was performed as described in (Letai and Ryan, 2013; Ryan et al., 2016).

In figure S1 and S2, cellular input for experiment was 1x10^4 of parental and senescent cells, or cell number indicated in figure. For figures 2-4, the mitochondrial input of the senescent cells was equivalent to that of 1x10^4 parental cells. The following senescent cell numbers were used: A549, 1.5x10^3 cells; MDA-MB-231, 1.4x10^3 cells; SUM159, 1.6x10^3 cells; RKO, 2.0x10^3 cells; Huh7, 2.5x10^3 cells; Hep3B, 4.1x10^3 cells; H358, 2.3x10^3 cells; HepG2, 2.8x10^3 cells; T47D, 3.7x10^3 cells; HCT116, 1.6x10^3 cells; SK-Mel-28, 2.1x10^3 cells; LoVo, 4.7x10^3 cells. Cells were profiled in 384-wells harboring various concentrations of BH3 peptides BIM, PUMA, BAD, and MS1; BH3 mimetics ABT-263, A-1331852, ABT-119, and S63845; and positive control alamethicin (25 µM) in a total of 30 µL MEB buffer (150 mM Mannitol, 10 mM HEPES-KOH [pH 7.5], 150 mM KCl, 1 mM EGTA, 1 mM EDTA, 0.1% BSA, 5 mM Succinate) + 0.001% w/v digitonin (#D5628, Sigma-Aldrich). After 50 min of incubation at 26 °C, cells were fixed for 10 min by adding 10 µL of 4% formaldehyde. The fixation was neutralized by the addition of 10 µL neutralization buffer (1.7 M Tris base, 1.25 M Glycine, pH 9.1). Finally, cells were stained overnight at 4 ° C with 10 µL of CytoC stain buffer (2% Tween20, 10% BSA (w/v) in PBS) containing 1,25 ug/ml Alexa Fluor 647 anti-cytochrome c antibody (Biolegend, cat#612310) and 10 ug/ml DAPI (Thermofisher Scientific, #D3571). Sample acquisition was performed on the High Throughput Sampler of the BD LSRFortessa Flow Cytometer (BD Biosciences) and analyzed using FlowJo (V10.7.1). The percentage of cytochrome c positive cells was determined in live, single, and DAPI positive cells. The percentage of cytochrome (cyto) c release was normalized to the DMSO control and calculated using the following equation:

$$\%Cyto\ c\ release = 100 - \frac{\%Cyto\ c\ positive_{Sample}}{\%Cyto\ c\ positive_{DMSO}}\ x\ 100$$

Mitochondrial quantification

Parental cells and senescent cells (see senescence-induction) were seeded into a 6-well. For parental cells, 5-2x 10^5 cells were seeded such that after 24h the confluency was around 80%. For senescent cells, one 70-80% confluent 150 mm dish with senescent cells (see senescence-induction) was reseeded into one 6-well plate (6 x 6-wells). The next day, the mitochondria were stained using MitoTracker™ Green FM (Invitrogen, #M7514) - hereafter referred to as MitoTracker - as recommended by the manufacturer. In short, the culture medium was replaced with medium containing 200 nM MitoTracker™ Green FM (Invitrogen, #M7514) and cells were incubated for 40-50 min under cell line growth conditions. After that, cells were trypsinized and resuspended in PBS containing 4',6-diamidino-2-phenylindole (DAPI) (10 µg/ml). Finally, samples were acquired using the Attune™ NxT (Invitrogen). The median fluorescence intensity (MFI) of MitoTracker was analysed in live, single and non-dead (DAPI negative) cells in FlowJo™ (v.10.7.1). To calculate the background corrected MFI

for independent experiments, the mean MFI of technical duplicates was subtracted by the MFI of a fluorescence minus one (FMO) control. To calculate the change in mitochondrial content, the background corrected MFI of the senescent cells was divided by the mean of two technical replicates of the parental cells.

Dose-response assay

SK-Mel-28 parental cells and senescent cells (see senescence-induction) were seeded into 96-wells and treated with various drug concentrations using the HP D300 Digital Dispenser. Parental cells were seeded in $1x10^3$ cells per 96-well. For the senescent cells, one 70-80% confluent 150 mm dish with senescent cells (see senescence-induction) was reseeded into one 96-well plate (96 x 96-wells). CellTiter-Blue assay for cell viability was performed with resazurin sodium salt (sigma-Aldrich, #R7017) and measured with EnVision 2104 Multilabel Reader (PerkinElmer). Half maximal inhibitory concentration (IC50) was estimated using the four-parameter logistic curve analyzed with GraphPad Prism (v9.0.0). As a positive control for killing, phenylarsine oxide (Sigma-Aldrich, cat:#P3075) was used, while DMSO served as a negative control. Assays were run in technical triplicates, in three independent experiments.

Westernblot

Senescence was induced for 7 days (see senescence-induction) and lysates were collected after 24h drug-washout. After that, cells were washed with cold PBS and lysed with RIPA buffer [25mM Tris-Cl (pH7.5), 1% NP40, 1% sodium deoxycholate, 0.1%SDS, and 150mM NaCl], supplemented with Halt™ Protease & Phosphatase Single-Use Inhibitor cocktail (Thermo Scientific, cat:#78442). Supernatant was separated after centrifugation for 30 min at 14.000 rpm at 4 °C. Protein concentrations were determined using Pierce™ BCA assay (Thermo Scientific, cat:# 23225), according to manufacturer's instructions. Samples were denatured with Bolt™ Sample Reducing Agent (Thermo Fisher, cat:#B0009) followed by 5 min incubation at 95 °C. After that, samples were run (SDS-PAGE) on a 5-15% Bis-Tris gel (Thermo Fisher) for 30 min at 200V. Proteins were transferred to a polyvinylidene fluoride (PVDF) membrane at 340 mA for 120 min. Blocking, incubation of primary and secondary antibody was performed under conditions recommended by the manufacturer. Primary antibodies detected BIM (Cell Signaling Technology Cat# 2933, RRID: AB_1030947), MCL-1 (Cell Signaling Technology Cat#5453, RRID: AB_10694494), NOXA (Abcam Cat# ab13654, RRID: AB_300536), Vinculin (Sigma-Aldrich Cat# V9131, RRID: AB_477629), P27 (BD Biosciences Cat# 610242, RRID: AB_397637), Phospho-S780 Rb (Cell Signaling Technology Cat# 8180, RRID: AB_10950972), Lamin B1 (Cell Signaling Technology Cat# 12586, RRID:AB_2650517), and Alpha-Tubulin (Sigma-Aldrich Cat# T9026, RRID: AB_477593). Membranes were incubated with a 1:10000 dilution of

4

secondary HRP conjugated anti-mouse (RRID: AB_11125547) or anti-rabbit (RRID: AB_11125142) antibody for 1 hour in blocking solution. After washing, proteins were visualized with a chemiluminescence substrate (ECL, Bio-Rad) on the ChemiDoc (Bio-Rad).

Senescence-Associated β-Galactosidase Activity (SA-β-Gal) Staining

Parental and senescent cells were seeded into 6-well plate (1×10^5 cells per well) one day before staining. SA-β-Gal staining was performed with the Senescence Cells Histochemical Staining Kit (cat#: CS0030) from Sigma-Aldrich, according to manufacturer's instructions. At least 100 cells per condition were scored for SA-β-gal positivity, from three independent experiments. Images were taken at 100x magnification.

References

Bhatt, S., Pioso, M.S., Olesinski, E.A., Yilma, B., Ryan, J.A., Mashaka, T., Leutz, B., Adamia, S., Zhu, H., Kuang, Y., et al. (2020). Reduced mitochondrial apoptotic priming drives resistance to BH3 mimetics in acute myeloid leukemia. Cancer Cell *38*, 872–890.

Bolomsky, A., Vogler, M., Köse, M.C., Heckman, C.A., Ehx, G., Ludwig, H., and Caers, J. (2020). MCL-1 inhibitors, fast-lane development of a new class of anti-cancer agents. J. Hematol. Oncol. *13*, 1–19.

Chang, J., Wang, Y., Shao, L., Laberge, R.-M., Demaria, M., Campisi, J., Janakiraman, K., Sharpless, N.E., Ding, S., Feng, W., et al. (2016). Clearance of senescent cells by ABT-263 rejuvenates aged hematopoietic stem cells in mice. Nat. Med. *22*, 78–83.

Czabotar, P.E., Lee, E.F., Van Delft, M.F., Day, C.L., Smith, B.J., Huang, D.C.S., Fairlie, W.D., Hinds, M.G., and Colman, P.M. (2007). Structural insights into the degradation of Mcl-1 induced by BH3 domains. Proc. Natl. Acad. Sci. U. S. A. *104*, 6217–6222.

Demaria, M., O'Leary, M.N., Chang, J., Shao, L., Liu, S., Alimirah, F., Koenig, K., Le, C., Mitin, N., Deal, A.M., et al. (2017). Cellular senescence promotes adverse effects of chemotherapy and cancer relapse. Cancer Discov.

Deng, J., Carlson, N., Takeyama, K., Dal Cin, P., Shipp, M., and Letai, A. (2007). BH3 Profiling Identifies Three Distinct Classes of Apoptotic Blocks to Predict Response to ABT-737 and Conventional Chemotherapeutic Agents. Cancer Cell *12*, 171–185.

Van Deursen, J.M. (2019). Senolytic therapies for healthy longevity. Science (80-.). *364*, 636–638.

Ewald, J.A., Desotelle, J.A., Wilding, G., and Jarrard, D.F. (2010). Therapy-induced senescence in cancer. J. Natl. Cancer Inst. *102*, 1536–1546.

Fan, H.Y., and Heerklotz, H. (2017). Digitonin does not flip across cholesterol-poor membranes. J. Colloid Interface Sci. *504*, 283–293.

Fraser, C., Ryan, J., and Sarosiek, K. (2019). BH3 Profiling: A Functional Assay to Measure Apoptotic Priming and Dependencies. Methods Mol. Biol. *1877*, 61–76.

Del Gaizo Moore, V., and Letai, A. (2013). BH3 profiling - Measuring integrated function of the mitochondrial apoptotic pathway to predict cell fate decisions. Cancer Lett. *332*, 202–205.

Goldstein, J.C., Waterhouse, N.J., Juin, P., Evan, G.I., and Green, D.R. (2000). The coordinate release of cytochrome c during apoptosis is rapid, complete and kinetically invariant. Nat. Cell Biol. 2, 156–162.

Gomex-Bougie, P., Ménoret, E., Juin, P., Dousset, C., Pellat-Deceunynck, C., and Amiot, M. (2011). Noxa controls Mule-dependent Mcl-1 ubiquitination through the regulation of the Mcl-1/USP9X. Biochem. Biophys. Res. Commun. *413*, 460–464.

González-Gualda, E., Pàez-Ribes, M., Lozano-Torres, B., Macias, D., Wilson, J.R., González-López, C., Ou, H.L., Mirón-Barroso, S., Zhang, Z., Lérida-Viso, A., et al. (2020). Galacto-conjugation of Navitoclax as an efficient strategy to increase senolytic specificity and reduce platelet toxicity. Aging Cell 1–19.

Hayflick, L., and Moorhead, P.S. (1961). The serial cultivation of human diploid cell strains. Exp. Cell Res.

He, Y., Zhang, X., Chang, J., Kim, H.N., Zhang, P., Wang, Y., Khan, S., Liu, X., Zhang, X., Lv, D., et al. (2020). Using proteolysis-targeting chimera technology to reduce navitoclax platelet toxicity and improve its senolytic activity. Nat. Commun. *11*.

Hernandez-Segura, A., Nehme, J., and Demaria, M. (2018). Hallmarks of Cellular Senescence. Trends Cell Biol. *28*, 436–453.

Hu, L., Li, H., Zi, M., Li, W., Liu, J., Yang, Y., Zhou, D., Kong, Q_.P., Zhang, Y., and He, Y. (2022). Why Senescent Cells Are Resistant to Apoptosis: An Insight for Senolytic Development. Front. Cell Dev. Biol. *10*, 1–17.

Hughes, D.L., Hughes, A., Soonawalla, Z., Mukherjee, S., and O'neill, E. (2021). Dynamic physiological culture of ex vivo human tissue: A systematic review. Cancers (Basel). *13*.

Jochems, F., Thijssen, B., De Conti, G., Jansen, R., Pogacar, Z., Groot, K., Wang, L., Schepers, A., Wang, C., Jin, H., et al. (2021). The Cancer SENESCopedia: A delineation of cancer cell senescence. Cell Rep. *36*, 109441.

Kale, J., Osterlund, E.J., and Andrews, D.W. (2017). BCL-2 family proteins: changing partners in the dance towards death. Cell Death Differ. *25*, 65–80.

Kalkavan, H., Chen, M.J., Crawford, J.C., Quarato, G., Fitzgerald, P., Tait, S.W.G., Goding, C.R., and Green, D.R. (2022). Sublethal cytochrome c release generates drug-tolerant persister cells. Cell *185*, 3356-3374.e22.

Kaur, J., and Farr, J.N. (2020). Cellular senescence in age-related disorders. Transl. Res. *226*, 96–104.

Khan, S., Zhang, X., Lv, D., Zhang, Q_., He, Y., Zhang, P.,

Liu, X., Thummuri, D., Yuan, Y., Wiegand, J.S., et al. (2019). A selective BCL-XL PROTAC degrader achieves safe and potent antitumor activity. Nat. Med. *25*, 1938–1947.

Kohli, J., Ge, C., Fitsiou, E., Doepner, M., Brandenburg, S.M., Faller, W.J., Ridky, T.W., and Demaria, M. (2022). Targeting anti-apoptotic pathways eliminates senescent melanocytes and leads to nevi regression. Nat. Commun. *13*, 7923.

Lafontaine, J., Cardin, G.B., Malaquin, N., Boisvert, J.S., Rodier, F., and Wong, P. (2021). Senolytic targeting of bcl-2 anti-apoptotic family increases cell death in irradiated sarcoma cells. Cancers (Basel). *13*, 1–20.

Letai, A. (2022). Apoptosis: Directly Targeted at Last. J. Clin. Oncol. *40*, 1693–1695.

Letai, A., and Ryan, J. (2013). BH3 Profiling in Whole Cells by Fluorimeter or FACS. Methods *61*, 156–164.

Martini, H., and Passos, J.F. (2022). Cellular senescence: all roads lead to mitochondria. FEBS J.

Michaloglou, C., Vredeveld, L.C.W., Soengas, M.S., Denoyelle, C., Kuilman, T., Van Der Horst, C.M.A.M., Majoor, D.M., Shay, J.W., Mooi, W.J., and Peeper, D.S. (2005). BRAFE600-associated senescence-like cell cycle arrest of human naevi. Nature *436*, 720–724.

Montero, J., Sarosiek, K.A., DeAngelo, J.D., Maertens, O., Ryan, J., Ercan, D., Piao, H., Horowitz, N.S., Berkowitz, R.S., Matulonis, U., et al. (2015). Drug-induced death signaling strategy rapidly predicts cancer response to chemotherapy. Cell *160*, 977–989.

Nakamura, M., Kondo, H., Shimada, Y., Waheed, A.A., and Ohno-Iwashita, Y. (2003). Cellular aging-dependent decrease in cholesterol in membrane microdomains of human diploid fibroblasts. Exp. Cell Res. *290*, 381–390.

Pan, R., Ryan, J., Pan, D., Wucherpfennig, K.W., and Letai, A. (2022). Augmenting NK cell-based immunotherapy by targeting mitochondrial apoptosis. Cell *185*, 1521-1538.e18.

Potter, D.S., Du, R., Bhola, P., Bueno, R., and Letai, A. (2021). Dynamic BH3 profiling identifies active BH3 mimetic combinations in non-small cell lung cancer. Cell Death Dis. *12*.

Rampino, N., Yamamoto, H., Li, Y., Sawai, H., Reed, J.C., and Perucho, M. (1997). Somatic Frameshift Mutations in the BAX Gene in Colon Cancers of the Microsatellite Mutator Phenotype. Science (80-.). *275*, 967–969.

Robin, T., Capes-Davis, A., and Bairoch, A. (2020). CLASTR: The Cellosaurus STR similarity search tool - A precious help for cell line authentication. Int. J. Cancer *146*, 1299–1306.

Ryan, J., Montero, J., Rocco, J., and Letai, A. (2016).

IBH3: Simple, fixable BH3 profiling to determine apoptotic priming in primary tissue by flow cytometry. Biol. Chem. *397*, 671–678.

Sarosiek, K.A., and Letai, A. (2016). Directly targeting the mitochondrial pathway of apoptosis for cancer therapy using BH3 mimetics – recent successes, current challenges and future promise. FEBS J. *283*, 3523–3533.

Shahbandi, A., Rao, S.G., Anderson, A.Y., Frey, W.D., Olayiwola, J.O., Ungerleider, N.A., and Jackson, J.G. (2020). BH3 mimetics selectively eliminate chemotherapy-induced senescent cells and improve response in TP53 wild-type breast cancer. Cell Death Differ.

Tait, S.W.G., Parsons, M.J., Liambi, F., Bouchier-Hayes, L., Connell, S., Muñoz-Pinedo, C., and Green, D.R. (2010). Resistance to caspase-indepedent cell death requires persistance of intact mitochondria. Dev Cell *18*, 802–813.

Taylor, R.C., Cullen, S.P., and Martin, S.J. (2008). Apoptosis: Controlled demolition at the cellular level. Nat. Rev. Mol. Cell Biol. *9*, 231–241.

Vo, T.T., Ryan, J., Carrasco, R., Neuberg, D., Rossi, D.J., Stone, R.M., Deangelo, D.J., Frattini, M.G., and Letai, A. (2012). Relative mitochondrial priming of myeloblasts and normal HSCs determines chemotherapeutic success in AML. Cell *151*, 344–355.

Wang, L., Lankhorst, L., and Bernards, R. (2022). Exploiting senescence for the treatment of cancer. Nat. Rev. Cancer *22*, 340–355.

Yosef, R., Pilpel, N., Tokarsky-Amiel, R., Biran, A., Ovadya, Y., Cohen, S., Vadai, E., Dassa, L., Shahar, E., Condiotti, R., et al. (2016). Directed elimination of senescent cells by inhibition of BCL-W and BCL-XL. Nat. Commun. *7*.

Zhu, Y., Tchkonia, T., Fuhrmann-Stroissnigg, H., Dai, H.M., Ling, Y.Y., Stout, M.B., Pirtskhalava, T., Giorgadze, N., Johnson, K.O., Giles, C.B., et al. (2016). Identification of a novel senolytic agent, navitoclax, targeting the Bcl-2 family of anti-apoptotic factors. Aging Cell *15*, 428–435.
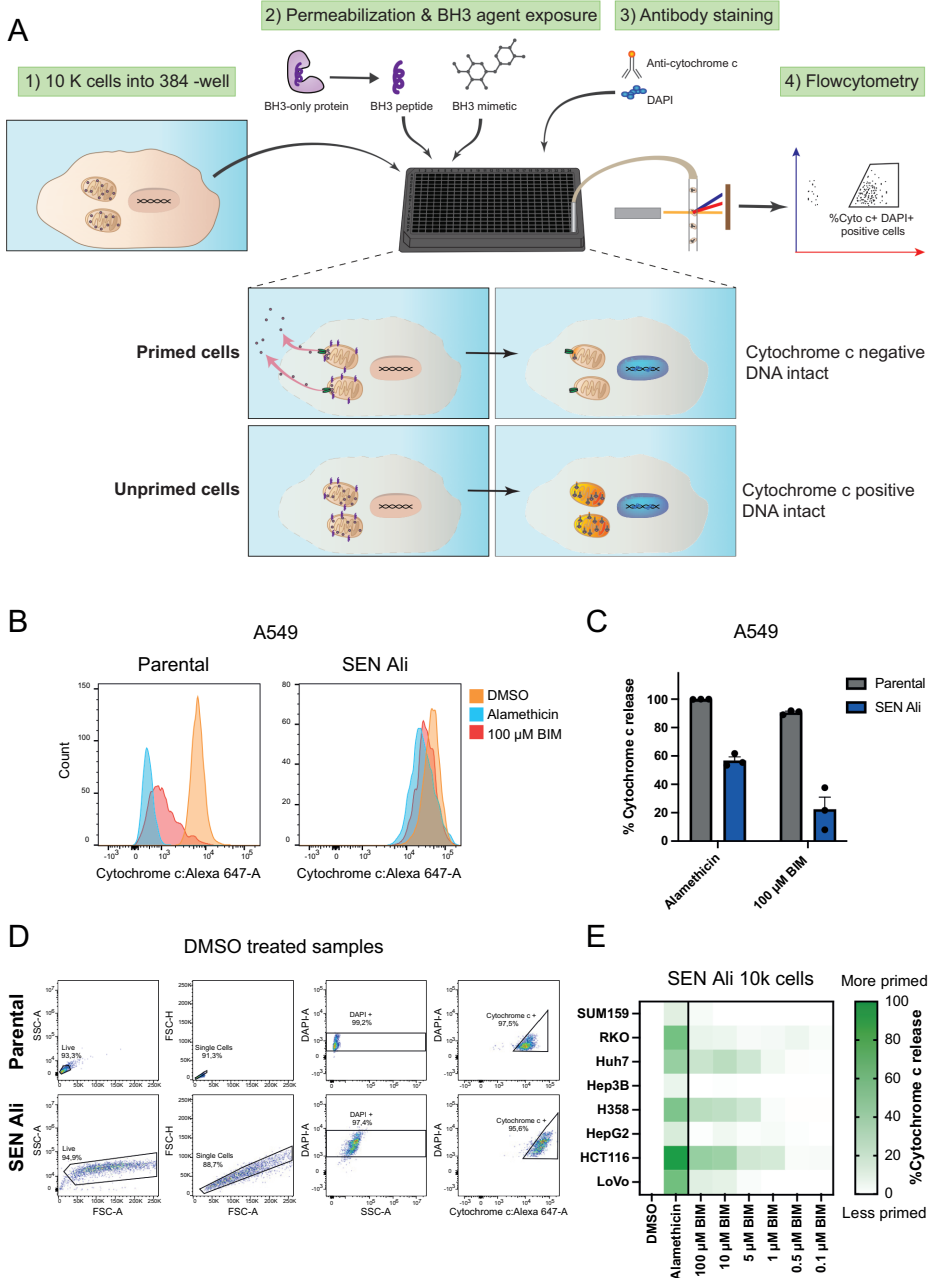
Supplementary figures

Figure S1: BH3 profiling of senescent cells shows incomplete cytochrome c release for alamethicin and BIM. (A) Outline of BH3 profiling procedure. Cells are seeded into 384-wells, permeabilized and exposed to various BH3 peptides and BH3 mimetics. After exposure, cells are stained with anti-cytochrome c antibody or DAPI. In this process, cells that activate MOMP upon

exposure to peptides will release cytochrome c into the cytosol, which will diffuse through the cellular membrane and exits the cell. This renders these cells cytochrome c negative. In contrast, cells that did not activate MOMP will stain cytochrome c positive. DAPI staining is performed to exclude cells from the analysis that show apoptosis-induced DNA degradation, which indicates that cells underwent apoptosis before the start of the assay. Lastly, profiled cells can be acquired by flow cytometry and will be analyzed for cytochrome c and DAPI positivity. (**B**) Histogram of cytochrome c:Alexa 647-A signal measured with flow cytometry. BH3 profiling was performed using DMSO as negative control, alamethicin as a positive control and high dose of BIM peptide. (**C**) Bar graph of the percentage of cytochrome c released upon BH3 profiling of parental and SEN Ali cells. Release is relative to DMSO. Data represents the mean ±SEM of triplicates. (**D**) Gating strategy for data acquired with flow cytometry for A549 parental and SEN Ali cells. Samples represent DMSO control samples from the same experiment as depicted in B and C. (**E**) Heatmap indicating the % of cytochrome c release upon BH3 profiling of various cell lines. Values indicate the mean of triplicates. Cell lines are ordered based on ABT-263 sensitivity.
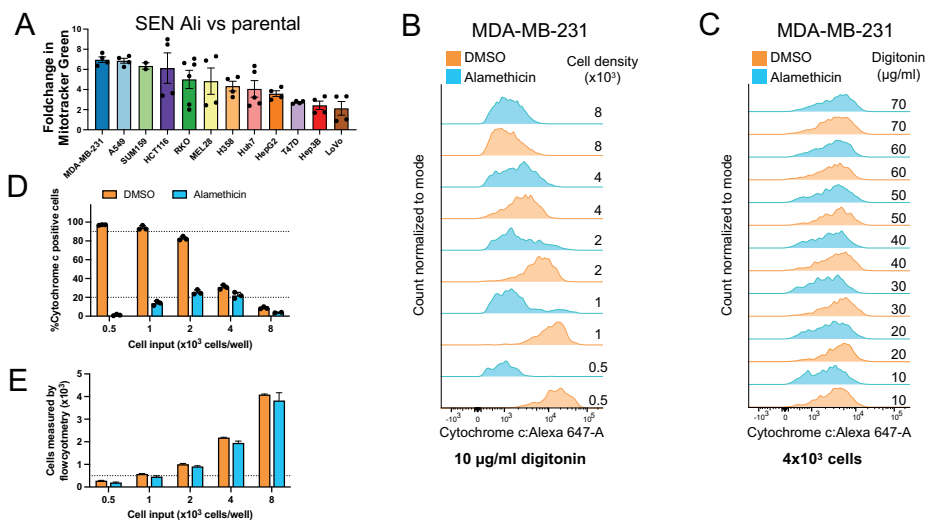

Figure S2: Separation between negative and positive controls is restored after correcting for mitochondrial content. (**A**) Bargraph of the foldchange in mitochondrial content measured by Mitotracker Green signal. Datapoints represent replicates that were obtained from two independent experiments. Cell lines are ordered based on change in mitochondria. (**B**) Histogram of cytochrome c:Alexa 647-A signal from iBH3 profiling assay that covers a range of cell densities as input for DMSO and alamethicin exposure. (**C**) Histogram of cytochrome c:Alexa 647-A signal from iBH3 profiling assay that covers a range of digitonin concentrations as input for DMSO and alamethicin exposure. (**D**) Bar graph of % of cytochrome c positive cells, determined for iBH3 assay covering various cell densities. Data was quantified from the representative results shown in B. (**E**) Bar graph of cell numbers measured by flow cytometry from iBH3 assay covering various cell densities.

4

CHAPTER 5

Exploring senescent cancer cell resistance to senolytic agent ABT-263

Fleur Jochems[1,3], Marlou Haverkamp[1,3], Ziva Pogacar[1],
Cor Lieftink[2], Hendrik J. Kuiken[2], Liqin Wang[2],
Roderick L. Beijersbergen[2,4], & René Bernards[1,4]

[1]Division of Molecular Carcinogenesis, Oncode Institute, Netherlands Cancer
Institute, Plesmanlaan 121, 1066 CX Amsterdam, The Netherlands
[2]Division of Molecular Carcinogenesis, The NKI Robotics and Screening Center,
Netherlands Cancer Institute, Plesmanlaan 121, 1066 CX Amsterdam, The
Netherlands
[3]These authors contributed equally
[4]These authors contributed equally

Abstract

Senescence is a cellular state triggered by various stress provoking insults, leading to a stable cell proliferation arrest and a phenotype switch. The senescence phenotype is characterized by an altered transcriptomic and epigenetic makeup, which renders senescent cells vulnerable to cytolytic agents called 'senolytics'. For example, in order to survive, senescent cells rely on the activity of anti-apoptotic proteins, which can be targeted by BH3 mimetic ABT-263. This compound is senolytic in both normal as well as in cancer senescent cells derived from various tissues. However, our lab and others have shown that certain senescent cancer cells remain resistant to this drug. To find possible resistance mechanisms to ABT-263, we performed a genome-wide functional genetic screen in senescent cells using CRISPR/Cas9 to find candidate genes that upon loss conferred resistance to ABT-263. This screen identified multiple players of the intrinsic apoptosis pathway (*BAX, VDAC2, CASP9*) and genes involved in counteracting the anti-apoptotic activity of MCL-1 and XIAP (*PMAIP1, DIABLO, HUWE1*) as involved in resistance to ABT-263. The latter might indicate that ABT-263-responsive senescent cells downregulate anti-apoptotic proteins *a priori* of senolytic treatment. Moreover, other candidate hits have been implicated in the negative regulation of the PI3K-AKT pathway (*VHL, RACK1*), indicating a pro-survival effect of this pathway. Conversely, VHL or RACK1 possibly abolish the pro-survival effect of PI3K-Akt signaling in senescent cells. Understanding mechanisms of resistance and increased sensitivity to ABT-263 will contribute to the design of future senolytic combination therapies or biomarkers of response to ABT-263.

5

Introduction

Cellular senescence is a phenotype that is elicited upon various stress-inducing events, like DNA-damage, nutrient deprivation, ROS accumulation and telomere-shortening (reviewed in Gorgoulis et al., 2019). This phenotype is characterized by a cell cycle arrest and transition in cell morphology (Hayflick, 1965), secretion of various factors known as the senescence-associated secretory phenotype (SASP) (Coppé et al., 2008), increase in SA-ß-galactosidase activity (Dimri et al., 1995), and remodeling of heterochromatin (Narita et al., 2003). However, senescent cells also display a heterogeneous gene expression (Basisty et al., 2020; Hernandez-Segura et al., 2017; Jochems et al., 2021). This heterogeneity forms the basis for the somewhat mixed reputation of senescent cells in the context of cancer: depending on the composition of their SASP and the stability of their cell cycle arrest, senescent cancer cells are either beneficial or detrimental for tumor propagation (Lee and Lee, 2014; Pérez-Mancera et al., 2014; Schosserer et al., 2017). As evidence is increasing that senescent cancer cells can resume proliferation, promote cancer stemness, and result in cancer relapse (Dirac and Bernards, 2003; Milanovic et al., 2018; Roberson et al., 2005; Saleh et al., 2017), it has been considered that the elimination of senescent cancer cells can be an attractive therapeutic strategy for the treatment of cancer (Wang et al., 2022a). Studies focused on the role of survival pathways in senescent cells led to the identification of various agents that activate apoptosis in senescent cells, so-called 'senolytics' (Soto-gamez et al., 2019).

In order to survive cellular insults, cells can adopt pro-survival strategies that counteract intrinsic and extrinsic apoptosis. Intrinsic apoptosis can be triggered by intracellular stress, depending on the intricate dance of BCL2 family member proteins (Kale et al., 2017), which are divided into three classes: the effectors, which orchestrate the mitochondrial outer membrane permeabilization (MOMP); the anti-apoptotic proteins, which inhibit the effectors; and the sensitizers that act as pro-apoptotic factors by inhibiting the anti-apoptotic proteins (Singh et al., 2019). After MOMP, cytochrome c is released into the cytoplasm where it interacts with APAF-1 to form the apoptosome, activating a cleaving cascade of Caspase 9 and Caspase 3/7, which dismantle the cell into apoptotic bodies (Taylor et al., 2008). During extrinsic apoptosis, cells respond to extracellular death signals, starting with death receptor activation, cleavage of Caspase 8, and activation of Caspase 3/6/7 (Elmore, 2007). Crosstalk between the intrinsic and extrinsic pathways occurs via BID, which is cleaved by Caspase 8 (Luo et al., 1998). In order to resist apoptosis, anti-apoptotic proteins BCL-XL, BCL-2, BCL-W, MCL-1 or BFL-1 play an important role in the intrinsic pathway, whereas cFLIP, an inhibitor of Death Receptor 5 (DR5) can prevent extrinsic apoptosis. Other proteins involved in apoptosis resistance are XIAP and Survivin, which act downstream of MOMP by inhibiting the activation of

5

Caspase 9, 3 and 7 (O'Brien and Kirby, 2008).

The survival of senescent cells has been attributed to BCL-XL, BCL-2, BCL-W, and/or cFLIP anti-apoptotic proteins, and targeting these players has a senolytic effect (Chang et al., 2016; Wang et al., 2022b; Zhu et al., 2016). A broad acting senolytic agent is ABT-263 (Navitoclax), which targets BCL-XL, BCL-2, and BCL-W (Zhu et al., 2016). ABT-263 shows enhanced tumor cell killing in a treatment regimen that first provokes senescence and subsequently applies this senolytic agent to remove senescent cancer cells, referred to as a 'one-two punch' (Saleh et al., 2020; Wang et al., 2017). Moreover, this senolytic agent reliefs age-related disease in preclinical models (Chang et al., 2016; Cristina et al., 2019; Sugihara et al., 2020), and reduces adverse effect of chemo or irradiation therapy (Chang et al., 2016; Demaria et al., 2017; Pan et al., 2017). Unfortunately, the clinical development of ABT-263 is partly encumbered by thrombocytopenia and neutropenia (Kaefer et al., 2014). Even though this drug showed acceptable toxicity in phase II clinical studies (clinicaltrials.gov; Brachet et al., 2022; de Vos et al., 2021), alternative ABT-263 therapies that circumvent these toxicities are under development. For instance, PROTACs PZ15227 and DT2216 rely on E3 ligase activity absent in platelets (He et al., 2020; Khan et al., 2019), and Nav-Gal, which consists of nanoparticles covered with a SA-ß-galactosidase cleavable moiety, releases ABT-263 in SA-ß-galactosidase positive cells only (González-Gualda et al., 2020).

ABT-263's effectiveness has been attributed to combined inhibition of BCL-XL and BCL-W (Yosef et al., 2016), as well as BCL-XL and BCL-2 (Zhu et al., 2016). Moreover, we and others have shown that responses of senescent cancer cells to ABT-263 are highly cell line dependent, ranging from highly responsive to refractory (Jochems et al., 2021; Shahbandi et al., 2020; Zhu et al., 2016). It has been suggested that the presence of Noxa is a prerequisite for ABT-263 sensitivity (Shahbandi et al., 2020). However, a full understanding of how certain senescent cancer cells can resist ABT-263 is currently lacking.

Here, we performed an unbiased genome-wide CRISPR/Cas9 knock-out screen in senescent cells and identified multiple candidate genes that upon loss cause resistance of senescent cancer cells to ABT-263.

Results

A549 encoding a doxycyclin-inducible Cas9 as a screening model

To identify genes involved in resistance to senolytic killing by ABT-263, we performed a genome-scale loss of function genetic screen in ABT-263-sensitive senescent cells, using the genome-wide Brunello library (Sanjana et al., 2014). We chose A549 cells as a screening model, as this cell line has the highest senolytic response to ABT-263 and showed a strong senescence response after treatment with aurora kinase A inhibitor

alisertib (Jochems et al., 2021).

In order to control the timing of gene editing, we transduced a doxycycline-inducible Cas9 lentiviral vector into A549 cells and selected a monoclonal population (A549-iCas9) that exhibited a similar response to alisertib as the parental, wild type (WT) cells, shown by the cellular response to various drug concentrations (Figure 1A). In addition, when A549-iCas9 cells as well as WT A549 cells were treated with 0.5µM alisertib, 100% of the cell populations stained positive for SA-ß-gal (Figure 1B-C), and protein markers of senescence - downregulation of Retinoblastoma protein (RB) phosphorylation and LaminB1, and upregulation of p21^{CIP1}- became evident after alisertib treatment (Figure 1D).

Next, we optimized the ABT-263 concentration for the screen to enable detection of true positive sgRNA hits over background noise. In general, positive selection CRISPR/Cas9 screens rely on the proliferation of a few drug-resistant knock-out clones, resulting in an increase in abundance of hit sgRNAs. However, in our set-up sgRNAs that confer resistance to ABT-263 may not show a large increase in abundance as the resistant cells may remain in a non-proliferative, surviving senescent state. For that reason, it was important to find an ABT-263 concentration that eliminates virtually all (inhibitory concentration 100% (IC_{100})) senescent cells. Testing a range of ABT-263 concentrations, the A549-iCas9 senescent cells showed a similar response to ABT-263 as the WT senescent cells (Figure 1E). We determined that a drug concentration of 1µM was sufficient to eliminate the entire population (Figure 1F), optimal for screening.

An additional consideration is that gene editing in senescent cells might be hindered by the presence of heterochromatin structures and lack of mitosis. To ensure adequate levels of gene editing, we first exposed proliferating and senescent A549-iCas9 cells to a range of doxycycline concentrations for three days. This resulted in a strong expression of Cas9 protein for 0.25-4µM doxycycline, both in proliferating and senescent cells (Figure G). Next, we assessed the targeting efficiency of Cas9 using the gene editing reporter vector pXPR_011 (Doench et al., 2014), which encodes the GFP gene and a sgRNA targeting this gene (Figure H). Both A549-iCas9 proliferating and senescent iCas9 populations were transduced with pXPR_011, cultured in the presence and absence of doxycycline, and subsequently analyzed by flow cytometry to determine the percentage of GFP+ cells. In proliferating cells, the targeting efficiency was >95% after 5 days of doxycycline treatment (Figure S1A), while senescent cells displayed a targeting efficiency of ~83% after 7 days (Figure S1B) and a targeting efficiency of >90% after 11 days of treatment (Figure 1I-J). We conclude that gene editing in senescence is slower than in the parental state, but extended doxycycline treatment can compensate for this difference.

In summary, the A549-iCas9 A549 cells are a suitable screening model based on the following observations: i) 100% senescence-induction efficiency with 0.5µM alisertib;

5

ii) complete senolytic response with 1µM ABT-263; iii) >90% gene editing efficiency with an inducible-Cas9 system and 11-day treatment with 1µg/ml doxycycline.
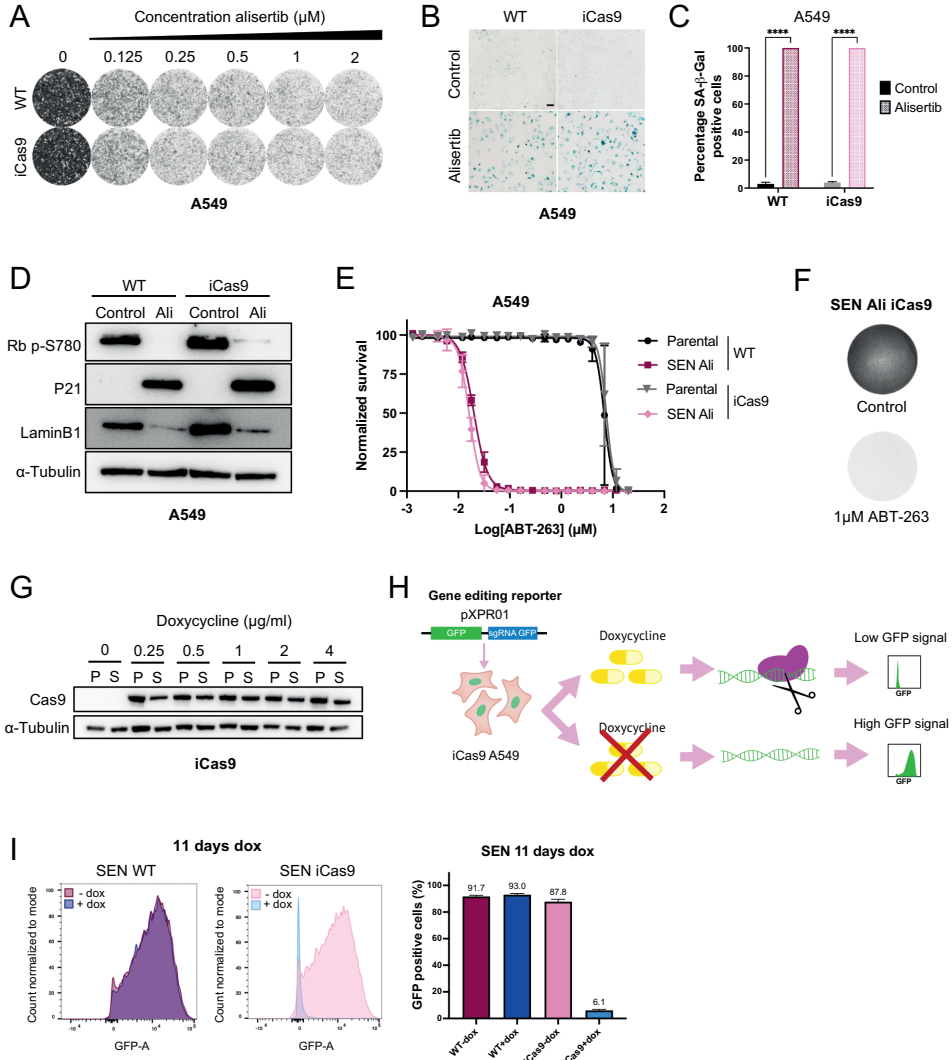

Figure 1. A549 encoding a doxycyclin-inducible Cas9 as a screening model. (A) Colony formation assay of A549 WT and A549 encoding doxycycline-inducible Cas9 (A549-iCas9). In a 6-well plate, 15 K cells were seeded and cultured for 7 days in the presence of various doses alisertib. **(B-G, I)** Cells were made senescent with 0.5 µM alisertib for 6-7 days. **(B)** Representative images of SA-ß-gal staining. The experiment was performed in two biological replicates and quantified in C. Scale bar = 100 µm. **(C)** Percentage of SA-ß-gal positive cells from two independent experiments. The data represents the mean ± SEM and was analyzed with a two-way ANOVA and Šídák's post-hoc test. ****p<0.0001 **(D)** Western blot for senescence markers. Alpha-tubulin served as a loading control. Ali, alisertib-induced senescent cells. **(E)** Dose-response curve for ABT-263. Parental and senescent cells were

seeded into a 96-well plate and treated with a range of ABT-263 concentrations for 5 days. Cell viability was measured by a cell titer blue assay and normalized to negative and positive controls. Each datapoint represents the mean of triplicate wells and are representative of two independent experiments. (**F**) Colony formation assay for screen optimization. 3 million A549-iCas9 cells were induced to senesce with 0.5 µM alisertib in 15-cm dishes. Next, cells were cultured for another 5 days in the presence or absence of 1 µM ABT-263 before fixation and staining. (**G**) Western blot for Cas9 protein in A549-iCas9 cells. Parental and senescent cells were treated with doxycycline for 3 days. P, parental; S, senescent. (**H**) Schematic outline of the gene editing reporter vector pXPR011 and the experimental set-up. pXP011 encodes GFP and a sgRNA targeting GFP. To determine the targeting efficiency of the doxycycline-inducible Cas9, cells were transduced with pXP011 and cultured with and without doxycycline. The percentage of GFP positive cells is determined by flowcytometry. (**I-J**) Senescent WT and A549-iCas9 A549 cells transduced with pXPR011 treated with doxycycline for 11 days. (**I**) Histogram of GFP signal measured by flowcytometry. Frequency was normalized to mode. (**J**) Quantification of GFP positive cells. WT, wildtype; A549-iCas9, doxycycline-inducible Cas9 monoclonal population.

Genetic screen in senescent cells identified 13 candidate genes for ABT-263 resistance

Using the optimized conditions as described above, we performed the screen as depicted in figure 2A. Briefly, A549-iCas9 cells were transduced in biological triplicates with the lentiGuide-Puro Brunello library (Doench et al., 2016) and selected for transduced cells. After selection, timepoint 0 (T0) samples were collected as a reference for sgRNA representation. Next, senescence was induced in the remaining cells by a 3-day treatment with alisertib, followed by 13 days of combined alisertib and doxycycline treatment to activate gene-editing. T1 samples were collected right before ABT-263 treatment, as another reference sample. The remaining cell populations were divided into two arms each and cultured in the presence or absence of ABT-263 for 5 days. Subsequently, T2-treated and T2-untreated samples were harvested and genomic DNA was isolated. The yield of genomic DNA from the T2-treated samples was low due to low number of cells collected in these samples, while for the T0, T1 and T2untreated samples sufficient gDNA was recovered to represent full library complexity. For this reason, we performed PCR using all of the genomic DNA for samples with a low DNA yield, and captured sgRNA regions using biotinylated primers in samples with sufficient DNA yield prior to PCR amplification to limit the number of PCRs for these samples.

To assess the technical quality of the screen we explored the similarity of each replicate and condition. As expected, hierarchical clustering of the read counts showed that the biological replicates of the T0, T1 and T2-untreated samples highly correlated with each other, while the T2-treated samples formed a distinct cluster away from the other samples (Figure 2B, S2A). The strong similarity between the T0, T1 and T2-untreated samples indicated that the library representation was well-maintained after senescence-induction, as also seen in the sgRNA rank plot (Figure S2B). In contrast to most CRISPR/Cas9 knockout screens, essential genes were

5

not depleted in T1 versus T0 samples, possibly due to most essential genes being required for survival of proliferating but not senescent cells (Figure S2C). Overall, the quality of the screen was sufficient to proceed with further analyses.

When comparing the sgRNA abundance of treated versus untreated and reference samples, 13 candidate genes were identified (Figure 2C), of which most were functionally-associated by STRING analysis and apoptosis-related (Figure 2D). The top hit was Bcl-2-associated X protein (*BAX*), which was already known to be required for ABT-263 activated apoptosis in senescent cells (Saleh et al., 2020). The second hit was Voltage-dependent anion-selective channel protein 2 (*VDAC2*), which is an anion-channel required for BAX to execute MOMP and loss of *VDAC2* phenocopies *BAX* knock-out cells in preventing apoptosis (Chin et al., 2018). Other hits that are part of the apoptotic pathway were Caspase 9 (*CASP9*), second mitochondria-derived activator of caspases (*DIABLO/SMAC*) and Phorbol-12-myristate-13-acetate-induced protein 1 (*PMAIP1,* encoding NOXA). Moreover, the hit E3 ligase HECT, UBA and WWE domain containing E3 ubiquitin protein ligase 1 (*HUWE1/MULE*) is also linked to apoptosis because it is required for MCL1 degradation (Zhong et al., 2005). Other hits were involved in the regulation of the PI3K-AKT pathway: Receptor for activated C kinase 1 (*GNB2L1/RACK1*), von Hippel-Lindau tumour suppressor (*VHL*), and Required for Cell Differentiation1 Homolog (*RQCD1*) (Ajiro et al., 2009; Mamidipudi and Cartwright, 2009; Yamaguchi et al., 2016). The remaining hits were: pre-mRNA processing factor 40 homolog A (*PRPF40A*), ring finger and WD repeat domain 2 (*RFWD2*), and AT-rich interaction domain 2 (*ARID2*).

In conclusion, we show that with specific adaptations, it is possible to perform a successful genome-wide functional genetic resistance screen in senescent cells. Moreover, we identified 13 candidate genes that upon knock-out mediate resistance to senolytic killing by ABT-263, of which six were related to the intrinsic apoptosis pathway, two to the PI3K-AKT pathway, and for five their role in apoptosis has not been described.
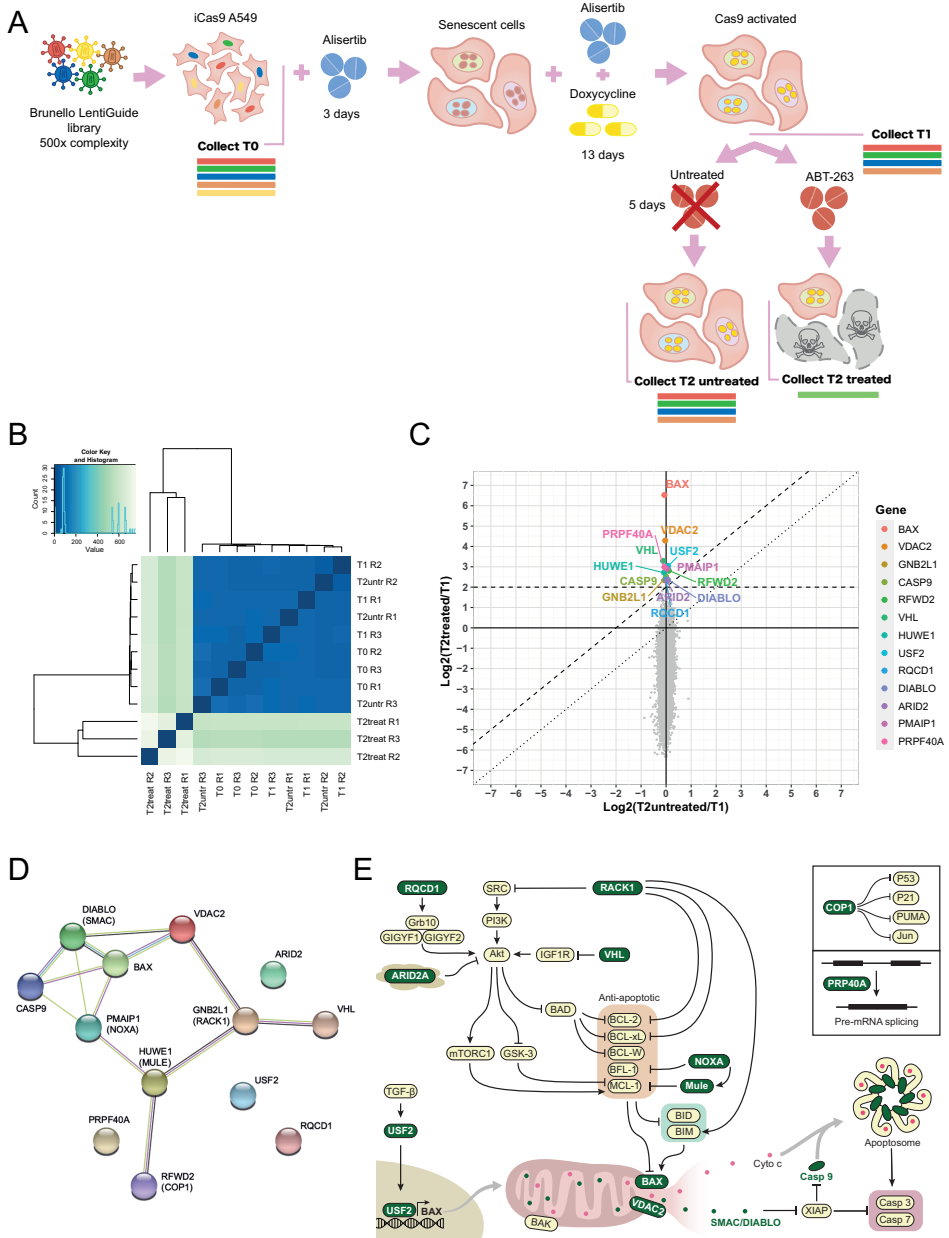
Figure 2. Genetic screen in senescent cells identified 13 candidate genes for ABT-263 resistance.
(**A**) Schematic outline of resistance screen for ABT-263 senolytic killing. First, A549 A549-iCas9 cells were transduced with the genome wide Brunello guide RNA library. After collecting reference sample T0, senescence was induced by 3 days of alisertib treatment followed by another 13 days of gene editing with combined doxycycline and alisertib treatment. At this point, the reference sample T1 was collected. After Cas9 activation, the senescent cells were maintained for 5 days with and without ABT-263, and T2-untreated and T2-treated samples were collected. T, timepoint.

(**B**) Heatmap of hierarchical clustering of the individual samples across various timepoints and biological replicates of the resistance screen. (**C**) Scatter plot in which each dot represents a gene, and the axes indicate the log2 fold change (Log2FC) calculated by DESeq2. RRA rank positions and FDR were used for hit selection (indicated in color), using two criteria: (i) T2-treated vs. T2-untreated FDR <=0.1 and RRA log2FC >= 2 (diagonal dashed line); (ii) T2-treated vs T1 FDR <= 0.1 and RRA log2FC >= 2 (horizontal dashed line). (**D**) Output from STRING analysis with the 13 hit candidate genes as input. (**E**) Schematic representation of the PI3K-Akt and BCL-2 family pathway, highlighting candidate genes in saturated colors.

Discussion

In this study, the aim was to uncover mechanisms of resistance to ABT-263 in senescent cells with the goal to identify candidate biomarkers of treatment response and putative targets for novel interventions that circumvent resistance. We performed a genome-wide functional genetic CRISPR/Cas9 knockout screen in senescent cells to identify genes that upon loss cause resistance to senolytic killing with ABT-263. We showed that performing resistance screens in senescent cells requires specific adaptations, and below we discuss guidelines for future screens. Candidate genes identified by the resistance screen are responsible for executing the apoptotic machinery, play a role in suppressing anti-apoptotic proteins, or are involved in the PI3K-Akt pathway. Furthermore, we discovered additional candidate genes that are not yet associated with these processes. First of all, additional experiments will be required to validate that knock-out of these genes confers resistance to ABT-263 in senescent cells. Below, we discuss how the candidate genes could be involved in the response to ABT-263 and their functional connections (Figure 2E). Finally, we consider opportunities for future biomarkers of ABT-263 treatment response and new treatment strategies that may enhance ABT-263 senolytic therapy.

Functional genetic screens are a valuable tool to identify a drug's mechanism of action, drug resistance mechanisms, or potential biomarkers to guide clinical practice (Mulero-Sánchez et al., 2019). Performing a resistance screen in senescent cells as opposed to proliferating cells comes with various challenges. An obvious difference between screening in a senescent versus proliferative setting is the inability of senescent cells to multiply. In the proliferative setting, the success of a resistance screens is attributed to the proliferation of a few resistant clones after prolonged treatment at $\sim$ IC_{80} drug concentration, resulting in an increase in abundance of the sgRNA sequences encoded by these cells over background noise caused by non-resistant cells that survived the treatment. Thus, in absence of proliferation such as in senescent cell populations, it is important to identify the lowest drug concentration at which only true positive resistant knock-out cells will be left behind, aiming at $\sim IC_{99}$ in non-edited cells. Nevertheless, this means that the number of cells in treated and untreated conditions will be unequal, which requires

additional adjustment in subsequent processing. For instance, we recommend to use a DNA-isolation method that can handle both small and large cell numbers. For example, a non-silica-based DNA isolation method in which reagent volumes can be adjusted, like with the DNeasy Blood and Tissue Kit (see methods for details). Moreover, after genomic DNA isolation, samples with low DNA yield can be directly used as template for PCR, while samples with a high DNA yield can be first processed using a DNA capture protocol to enrich sgRNA encoding DNA fragments, which will limit the number of PCR reactions for these samples.

Other considerations for resistance screening in senescent cells are: (i) an inducible-Cas9 system is required to activate gene-editing after senescence-induction to prevent screening for resistance against the senescence-inducing drug; (ii) after Cas9 activation with doxycycline, senescent cells need longer time (11 days) than parental cells (5 days) to reach a gene-editing efficiency of >90%; (iii) classical 'essential genes' for proliferating cells may not be required for the survival of senescent cells, which means that other genes have to be considered as positive controls for gene editing (e.g. *BCL2L1* and *CFLAR* in A549); (iv) on a per cell basis, the cellular mass of senescent cells is strongly increased compared to parental cells. We have observed that this can decrease the efficiency of DNA isolation methods for untreated senescent samples, and recommend to optimize the senescent cell number input such that protein contamination is prevent. The final cell number might be lower than instructed by the manufacturer; (v) senescent cells often become multinucleated, therefore it has to be considered that the actual library coverage calculated using the DNA concentration or read counts is lower in reality. Overall, we have shown that implementing the adaptations mentioned above make it possible to effectively perform drug resistance screens in senescent cells.

The ABT-263 resistance screen in senescent A549 cells yielded 13 candidate hits. The two most significant hits, *BAX* and *VDAC2,* as well as *CASP9* were considered to be positive controls because these genes are required for the execution of apoptosis and thus, knocking out these genes would abolish apoptosis. Specifically, BAX is essential for ABT-263-induced killing (Inoue-Yamauchi et al., 2017; Saleh et al., 2020), and VDAC2 is required for BAX-mediated MOMP (Chin et al., 2018). Moreover, *CASP9* forms the core of the apoptosome (Rodriguez and Lazebnik, 1999). Loss-of function mutations in *BAX, CASP9,* or *VDAC2* will likely hinder ABT-263-induced apoptosis, and might serve as biomarkers of treatment response. Interestingly, the colon cancer cell lines LoVo and HCT116 harbor mutations in *BAX,* which probably explains why senescent LoVo and HCT116 cells remain largely unresponsive to ABT-263 (Jochems et al., 2021). To conclude, the fact that our screen was able to identify validated known, key players involved in ABT-263-induced cell death increases the credibility that other candidate genes are involved in ABT-263 senolytic resistance.

The most interesting hits from the screen were those involved in the negative

5

regulation of anti-apoptotic proteins, as the latter could be exploited therapeutically by combining ABT-263 with a drug targeting these anti-apoptotic proteins. In our screen, we found multiple candidate genes involved in the downregulation of MCL1. For instance, *PMAIP* (encoding NOXA) and E3 ligase *HUWE1* (also referred to as MULE) are both involved in the degradation of anti-apoptotic protein MCL1. NOXA interacts and sequesters MCL1, and allows MULE to ubiquitinate MCL-1 for proteasomal degradation and inhibits the USP9X/MCL-1 interaction, preventing deubiquitylation (Gomex-Bougie et al., 2011). These results indicate that degradation of MCL-1 by NOXA and MULE is required for the killing activity of ABT-263. This is also in line with work from others showing that ABT-263's effectiveness is attributed to a reduction of MCL-1 during mitotic arrest and that the level of NOXA in senescent cells correlates with ABT-263 response (Shahbandi et al., 2020; Shi et al., 2008). Consequently, a combination treatment with MCL-1 inhibitor S63845 and ABT-263 was able to induce cell death in senescent ABT-263 resistant cells (Shahbandi et al., 2020).

Another candidate hit involved in the negative regulation of anti-apoptotic proteins was *SMAC/DIABLO*. This protein inhibits the pro-survival protein XIAP. As *Smac/Diablo*^{-/-}-mice are still able to develop normally and activate apoptosis (Okada et al., 2002), it raises the question whether SMAC/DIABLO is required for execution of apoptosis in general, or whether this is specific for the senescent state. A recent preprint from Colville et al. described a genetic screening method in which apoptotic, floating cells as well as live attached cells were sequenced after short-term treatment with ABT-263, referred to as 'Death-seq'. Using this method in doxorubicin-induced senescent IMR-90 cells, they found *SMAC/DIABLO* to be involved in ABT-263 resistance, and showed that inhibition of XIAP with Birinapant synergizes with ABT-263 in senescent, but not in proliferating cells (Colville et al., 2022). In future studies, it will be interesting to test whether this synergy is also observed in senescent cancer cells and whether the requirement of SMAC/DIABLO in apoptosis is dependent on the apoptosis-trigger, cell line or cell state.

Other hits were involved in the regulation of the PI3K-Akt pathway: *RACK1, VHL*, and *RQCD1*. RACK1 and VHL negatively regulate Akt, while RQCD1 has an activating effect (Ajiro et al., 2009; Mamidipudi and Cartwright, 2009; Yamaguchi et al., 2016). Moreover, it has been shown that RACK1 influences apoptosis and Akt signaling in multiple ways: i) inhibition of SRC (proto-oncogene tyrosine-protein kinase), which subsequently leads to a downregulation of PI3K and Akt activity; ii) increasing levels of BCL-2 and BCL-XL, while reducing levels of BIM; and, iii) activation and translocation of BAX via a SRC-independent mechanism (Mamidipudi and Cartwright, 2009). The candidate hit VHL is involved in multiple cellular processes (Li and Kim, 2011), but also inhibits *IGF1R* expression. Loss of VHL has been shown to activate AKT and cause resistance to 2-deoxyglucose-ABT-263 combination therapy

(Yamaguchi et al., 2016). In contrast to the other hits, RQCD1 has been described to promote Akt activity via interaction with the growth factor receptor binding protein 10 (Grb10) and its interacting molecules, and silencing of RQCD1 was found to reduce Ser 473 phosphorylation of Akt (Ajiro et al., 2009). More research will be required to identify if and potentially how the PI3K-Akt is involved in resistance to ABT-263, and whether suppression of this pathway is a prerequisite for ABT-263 response in senescent cells.

Interestingly, Akt activation can also lead to increased MCL-1 levels, which might be the connection between the PI3K/Akt pathway and resistance to ABT-263-induced senolysis (Figure 2E). Akt can activate MCL-1 via two mechanisms: (1) activation of mammalian target of rapamycin complex 1 (mTORC1), possibly leading to elF4F mediated cap-dependent translation that reduces MCL-1 levels (Senichkin et al., 2020); (2) negative regulation of glycogen synthase kinase-3 (GSK-3), which usually phosphorylates MCL-1 for proteasomal degradation, leading to stabilization of MCL-1 (Maurer et al., 2006). Notwithstanding, the PI3K-Akt pathway can contribute to cell survival in various other ways. For example, Akt can block apoptosis through phosphorylating caspase-9, BAD, and FOXO subfamily of forkhead transcription factors (Fresno Vara et al., 2004). Senolytic agents dasatinib, quercetin, and fisetin are thought to -besides possible other targets- induce senolysis by inhibiting Src and PI3K-Akt signaling (Wang et al., 2022a). Even though it is proposed that these drugs result in BCL-XL suppression, the exact mechanism of apoptosis induction remains to be discovered. This shows that combining ABT-263 with PI3K/Akt inhibitors could potentially enhance ABT-263 response. Notably, it has been shown that a combination of ABT-263 and inhibition of mTORC1 - downstream of Akt - with AZD8055 induces apoptosis in non-senescent ABT-263-resistant small cell lung cancer cells (Faber et al., 2015). In addition, single AZD8055 treatment has been shown to be senolytic in CDC7 inhibitor-induced but not alisertib-induced senescent liver cancer cells (Wang et al., 2019). Since aurora kinase A can activate the ERK1/2/mTOR axis, alisertib treatment results in mTOR suppression (Zhang et al., 2019), possibly blocking the PI3K/Akt/mTORC1 pro-survival pathway in alisertib-induced senescent cells, rendering them sensitive to ABT-263. Overall, the PI3K-Akt pathway plays an important role in cell survival, and it remains to be determined whether inhibition of this pathway influences MCL-1 or BCL-XL levels in senescent cells and whether this occurs via mTORC1, GSK-3 or BAD.

The remaining hits were not clearly linked to apoptosis or the PI3K-Akt pathway. The hit *USF2* is possibly linked to *BAX* expression, as transforming growth factor TGF-β can increase BAX expression via transcription factor USF2 (Sato et al., 2011). However, it is unclear whether this protein is solely required for BAX expression. Other candidate genes were *PRPF40A*, *RFWD2*, and *ARID2*. PRPF40A is a putative homolog of Pre-mRNA processing protein 40 and is important in pre-mRNA

5

splicing (Kao and Siliciano, 1996). Its expression is linked to hypoxia in lung cancer (Oleksiewicz et al., 2017) and has been proposed as a potential biomarker for poor prognosis in pancreatic cancer (Huo et al., 2019). The latter might indicate a role in cell survival. RFWD2, also known as COP1 (constitutively photomorphogenic 1), acts as a E3 ubiquitin ligase for p53 degradation (Dornan et al., 2004), and knock out of RFWD2 may thus potentially activate the anti-apoptotic effects of p53 (Jänicke et al., 2008). In contrast, silencing of COP1 in breast cancer cells was found to lead to the expression of p53 target genes *CDKN1A* and *PUMA* (p53-upregulated modulator of apoptosis). The latter exerts a pro-apoptotic rather than a survival effect (Ka et al., 2018). ARID2 is part of the polybromo-associated BAF (PBAF) SWI/SNF complexes, which are heterochromatin-remodelers implicated in transcriptional regulation and DNA damage repair. For that reason, ARID2 is involved in a variety of signaling pathways, and one study suggests that ARID2 overexpression can potentially activate Akt signaling (Tao et al., 2017). Overall, validating *PRPF40A*, *RFWD2* and *ARID2* might uncover important pathway interactions that could explain ABT-263 resistance.

In conclusion, our resistance screen for senolytic killing with ABT-263 identified several genes that are possibly involved in negatively regulating anti-apoptotic proteins and the PI3K-Akt pathway. If these candidate hits validate, the outstanding question is whether resistance to ABT-263 occurs via the activation of the PI3K-Akt pathway and (subsequent) upregulation of MCL-1 or through activation of mTORC1, GSK-3 or Bad. Other questions include: (i) Are RACK1, ARID2A and VHL responsible for the negative regulation of Akt signaling in senescent cells? (ii) Is alisertib normally reducing mTORC1 in senescent cells, leading to a reduction of PI3K/Akt/mTORC1, but when counteracted, this is causing resistance? (iii) Could loss-of-function mutations in these genes or activating mutations in PI3K/Akt serve as biomarkers for response? (iv) Can we overcome resistance to ABT-263-induced senolysis by combining an Akt inhibitor with ABT-263? Future experiments are needed to address these questions. Overall, we show how to effectively screen for resistance against senolytic agents in senescent cells, which can help future researchers to identify resistance mechanisms, resistance biomarkers, or the mechanism of action of other senolytic agents.

Methods

Cell lines

All cell lines were acquired from ATCC. The A549 non-small lung cancer cell line was cultured in RPMI (GIBCO) supplemented with 10% fetal bovine serum (Serana), 1% L-glutamine (GIBCO), and 1% penicillin/streptomycin (GIBCO). The transformed human embryonic kidney cells HEK293T were cultured in DMEM (GIBCO)

supplemented with 10% fetal bovine serum (Serana), 1% L-glutamin (GIBCO), and 1% penicillin/streptomycin (GIBCO). The doxycycline-inducible Cas9 monoclonal population was created by lentiviral transduction (see method section of lentiviral infection) of Inducible Lentiviral hEF1α-Blast-Cas9 Nuclease Plasmid DNA (Edit-R™, Horizon Discovery, cat: #CAS11229). Next, monoclonal populations were hand-picked and we selected the clone with the lowest background expression and highest Cas9 induction after doxycycline treatment.

All cell lines were regularly tested for mycoplasma and cell line identity was confirmed using STR profiling (Eurofins Genomics) and CLASTR (Robin et al., 2020).

Colony formation assay and crystal violet staining
Cells were seeded into 6-well plates at 15k cells per well and cultured for 7 days in the presence or absence of alisertib. Drug containing growth media was replaced every 3-4 days. After treatment, cells were fixed with 4% paraformaldehyde (v/v) for 20 min. Then, cells were stained for 10 min with 0.5% crystal violet (w/v) for visualization and scanned.

Senescence-associated ß-galactosidase activity staining
One day before staining, ~200k senescent and parental cells were seeded into a 6-well plate. The staining was performed using the Senescence Cells Histochemical Staining Kit (cat#: CS0030, Sigma-Aldrich), following manufacturer's recommendations. For each condition, 5 images were taken and at least 100 cells were manually counted for SA-ß-gal positivity. The experiment was performed two independent times, in technical triplicates.

Westernblot
In a 15-cm dish, 1 M cells were seeded and treated with 0.5 µM alisertib for 7 days. After 24 hours drug washout, cells were washed with cold PBS and lysed in RIPA buffer [25 mM Tris-Cl (pH 7.5), 1% NP40, 1% sodium deoxycholate, 0.1% SDS, and 150 mM NaCl], supplemented with Halt Protease & Phosphatase Single-Use Inhibitor cocktail (Thermo Scientific, cat:#78442). Samples were resolved and visualized on gel as described in before (Jochems et al., 2021). Briefly, samples were separated on a NuPAGE™ 4% - 12% Bis-Tris gel (Thermo Fisher) and transferred to a polyvinylidene fluoride (PVDF) membrane. Primary antibodies detecting Phospho-S780 Rb (RRID: AB_10950972), Lamin B1 (RRID: AB_2650517), P21 (RRID: AB_2890611), Alpha-Tubulin (RRID: AB_477593), Vinculin (RRID: AB_477629) were used. Proteins were visualized using secondary HRP conjugated antibodies anti-mouse (RRID: AB_11125547) or anti-rabbit (RRID: AB_11125142) and chemiluminescence substrate (ECL, Bio-Rad), measured on the ChemiDoc (Bio-Rad).

5

Dose-response assay

For the senescent cells, 1 M cells were treated for 7 days with 0.5 μM alisertib in a 15-cm dish to create an 80% confluent dish with senescent cells, of which 1/120 was seeded per 96-well. Parental cells (10 k per 96-well) and senescent cells were cultured for 5 days in the presence of various ABT-263 concentrations. ABT-263 was dispensed using a HP D300 digital dispenser. To measure cell viability, cells were incubated in the presence of resazurin sodium salt (Sigma-Aldrich, #R7017) for 3 hours at 37 °C and fluorescence was measured with an Envision 2104 Multilabel Reader (PerkinElmer). Data was collected in technical triplicate and biological duplicates. DMSO was used as a negative control and phenylarsine oxide (Sigma-Aldrich, cat:#P3075) as a positive control for maximum killing. The half maximal inhibitory concentration was estimated using the four-parameter logistic regression model in Graphpad Prism (v8.4.3).

Determining Cas9 editing efficiency by flowcytometry

Cells transduced with pXPR011 (Addgene, cat#59702) were harvested and stained with 4',6-diamidino-2-phenylindole (DAPI) (10 μg/ml) before they were acquired on the Attune™ NxT (Invitrogen). The GFP intensity was determined for the live, single and DAPI negative population. The editing efficiency was determined by the % of GFP negative cells in the doxycycline treated sample minus the untreated control.

Lentiviral infection

To produce lentivirus, packaging vector psPAX2 (Addgene, cat:#12260), envelope vector pCMV-VSV-G (Addgene, cat:#8454) and transfer vector of interest were co-transfected in HEK293T cells. Lentiviral supernatant was collected and filtered through 0.45 μm filter. Cells were infected at a multiplicity of infection (MOI) < 0.3 in the presence of 8 μg/mL polybrene and transduced cells were selected for 48 hours with 2 μg/mL puromycin.

Functional genetic screen

Lentivirus was produced from the Brunello lentiGuide library (Addgene, cat:#73178; (Doench et al., 2016), as described earlier (Evers et al., 2016). The screen was performed at 500x complexity and a MOI < 0.3. The A549-iCas9 monoclonal cell line was seeded into 129x 15-cm dishes with 5M cells per dish. The next day, cells were transduced with lentivirus library for 24 hours and transduced cells were selected with 2 μg/mL puromycin for 72 hours. Medium with puromycin was refreshed after 48 hours. After selection, T0 samples were collected and the remaining cells were reseeded into 180x 15-cm dishes with 3 M cells per dish. These plates were subsequently treated with 0.5 μM alisertib for 3 days to induce senescence, followed by another 13 days of combined alisertib and 1 μg/ml doxycycline. After the senescence-induction and

gene-editing, T1 samples were collected and the remaining plates were divided into one arm with and one without treatment. Cells were kept in culture for another 5 days in the presence or absence of 1 μM ABT-263 before T2-treated and T2-untreated samples were collected, respectively.

DNA was isolated using the DNasy Blood and Tissue Kit (Qiagen, cat:#69506), with upscaled quantities. Briefly, snap-frozen parental cells (60 M per 50 mL tube) and senescent cells (20 M per 50 mL tube) were resuspended in 10 mL cell lysis solution. RNA was degraded with 50 μL RNAse A solution (10 mg/mL) and protein was precipitated with 3 mL precipitation solution. DNA precipitation was performed with 10 mL isopropanol and 10 mL 70% ethanol. Finally, the DNA was dissolved in 1200 μL DNA hydration solution. For samples that contained visible protein pellets, we applied the Appendix C from the DNasy Blood and Tissue Kit (Qiagen, cat:#69506): 'repurifying DNA samples'.

To limit the number of PCR reactions, we performed the DNA capture protocol described before (Jastrzebski et al., 2016), with the following modifications: we used 50 μg of DNA per capture reaction and digested the DNA with *NdeI* and *PstL-HF* restriction enzymes. The sequence of the 5'biotinylated (BITEG) capture oligos were: NdeI_2786/340_FW: /5BiotinTEG/TGCTTACCGTAACTTGAAAGTATTTCGATTTCTTG-GCTTTATATATCTTG; PstI_1135_RV: /5BiotinTEG/TGCAGCCAGGTGGAAGTAAT-TCAAGGCACGCAAGGGCCATAACCCGTAAA.

The T0, T1 and T2-untreated samples were first subjected to capture, while the T2-treated sample were directly used for PCR. Two PCR reactions were performed to amplify the region of interest, as described before (Evers et al., 2016). The following primers were used: PCR_1_FW ACACTCTTTCCCTACACGACGCTCTTCCGATCTNN-NNNNGGCTTTATATATCTTGTGGAAAGGACG; PCR_1_RV GTGACTGGAGTTCAGAC-GTGTGCTCTTCCGATCTTCTACTATTCTTTCCCCTGCACTGT; PCR_2_FW AATGATAC-GGCGACCACCGAGATCTACACTCTTTCCCTACACGACGCTCTTCCGATCT; PCR_2_RV CAAGCAGAAGACGGCATACGAGATNNNNNNGTGACTGGAGTTCAGACGTGT-GCTCTTCCGATCT. The NNNNN represents various barcode and index sequences. After PCR, the DNA concentrations were measured by Qubit (Thermo Fisher Scientific) and pooled equimolarly.

sgRNA counts were determined by sequencing with the Illumina NextSeq550 at the Genomics Core Facility (NKI, The Netherlands). For normalization of the samples for sequence depth, relative total size factors were calculated by dividing the total of each sample by the geometric mean of all totals. Subsequently, all values within a sample were divided by the respective total size factor. A paired differential test was performed on the sgRNA level using DESeq2 (Love et al., 2014) for T2treated vs T1, T2untreated vs T1 and T2treated vs T2untreated. Results were then sorted on the DESeq2 test statistic and used as input for an enrichment analysis on the gene level with MAGeCK's Robust Rank Algorithm (RRA). The results of RRA contains

a rank position, p-value and a corrected p-value for multiple testing (FDR). In addition, per gene a median log2 fold change was calculated over the sgRNAs of a gene based on the log2 fold change calculated by DESeq2. Hits were selected using the following criteria *(i) T2treated vs T2untreated FDR <=0.1 and median log2FC >= 2; (ii) T2treated vs T1 FDR <= 0.1 and median log2FC >= 2.*

References

Ajiro, M., Katagiri, T., Ueda, K., Nakagawa, H., Fukukawa, C., Lin, M.-L., Park, J.-H., Nishidate, T., Daigo, Y., and Nakamura, Y. (2009). Involvement of RQCD1 overexpression, a novel cancer-testis antigen, in the Akt pathway in breast cancer cells. Int. J. Oncol. 35, 547–557.

Basisty, N., Kale, A., Jeon, O.H., Kuehnemann, C., Payne, T., Rao, C., Holtz, A., Shah, S., Sharma, V., Ferrucci, L., et al. (2020). A proteomic atlas of senescence-associated secretomes for aging biomarker development. PLoS Biol. 18, e3000599.

Brachet, P.E., Fabbro, M., Leary, A., Medioni, J., Follana, P., Lesoin, A., Frenel, J.-S., Abadie Lacourtoisie, S., Floquet, A., Gladieff, L., et al. (2022). A GINECO phase II study of Navitoclax (ABT 263) in women with platinum resistant/refractory recurrent ovarian cancer (ROC). Gynecol. Oncol. 165, 30–39.

Chang, J., Wang, Y., Shao, L., Laberge, R.-M., Demaria, M., Campisi, J., Janakiraman, K., Sharpless, N.E., Ding, S., Feng, W., et al. (2016). Clearance of senescent cells by ABT-263 rejuvenates aged hematopoietic stem cells in mice. Nat. Med. 22, 78–83.

Chin, H.S., Li, M.X., Tan, I.K.L., Ninnis, R.L., Reljic, B., Scicluna, K., Dagley, L.F., Sandow, J.J., Kelly, G.L., Samson, A.L., et al. (2018). VDAC2 enables BAX to mediate apoptosis and limit tumor development. Nat. Commun. 9, 1–13.

Colville, A., Liu, J.-Y., Thomas, S., Ishak, H.D., Zhou, R., Klein, J.D.D., Morgens, D.W., Goshayeshi, A., Salvi, J.S., Yao, D., et al. (2022). Death-seq identifies regulators of cell death and senolytic therapies. BioRxiv 2022.04.01.486768.

Coppé, J.P., Patil, C.K., Rodier, F., Sun, Y., Muñoz, D.P., Goldstein, J., Nelson, P.S., Desprez, P.Y., and Campisi, J. (2008). Senescence-associated secretory phenotypes reveal cell-nonautonomous functions of oncogenic RAS and the p53 tumor suppressor. PLoS Biol. 6, 2853–2868.

Cristina, A.-M., Joshua, A., Lee Jr, T.B., Ayush, M., Talemal, L., Chipashvili, V., Hollister-Lock, J., Van deursen, J., Weir, G., and Bonner-Weir, S. (2019). Acceleration of β-cell aging determines diabetes and senolysis improves disease outcomes. 30, 129–142.

Demaria, M., O'Leary, M.N., Chang, J., Shao, L., Liu, S., Alimirah, F., Koenig, K., Le, C., Mitin, N., Deal, A.M., et al. (2017). Cellular Senescence Promotes Adverse Effects of Chemotherapy and Cancer Relapse. Cancer Discov. 7, 165–176.

Dimri, G.P., Lee, X., Basile, G., Acosta, M., Scott, G., Roskelley, C., Medrano, E.E., Linskens, M., Rubelj, I., Pereira-Smith, O., et al. (1995). A biomarker that identifies senescent human cells in culture and in aging skin in vivo. Proc. Natl. Acad. Sci. U. S. A. 92, 9363–9367.

Dirac, A.M.G., and Bernards, R. (2003). Reversal of senescence in mouse fibroblasts through lentiviral suppression of p53. J. Biol. Chem. 278, 11731–11734.

Doench, J.G., Hartenian, E., Graham, D.B., Tothova, Z., Hegde, M., Smith, I., Sullender, M., Ebert, B.L., Xavier, R.J., and Root, D.E. (2014). Rational design of highly active sgRNAs for CRISPR-Cas9-mediated gene inactivation. Nat. Biotechnol. 32, 1262–1267.

Doench, J.G., Fusi, N., Sullender, M., Hegde, M., Vaimberg, E.W., Donovan, K.F., Smith, I., Tothova, Z., Wilen, C., Orchard, R., et al. (2016). Optimized sgRNA design to maximize activity and minimize off-target effects of CRISPR-Cas9 Synthesis of an arrayed sgRNA library targeting the human genome. Nat. Biotechnol. 34, 184–191.

Dornan, D., Wertz, I., Shimizu, H., Arnott, D., Frantz, G.D., Dowd, P., O'Rourke, K., Koeppen, H., and Dixit, V.M. (2004). The ubiquitin ligase COP1 is a critical negative regulator of p53. Nature 429, 86–92.

Elmore, S. (2007). Apoptosis: A review of programmed cell death. Toxicol Pathol 23, 495–516.

Evers, B., Jastrzebski, K., Heijmans, J.P.M., Grernrum, W., Beijersbergen, R.L., and Bernards, R. (2016). CRISPR knockout screening outperforms shRNA and CRISPRi in identifying essential genes. Nat. Biotechnol. 34, 11–14.

Faber, A.C., Farago, A.F., Costa, C., Dastur, A., Gomez-Caraballo, M., Robbins, R., Wagner, B.L., Rideout, W.M., Jakubik, C.T., Ham, J., et al. (2015). Assessment of ABT-263 activity across a cancer cell line collection leads to a potent combination therapy for small-cell lung cancer. Proc. Natl. Acad. Sci. 112, E1288–E1296.

Fresno Vara, J.Á., Casado, E., de Castro, J., Cejas, P., Belda-Iniesta, C., and González-Barón, M. (2004). PI3K/Akt signalling pathway and cancer. Cancer Treat. Rev. 30, 193–204.

Gomex-Bougie, P., Ménoret, E., Juin, P., Dousset, C., Pellat-Deceunynck, C., and Amiot, M. (2011). Noxa controls Mule-dependent Mcl-1 ubiquitination through the regulation of the

5

Mcl-1/USP9X. Biochem. Biophys. Res. Commun. *413*, 460–464.

González-Gualda, E., Pàez-Ribes, M., Lozano-Torres, B., Macias, D., Wilson, J.R., González-López, C., Ou, H.L., Mirón-Barroso, S., Zhang, Z., Lérida-Viso, A., et al. (2020). Galacto-conjugation of Navitoclax as an efficient strategy to increase senolytic specificity and reduce platelet toxicity. Aging Cell 1–19.

Gorgoulis, V., Adams, P.D., Alimonti, A., Bennett, D.C., Bischof, O., Bishop, C., Campisi, J., Collado, M., Evangelou, K., Ferbeyre, G., et al. (2019). Cellular Senescence: Defining a Path Forward. Cell *179*, 813–827.

Hayflick, L. (1965). The limited in vitro lifetime of human diploid cell strains. Exp. Cell Res. *37*, 614–636.

He, Y., Zhang, X., Chang, J., Kim, H.N., Zhang, P., Wang, Y., Khan, S., Liu, X., Zhang, X., Lv, D., et al. (2020). Using proteolysis-targeting chimera technology to reduce navitoclax platelet toxicity and improve its senolytic activity. Nat. Commun. *11*.

Hernandez-Segura, A., de Jong, T. V., Melov, S., Guryev, V., Campisi, J., and Demaria, M. (2017). Unmasking Transcriptional Heterogeneity in Senescent Cells. Curr. Biol. *27*, 2652–2660.

Huo, Z., Zhai, S., Weng, Y., Qian, H., Tang, X., Shi, Y., Deng, X., Wang, Y., and Shen, B. (2019). PRPF40A as a potential diagnostic and prognostic marker is upregulated in pancreatic cancer tissues and cell lines: An integrated bioinformatics data analysis. Onco. Targets. Ther. *12*, 5037–5051.

Inoue-Yamauchi, A., Jeng, P.S., Kim, K., Chen, H.C., Han, S., Ganesan, Y.T., Ishizawa, K., Jebiwott, S., Dong, Y., Pietanza, M.C., et al. (2017). Targeting the differential addiction to anti-apoptotic BCL-2 family for cancer therapy. Nat. Commun. *8*, 1–14.

Jänicke, R.U., Sohn, D., and Schulze-Osthoff, K. (2008). The dark side of a tumor suppressor: Anti-apoptotic p53. Cell Death Differ. *15*, 959–976.

Jastrzebski, K., Evers, B., and Beijersbergen, R.L. (2016). Pooled shRNA Screening in Mammalian Cells as a Functional Genomic Discovery Platform. Methods Mol. Biol. *1470*, 49–73.

Jochems, F., Thijssen, B., De Conti, G., Jansen, R., Pogacar, Z., Groot, K., Wang, L., Schepers, A., Wang, C., Jin, H., et al. (2021). The Cancer SENESCopedia: A delineation of cancer cell senescence. Cell Rep. *36*, 109441.

Ka, W.H., Cho, S.K., Chun, B.N., Byun, S.Y., and Ahn, J.C. (2018). The ubiquitin ligase COP1 regulates cell cycle and apoptosis by affecting p53 function in human breast cancer cell lines. Breast Cancer *25*, 529–538.

Kaefer, A., Yang, J., Noertersheuser, P., Mensing, S., Humerickhouse, R., Awni, W., and Xiong, H. (2014). Mechanism-based pharmacokinetic/pharmacodynamic meta-analysis of navitoclax (ABT-263) induced thrombocytopenia. Cancer Chemother. Pharmacol. *74*, 593–602.

Kale, J., Osterlund, E.J., and Andrews, D.W. (2017). BCL-2 family proteins: changing partners in the dance towards death. Cell Death Differ. *25*, 65–80.

Kao, H.Y., and Siliciano, P.G. (1996). Identification of Prp40, a novel essential yeast splicing factor associated with the U1 small nuclear ribonucleoprotein particle. Mol. Cell. Biol. *16*, 960–967.

Khan, S., Zhang, X., Lv, D., Zhang, Q., He, Y., Zhang, P., Liu, X., Thummuri, D., Yuan, Y., Wiegand, J.S., et al. (2019). A selective BCL-XL PROTAC degrader achieves safe and potent antitumor activity. Nat. Med. *25*, 1938–1947.

Lee, M., and Lee, J.S. (2014). Exploiting tumor cell senescence in anticancer therapy. BMB Rep. *47*, 51–59.

Li, M., and Kim, W.Y. (2011). Two sides to every story: The HIF-dependent and HIF-independent functions of pVHL. J. Cell. Mol. Med. *15*, 187–195.

Li, W., Xu, H., Xiao, T., Cong, L., Love, M.I., Zhang, F., Irizarry, R.A., Liu, J.S., Brown, M., and Liu, X. (2014). MAGeCK enables robust identification of essential genes from genome-scale CRISPR/Cas9 knockout screens. Genome Biol. *15*, 554.

Love, M.I., Huber, W., and Anders, S. (2014). Moderated estimation of fold change and dispersion for RNA-seq data with DESeq2. Genome Biol. *15*.

Luo, X., Budihardjo, I., Zou, H., Slaughter, C., and Wang, X. (1998). Bid, a Bcl2 interacting protein, mediates cytochrome c release from mitochondria in response to activation of cell surface death receptors. Cell *94*, 481–490.

Mamidipudi, V., and Cartwright, C.A. (2009). A novel pro-apoptotic function of RACK1: Suppression of Src activity in the intrinsic and Akt pathways. Oncogene *28*, 4421–4433.

Maurer, U., Charvet, C., Wagman, A.S., Dejardin, E., and Green, D.R. (2006). Glycogen synthase kinase-3 regulates mitochondrial outer membrane permeabilization and apoptosis by destabilization of MCL-1. Mol. Cell *21*, 749–760.

Milanovic, M., Fan, D.N.Y., Belenki, D., Däbritz, J.H.M., Zhao, Z., Yu, Y., Dörr, J.R., Dimitrova, L., Lenze, D., Monteiro Barbosa, I.A., et al. (2018). Senescence-associated reprogramming promotes cancer stemness. Nature *553*, 96–100.

Mulero-Sánchez, A., Pogacar, Z., and Vecchione, L. (2019). Importance of genetic screens in precision oncology. ESMO Open *4*, 1–10.

Narita, M., Nūnez, S., Heard, E., Narita, M., Lin, A.W., Hearn, S.A., Spector, D.L., Hannon, G.J., and Lowe, S.W. (2003). Rb-mediated heterochromatin formation and silencing of E2F target genes during cellular senescence. Cell *113*, 703–716.

O'Brien, M.A., and Kirby, R. (2008). Apoptosis: A review of pro-apoptotic and anti-apoptotic pathways and dysregulation in disease. J. Vet. Emerg. Crit. Care *18*, 572–585.

Okada, H., Suh, W.-K., Jin, J., Woo, M., Du, C., Elia, A., Duncan, G.S., Wakeham, A., Itie, A., Lowe, S.W., et al. (2002). Generation and Characterization of Smac/DIABLO-Deficient Mice. Mol. Cell. Biol. *22*, 3509–3517.

Oleksiewicz, U., Liloglou, T., Tasopoulou, K.M., Daskoulidou, N., Gosney, J.R., Field, J.K., and Xinarianos, G. (2017). COL1A1, PRPF40A, and UCP2 correlate with hypoxia markers in non-small cell lung cancer. J. Cancer Res. Clin. Oncol. *143*, 1133–1141.

Pan, J., Li, D., Xu, Y., Zhang, J., Wang, Y., Chen, M., Lin, S., Huang, L., Chung, E.J., Citrin, D., et al. (2017). Inhibition of BCL-2/xl with ABT-263 Selectively Kills Senescent Type II Pneumocytes and Reverses Persistent Pulmonary Fibrosis Induced by Ionizing Radiation in Mice. Int. J. Radiat. Oncol. Biol. Phys. *99*, 353–361.

Pérez-Mancera, P.A., Young, A.R.J., and Narita, M. (2014). Inside and out: the activities of senescence in cancer. Nat. Rev. Cancer *14*, 547–558.

Roberson, R.S., Kussick, S.J., Vallieres, E., Chen, S.Y.J., and Wu, D.Y. (2005). Escape from therapy-induced accelerated cellular senescence in p53-null lung cancer cells and in human lung cancers. Cancer Res. *65*, 2795–2803.

Robin, T., Capes-Davis, A., and Bairoch, A. (2020). CLASTR: The Cellosaurus STR similarity search tool - A precious help for cell line authentication. Int. J. Cancer *146*, 1299–1306.

Rodriguez, J., and Lazebnik, Y. (1999). Caspase-9 and APAF-1 form an active holoenzyme. Genes Dev. *13*, 3179–3184.

Saleh, T., Cudjoe, E.K., Kyte, S.L., Henderson, S.C., Elmore, L.W., and Gewirtz, D. (2017). Reversibility of chemotherapy-induced senescence is independent of autophagy and a potential model for tumor dormancy and cancer recurrence. BioRxiv 804–828.

Saleh, T., Carpenter, V.J., Tyutyunyk-Massey, L., Murray, G., Leverson, J.D., Souers, A.J., Alotaibi, M.R., Faber, A.C., Reed, J., Harada, H., et al. (2020). Clearance of therapy-induced senescent tumor cells by the senolytic ABT-263 via interference with BCL-XL–BAX interaction. Mol. Oncol. *14*, 2504–2519.

Sanjana, N.E., Shalem, O., and Zhang, F. (2014). Improved vectors and genome-wide libraries for CRISPR screening. Nat. Methods *11*, 783–784.

Sato, A.Y.S., Antonioli, E., Tambellini, R., and Campos, A.H. (2011). ID1 inhibits USF2 and blocks TGF-β-induced apoptosis in mesangial cells. Am. J. Physiol. - Ren. Physiol. *301*, 1260–1269.

Schosserer, M., Grillari, J., and Breitenbach, M. (2017). The Dual Role of Cellular Senescence in Developing Tumors and Their Response to Cancer Therapy. Front. Oncol. 7, 278.

Senichkin, V. V., Streletskaia, A.Y., Gorbunova, A.S., Zhivotovsky, B., and Kopeina, G.S. (2020). Saga of Mcl-1: regulation from transcription to degradation. Cell Death Differ. *27*, 405–419.

Shahbandi, A., Rao, S.G., Anderson, A.Y., Frey, W.D., Olayiwola, J.O., Ungerleider, N.A., and Jackson, J.G. (2020). BH3 mimetics selectively eliminate chemotherapy-induced senescent cells and improve response in TP53 wild-type breast cancer. Cell Death Differ.

Shi, J., Zhou, Y., Huang, H., and Mitchison, T.J. (2008). Navitoclax (ABT-263) accelerates apoptosis during drug-induced mitotic arrest by antagonizing Bcl-xL. North *29*, 1883–1889.

Singh, R., Letai, A., and Sarosiek, K. (2019). Regulation of apoptosis in health and disease: the balancing act of BCL-2 family proteins. Nat. Rev. Mol. Cell Biol. *20*, 175–193.

Soto-gamez, A., Quax, W.J., and Demaria, M. (2019). Regulation of Survival Networks in Senescent Cells: From Mechanisms to Interventions. J. Mol. Biol. *431*, 2629–2643.

Sugihara, H., Teramoto, N., Nakamura, K., Shiga, T., Shirakawa, T., Matsuo, M., Ogasawara, M., Nishino, I., Matsuwaki, T., Nishihara, M., et al. (2020). Cellular senescence-mediated exacerbation of Duchenne muscular dystrophy. Sci. Rep. *10*, 1–17.

Szklarczyk, D., Gable, A.L., Nastou, K.C., Lyon, D., Kirsch, R., Pyysalo, S., Doncheva, N.T., Legeay, M., Fang, T., Bork, P., et al. (2021). The STRING database in 2021: Customizable protein-protein networks, and functional characterization of user-uploaded gene/measurement sets. Nucleic Acids Res. *49*, D605–D612.

Tao, B., Yi, J., Huang, C., Xu, W., Qin, C., Chen, L., Chen, J., Gao, Y., and Wang, R. (2017). MicroRNA-96 regulates the proliferation of nucleus pulposus cells by targeting ARID2/AKT signaling. Mol. Med. Rep. *16*, 7553–7560.

Taylor, R.C., Cullen, S.P., and Martin, S.J. (2008). Apoptosis: Controlled demolition at the cellular level. Nat. Rev. Mol. Cell Biol. *9*, 231–241.

de Vos, S., Leonard, J.P., Friedberg, J.W., Zain, J., Dunleavy, K., Humerickhouse, R., Hayslip,

5

J., Pesko, J., and Wilson, W.H. (2021). Safety and efficacy of navitoclax, a BCL-2 and BCL-XL inhibitor, in patients with relapsed or refractory lymphoid malignancies: results from a phase 2a study. Leuk. Lymphoma *62*, 810–818.

Wang, C., Vegna, S., Jin, H., Benedict, B., Lieftink, C., Ramirez, C., de Oliveira, R.L., Morris, B., Gadiot, J., Wang, W., et al. (2019). Inducing and exploiting vulnerabilities for the treatment of liver cancer. Nature *574*, 268–272.

Wang, L., Leite de Oliveira, R., Wang, C., Fernandes Neto, J.M., Mainardi, S., Evers, B., Lieftink, C., Morris, B., Jochems, F., Willemsen, L., et al. (2017). High-Throughput Functional Genetic and Compound Screens Identify Targets for Senescence Induction in Cancer. Cell Rep. *21*, 773–783.

Wang, L., Lankhorst, L., and Bernards, R. (2022a). Exploiting senescence for the treatment of cancer. Nat. Rev. Cancer *22*, 340–355.

Wang, L., Jin, H., Jochems, F., Wang, S., Lieftink, C., Martinez, I.M., De Conti, G., Edwards, F., de Oliveira, R.L., Schepers, A., et al. (2022b). cFLIP suppression and DR5 activation sensitize senescent cancer cells to senolysis. Nat. Cancer *3*, 1284–1299.

Yamaguchi, R., Harada, H., and Hirota, K. (2016). VHL-deficient renal cancer cells gain resistance to mitochondria-activating apoptosis inducers by activating AKT through the IGF1R-PI3K pathway. Tumor Biol. *37*, 13295–13306.

Yosef, R., Pilpel, N., Tokarsky-Amiel, R., Biran, A., Ovadya, Y., Cohen, S., Vadai, E., Dassa, L., Shahar, E., Condiotti, R., et al. (2016). Directed elimination of senescent cells by inhibition of BCL-W and BCL-XL. Nat. Commun. *7*.

Zhang, W., Xia, D., Li, Z., Zhou, T., Chen, T., Wu, Z., Zhou, W., Li, Z., Li, L., and Xu, J. (2019). Aurora-A/ERK1/2/mTOR axis promotes tumor progression in triple-negative breast cancer and dual-targeting Aurora-A/mTOR shows synthetic lethality. Cell Death Dis. *10*, 606.

Zhong, Q., Gao, W., Du, F., and Wang, X. (2005). Mule/ARF-BP1, a BH3-only E3 ubiquitin ligase, catalyzes the polyubiquitination of Mcl-1 and regulates apoptosis. Cell *121*, 1085–1095.

Zhu, Y., Tchkonia, T., Fuhrmann-Stroissnigg, H., Dai, H.M., Ling, Y.Y., Stout, M.B., Pirtskhalava, T., Giorgadze, N., Johnson, K.O., Giles, C.B., et al. (2016). Identification of a novel senolytic agent, navitoclax, targeting the Bcl-2 family of anti-apoptotic factors. Aging Cell *15*, 428–435.
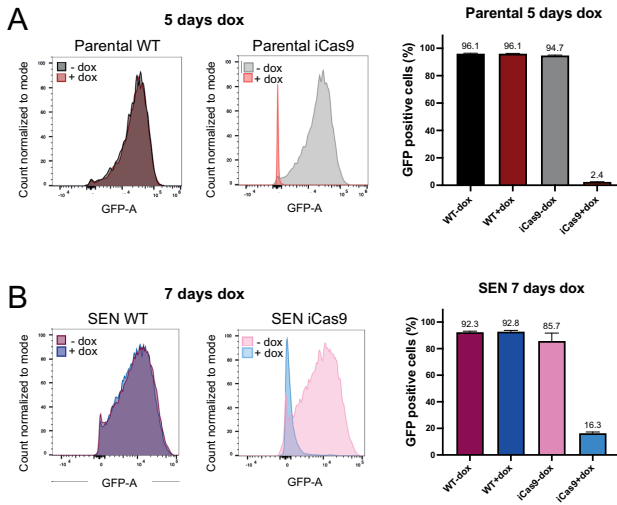
Supplementary figures

Figure S1. Editing efficiency in parental and senescent cells, related to figure 1. (A) Histogram of GFP signal and quantification of GFP positive cells of pXPR011-carrying parental WT and A549-iCas9 A549 cells treated with doxycycline for 5 days. **(B)** Histogram of GFP signal and quantification of GFP positive senescent WT and A549-iCas9 A549 cells transduced with pXPR011 and treated with doxycycline for 7 days.
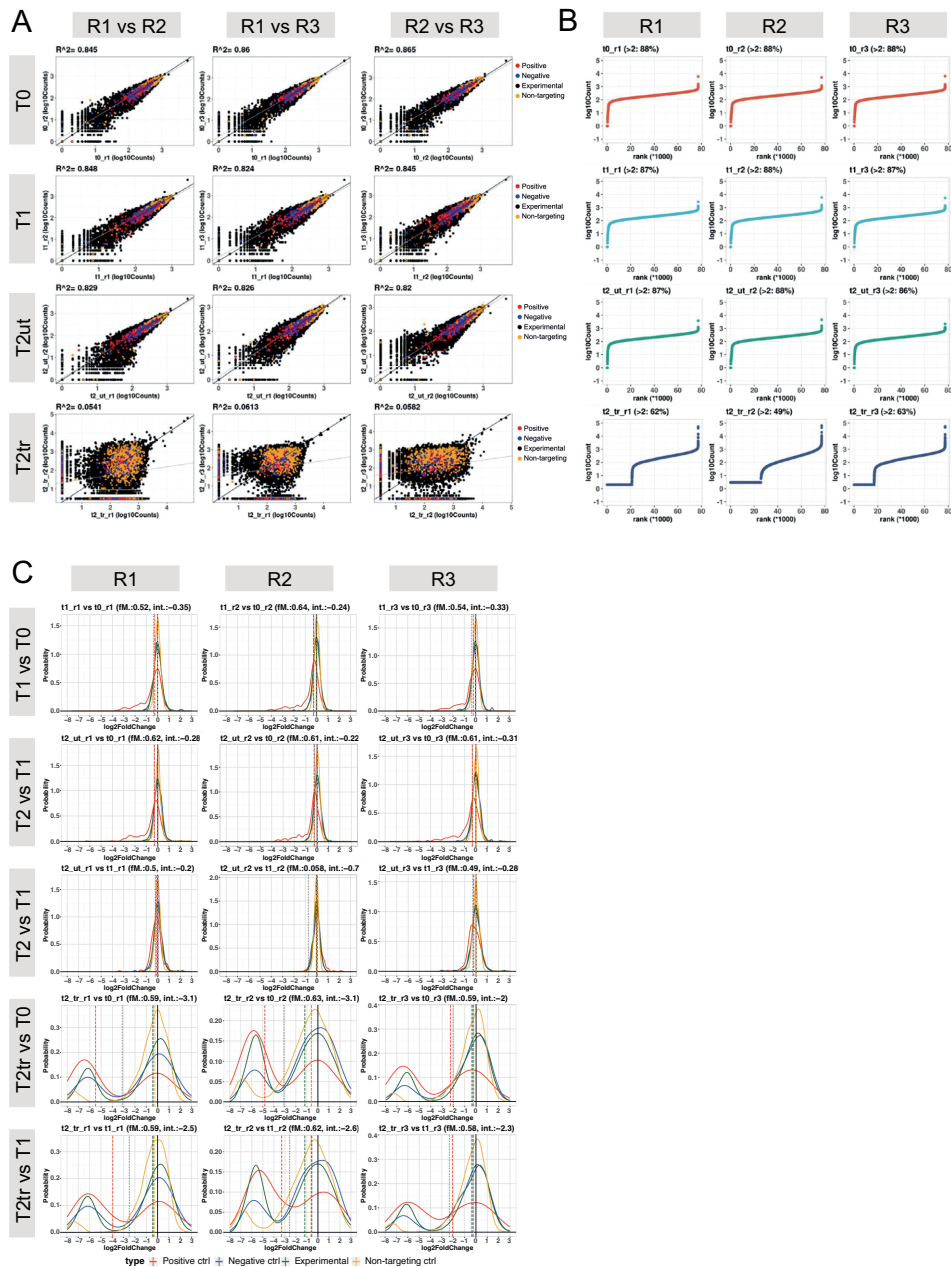
5

Figure S2. Quality control of resistance screen for ABT-263 senolytic killing. (A) Pearson correlation plots of the different time points and biological replicates. Each dot indicates a sgRNA targeting a gene. Yellow, non-targeting sgRNAs; blue, sgRNAs targeting non-essential genes; red, sgRNAs targeting essential genes; black, sgRNAs targeting experimental genes. **(B)** Rank distributions of sgRNA counts to assess the library complexity. Each dot represents a sgRNA. **(C)** Probability distributions for positive controls targeting essential genes (red), negative controls targeting non-essential genes (blue), experimental genes (green) and non-targeting controls (yellow).

CHAPTER

cFLIP suppression and DR5 activation sensitize senescent cancer cells to senolysis

6

Liqin Wang[1,#,*], Haojie Jin[1,2,#], Fleur Jochems[1], Siying Wang[2],
Cor Lieftink[4], Isabel Mora Martinez[1], Giulia De Conti[1],
Finn Edwards[1], Rodrigo Leite de Oliveira[1], Arnout Schepers[1],
Yangyang Zhou[2], Jiaojiao Zheng[2], Wei Wu[2], Xingling Zheng[2],
Shengxian Yuan[3], Jing Ling[2], Kathy Jastrzebski[1],
Matheus Dos Santos Dias[1], Ji-Ying Song[5],
Patrick N. H. Celie[6], Hideo Yagita[7], Ming Yao[2], Weiping Zhou[3],
Roderick L. Beijersbergen[4], Wenxin Qin[2,*] and René Bernards[1,2,*]

[#] These authors contributed equally to this work.
[1] Division of Molecular Carcinogenesis, Oncode Institute. The Netherlands Cancer Institute, Plesmanlaan 121, 1066 CX Amsterdam, The Netherlands
[2] State Key Laboratory of Oncogenes and Related Genes, Shanghai Cancer Institute, Renji Hospital, Shanghai Jiao Tong University School of Medicine, Shanghai, China
[3] The Third Department of Hepatic Surgery, Eastern Hepatobiliary Surgery Hospital, Shanghai, China
[4] Division of Molecular Carcinogenesis, NKI Robotic and Screening Center, The Netherlands Cancer Institute, Plesmanlaan 121, 1066 CX Amsterdam, The Netherlands
[5] Division of Experimental Animal Pathology, The Netherlands Cancer Institute, Plesmanlaan 121, 1066 CX Amsterdam, The Netherlands
[6] Division of Biochemistry, Protein facility, Oncode Institute. The Netherlands Cancer Institute, Plesmanlaan 121, 1066 CX Amsterdam, The Netherlands
[7] Department of Immunology, Juntendo University School of Medicine. 2-1-1 Hongo, Bunkyo-ku Tokyo 113-8421, Japan.

Abstract

Senolytics, drugs that kill senescent cells, have been proposed to improve the response to pro-senescence cancer therapies. However, this remains challenging due to a lack of broadly-acting senolytic drugs. Using CRISPR/Cas9-based genetic screens in different senescent cancer cell models, we identify here loss of the death receptor inhibitor cFLIP as a common vulnerability of senescent cancer cells. Senescent cells are primed for apoptotic death by NF-kB-mediated upregulation of Death Receptor 5 (DR5) and its ligand TRAIL, but are protected from death by increased cFLIP expression. Activation of DR5 signalling by agonistic antibody, which can be enhanced further by suppression of cFLIP by BRD2 inhibition, leads to efficient killing of a variety of senescent cancer cells. Moreover, senescent cells sensitise adjacent non-senescent cells to killing by DR5 agonist through a bystander effect mediated by secretion of cytokines. We validate this "one-two punch" cancer therapy by combining pro-senescence therapy with DR5 activation in different animal models.

Introduction

Senescence can be triggered by a variety of stresses and is considered a fail-safe mechanism against oncogenic transformation (Hayflick, 1965; Serrano et al., 1997). Senescence has also been recognized as a stress response to anti-cancer therapies (Nardella et al., 2011). While at first glance such proliferation arrest would seem beneficial, multiple studies have highlighted that the senescence-associated secretory phenotype (SASP) produced by senescent tumour cells represents a potentially double-edged sword for tumour control (Coppé et al., 2010). On the one hand, the SASP can inhibit tumour growth by triggering an immunological response (Eggert et al., 2016; Ruscetti et al., 2018). On the other hand, the long-term presence of SASP can potentially be deleterious, causing chronic inflammation, immunosuppression, stimulating epithelial-to-mesenchymal transition, inducing a stem cell-like state, or promoting tumour migration and metastasis (Demaria et al., 2017; Faget et al., 2019; Kuilman et al., 2008; Laberge et al., 2012). Therefore, while the senescence growth arrest may represent an initial desirable outcome of treatment, prolonged presence of senescent cells can be deleterious.

Senolytics, drugs that preferentially kill senescent cells, can potentially be combined with pro-senescence therapies to avoid the long-term deleterious effects of persistent senescent cells in a tumour. However, this therapeutic strategy is limited by a lack of broadly-acting senolytic agents that act selectively on senescent cancer cells in a context-independent fashion with acceptable toxicity profile (Carpenter et al., 2021; Dörr et al., 2013; Guerrero et al., 2019; Muñoz-Espín et al., 2018; Shahbandi et al., 2020; Wang et al., 2019, 2017). Here we use unbiased genetic screens to identify vulnerabilities of senescent cancer cells.

Results

CRISPR-based senolytic screen identifies cFLIP as a senolytic target

To identify genes whose inactivation cause cell death selectively in senescent cancer cells, we developed a genome-scale loss of function genetic screen using a doxycycline-inducible CRISPR/Cas9 vector system (Figure 1A, S1A-F). We used as the screening model A549 *KRAS* mutant lung cancer cells treated with three potent senescence inducers: the aurora kinase A inhibitor alisertib, the PLK4 inhibitor CFI-400945 and the topoisomerase II inhibitor etoposide (Figure S1A-C) (Jochems et al., 2021). In short, we first introduced the lentiviral gRNA library in proliferating A549 cells, followed by selection for lentiviral integration. The gRNA expressing cells were treated with one of the three agents to induce senescence. After this, CAS9 expression was activated by doxycycline treatment to induce gene knock-outs.

The senescent cell populations were cultured for 10 days to allow for depletion of gRNAs in the senescent cells (Figure 1A). A control arm of proliferating cells was also included in the screen. We selected sgRNAs preferentially depleted from cells made senescent by all three agents, with little or no effect in the proliferating arms. Using this criterium, we identified cFLIP (encoded by the *CFLAR* gene), an inhibitor of death receptor-mediated apoptosis, as the top common hit (Figure 1B). For validation, we generated two cFLIP^{KO} clones from A549-iCas9 cells (Figure 1C). Loss of cFLIP selectively induced cell death not only in alisertib-induced senescent cells, but also in cells made senescent by other agents, such as the PLK4 inhibitor, etoposide or the aurora kinase B inhibitor barasertib, but not in proliferating cells (Figure 1D). Using the Incucyte imaging system, we observed that the cFLIP^{KO} cells treated with different senescence inducers undergo a series of morphological and biochemical changes typical for apoptosis, such as shrinkage of the cell, fragmentation into membrane-bound apoptotic bodies and massive staining with a caspase 3/7-activated dye (Figure 1E). Consistent with this, the apoptosis-mediated cell death phenotype can be rescued by the caspase inhibitor Z-VAD-FMK (Figure 1F).

We also performed the CRISPR screen described above in SK-Hep1 hepatocellular and PC3 prostate carcinoma cells made senescent with alisertib. In these additional cell lines, cFLIP was again identified as the top hit indicating context independency (Figure S2A,B). Using a SK-Hep1 cFLIP^{KO} clone and PC3 cells with cFLIP suppression by shRNAs, we also observed similar apoptosis-mediated senolytic effects upon treatment with four independent senescence inducers (Figure S2C-I).
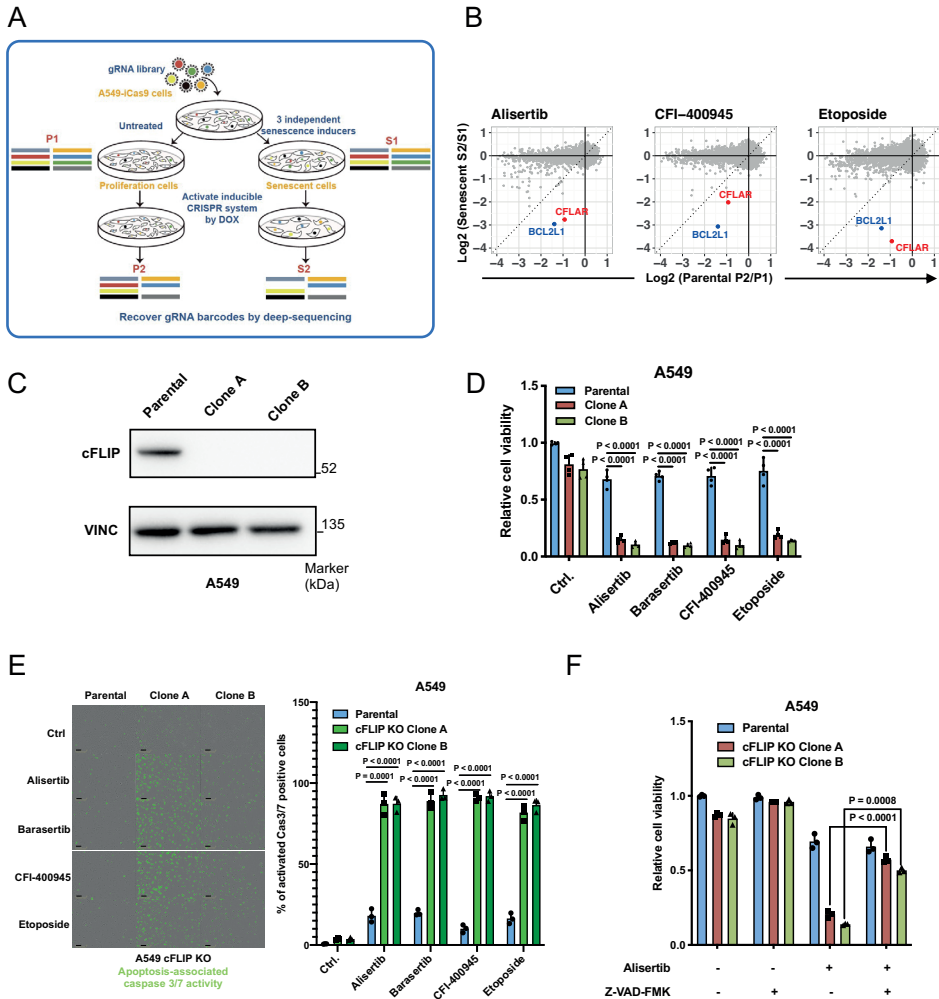
6

Figure 1. A doxycycline-inducible CRISPR screen identifies cFLIP as a senolytic target.
(**A**) Schematic of CRISPR-based senolytic screen workflow. Genome-wide lentiviral Brunello gRNA collection was introduced to A549-iCas9 cells. After 7 days of senescence inducer treatment (0.5 µM alisertib, 50nM CFI-400945, 2 µM Etoposide), cells were switched to 1 µg/ml doxycycline (DOX) for 10 days. Non-senescent cells were included as the control arm. Changes in gRNA abundance were identified by deep sequencing. (**B**) Top hits were selected based on the fold depletion of (S2 vs S1) divided by (P2 vs P1). BCL2L1 is considered to be a positive control. (**C**) Western blot of cFLIP and vinculin (loading control) in A549 parental cells and cFLIP^KO clones. (**D**) CellTiter-Blue quantification of cells treated with 0.5 µM alisertib, 1 µM Barasertib, 50nM CFI-400945 or 2 µM Etoposide as different senescence inducers for one week. (**E**) Senescence inducers treated A549 parental and cFLIP^KO cells incubated with caspase-3/7 green apoptosis assay reagent. The black scale bars represent 100 µm. (**F**) Relative cell viability accessed by colony formation assay in the A549 parental and cFLIP^KO cells. The cells were treated with 0.5 µM alisertib and 10 µM Z-VAD-FMK for one week. Error bars in this figure represent the mean ± standard deviations from biological triplicates (*P≤0.05, ** P≤0.01, *** P≤0.001, two-tailed t-test).

NF-kB primes senescent cancer cells for extrinsic apoptosis

To gain mechanistic insight into why *cFLIP* knockout induces senolysis, we performed transcriptome analysis on alisertib-treated A549 cells. This showed that multiple NF-kB signalling gene signatures are highly enriched in the senescent cells (Figure 2A), which was confirmed by activation of a NF-kB-luciferase reporter construct (Wilson et al., 2013) following treatment with different senescence inducers (Figure 2B). Real-time PCR confirmed the upregulation of a group of NF-kB target genes is highly upregulated, including *cFLIP* (Figure 2C). Moreover, transcriptome analyses of 13 cell lines from four different tissue types made senescent by either alisertib or etoposide showed increased levels of cFLIP following senescence induction (Figure 2D). In addition to cFLIP, other components of the death receptor pathway are also activated during senescence, including death receptor 5 (*DR5/TNFRSF10B*) and its ligand *TRAIL* (Figure 2C-F, and S3A,G). However, other death receptor family members, such as *TNFRSF10C*, *TNFRSF10D*, *TNFRSF10A*, *TNFA* and *TNFRSF1A* were not strongly affected (Figure S3B-F). Suppression of the essential NF-kB subunit p65 using two independent shRNAs or using an IKBα-mutant as a NF-kB super repressor resulted in attenuated *DR5*, *TRAIL* and *cFLIP* induction in the senescent cells (Figure 2G, H). We conclude that NF-kB activity is upregulated in the senescent cells, which leads to increased expression of both DR5 and its ligand TRAIL to prime senescent cells for apoptosis. However, senescent cells are protected from apoptotic death by a concomitant increase in cFLIP. When cFLIP is suppressed, senescent cells are no longer protected from extrinsic apoptosis mediated by the increased levels of TRAIL and DR5. To test this model, we suppressed TRAIL and DR5 expression using shRNAs in cFLIP-deficient A549 and SK-Hep1 cells. Indeed, suppression of either gene could partially rescue the cFLIP deficient cells from the alisertib-induced senolytic effect (Figure 2I, J, and S3H, I). Together, these data support the notion that senescent cancer cells are sensitized to death receptor mediated killing, at least in part, by activation of NF-kB. Our data also suggest that perturbation of this balance in death receptor signalling could be a therapeutic strategy to drive senescent cells to apoptotic death.
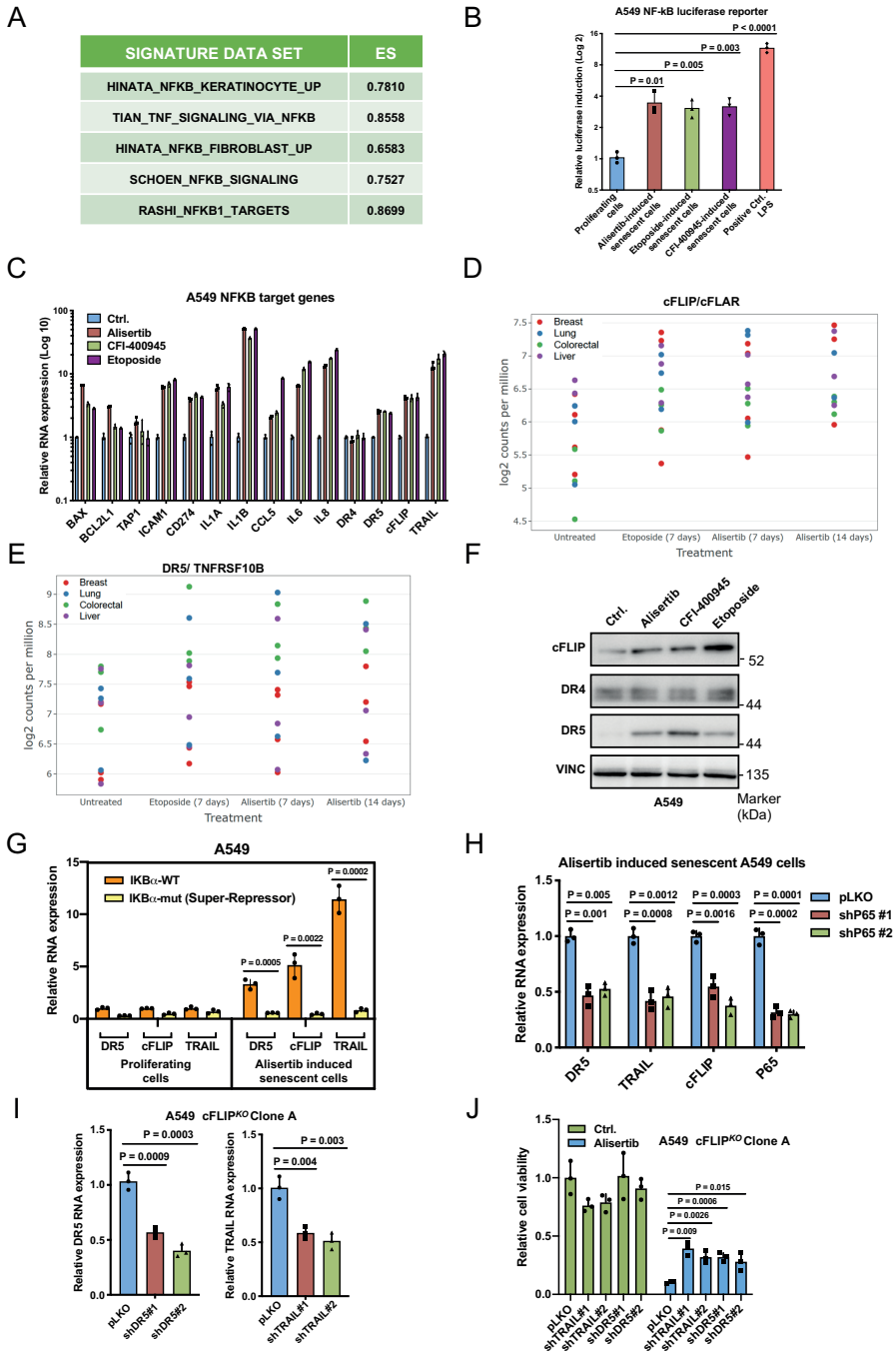
Figure 2. NF-kB drives extrinsic apoptosis priming in senescent cancer cells. (**A**) RNA sequencing was performed on A549 cells treated with 0.5 μM alisertib for 1 week, and followed by gene set enrichment analysis (GSEA) of alisertib treated cells versus untreated control for multiple independent NF-KB signaling gene sets. (**B**) A549 cells were treated with 0.5 μM alisertib, 50nM

CFI-400945, 2 μM Etoposide for one week to induce senescence and NF-kB signaling activation was measured using a luciferase-based NF-kB reporter. **(C)** Gene expression measured by real-time PCR of a panel of NF-kB target genes in cells treated with senescence inducers. **(D-E)** cFLIP **(D)** and DR5 **(E)** expression derived from RNAseq on a cell line panel made senescent with alisertib or etoposide. **(F)** Western blot of DR4, DR5, cFLIP in A549 cells treated with different senescence inducers. **(G)** Real-time PCR analysis of DR5, cFLIP and TRAIL on dominant repressor mutant IKB-alpha viral vector infected A549. Wildtype IKB-alpha viral vector infected cells were used as the control. **(H)** Real-time PCR of DR5, cFLIP, and TRAIL expression in in alisertib-induced senescent A549 cells having two shRNA against p65. **(I)** Real-time PCR of TRAIL and DR5 in A549 cFLIP^{KO} cells with shRNAs against these genes. **(J)** Cell viability based on the colony formation in the A549 cFLIP^{KO} cells with shRNAs against TRAIL or DR5, and treated with 0.5 μM alisertib for one week. Error bars in this figure represent the mean ± standard deviations from biological triplicates (*P≤0.05, ** P≤0.01, *** P≤0.001, two-tailed t-test).

Death receptor 5 agonists have widespread senolytic activity

To validate this model further, we used a recombinant trimeric TRAIL protein (Lz-TRAIL) to activate death receptor signalling in senescent cells. These experiments showed that ligand activation of death receptors DR4 and DR5 indeed resulted in preferential killing of senescent cells over proliferating cells in multiple cell models, including lung (A549, H358, H2030), breast (MDA-MB-231, MCF-7), colon (HCT116, RKO, SW480) and liver (SK-Hep1, Huh7) cancer models (Figure 3A and Figure S4A-E). Using Incucyte imaging, we also observed a massive induction of caspase 3/7 activity in senescent A549 cells treated with Lz-TRAIL (Figure 3B), indicating the dominant involvement of apoptosis in the eradication of senescent cells. This notion is supported further by western blot analysis showing that Poly ADP-ribose polymerase (PARP) protein was cleaved upon Lz-TRAIL treatment only in the senescent cells (Figure 3C). Death receptor signalling can trigger both apoptosis and necroptosis. To investigate which form of cell death contributes to this senolytic effect, we compared the rescue efficiency between Z-VAD-FMK (apoptosis inhibitor) and necrosulfonamide (necroptosis inhibitor) on the senescent cells treated with Lz-TRAIL. We observed that only apoptosis inhibition could rescue the phenotype (Figure 3d). This data is consistent with our findings above and in another model (SK-Hep1, Figure S5A, B) showing that about 90% of cells stained positive for caspase 3/7 activity, indicating that apoptosis plays a dominant role in death receptor signal mediated senolysis.

TRAIL is the ligand for both death receptor DR4 and DR5. To examine the contribution of apoptosis from each receptor, we generated either DR4, DR5 or DR4/5 knockout senescent cells and treated with Lz-TRAIL. DR5 knockout, but not DR4 knockout, attenuated Lz-TRAIL mediated senolysis (Figure 3E, F). Moreover, the senolytic effect was not observed by treating senescent cells with a specific DR4 agonist antibody mapatumumab (Figure 3G). These observations are consistent with our findings (Figure 2C, E, F) showing that only DR5 is upregulated upon senescence induction. These results suggest that activation of DR5 is a significant

contributor to sensitizing senescent cells to death receptor pathway agonists.

TRAIL has poor bioavailability and binds to decoy receptors (DcR1 and DcR2), which suppress apoptosis induction. TRAIL also activates DR4 which does not contribute to senolysis (Fig 3F, G) (Soto-Gamez et al., 2022). To overcome these potential limitations of using TRAIL as a senolytic, we tested whether the DR5 agonistic antibody conatumumab can also preferentially kill senescent cancer cells. We found that conatumumab also leads to selective killing of alisertib induced senescent cells via apoptosis induction (Figure 4A-C and Figure S5C). We also validated the senolytic effect of conatumumab and recombinant TRAIL in other models in which senescence was induced by barasertib, the PLK4 inhibitor CFI-400945, etoposide or ionizing radiation (Figure 4D and Figure S5D-K).

Next, we tested whether NF-kB activation by itself is sufficient to confer sensitivity to conatumumab killing. We found that activation of NF-kB by LPS is not sufficient to sensitize to DR5 agonist killing (Figure 2B and Figure S5L). This is most likely explained by our finding that senescence induces higher levels of TRAIL, DR5 and cFLIP than NF-kB activation by LPS (Figure S5M). Thus, our combined data show that NF-kB activation is necessary, but not sufficient, for inducing sensitivity to DR5 agonist killing.

These results indicate that a DR5 agonist can act as a senolytic agent that can be combined with different classes of pro-senescence therapies. To test the context-independence of this senolytic effect, we studied the effects of conatumumab in a panel of senescent cancer cells, including lung (A549, H2030, PC9), breast (MB-MDA-231, MCF-7), colon (HCT116, Lovo), pancreatic (MIA PaCa-2), melanoma (A375), bile duct (EGI-1, TFK-1) and liver (SK-Hep1, Hep3B, Huh7) cancer (Figure 4E). For these 14 cell models, we also compared the senolytic effect of conatumumab to that of one of the most established senolytic agents, the BCL-2 family inhibitor navitoclax (ABT-263) (Chang et al., 2016). Based on cell viability, we determined IC50 values of senescent and proliferating cells upon treatment with these two senolytic agents and calculated senolytic indexes (IC50 of drug in proliferating cells divided by IC50 in senescent cells) as a measure of senescence-selectivity. We observed that conatumumab could induce senolysis in all 14 cell models, including the 6 models that were insensitive to navitoclax (H2030, MIA PaCa-2, HCT116, Lovo, TFK-1 and EGI-1). In all cases, senescent cells were 5-10-fold more sensitive to conatumumab than their proliferating counterparts (Fig 4E). This indicates that DR5 agonist can act as a selective senolytic agent having broader activity than navitoclax.
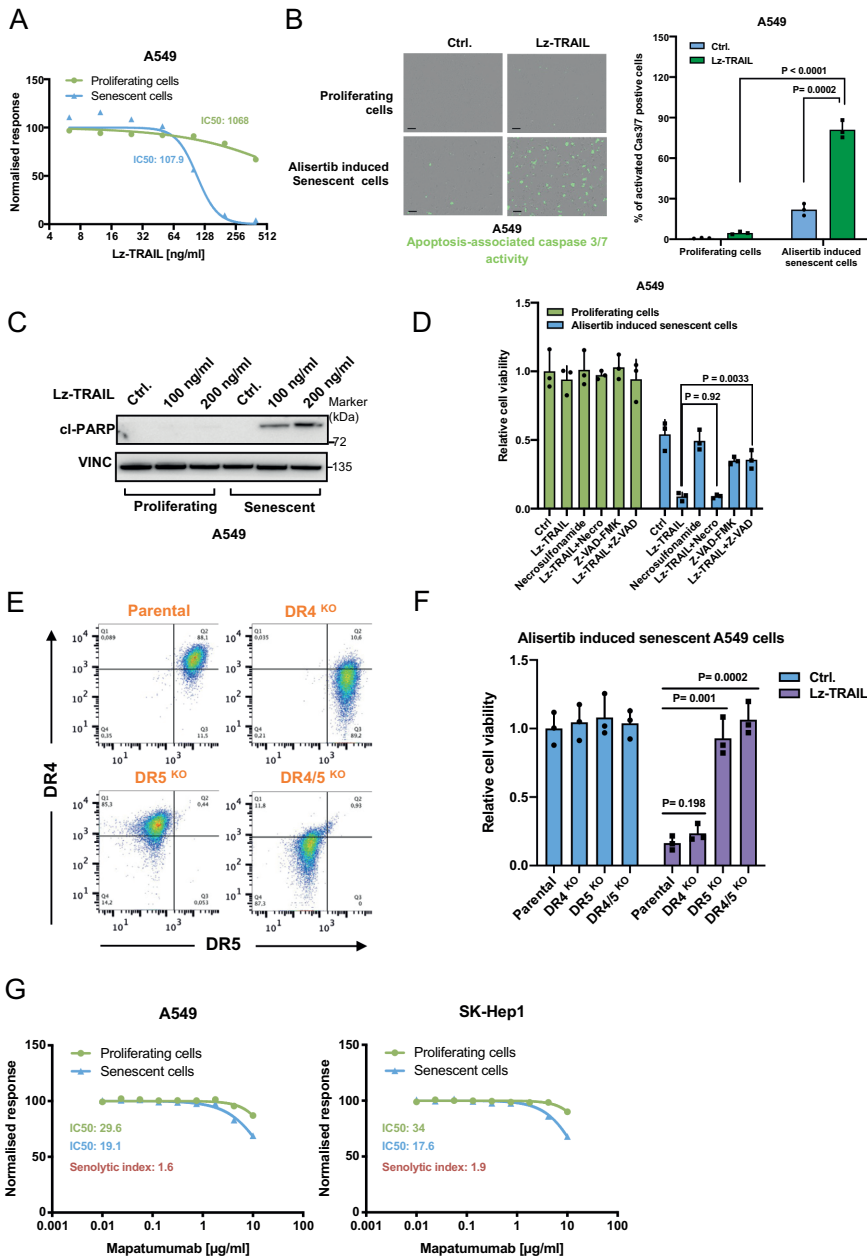
6

Figure 3. DR5 activation sensitize senescent cancer cells to senolysis. (A) Dose-response curve of 0.5 μM alisertib-induced senescent and proliferating A549 cells treated with Lz-TRAIL. **(B)** Caspase-3/7 green apoptosis assay on alisertib-induced senescent A549 cells treated with 200 ng/ml Lz-TRAIL. The black scale bars represent 100 μm. **(C)** Western blot of cl-PARP in A549 cells treated with Lz-TRAIL. **(D)** Cell viability based on the colony formation in the senescent and proliferating A549 parental cells treated with 200 ng/ml Lz-TRAIL, 10 μM Z-VAD-FMK, and 10 μM necrosulfonamide. **(E)** Flow cytometry analysis of DR4, DR5, and DR4/5 knockout A549 clones. **(F)** Cell viability based on the colony formation assay in the DR5, DR4, and DR4/5 knockout A549 cells treated with 0.5

µM alisertib to induce senescence, and then switched to 200 ng/ml Lz-TRAIL. **(G)** Dose-response curve of 0.5 µM alisertib-induced senescent and proliferating A549 and SK-Hep1 cells treated with mapatumumab. Error bars in this figure represent the mean ± standard deviations from biological triplicates (*P≤0.05, ** P≤0.01, *** P≤0.001, two-tailed t-test).

To test the effect of pro-senescence/senolytic treatment *in vivo*, we established a hepatocellular carcinoma patient-derived xenograft (PDX) model and engrafted A549 and SK-Hep1 cells into immunodeficient nude mice. Due to tumour heterogeneity, senescence is likely not induced synchronously in the tumours. Therefore, we used the pro-senescence and senolytic drugs in combination. When tumours reached approximately 150 mm³, mice were randomized into different cohorts and treated with vehicle, alisertib or barasertib, conatumumab or drug combinations. Treatment with single agent alisertib or conatumumab resulted in limited tumour growth inhibition. However, treatment with the combination of two drugs resulted in persistent suppression of tumour growth throughout the experiment in all three cancer models (Figure 4F and Figure S6A, B). To assess the selective killing of senescent tumour cells in the in vivo models upon DR5 activation, we collected the tumours and stained them for p21^{cip1} as a senescence marker. We observed alisertib treatment induced senescence in the tumours as judged by p21^{cip1} induction. In the combination treatments with conatumumab, the senescent cells were significantly depleted (Figure 4G, H, Figure S6C-E).

To identify genes whose inactivation results in resistance to death receptor activation in senescent cancer cells, we performed a CRISPR screen in SK-Hep1 cells having a gene knockout for *cFLIP* (Figure S7A). These cells undergo apoptosis upon senescence induction (Figure S2C-F). A number of crucial extrinsic apoptosis signalling components were identified as the top hits from the screen, including DR5, FADD, CASP8 and BID. Knockdown of these genes by shRNAs indeed conferred resistance to DR5 activation mediated senolysis (Figure S7B-H). Moreover, the liver cancer cell line PLC/PRF/5 which carries a loss of function mutation in *FADD* (Suzuki et al., 1999), was also resistant to DR5 agonist-mediated senolysis, and this resistance could be reversed by expressing wild type *FADD* (Figure S7I-K). These observations support our hypothesis that extrinsic apoptotic signalling plays a dominant role in killing senescent cancer cells.

Next, we tested conatumumab-mediated senolysis in the senescence competent versus defective cell model. We used primary human BJ fibroblasts expressing an inducible *RAS* oncogene and an *TP53* knockdown vector (Nijwening et al., 2011). We observed that *TP53* suppression resulted in senescence bypass and attenuated conatumumab-mediated senolysis (Figure S8A-C). However, many models used here are *TP53* deficient, can be induced to become senescent and respond to conatumumab, indicating that *TP53* status is not a biomarker of conatumumab response.
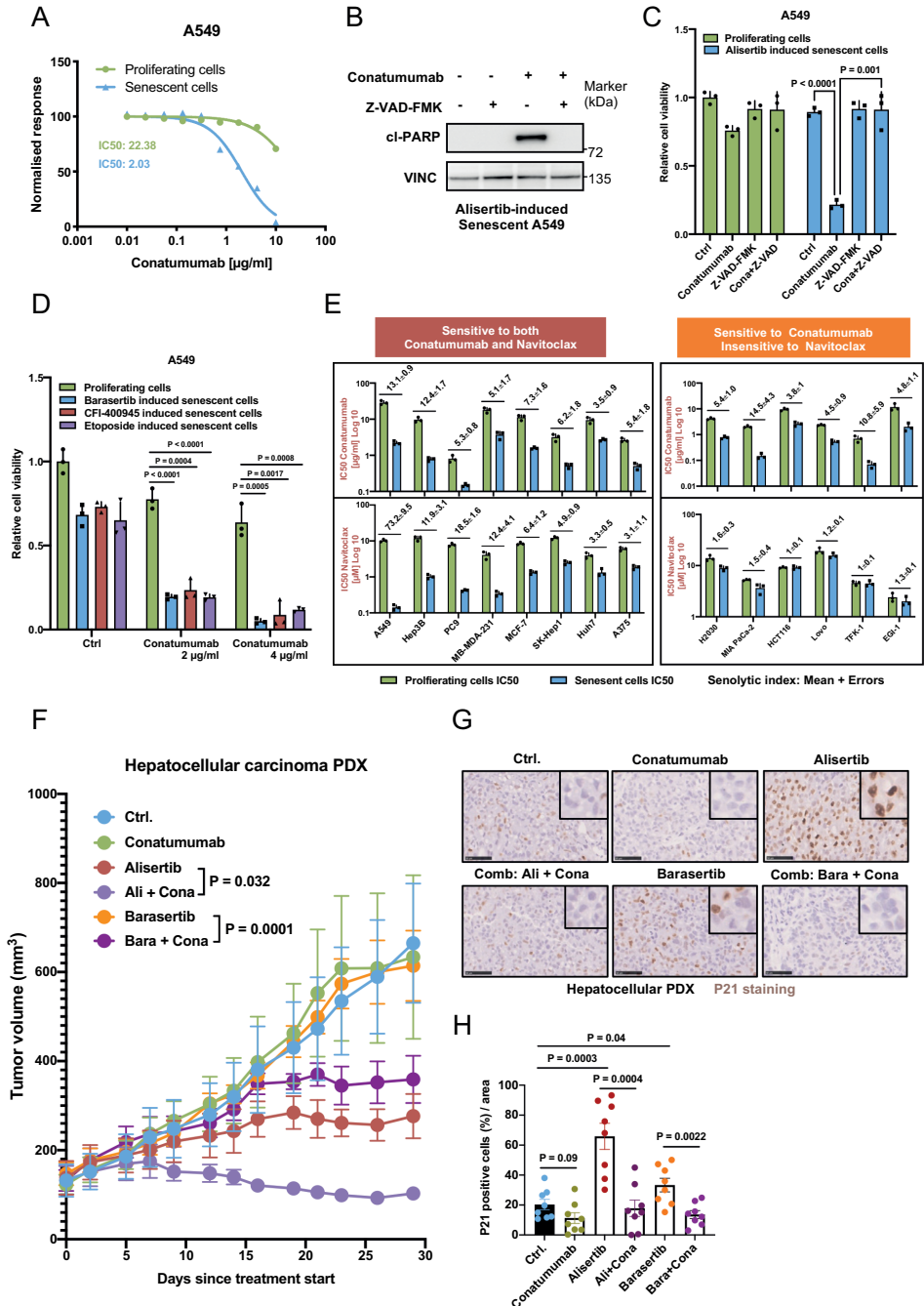
6

Figure 4. DR5 agonists have a broad spectrum senolytic activity. (A) Dose-response curve of alisertib-induced senescent and proliferating A549 cells treated with conatumumab. **(B)** Western blot of cleaved PARP in alisertib-induced senescent A549 cells with 4 μg/ml conatumumab and 10 μM Z-VAD-FMK. **(C)** CellTiter-Blue measurement in the 0.5 μM alisertib-induced senescent A549 cells treated with 4μg/ml conatumumab and 10 μM Z-VAD-FMK. **(D)** Cell viability based on the

colony formation in 1 μM barasertib, 50nM CFI-400945 or 2 μM Etoposide senescent A549 cells upon conatumumab treatment. **(E)** Alisertib-induced senescent and proliferating cell line panels with conatumumab or navitoclax. Senolytic indexes were calculated by IC50 of proliferating cells divided by IC50 of senescent cells. Error bars in the *in vitro* studies in this figure represent the mean ± standard deviations from biological triplicates (*P≤0.05, ** P≤0.01, *** P≤0.001, two-tailed t-test). **(F)** Tumour growth of hepatocellular carcinoma PDX in flanks of Balb/c nude mice subcutaneously implanted with liver tumour pieces, when tumors reached approximately 150 mm³, assigned to either vehicle control, 25 mg/kg alisertib, 50 mg/kg barasertib, 10 μg/dose conatumumab and two combinations (n=5). The data is presented as mean ± SEM. Two-way ANOVA test was applied for the *in vivo* study statistical analysis. (*P≤0.05, ** P≤0.01, *** P≤0.001). **(G)** Fixed tissues were dehydrated and embedded in paraffin. Sections of 2-4 μm were prepared and immunostained with P21 to indicate senescent cells in the tumors of liver PDX. The black scale bars represent 50 μm. **(H)** For Immunohistochemistry analysis, error bars in this figure represent the mean ± standard deviations from biological triplicates (* P≤0.05, ** P≤0.01, *** P≤0.001, two-tailed t-test).

BRD2 inhibition enhances DR5 agonist-mediated senolysis

Several DR5 agonistic antibodies have shown considerable toxicity in the clinic (Finnberg et al., 2016; Takeda et al., 2008). Our finding that senescent cancer cells display a 5-10-fold lower IC50 for DR5-agonistic antibody mediated killing (Figure 4E) may help address this issue, in that combination with a pro-senescence therapy may require lower doses of DR5 antibody to obtain efficient cell killing. A potential strategy to further reduce DR5 antibody toxicity could be the use of drug combinations based on synthetic lethal interactions with DR5 agonistic antibodies. To find such potential DR5 synergistic drug targets, we performed a CRISPR/Cas9 based synergy screen with a custom kinome and epigenome library of some 1000 genes (Wang et al., 2019, 2017) to identify genes whose inactivation can sensitize PC9 lung cancer cells to conatumumab (Figure 5A). Using this approach, we identified the bromodomain and extra-terminal (BET) motif protein family member BRD2 as the top hit (Figure 5B). To validate BRD2 as a hit, we used a small molecule inhibitor NEO2734 (Spriano et al., 2018) to inhibit BRD protein function or a proteolysis-targeting chimera (PROTAC) molecule ARV-771 (Raina et al., 2016) to degrade the BRD proteins. Indeed, the synthetic lethality interaction between inhibition of BRD family proteins and DR5 activation validated in the multiple cancer cell models (Figure 5C, D). Moreover, we did not detect any cell killing in two primary human cells, a retinal pigment epithelial cell (Rpe1) and a fibroblast (BJ) when using the same drug concentrations of conatumumab and NEO2734 that efficiently killed PC9 and SK-Hep 1 cancer cells, indicating cancer-selectivity of this drug combination (Figure 5C).

To obtain insight in the potential mechanism for the observed drug synergy, we performed a transcriptome analysis on PC9 and SK-Hep1 cells treated for 7 days with NEO2734. Among the death receptor signalling genes, *cFLIP* was down-regulated upon drug treatment in both cell lines (Figure 5E). This finding was also validated with real-time PCR and indicated the significant suppression of *cFLIP* within 24

6

hours of drug treatment (Figure 5F). To date, BRD inhibitors target the BET domains of all BRD proteins, and no specific BRD2 inhibitor has been developed. To rule out the potential drug off-target effect, we genetically suppressed BRD2 and BRD4 using shRNAs. We observed that only BRD2 knockdown suppressed cFLIP expression and synergized with DR5 activation to kill the cells (Figure 5G, H).

These observations agree with the results of the CRISPR screen in senescent cells, which also identified loss of cFLIP as a major inducer of senolytic activity. Taking advantage of this newly discovered mechanism of cFLIP suppression, we tested BRD inhibition as a senolytic in senescent cancer cells. As shown in Figure 6A-B, BRD inhibition can preferentially eradicate senescent cancer cells with a lesser effect on proliferating cells. Next, we asked whether a low dose conatumumab plus low dose NEO2734 as a potent senolytic cocktail. As can be seen in Figure 6C and Figures S8D-F, this low dose cocktail is active in multiple senescent cancer models. Overexpression of cFLIP in the senescent A549 or SK-Hep1 cells prevented senolysis by the combination of conatumumab and either NEO2734 or ARV-771 (Figure 6D, E). Similar observations were also made using FADD, CASP8 or DR5 null A549 cells (Figure S8G-I). Together, our data show that either overexpression cFLIP or loss of FADD, CASP8, DR5 can rescue cells from this drug combination-mediated senolysis, indicating that these genes are crucial to mediate senescent cell death.

To test this senolytic cocktail *in vivo*, we used both immunodeficient and immunocompetent mouse models. We engrafted A549 cells into immunodeficient nude mice and Hepa1-6 liver cancer cells in syngeneic immunocompetent C57bl/6 mice. After tumours were established, we treated with alisertib to induce senescence and combinations of the two senolytic drugs. Treatment with single agent alisertib, NEO2734 or DR5 agonist antibodies (conatumumab for A549, mouse DR5 antibody MD5-1 for Hepa1-6) resulted in limited tumour growth inhibition. Treatment with the combination of two drugs resulted in some tumour control, but the strongest effect was seen with the three-way combination, without affecting bodyweight of the mice (Figure 7A-D). To assess the selective killing of senescent tumour cells in the in vivo models upon DR5 activation, we collected the tumours and stained them for p21^{cip1} as a senescence marker. We observed alisertib treatment massively induced senescence in the tumours as judged by p21^{cip1} induction. In the combination treatments with conatumumab, the senescent cells were significantly depleted. (Figure S9A, B). CD95/FAS is also upregulated in senescent cells and FAS ligand (FASLG) induces preferential killing of senescent cells (Figure S9C, D). This raises the possibility that FASLG produced by activated tumour-infiltrating lymphocytes also contribute to senolysis.
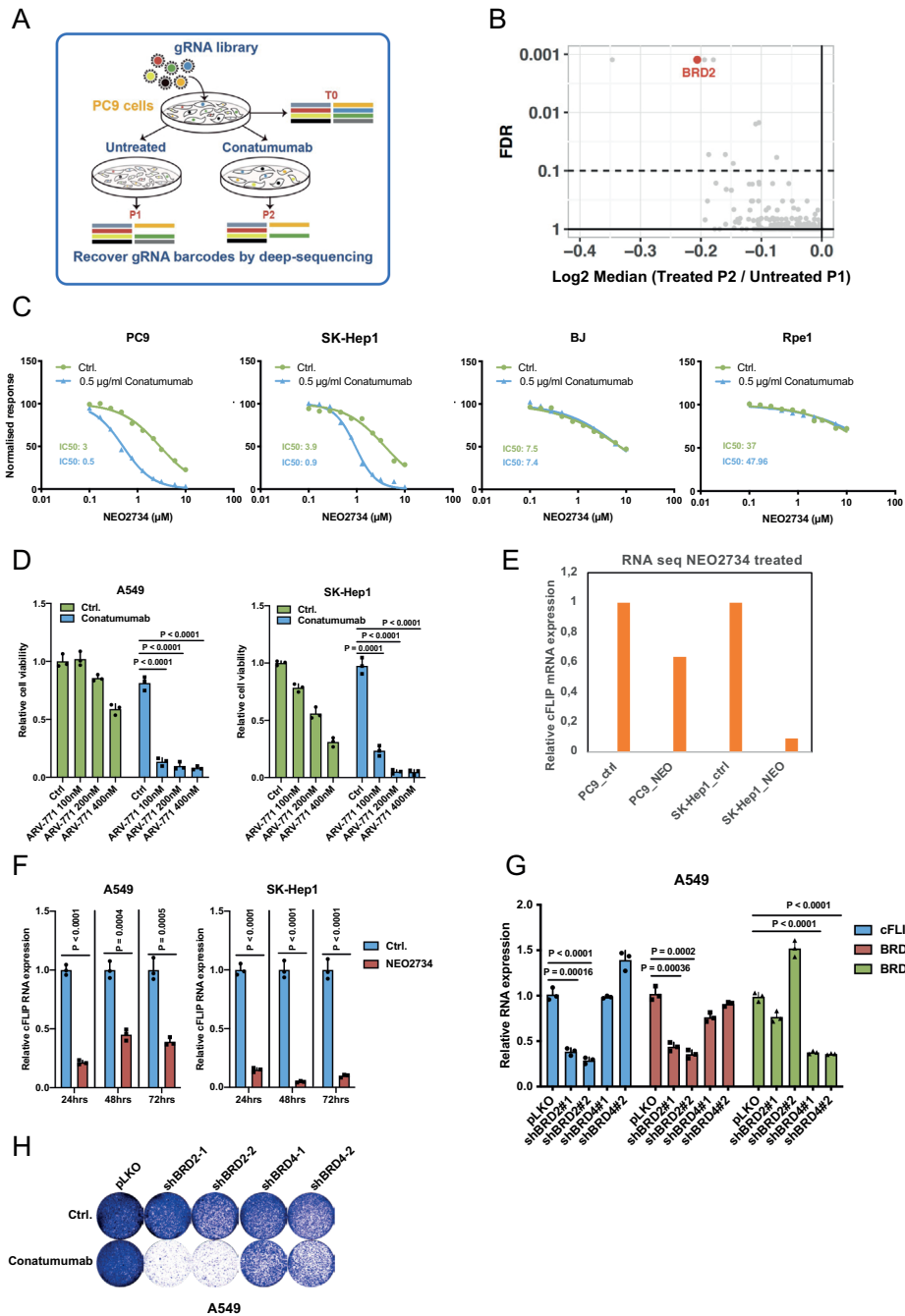
Figure 5. BRD2 inhibition suppresses cFLIP and enhances DR5 agonist-mediated cell killing.
(**A**) CRISPR-based synergy screen in PC9 to identify genes whose inhibition synergizes with 0.125 µg/ml conatumumab in causing cell death. PC9 cells were infected with kinome and epigenome CRISPR library virus and cultured with conatumumab for 7 days. Deep-sequencing was used to determine changes in gRNA representation. (**B**) Top hits were selected by the fold depletion upon

6

conatumumab treatment. **(C)** Dose-response curve of PC9, SK-Hep1, BJ, and Rpe1 cells treated with conatumumab and NEO2734. **(D)** Colony formation assay in the A549 and SK-Hep1 cells with ARV-771 and conatumumab (4 μg/ml for A549, 0.5 μg/ml for SK-Hep1) treatment. **(E)** cFLIP expression from RNAseq of PC9 and SK-Hep1 upon 1 μM NEO2734 treatment. **(F)** Real-time PCR of cFLIP expression on A549 and SK-Hep1 upon 1 μM NEO2734 treatment on different time points. **(G)** Real-time PCR of cFLIP, BRD2 and BRD4 in A549 cells with shRNA against BRD2 and BRD4. **(H)** Colony formation in the A549 cells with shRNA against BRD2 or BRD4 and treated with 4 μg/ml conatumumab. Error bars in the *in vitro* studies in this figure represent the mean ± standard deviations from biological triplicates (*P≤0.05, ** P≤0.01, *** P≤0.001, two-tailed t-test).

It may be challenging to induce senescence evenly in heterogeneous tumours and any remaining non-senescent cancer cells might escape senolytic therapy. However, it is possible that SASP factors, including TRAIL and cytokines like IL6 and IL8 that activate NF-kB signalling in recipient non-senescent cells, could sensitise such cells to a DR5 agonist. Such a "bystander" effect on non-senescent cells could increase the efficiency of pro-senescence/senolytic therapy. To test this, we collected conditioned culture medium from therapy-induced senescent cells and used this to treat proliferating cells. SASP media treated proliferating cells did not become senescent, but show decreased cell survival in the presence of NEO2734 and conatumumab (Figure S9E-H). Notably, this bystander effect of senescent cells on killing of non-senescent cells in the population is limited to DR5 agonist plus BRD inhibitor cocktail and not seen with navitoclax (Figure S10A). This is most readily explained by the notion that secreted TRAIL and NF-kB activation sensitize to activation of extrinsic apoptosis signalling and not to enhancement of intrinsic apoptosis signalling. This highlights the unique nature of DR5 activation as a senolytic in oncology. Moreover, the responsiveness was SASP concentration-dependent (Figure S10B). To further study this bystander effect, we also tested our senolytic cocktail in an *in vitro* competition assay using different ratios of senescent and proliferating cells. The result shows that non-senescent cells in the experiment having a higher senescent cell density responded best to senolytic treatment (Figure S10C). Transcriptomic analysis of SASP medium treated proliferating cells showed that NF-kB signalling was activated (Figure S10D). Furthermore, the suppression of p65 using shRNAs rescues the SASP treated proliferating cells from senolysis (Figure S10E). These results indicate that the senolytic responsiveness of the non-senescent cells by SASP factors is driven in part by NF-kB activation. Our data support a model in which pro-senescence therapies prime senescent cancer cells for cell death through enforced extrinsic apoptosis signalling. We show that a DR5 agonistic antibody, potentially combined with BRD inhibition to suppress cFLIP expression, leads to effective induction of apoptosis in senescent cancer cells (Figure 7E).
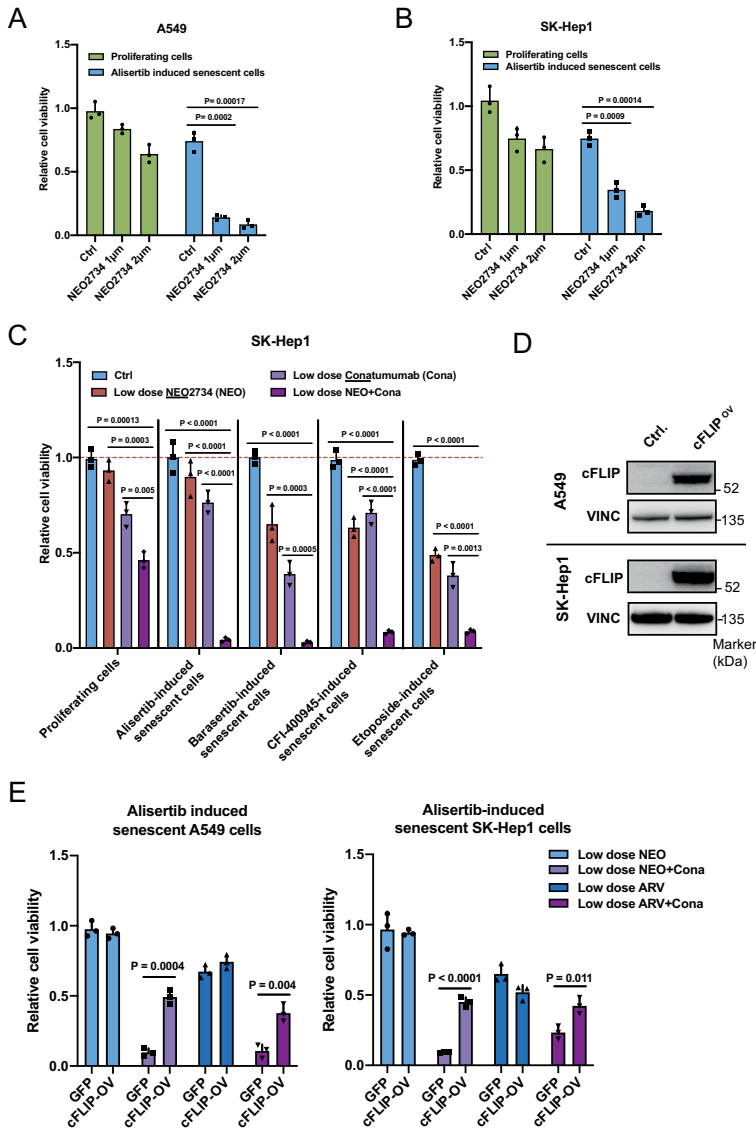
Figure 6. cFLIP suppression and DR5 activation sensitize senescent cancer cells to senolysis. (A-B) CellTiter-Blue measurement on the senescent and proliferating A549 **(A)** and SK-Hep1 **(B)** cells upon NEO2734 treatment. **(C)** Colony formation using low dose 0.25 μM of NEO2734 and 0.125 μg/ml conatumumab on SK-Hep1 cells made senescent by one-week treatment of 0.5μM alisertib, 1 μM barasertib, 50nM CFI-400945 or 2 μM Etoposide. Viabilities were normalized to non-conatumumab and non-NEO2734 treated cells. **(D)** Western blot of cFLIP overexpressed A549 and SK-Hep1 cells. **(E)** Cell viability based on the colony formation in cFLIP overexpressing A549 and SK-Hep1 senescent cells treated with 0.25 μM NEO2734 and conatumumab (0.125 μg/ml for SK-Hep1 and 1 μg/ml for A549). Error bars in this figure represent the mean ± standard deviations from biological triplicates (*P≤0.05, ** P≤0.01, *** P≤0.001, two-tailed t-test).
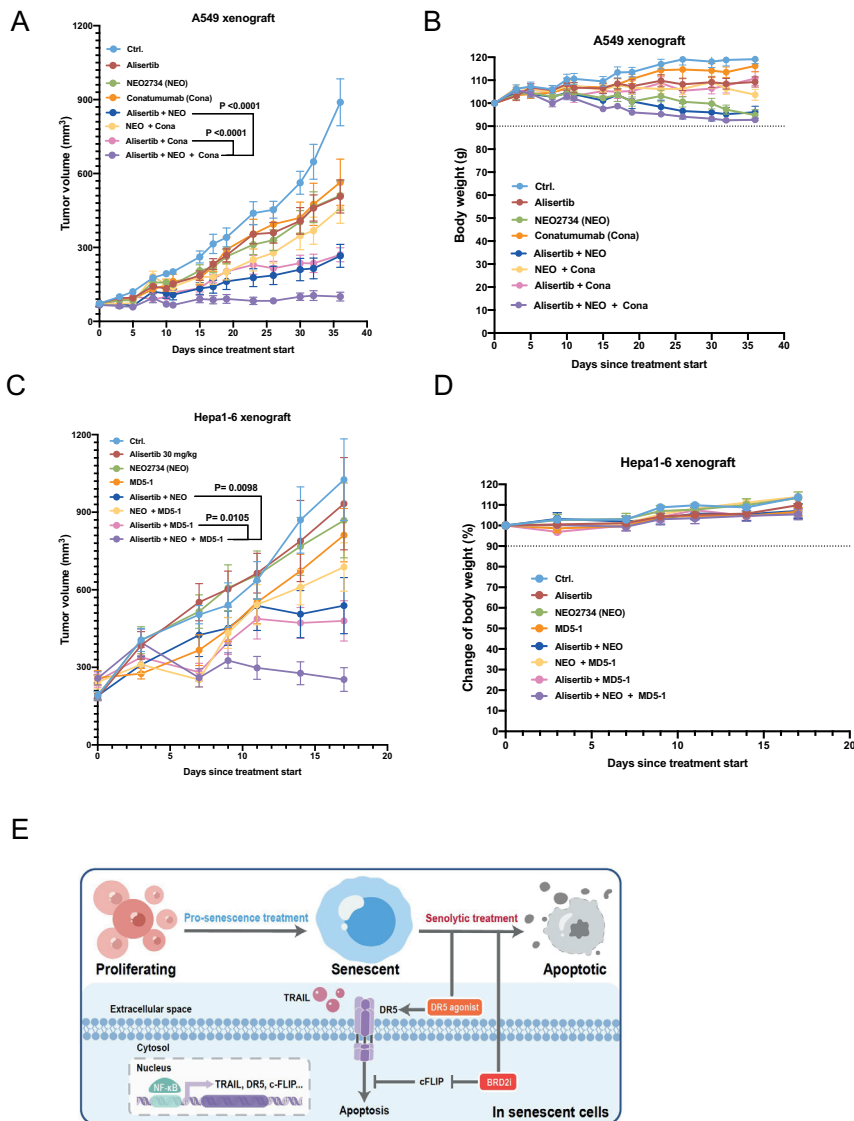
Figure 7. *In vivo* validation of BRD inhibitor and DR5 agonist combination as a senolytic cocktail. (A) Tumour growth of A549 lung cancer cells in the flank immunodeficient nude mice. When tumors reached approximately 100 mm³, assigned to either vehicle control, 30 mg/kg alisertib, 4 mg/kg NEO2734 (NEO), 5 μg/dose conatumumab (Cona), the two-way combinations of 4 mg/kg NEO2734 plus 5 μg/dose conatumumab and 30 mg/kg alisertib plus 5 μg/dose conatumumab, and then three-way combination of 30 mg/kg alisertib plus 4 mg/kg NEO2734 plus 2.5 μg/dose conatumumab (n=8). **(B)** Body weight of *in vivo* experiment with A549 lung cancer cells engrafted into immunodeficient nude mice. **(C)** Tumour growth of Hepa1-6 liver cancer cells in syngeneic immunocompetent C57bl/6 mice. When tumours reached approximately 250 mm³, animals were assigned to either vehicle control, 30 mg/kg alisertib, 4 mg/kg NEO2734 (NEO), 0.3 μg/dose MD5-1, the two-way combinations of 4 mg/kg NEO2734 plus 0.3 μg/dose MD5-1 and 30 mg/kg alisertib plus 0.3 μg/dose MD5-1, and then three-way combination of 30 mg/kg alisertib plus 4 mg/kg NEO2734 plus 0.3 μg/dose MD5-1 (n=9). **(D)** Body weight of *in vivo* experiment with Hepa1-6 liver cancer cells

in syngeneic immunocompetent C57bl/6 mice. The data is presented as mean ± SEM. Two-way ANOVA test was applied for the *in vivo* statistical analysis. (*P≤0.05, ** P≤0.01, *** P≤0.001). **(E)** Model of combining pro-senescence and senolytic therapies.

Discussion

Therapy-induced senescence is a well-established side effect of multiple cancer drugs (Nardella et al., 2011) and such senescent cancer cells may evoke a more aggressive behaviour of the non-senescent cells in the tumour population through paracrine effects of the secreted SASP (Wang et al., 2020). Senolytic drugs can therefore also have future use in combination with cancer drugs with senescence inducing activity. Aurora kinase inhibitors are potent inducers of senescence in cell culture (Liu et al., 2015; Wang et al., 2017). Nevertheless, multiple aurora kinase inhibitors have failed in the clinical trials due to lack of single agent activity (Borisa and Bhatt, 2017; O'Connor et al., 2019). Our study indicates that combinations of pro-senescence drugs and DR5 agonists or together with BRD inhibitors may achieve better treatment response. There is precedent for the notion that drugs lacking single agent activity become very potent in combination. In *BRAF* mutant colon cancer the combination of BRAF and EGFR inhibitors is now approved for clinical use, but the two drugs lack single agent activity in this cancer (Tabernero et al., 2021). Finally, the inducible CRISPR screening platform described here may have utility to find vulnerabilities of other types of proliferation-arrested cancer cells, such as drug tolerant persisters (Sharma et al., 2010) or cells that have entered diapause-like state after drug treatment (Dhimolea et al., 2021; Lin and Zhu, 2021; Rehman et al., 2021).

6

Methods

Ethical approvals

Human NK cells were isolated from blood collars of healthy donors obtained under Institutional Review Board-approved protocols of the Dana-Farber Cancer Institute (DFCI) and Boston Children's Hospital. All human tumor specimens were obtained under an Institutional Review Board-approved protocol of St Jude Children's Research Hospital, and informed consent was obtained from all subjects. All mouse experiments were performed with approval from the DFCI Institutional Animal Care and Use Committee (IACUC).

This study complied with all relevant ethical regulations and was approved by the Ethics Committee of Peking University. All participants were provided with written informed consent.

This study complies with all relevant ethical regulations. The use of patient information, tissues and genomic data was performed according to the guidelines of the European Network of Research Ethics Committees, following European, national and local laws as detailed below for each case. Experiments with mice were approved by the Animal Care and Use Committee of Barcelona Science Park under protocols CEEA-PCB-14-000053, CEEA-PCB-14-000275, CEEA-PCB-14-000276, CEEA-PCB-14-000285 and CEEA-PCB-15-000075.

Ethics approval and consent to participate

Mice (male/female) received standard chow diet freely and were housed in conditions of 12:12h dark:light cycle, 22±1°C ambient temperature and 50±10% humidity at Peking University Health Science Center animal facility. All animal experiments were performed in accordance with a protocol approved by the Department of Laboratory Animal Science of Peking University Health Science Center and supervised by the institutional review board of Peking University.

The primary tumor cell lines, hCAFs, human TMA samples were collected from PDAC patients (male/female) aged 34–82years diagnosed with PDAC at the Department of Pancreatic Surgery, Huashan Hospital. All manipulations about human patient samples were approved by the Research Ethics Committee of Huashan Hospital, Fudan University. All patients provided written informed consent before enrollment and have consented to the data reporting provided in Supplementary Table 4.

Cell lines

All cell lines were obtained from ATCC. Cell lines A549, PC9, H2030, H358, MIA PaCa-2, TFK-1, EGI-1, HCT116, SW480 and Lovo were cultured in a RPMI-based medium supplemented with 10% FBS, 1% penicillin/streptomycin and 2mM L-glutamine. Cell lines Hepa1-6, BJ, RPE1, SK-Hep1, Hep3B, PLC/PRF/5, Huh7, A375, MB-MDA-231

and MCF-7 were cultured in a DMEM-based medium supplemented with 10% FBS, 1% penicillin/streptomycin and 2mM L-glutamine. Monoclonal A549-iCas9, SK-Hep1-iCas9, PC3-iCas9 cells were generated from A549, SK-Hep1 and PC3 parental cells infected by the edit-R Inducible Lentiviral Cas9 vector. BJ-ER: HRAS and BJ-ER: HRAS-shTP53 cells were gifts from Dr. Roderick Beijersbergen, Netherlands Cancer institute, Amsterdam, the Netherlands. All the Cell lines have been validated by STR profiling and regularly tested for Mycoplasma spp with PCR-based assay.

Compounds and antibodies

Alisertib (#201931), Barasertib (#200420), Etoposide (#100330), Navitoclax (#201970), ARV-771 (#206827), PF-06873600 (#206997), Doxorubicin (#100280), Palbociclib (#202173), Trametinib (#201458), Bleomycin (#100090), Necrosulfonamide (#525389) and Z-VAD-FMK (#533011) were purchased from Medkoo Biosciences. CFI-400945 (#S7552) and NEO2734 (#S9648), were purchased from Selleck Chemicals. Lz-TRAIL (#LS-G3910) was purchased from LSBio. Conatumumab (#TAB-203) was purchased from Creative Biolabs. The antibodies for western blot analysis were used with dilution 1:1000, Anti-cFLIP (clone 7F10, #ALX-804-961-0100) was purchased from Enzo Life Sciences. Anti-VINC (clone hVIN-1, #V9131) was purchased from Sigma-Aldrich. Anti-DR4 (polyclonal, #AB16955) and anti-DR5 (polyclonal, #AB16942) were purchased from MERCK. Anti-cleaved PARP (Asp214) (clone D64E10, # 5625), Anti-phospho-MEK1/2 (Ser217/221) (Clone 41G9, # 9154), Anti-MEK1/2 (Clone L38C12, # 4694), Anti-phospho-Rb (Ser780) (polyclonal, # 39033) Anti-TRAIL (Clone C92B9, #3219) were purchased from Cell Signaling. Anti-P21 (polyclonal, #sc-397), Anti-HSP90 (polyclonal, #sc-7947) was purchased from Santa Cruz Biotechnology. For FACS related experiments, Anti-DR4-APC (DJR1, Biolgend #307207), anti-DR5 antibody-PE (DJR2-4 (7-8), Biolgend #307405). MD5-1 antibody was provided by From Dr. Hideo Yagita from Department of Immunology, Juntendo University School of Medicine, Tokyo, Japan. InVivoMAb polyclonal Armenian hamster IgG (#BE0091) was used as the isotype Control of MD5-1 were purchased from BioXcell.

Plasmids and Primers

All the primers and individual shRNA vectors were collected from the TRC library. (Supplementary Table 1). The FADD and cFLIP overexpression lenti-viral vectors were collected from BROAD ORF cDNA library. The luciferase-based NF-kB reporter pHAGE NFkB-TA-LUC-UBC-GFP-W (#49343) (Wilson et al., 2013), IKB suppressor vectors pBabe-Puro-IKBalpha-wt (#15290) (Boehm et al., 2007), pBabe-Puro-IKBalpha-mut (super repressor) (#15291) (Boehm et al., 2007), gene editing assay vector pXPR_011 (#59702) (Doench et al., 2014), gRNA cloning vector pLentiGuide-puro (#52963) (Sanjana et al., 2014), Human CRISPR Knockout Pooled Library (Brunello) (#73178) (Doench et al., 2016) were purchased from addgene. The edit-R Inducible

6

Lentiviral Cas9 vector (#NC1606271) was purchased from Dharmacon.

CRISPR/Cas9 based genetic screens
The CRISPR-based senolytic screen platform in Figure 1A requires cell models, which can be homogenously induced to senescence while efficiently performing gene editing. Monoclonal cells with a high CAS9 induction need to be selected from the doxycycline-inducible Cas9 vector embedded cells. To test gene-editing efficiency of the selected clone, the cells can be infected with lentiviral vector pXPR-011 containing EGFP with gRNA against EGFP and analyzed by flow cytometry after 1 week 1 µg/ml doxycycline treatment (Figure S1A-G). The CRISPR-based senolytic screen in Figure 1A, A549 cells were infected with a doxycycline-inducible Cas9 (iCas9) lentiviral vector, and single clones with high CAS9 induction were picked and checked on gene editing efficiency using pXPR-011 vector. Next, Brunello lentiviral whole genome-wide gRNA collection virus was introduced to the A549-iCas9 cells with MOI 0.3 and 500-times coverage. These infected cells were firstly treated with 0.5 µM alisertib for 7 days to drive them into senescence. Afterwards, these cells were suspended from alisertib then switched to 1 µg/ml doxycycline treatment for 10 days. Non-senescent cells were included as the control arm to filter out the straight lethal genes and also treated with doxycycline. Changes in library representation after 10 days doxycycline treatment were determined by Illumina deep-sequencing. Proliferating cells were also taken as the control to filter out the essential genes and to determine the selective senolytic activity. gRNAs prioritized for further analysis were selected by the fold depletion of abundance in pre-and post-dox treatment in both alisertib induced senescent and proliferating cells (For A549, S2 and S1 samples compared to P2 and P1 samples. For SK-Hep1 and PC3 (Figure S1G-I) as a validation screen, only senescent arm was used, S2 compared to S1).

CRISPR-based synergy screen shown in Figure 4 was performed on PC9 to identify genes whose inhibition can synergistically result in apoptosis with conatumumab. Polyclonal human "kinome and epigenome" CRISPR library virus (5,971 CRISPR vectors targeting 504 kinases, 5,130 vectors targeting 446 epigenetic factors, 100 vectors for 10 essential genes and 50 non-targeting gRNAs) was generated to infect PC9 cells. These cells were then cultured with 0.2 µg/ml conatumumab and collected after 7 days. Changes in library representation were determined by Illumina deep-sequencing. Non-treated cells were also taken as the control to identify genes, which were only depleted in the treated arm. gRNAs prioritized for further analysis were selected by the fold depletion due to conatumumab treatment.

Apoptosis resistance screen in Figure S6 was performed on using Hep1-iCas9 cFLIP null cells to identify genes whose inhibition can result in resistance to apoptosis with alisertib. The cells were infected with Brunello lentiviral whole genome-wide gRNA collection virus. After puromycin selecting the infected cells. To arm were taken as

one of the controls. Afterwards, the cells were pre-treated with 0.5 μg/ml doxycycline for 4 days. Next, the cells were divided to two arms with or without alisertib treatments for 2 weeks. Doxycycline was kept in both arms through the experiment. At the end of experiment, the cells from both arms were collected. Changes in library representation were determined by Illumina deep-sequencing. Cells before alisertib and non-alisertib treated cells were also taken as the control to identify genes, which were only enriched in the treated arm. gRNAs prioritized for further analysis were selected by the fold enrichment due to alisertib treatment. The primary selection is on the significant and substantial increase when comparing alisertib treated versus untreated. However, as an increase in treated versus untreated can also come from a decrease in untreated versus To, instead of an increase in Ttreated versus To. In this case, we applied a second criterion that there should also be significant and substantial increase when comparing Treated versus To.

All CRISPR screens were performed with three biological replicates with the independent viral infection. Hits in the three CRISPR screens for senolytics, as depicted in Figure 1, were selected based on higher depletion in the senescence condition compared to the parental condition in all three screens. Other screens were analysed in the following way. First, a differential analysis on the sgRNA level between two conditions was done with DESeq2. The results of this analysis were sorted on the DESeq2 test statistic putting the most depleted sgRNA at the top. We then used MAGeCK's RRA tool to look for each gene for the enrichment of the sgRNAs towards the top. The p-value of this enrichment analysis was then corrected for multiple testing using the Benjamini-Hochberg method. As hits we selected the genes with an FDR smaller or equal than 0.1 (Evers et al., 2016; Li et al., 2014; Love et al., 2014).

CRISPR-mediated knockout of cFLIP, CASP8, FADD, DR4 and DR5

For A549 cFLIP null cells, the gRNA (5'-ATTACCTATAGTCCGAAACA-3') was generate as flowing, oligonucleotides containing gRNA sequences flanked by 20-30 nt of overlapping backbone sequence were obtained from ThermoFisher scientific. Guide RNA (gRNA) were cloned into LentiGuide-puro (addgene plasmid #52963) via *BsmB*I sites, using Gibson Assembly® Master Mix (#E2611 from NEB). Afterwards, gRNA-cFLIP was introduced into A549-iCas9 cells with lentiviral infection. After 48 hours of doxycycline treatment, the cFLIP^{KO} clones were picked. For Hep1 cFLIP null cells, the gRNA (GUCUGCUGAAGUCAUCCAUC - Modified) was purchased from Synthego Corporation, and introduced into Hep1 with Lipofectamine™ CRISPRMAX™ Cas9 Transfection Reagent (#CMAX00008 From Thermo Fisher). Afterwards, the cFLIP^{KO} clone was picked. A549 Casp8, FADD, DR4, DR5 knockout cells were generated as Hep1 cFLIP null cells described above using gRNAs Casp8 (CAGAAAUCUUUAUGAUAUUG - Modified), FADD (ACAGCGAGUGCAGCAGCACC -

Modified), TNFRSF10A/DR4 (AAACAAAUUGUUGGAAGCAU - Modified), TNFRSF10B/ DR5 (GCUGGACCUCUUUUGUUGUG - Modified). DR4/5 double knockout cells were generated by mixing gRNAs against DR4 and DR5, and then followed the same rest of procedures.

Lentiviral transduction
A third-generation lentivirus packaging system consisting of pCMV-VSV-G (addgene#8454), pRSV-Rev (Addgene#12253) and pMDLg/pRRE (Addgene#12251) was used to create virus particles of the modified reporter plasmids. A transient transfection was performed in 293T cells and lentiviral supernatants were produced. Destination cells were infected with lentiviral supernatants, using 8μg/ml polybrene and low virus titer. After 48h of incubation, the supernatant was replaced by a medium containing 10 μg/ml blasticidin or 2 μg/ml puromycin. After 48h, selection of viral transduced cell lines was completed.

Drug treatments
Used concentrations of drugs in the colony formation, CellTiter-blue measurement, Incucyte proliferation and apoptosis assays, western blot and real-time PCR. senescence inducers: 0.5 μM alisertib, 1 μM Barasertib, 50 nM CFI-400945, 2 μM Etoposide, 10 Gy ionizing radiation. Drugs induce senescence for a week. Pan-caspase inhibitor: 10 μM Z-VAD-FMK, Necroptosis inhibitor: 10 μM necrosulfonamide, DR5 agonists: Lz-TRAIL 200 ng/ml, conatumumab used 4 μg/ml for A549 and 1 μg/ml for Hep1. Low dose of conatumumab used 1 μg/ml for A549 and 0.125 μg/ml for Hep1. BCL2-family inhibitor: 1 μM Navitoclax. Refresh the drugs and medium every 3 days. BRD inhibitors: NEO2734 treatment in RNA seq and real-time PCR was 1 μM for 1 week or indicated time points. Low dose of NEO2734 used 0.25 μM. Low dose of ARV-771 used 50 nM. Other doses of drugs were indicated in the figures.

NF-kB signaling measurement
NF-kB signaling activation was measured by A549 cells with an integrated NF-kB-luciferase reporter construct a luciferase-based NF-kB reporter (pHAGE NFkB-TA-LUC-UBC-GFP-W, addgene plasmid #49343) (Wilson et al., 2013). Luciferase signal was carried out using Luciferase Assay System (#E1500) from Promeg according to the manufacturer's instructions.

Colony formation assay
Cells were seeded into 12-well plates (40,000 cells per well) and cultured both in the absence and presence of drugs as indicated for 5 days. Drug-induced senescent cells were firstly treated with one of the senescence inducers for 7 days. Next, cells were trypsinized, suspended from senescence treatment and seeded equal cell density

in the plates as the proliferating arm. Afterwards, the cells were switched to other drug treatments for another 5 days. At the end of the assay, cells were fixed with 4% of formaldehyde (#1.04002, Millipore) diluted in PBS, stained with 2% of crystal violet (#HT90132 Sigma-Aldrich) diluted in water, photographed and quantified using Fiji.

IncuCyte cell proliferation assays

For IncuCyte proliferation assays, cells were seeded in 96-well plates (3,000 cells per well) and cultured in absence or presence of drugs as indicated. Apoptosis marker staining was accessed by caspase-3/7 green apoptosis assay reagent (#4440 from Essen Bioscience, 1000 times dilution to each well). Cell confluence and GFP signal were measured and quantified by the IncuCyte imaging system (Essen Bioscience).

Cell viability measurement

Cell viability was detected using CellTiter-Blue® Cell Viability Assay Kit (G8081, Promega) according to the manufacturer's instructions. Drug-induced senescent cells were firstly treated with one of the senescence inducers for 7 days. Next, cells were trypsinized, suspended from senescence treatment and seeded equal cell density in the plates as the proliferating arm. Afterwards, the cells were switched to other drug treatments for another 5 days. At the end of assay, CellTiter-Blue reagent was added and measurement was performed using EnVision multi-label plate reader (PerkinElmer). Dose-response curve. IC50 values were calculated by PRISM.

Senolytic index calculation

Cell viability was measured from 3 technical replicates using CellTiter-Blue to generate dose-response curves to calculate IC50. Senolytic indexes were calculated by IC50 of proliferating cells divided by IC50 of senescent cells.

Protein lysate preparation and immunoblotting

Cells were seeded in the culture medium in the absence or presence of drugs. Afterwards, the cells were washed with PBS and lysed with RIPA buffer supplemented with protease inhibitors (cOmplete, Roche) and phosphatase inhibitor cocktails II and III (Sigma). All lysates were freshly prepared and processed with Novex NuPAGE Gel Electrophoresis Systems (Invitrogen).

Real-time PCR

Total RNA was extracted from cells using TRIzol reagent from Invitrogen or Quick-RNA™ MiniPrep (#R1055) from Zymo Research. cDNA synthesis was performed using Maxima Universal First Strand cDNA Synthesis Kit (#K1661) from Thermo scientific. qPCR reactions were performed with FastStart Universal SYBR Green Master (Rox) from Roche. The experiments were performed according to the manufacturer's

instructions. The sequences of the primers used for qRT–PCR analyses are described in the key resource table online: 'https://www.nature.com/articles/s43018-022-00462-2'. All reactions were run in triplicate. The CT values were calculated using the Standard Curve Method.

Staining for senescence associated β-galactosidase activity

β-galactosidase activity in cells was detected using Histochemical Staining Kit (CS0030-1KT) from Sigma-Aldrich. β-galactosidase detection was carried out according to the manufacturer's instructions. SA-beta-gal staining positive cells were quantified based on 3 independent images.

Cell line-derived xenografts

All animals were manipulated according to protocols approved by the Shanghai Medical Experimental Animal Care Commission and Shanghai Cancer Institute. The maximal tumor size/burden is 2000mm³. All the in vivo experiments have not exceeded the maximal tumor size. Six- to 8-week-old male BALB/c nude mice were used in the studies. In figure 4G, A549 cells (1×10^7 cells per mouse) were injected subcutaneously into the flanks of nude mice (8 mice per group). After tumour establishment, mice were randomly assigned to 5 days/week treatment (drug-off in weekend) and given vehicle, conatumumab (intraperitoneal injection), alisertib (Oral gavage), NEO2734 (Oral gavage) or combinations. In figure 4h Hepa1-6 mouse liver cancer line cells (5×10^6 cells per mouse) were injected subcutaneously into the flanks of in syngeneic immunocompetent C57bl/6 mice (9 mice per group). After tumour establishment, mice were randomly assigned to 5 days per week treatment (drug-off in weekend) and given vehicle, alisertib, NEO2734 or related combinations. In the treatment arms involved mouse DR5 agonist MD5-1, MD5-1 were 2 times intraperitoneal injected per week, respectively. InVivoMAb polyclonal Armenian hamster IgG were used in the control groups. In Figure S5, A549 cells (5×10^6 cells per mouse) or SK-Hep1 cells (1×10^7 cells per mouse) were injected subcutaneously into the flanks of nude mice (6 mice per group for A549, 8 mice per group for Hep1). After tumour establishment, mice were randomly assigned to 5 days/week treatment and given vehicle, conatumumab (intraperitoneal injection), alisertib or combination. Tumour volume based on calliper measurements was calculated by the modified ellipsoidal formula: tumour volume = ½ length × width². The data is presented as mean ± SEM.

Patient-derived xenografts

In compliance with the protocol approved by the Institutional Review Board of Naval Military Medical University Affiliated Eastern Hepatobiliary Hospital and with the subjects' informed consent, fragments of surgically resected tumour tissues from HCC patients were used for xenotransplantation. The maximal tumor size/

burden is 2000mm³. The in vivo experiments have not exceeded the maximal tumor size. Briefly, patient samples were collected, trimmed, cut into 20-30 mm³ fragments and implanted subcutaneously in the fore flanks of anesthetized 6- to 8-week-old male BALB/c nude mice within three hours. After tumour volume reaching around 100 mm³, mice were randomly assigned to 5 days / week treatment with vehicle, Conatumumab (intraperitoneal injection), Alisertib/barasertib (oral gavage) or combination. (5 mice per group). Tumour volume based on calliper measurements was calculated by the modified ellipsoidal formula: tumour volume = ½ length × width². The data is presented as mean ± SEM. All procedures and protocols were approved by the Institutional Animal Care and Use Committee of WuXi AppTec.

Flow cytometry

The cells were trypsinized and washed one with PBS. Next, the cells were incubated for 30 minutes with dilution 1:100 using Anti-DR4-APC (DJR1, Biolgend #307207), anti-DR5 antibody-PE (DJR2-4 (7-8), Biolgend #307405). After PBS washing, the cells were measured by flow cytometry BD LSRFortessa and analyzed by Flowjo V10.

Immunohistochemistry

Formalin-fixed paraffin-embedded samples were also obtained from xenograft tumours and then probed with antibodies against p21 Waf1/Cip1 (#2947, Cell signalling; 1:50). Following incubation with the primary antibodies, positive cells were visualized using DAB+ as a chromogen. Quantification of p21 staining were performed by analyzing percentage of positive cells from 12 biologically independent nodules each treatment at a magnification of 20X. The analysis is performed by HALO® image analysis software.

Senescence conditional (SASP) medium related experiments

A549 or SK-Hep1 cells were seeded in 4-5 million cells in the 15cm dishes and treated with different senescence inducers for one week, such as 0.5 µM alisertib, 1 µM barasertib, 50 nM CFI-400945, 0.5 µM PF-06873600, 2 µM etoposide or 100 nM doxorubicin. The drugs were refreshed twice within a week. Afterwards, the drugs were suspended, the senescent cells were cultured and refreshed twice with a standard medium for one week. After the second time fresh, the SASP medium was collected after three days and diluted with fresh standard medium either one time or two times to generate ½ SASP or ¼ SASP media. The control medium in the experiments was generated as described below. 2-3 million proliferating cells were cultured with a standard medium for three days. The cultured medium was collected and diluted with a freshly standard medium one time. The control medium and SASP medium were added to the A549 or SK-Hep1 proliferating cells and treated with the senolytic agents.

Transcriptomic data

RNA sequencing data of lung cancer lines: A549, H358, PC9, liver cancer lines: HepG2, Huh7, Hep3B, breast cancer lines: MCF-7, T47D, MDA-MB-231, SUM159 and colon cancer lines: HCT116, LoVo, RKO in parental, alisertib-induced senescent and etoposide-induced senescent state can be found under accession number E-MTAB-9970 in ArrayExpress (Jochems et al. 2021). Beeswarm plots for the gene expression of extrinsic apoptosis related genes. Each dot represents a cell line (Red for breast, green for colon, blue for lung and purple for liver cancer lines). The data can be accessed via https://ccb.nki.nl/publications/cancer-senescence/.

Statistics and Reproducibility

Throughout all figures: *p<0.05, **p<0.01, and ***p<0.001 and NS (Not Significant) p>0.05. *In vitro* experiment statistical two-tailed t-test were analyzed with two-tailed and performed using Microsoft Excel. *In vivo* experiment statistical two-way ANOVA analyses were performed using Prism version 8.0 (GraphPad). All the in vitro experiments (except RNA sequencing, due to the high cost) were repeated in at least three independent experiments and showed comparable results between experiments. Further information on research design is available in the Nature Research Reporting Summary linked to this article.

Raw numerical data and statistical analysis of all repeats for all figures and are provided in the Source data. Information about experimental replicates is included in the figure legends. Statistical analysis was performed using the SPSS statistical software package (standard v.20; SPSS Inc.). For two-group statistical analyses, unpaired Student's *t*-test was used. Error bars represent SD, as indicated in the legends. For more than two-group statistical analyses, Dunnett's test were used.

Littermate animals from different cages were randomly assigned to the experimental groups. Tumor weight measurements were performed in a blinded manner. All other data collection and analysis were not performed blind to the conditions of the experiments. Data distribution was assumed to be normal but not formally tested. No data were excluded from the analyses.

No statistical method was used to predetermine sample size in all the highly controlled in vitro or in vivo experiments, but our sample sizes are similar to those reported in previous publications. For each experiment, we aimed for a number of at least of three samples or animals per group to allow basic statistical significance. The exact sample size was indicated in the figure legend. All animals were randomized and exposed to the same environment.

References

Boehm, J.S., Zhao, J.J., Yao, J., Kim, S.Y., Firestein, R., Dunn, I.F., Sjostrom, S.K., Garraway, L.A., Weremowicz, S., Richardson, A.L., et al. (2007). Integrative Genomic Approaches Identify IKBKE as a Breast Cancer Oncogene. Cell *129*, 1065–1079.

Borisa, A.C., and Bhatt, H.G. (2017). A comprehensive review on Aurora kinase: Small molecule inhibitors and clinical trial studies. Eur. J. Med. Chem. *140*, 1–19.

Carpenter, V.J., Saleh, T., and Gewirtz, D.A. (2021). Senolytics for cancer therapy: Is all that glitters really gold? Cancers (Basel).

Chang, J., Wang, Y., Shao, L., Laberge, R.-M., Demaria, M., Campisi, J., Janakiraman, K., Sharpless, N.E., Ding, S., Feng, W., et al. (2016). Clearance of senescent cells by ABT-263 rejuvenates aged hematopoietic stem cells in mice. Nat. Med. *22*, 78–83.

Coppé, J.P., Desprez, P.Y., Krtolica, A., and Campisi, J. (2010). The senescence-associated secretory phenotype: The dark side of tumor suppression. Annu. Rev. Pathol. Mech. Dis. *5*, 99–118.

Demaria, M., O'Leary, M.N., Chang, J., Shao, L., Liu, S., Alimirah, F., Koenig, K., Le, C., Mitin, N., Deal, A.M., et al. (2017). Cellular senescence promotes adverse effects of chemotherapy and cancer relapse. Cancer Discov.

Dhimolea, E., de Matos Simoes, R., Kansara, D., Al'Khafaji, A., Bouyssou, J., Weng, X., Sharma, S., Raja, J., Awate, P., Shirasaki, R., et al. (2021). An Embryonic Diapause-like Adaptation with Suppressed Myc Activity Enables Tumor Treatment Persistence. Cancer Cell *39*, 240-256. e11.

Doench, J.G., Hartenian, E., Graham, D.B., Tothova, Z., Hegde, M., Smith, I., Sullender, M., Ebert, B.L., Xavier, R.J., and Root, D.E. (2014). Rational design of highly active sgRNAs for CRISPR-Cas9-mediated gene inactivation. Nat. Biotechnol. *32*, 1262–1267.

Doench, J.G., Fusi, N., Sullender, M., Hegde, M., Vaimberg, E.W., Donovan, K.F., Smith, I., Tothova, Z., Wilen, C., Orchard, R., et al. (2016). Optimized sgRNA design to maximize activity and minimize off-target effects of CRISPR-Cas9. Nat. Biotechnol. *34*.

Dörr, J.R., Yu, Y., Milanovic, M., Beuster, G., Zasada, C., Däbritz, J.H.M., Lisec, J., Lenze, D., Gerhardt, A., Schleicher, K., et al. (2013). Synthetic lethal metabolic targeting of cellular senescence in cancer therapy. Nature *501*, 421–425.

Eggert, T., Wolter, K., Ji, J., Ma, C., Yevsa, T., Klotz, S., Medina-Echeverz, J., Longerich, T., Forgues, M., Reisinger, F., et al. (2016). Distinct Functions of Senescence-Associated Immune Responses in Liver Tumor Surveillance and Tumor Progression. Cancer Cell *30*, 533–547.

Evers, B., Jastrzebski, K., Heijmans, J.P.M., Grernrum, W., Beijersbergen, R.L., and Bernards, R. (2016). CRISPR knockout screening outperforms shRNA and CRISPRi in identifying essential genes. Nat. Biotechnol. *34*, 11–14.

Faget, D. V., Ren, Q., and Stewart, S.A. (2019). Unmasking senescence: context-dependent effects of SASP in cancer. Nat. Rev. Cancer *19*, 439–453.

Finnberg, N.K., Gokare, P., Navaraj, A., Kuhs, K.A.L., Cerniglia, G., Yagita, H., Takeda, K., Motoyama, N., and El-Deiry, W.S. (2016). Agonists of the TRAIL death receptor DR5 sensitize intestinal stem cells to chemotherapy-induced cell death and trigger gastrointestinal toxicity. Cancer Res. *76*, 700–712.

Guerrero, A., Herranz, N., Sun, B., Wagner, V., Gallage, S., Guiho, R., Wolter, K., Pombo, J., Irvine, E.E., Andrew, J., et al. (2019). Cardiac glycosides are broad-spectrum senolytics. Nat. Metab. *1*, 1074–1088.

Hayflick, L. (1965). The limited in vitro lifetime of human diploid cell strains. Exp. Cell Res. *37*, 614–636.

Jochems, F., Thijssen, B., De Conti, G., Jansen, R., Pogacar, Z., Groot, K., Wang, L., Schepers, A., Wang, C., Jin, H., et al. (2021). The Cancer SENESCopedia: A delineation of cancer cell senescence. Cell Rep. *36*, 109441.

Kuilman, T., Michaloglou, C., Vredeveld, L.C.W., Douma, S., van Doorn, R., Desmet, C.J., Aarden, L.A., Mooi, W.J., and Peeper, D.S. (2008). Oncogene-Induced Senescence Relayed by an Interleukin-Dependent Inflammatory Network. Cell *133*, 1019–1031.

Laberge, R.M., Awad, P., Campisi, J., and Desprez, P.Y. (2012). Epithelial-mesenchymal transition induced by senescent fibroblasts. Cancer Microenviron. *5*, 39–44.

Li, W., Xu, H., Xiao, T., Cong, L., Love, M.I., Zhang, F., Irizarry, R.A., Liu, J.S., Brown, M., and Liu, X. (2014). MAGeCK enables robust identification of essential genes from genome-scale CRISPR/Cas9 knockout screens. Genome Biol. *15*, 554.

Lin, Y.H., and Zhu, H. (2021). A Malignant Case of Arrested Development: Cancer Cell Dormancy Mimics Embryonic Diapause. Cancer Cell *39*, 142–144.

6

Liu, Y., Hawkins, O.E., Vilgelm, A.E., Pawlikowski, J.S., Ecsedy, J.A., Sosman, J.A., Kelley, M.C., and Richmond, A. (2015). Combining an Aurora Kinase Inhibitor and a Death Receptor Ligand/Agonist Antibody Triggers Apoptosis in Melanoma Cells and Prevents Tumor Growth in Preclinical Mouse Models. Clin. Cancer Res.

Love, M.I., Huber, W., and Anders, S. (2014). Moderated estimation of fold change and dispersion for RNA-seq data with DESeq2. Genome Biol. *15*.

Muñoz-Espín, D., Rovira, M., Galiana, I., Giménez, C., Lozano-Torres, B., Paez-Ribes, M., Llanos, S., Chaib, S., Muñoz-Martín, M., Ucero, A.C., et al. (2018). A versatile drug delivery system targeting senescent cells. EMBO Mol. Med. *10*, 1–18.

Nardella, C., Clohessy, J.G., Alimonti, A., and Pandolfi, P.P. (2011). Pro-senescence therapy for cancer treatment. Nat. Rev. Cancer.

Nijwening, J.H., Kuiken, H.J., and Beijersbergen, R.L. (2011). Screening for modulators of cisplatin sensitivity: Unbiased screens reveal common themes. Cell Cycle *10*, 380–386.

O'Connor, O.A., Ozcan, M., Jacobsen, E.D., Roncero, J.M., Trotman, J., Demeter, J., Masszi, T., Pereira, J., Ramchandren, R., Beaven, A., et al. (2019). Randomized phase III study of alisertib or investigator's choice (selected single agent) in patients with relapsed or refractory peripheral T-cell lymphoma ¨. In Journal of Clinical Oncology, pp. 613–623.

Raina, K., Lu, J., Qian, Y., Altieri, M., Gordon, D., Rossi, A.M.K., Wang, J., Chen, X., Dong, H., Siu, K., et al. (2016). PROTAC-induced BET protein degradation as a therapy for castration-resistant prostate cancer. Proc. Natl. Acad. Sci. U. S. A.

Rehman, S.K., Haynes, J., Collignon, E., Brown, K.R., Wang, Y., Nixon, A.M.L., Bruce, J.P., Wintersinger, J.A., Singh Mer, A., Lo, E.B.L., et al. (2021). Colorectal Cancer Cells Enter a Diapause-like DTP State to Survive Chemotherapy. Cell *184*, 226-242.e21.

Ruscetti, M., Leibold, J., Bott, M.J., Fennell, M., Kulick, A., Salgado, N.R., Chen, C.C., Ho, Y. jui, Sanchez-Rivera, F.J., Feucht, J., et al. (2018). NK cell–mediated cytotoxicity contributes to tumor control by a cytostatic drug combination. Science (80-.).

Sanjana, N.E., Shalem, O., and Zhang, F. (2014). Improved vectors and genome-wide libraries for CRISPR screening. Nat. Methods *11*, 783–784.

Serrano, M., Lin, A.W., McCurrach, M.E., Beach, D., and Lowe, S.W. (1997). Oncogenic ras provokes premature cell senescence associated with accumulation of p53 and p16(INK4a). Cell *88*, 593–602.

Shahbandi, A., Rao, S.G., Anderson, A.Y., Frey, W.D., Olayiwola, J.O., Ungerleider, N.A., and Jackson, J.G. (2020). BH3 mimetics selectively eliminate chemotherapy-induced senescent cells and improve response in TP53 wild-type breast cancer. Cell Death Differ.

Sharma, S. V., Lee, D.Y., Li, B., Quinlan, M.P., Takahashi, F., Maheswaran, S., McDermott, U., Azizian, N., Zou, L., Fischbach, M.A., et al. (2010). A Chromatin-Mediated Reversible Drug-Tolerant State in Cancer Cell Subpopulations. Cell *141*, 69–80.

Soto-Gamez, A., Wang, Y., Zhou, X., Seras, L., Quax, W., and Demaria, M. (2022). Enhanced extrinsic apoptosis of therapy-induced senescent cancer cells using a death receptor 5 (DR5) selective agonist. Cancer Lett. *525*, 67–75.

Spriano, F., Gaudio, E., Tarantelli, C., Golino, G., Cascione, L., Zucca, E., Stathis, A., Giles, F.J., and Bertoni, F. (2018). Targeting Both BET and Crebbp/EP300 Proteins with the Novel Dual Inhibitor NEO2734 Leads to More Preclinical Anti-Tumor Activity in Diffuse Large B Cell Lymphomathan with Single BET or Crebbp/EP300 Inhibitors. Blood *132*, 4174–4174.

Suzuki, A., Araki, T., Miura, M., and Tsutomi, Y. (1999). Functional absence of FADD in PLC/PRF/5 hepatoma cells: Possible involvement in the transformation to hepatoma in HBV-infected hepatocytes. Proc. Soc. Exp. Biol. Med. *221*, 72–79.

Tabernero, J., Grothey, A., van Cutsem, E., Yaeger, R., Wasan, H., Yoshino, T., Desai, J., Ciardiello, F., Loupakis, F., Hong, Y.S., et al. (2021). Encorafenib plus cetuximab as a new standard of care for previously treated BRAF V600E-mutant metastatic colorectal cancer: Updated survival results and subgroup analyses from the BEACON study. J. Clin. Oncol. *39*, 273–284.

Takeda, K., Kojima, Y., Ikejima, K., Harada, K., Yamashina, S., Okumura, K., Aoyama, T., Frese, S., Ikeda, H., Haynes, N.M., et al. (2008). Death receptor 5 mediated-apoptosis contributes to cholestatic liver disease. Proc. Natl. Acad. Sci. U. S. A. *105*, 10895–10900.

Wang, B., Kohli, J., and Demaria, M. (2020). Senescent Cells in Cancer Therapy: Friends or Foes? Trends in Cancer.

Wang, C., Vegna, S., Jin, H., Benedict, B., Lieftink, C., Ramirez, C., de Oliveira, R.L., Morris, B., Gadiot, J., Wang, W., et al. (2019). Inducing and exploiting vulnerabilities for the treatment of liver cancer. Nature *574*, 268–272.

Wang, L., Leite de Oliveira, R., Wang, C., Fernandes Neto, J.M., Mainardi, S., Evers, B., Lieftink, C., Morris, B., Jochems, F., Willemsen, L., et al. (2017). High-Throughput Functional Genetic

and Compound Screens Identify Targets for Senescence Induction in Cancer. Cell Rep. *21*, 773–783.

Wilson, A.A., Kwok, L.W., Porter, E.L., Payne, J.G., McElroy, G.S., Ohle, S.J., Greenhill, S.R., Blahna, M.T., Yamamoto, K., Jean, J.C., et al. (2013). Lentiviral delivery of RNAi for in vivo lineage-specific modulation of gene expression in mouse lung macrophages. Mol. Ther. *21*, 825–833.
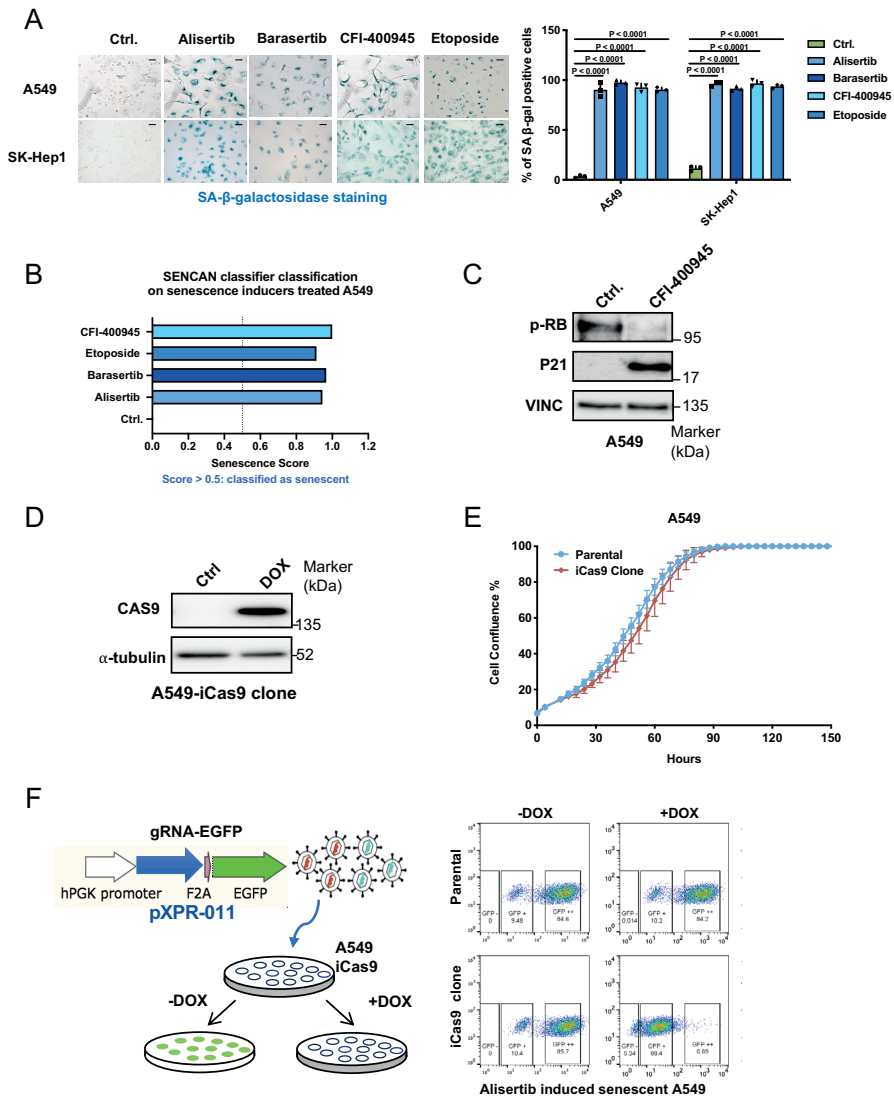
6

Supplementary figures

Figure S1. Senolytic screen optimization. **(A)** Senescence associated beta-galactosidase staining in A549 and SK-Hep1 cells treated for one week with senescence inducers (0.5 μM Alisertib, 1 μM Barasertib, 50 nM CFI-400951 or 2 μM Etoposide). The black scale bars represent 100 μm. **(B)** SENCAN classifier analysis (Jochems et al. 2021) on different senescence inducer treated A549 cells. **(C)** Western blot analysis of P21 and phosp-RB in A549 treated with 50 nM CFI-400945 for 1 week. **(D)** Western blot analysis of CAS9 expression in A549-iCas9 clone treated for 24 hours with 1 μg/ml doxycycline. **(E)** IncuCyte growth curve for A549-iCas9 and the parental cells. **(F)** A549 cells were infected with pXRP-011 and treated with or without 1 μg/ml doxycycline for a week. Afterwards, the GFP signals were measured by flow cytometry to determine gene editing efficiencies. Error bars in this figure represent the mean ± standard deviations from biological triplicates (* P≤0.05, ** P≤0.01, *** P≤0.001, two-tailed t-test).
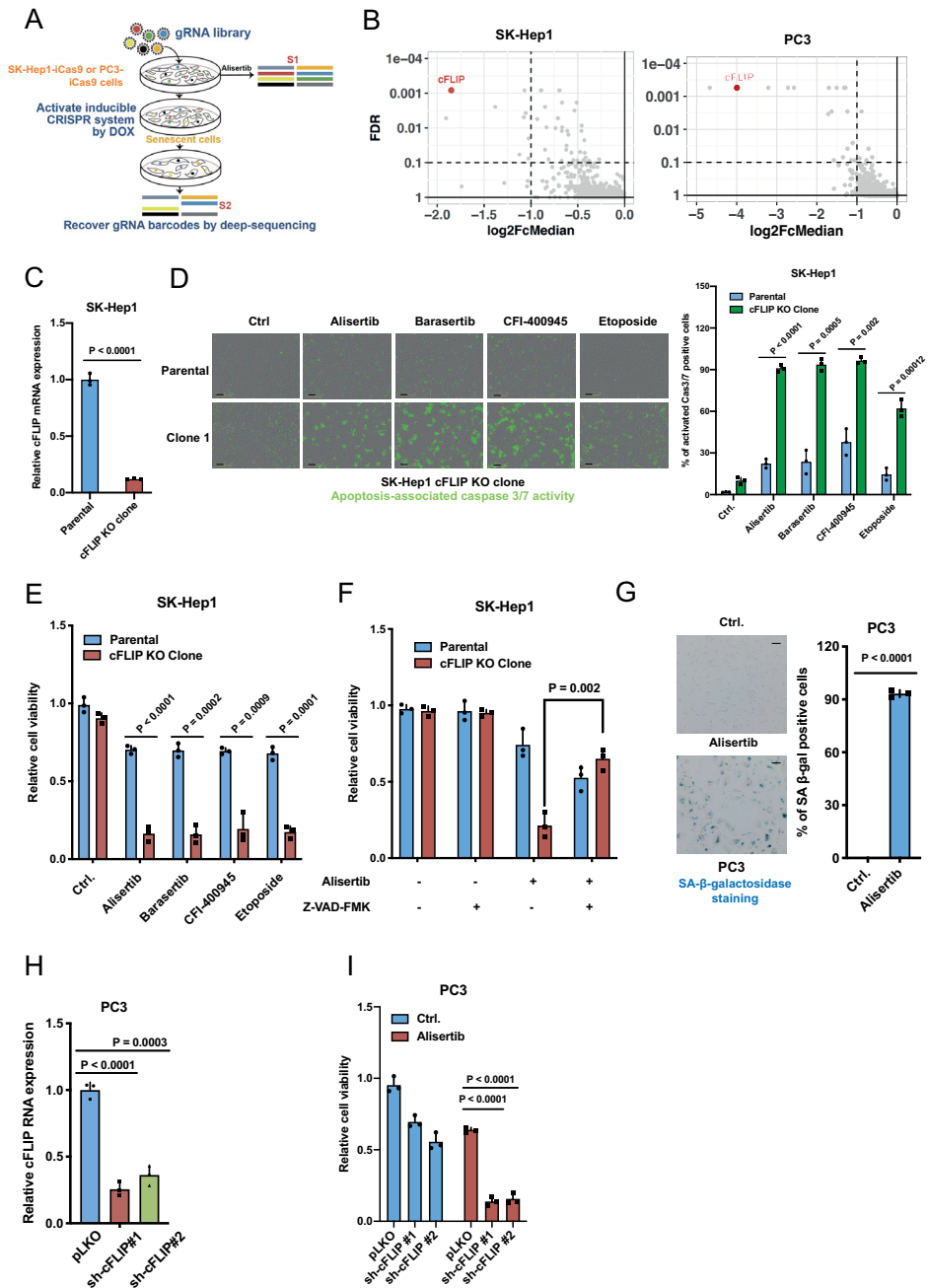
Figure S2. Senolytic screens and validation in additional models. (A) Schematic of CRISPR-based senolytic screen workflow in SK-Hep1 and PC3. Genome-wide Brunello gRNA collection lentivirus was introduced to the SK-Hep1-iCas9 or PC3-iCas9 cells. After 7 days of 0.5µM alisertib treatment, cells were switched to 1 µg/ml doxycycline (DOX) for 10 days. Illumina deep-sequencing was used to determine changes in library representation. **(B)** Top hits from SK-Hep1 and PC3 were selected based on the fold depletion of S2 divided by S1. **(C)** Real-time PCR analysis of cFLIP expression on SK-Hep1

cFLIP^{KO} clone. **(D)** Senescence inducers treated SK-Hep1 parental and cFLIP^{KO} cells were incubated with caspase-3/7 green apoptosis assay reagent. The black scale bars represent 100 μm. **(E)** CellTiter-Blue measurement in the SK-Hep1 parental and *cFLIP^{KO}* cells treated with senescence inducers for one week. **(F)** Quantification of colony formation assay for A549 parental and cFLIP-KO cells treated with 0.5 μM alisertib and 10 μM Z-VAD-FMK. **(G)** Senescence associated beta-galactosidase staining on PC3 cells with one week of 0.5 μM Alisertib treatment. The black scale bars represent 100 μm. **(H)** Real-time PCR analysis of cFLIP expression on PC3 cells infected with shRNAs against cFLIP. **(I)** Quantification of colony formation assay for PC3 cells treated with 0.5 μM alisertib and infected with shRNAs against cFLIP. Error bars in this figure represent the mean ± standard deviations from biological triplicates (* P≤0.05, ** P≤0.01, *** P≤0.001, two-tailed t-test).
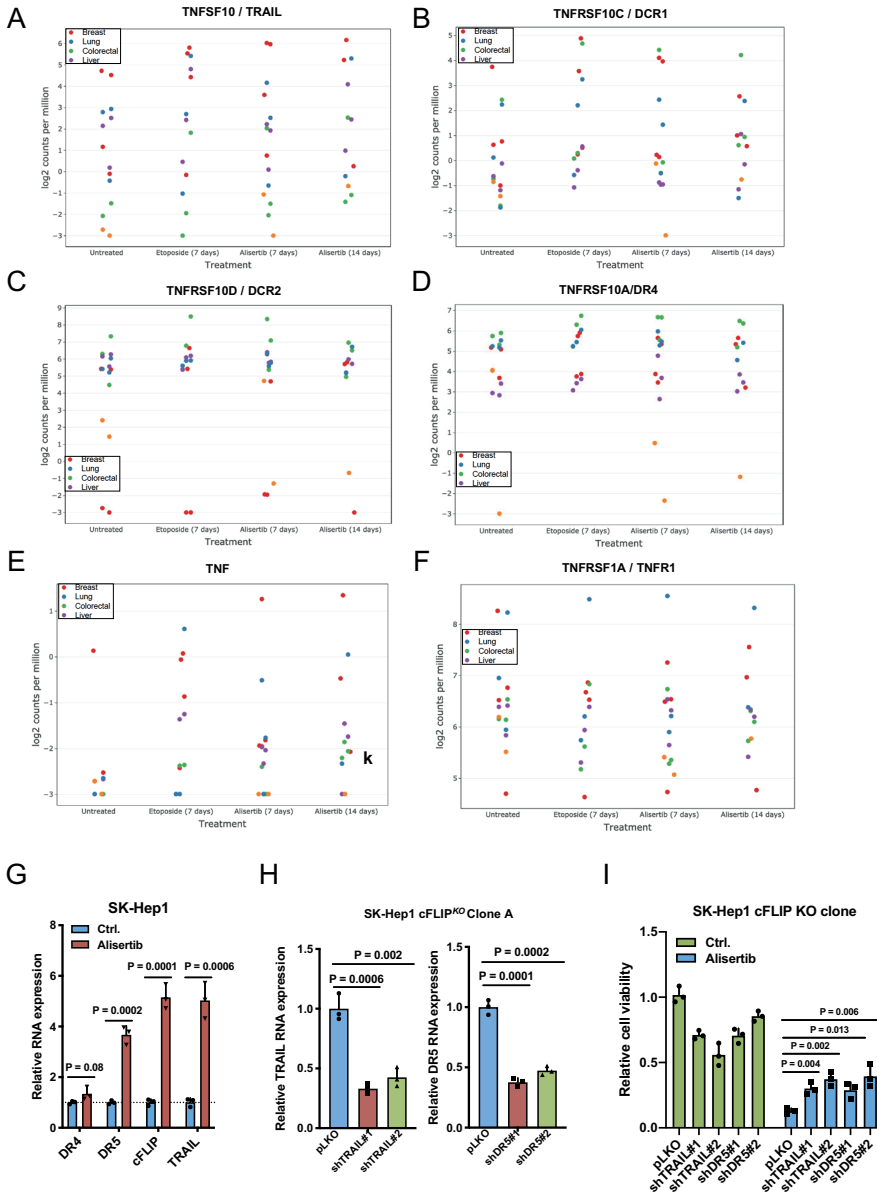
Figure S3. Enrichment of NF-kB signatures, death receptor related gene expression upon senescence induction and extrinsic apoptosis priming in senescent cells. (**A-F**) Transcriptomic analysis of death receptor genes TNFSF10 (TRAIL), TNFRSF10C (DCR1), TNFRSF10D (DCR2), TNFRSF10A (DR4), TNF and TNFRSF1A (TNFR1) from 13 cell lines made senescent by etoposide and alisertib (ArrayExpress E-MTAB-9970). (**G**) Real-time PCR analysis of DR4, DR5, cFLIP, and TRAIL in SK-Hep1 cells treated with 0.5 µM alisertib. (**H**) Real-time PCR analysis of TRAIL and DR5 in cFLIP knock-out SK-Hep1 cells with shRNAs against these genes. (**I**) Cell viability assessed by colony formation assay in cFLIP^{KO} cells with shRNAs against TRAIL or DR5 and treated with 0.5 µM alisertib for 7 days. Error bars in this figure represent the mean ± standard deviations from biological triplicates (* P≤0.05, ** P≤0.01, *** P≤0.001, two-tailed t-test).
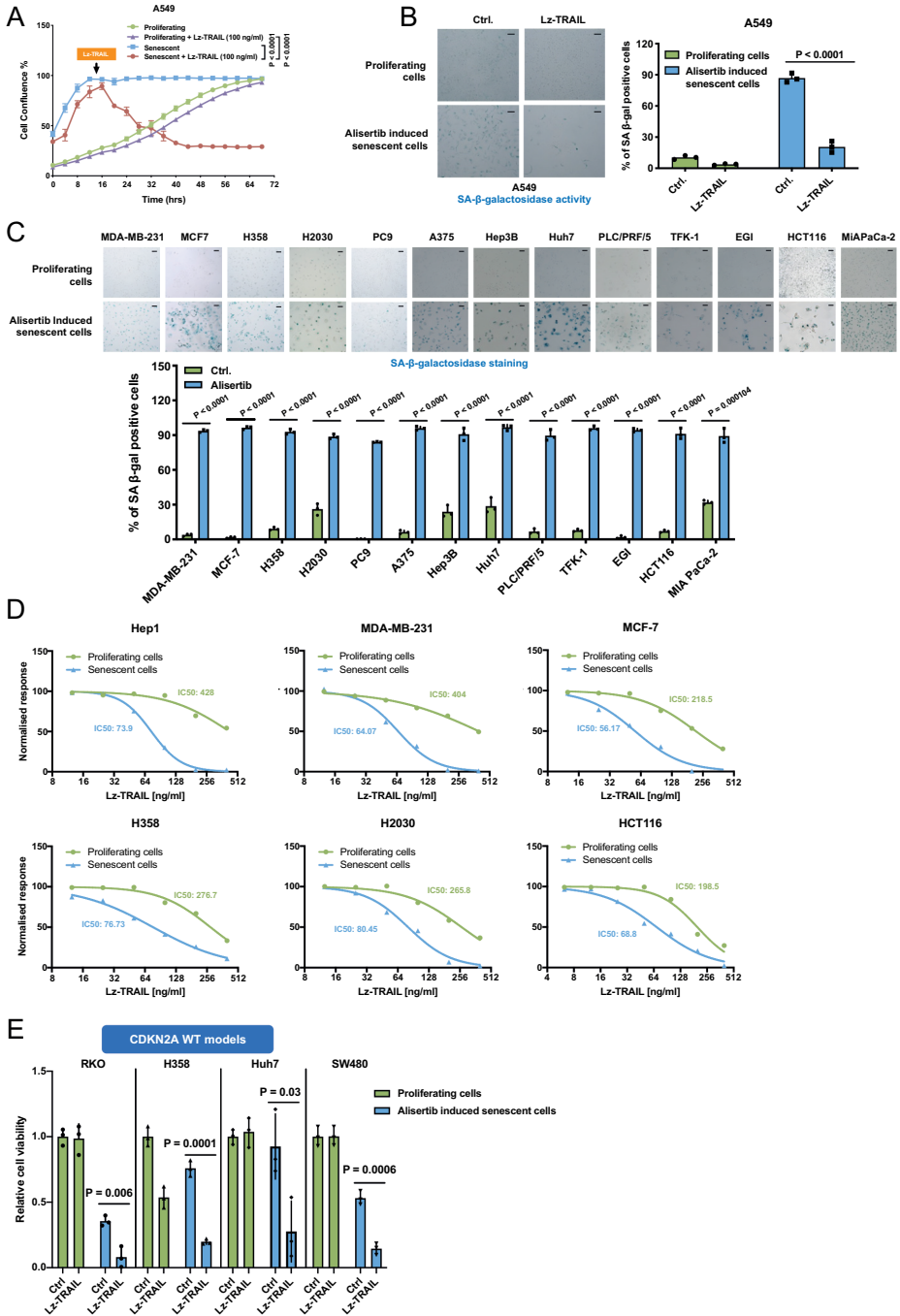
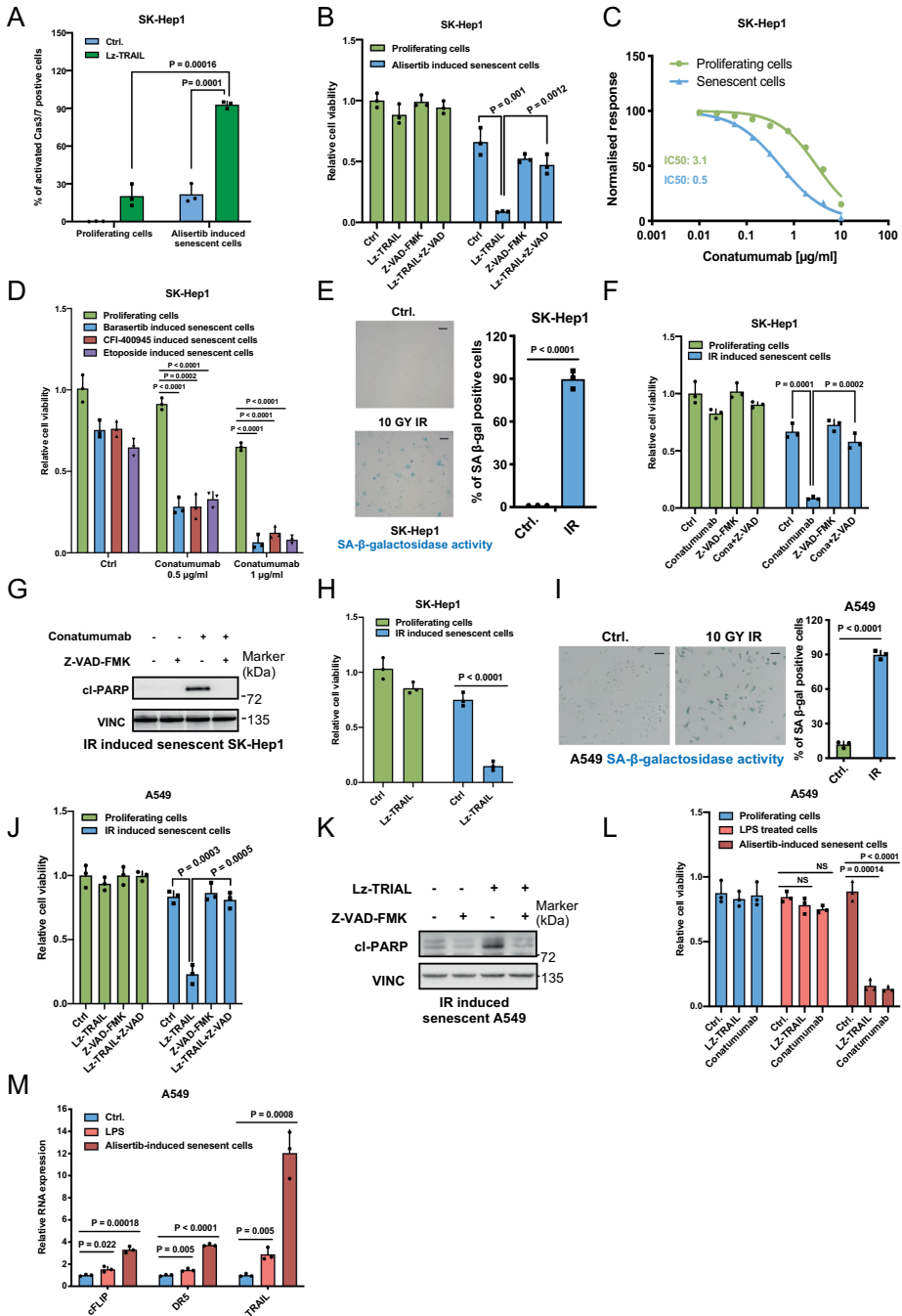**Figure S4. Lz-TRAIL-mediated senolysis in additional alisertib-induced senescent cell models. (A)** Incucyte cell proliferation assay showing 0.5 µM alisertib-induced senescent A549 cells treated with 100 ng/ml Lz-TRAIL. **(B)** Senescence associated with beta-galactosidase staining in A549 parental and alisertib-induced senescent cells treated with 200 ng/ml Lz-TRAIL. **(C)** Senescence associated beta-galactosidase staining in a panel of cell lines treated with alisertib. The black scale

bars represent 100 μm. **(D)** Dose-response curves of alisertib-induced senescent and proliferating *CDKN2A* mutant cell models upon Lz-TRAIL treatment. **(E)** Cell viability based on colony formation assay with alisertib-induced senescent and proliferating *CDKN2A* wild type cell models upon 100 ng/ml Lz-TRAIL treatment. Error bars in this figure represent the mean ± standard deviations from biological triplicates (* P≤0.05, ** P≤0.01, *** P≤0.001, two-tailed t-test).

6

Figure S5. Death receptor agonist-mediated senolysis in additional models induced by different senescence inducers. (A) Caspase-3/7 green apoptosis assay on alisertib-induced senescent SK-Hep1 cells treated with 100 ng/ml Lz-TRAIL. **(B)** Cell viability accessed by colony formation in the alisertib-induced senescent and proliferating SK-Hep1 cells treated with 100 ng/ml Lz-TRAIL, 10 μM Z-VAD-FMK. **(C)** Dose-response curve of 0.5 μM alisertib-induced senescent and proliferating SK-

Hep1 cells treated with conatumumab. **(D)** Colony formation assay in drug-induced (one week of 1 μM Barasertib, 100 nM CFI-400945, 2 μM Etoposide treatment) senescent SK-Hep1 cells treated with conatumumab. **(E)** Senescence associated beta-galactosidase staining in 7 days post-IR 10Gy on SK-Hep1 cells. The black scale bars represent 100 μm. **(F-G)** Colony formation **(F)** and Western blot of cl-PARP **(G)** in the IR-induced senescent and proliferating SK-Hep1 cells treated with 1 μg/ml conatumumab and 10 μM Z-VAD-FMK. **(H)** Cell viability accessed by colony formation in the IR-induced senescent and proliferating SK-Hep1 cells treated 100 ng/ml Lz-TRAIL. **(I)** Senescence associated beta-galactosidase staining in 7 days 10Gy post-ionizing irradiated (IR) A549 cells. The black scale bars represent 100 μm. **(J-K)** Colony formation assay **(J)** and western blot of cl-PARP **(K)** in the 10 Gy IR-induced senescent and proliferating A549 cells treated with 100ng/ml Lz-TRAIL and 10 μM Z-VAD-FMK. **(L)** Cell viability accessed by colony formation of 0.5 μM alisertib-induced senescent and 10 μg/ml LPS cultured cells treated with the 4 μg/ml conatumumab or 200 ng/ml Lz-TRAIL. **(M)** Real-time PCR for DR5, cFLIP, TRAIL in LPS treated and alisertib-induced senescent A549 cells. Error bars in this figure represent the mean ± standard deviations from biological triplicates (* P≤0.05, ** P≤0.01, *** P≤0.001, two-tailed t-test).
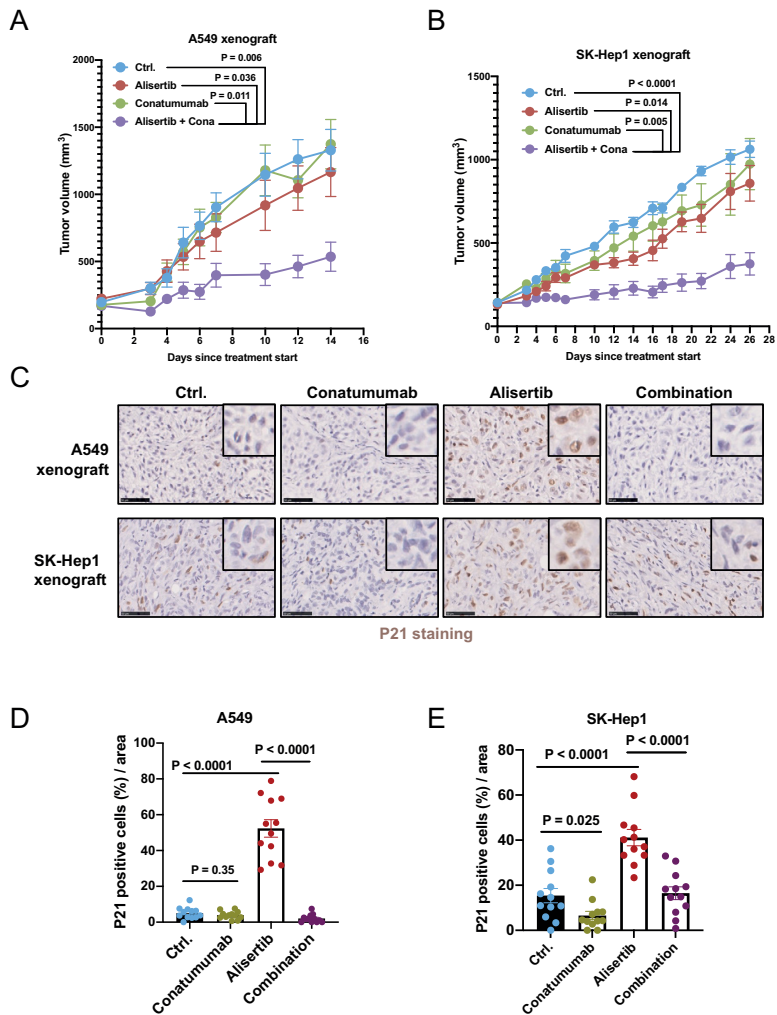
6

Figure S6. *In vivo* study of conatumumab-mediated senolysis. (A-B) Tumor growth of A549 **(A)** and SK-Hep1 **(B)** cells in flanks of Balb/c nude mice subcutaneously injected with 5 million cells. When tumors reached approximately 150mm³, mice were assigned to either vehicle control, 25 mg/kg alisertib, conatumumab (5 µg/dose for SK-Hep1, 10 µg/dose for A549) or combination (6 mice per group for A549, 8 mice per group for SK-Hep1). The data is presented as mean ± SEM. **c,** Fixed tissues were dehydrated and embedded in paraffin. Sections of 2-4 µm were prepared and immunostained with P21 to indicate senescent cells in the tumors of A549 and SK-Hep1. The black scale bars represent 50 µm. **(D-E)** For Immunohistochemistry analysis, error bars in this figure represent the mean ± standard deviations from biological triplicates (* P≤0.05, ** P≤0.01, *** P≤0.001, two-tailed t-test). Two-way ANOVA test was applied for xenograft experiments for statistical analysis. (* P≤0.05, ** P≤0.01, *** P≤0.001)
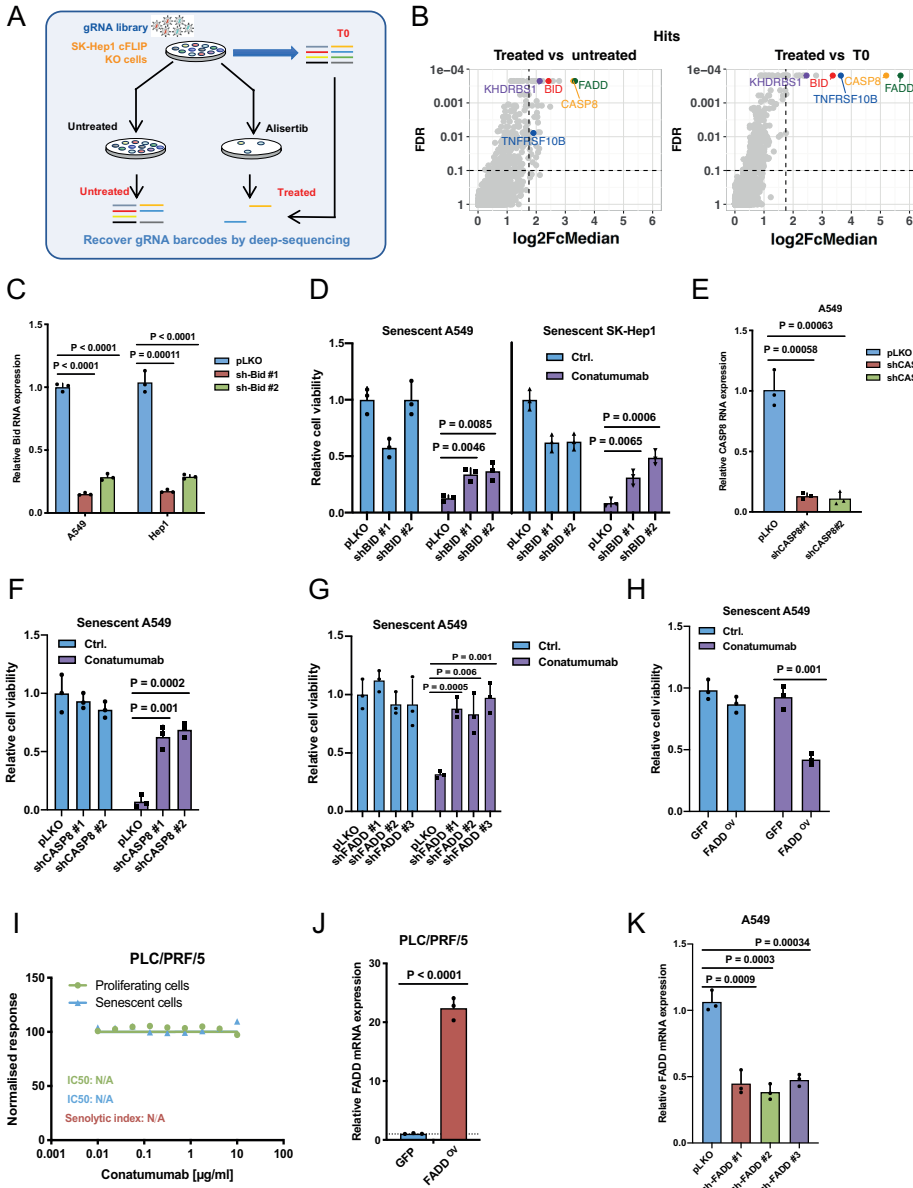
Figure S7. Potential resistance mechanisms of death receptor activation-mediated senolysis.
(**A**) CRISPR-based resistance screen was performed on cFLIP null SK-Hep1 cells to identify genes whose inhibition can result in resistance to alisertib-mediated senolysis. The cFLIP null SK-Hep1 cells were infected with genome-wide Brunello gRNA collection lentivirus and cultured with 0.5 μM alisertib and 1 μg/ml doxycycline for 14 days. The control arm is without alisertib. Deep-sequencing was used to determine changes in library representation. (**B**) Top hits were selected by the fold enrichment upon senolysis. (**C**) Real-time PCR of Bid in A549 and SK-Hep1 cells transduced with shRNAs against Bid. (**D**) Cell viability accessed by colony formation assay on Bid knockdown senescent A549 and SK-Hep1 cells treated with conatumumab. (**E**) Real-time PCR of Caspase 8 in cells A549 with shRNAs against CASP8. (**F**) Cell viability on CASP8 knockdown senescent A549 cells

treated with conatumumab. **(G)** Cell viability on FADD suppressed senescent A549 cells treated with Lz-TRAIL. **(H)** Real-time PCR of FADD in cells A549 with shRNA against FADD. **(I)** Dose-response curve in 1 μM alisertib-induced senescent PLC/PRF/5 cells treated with conatumumab. **(J)** Real-time PCR of FADD in A549 cells infected with FADD overexpression vector. **(K)** Cell viability on FADD overexpressed senescent A549 cells treated with Lz-TRAIL. Error bars in this figure represent the mean ± standard deviations from biological triplicates (* P≤0.05, ** P≤0.01, *** P≤0.001, two-tailed t-test).
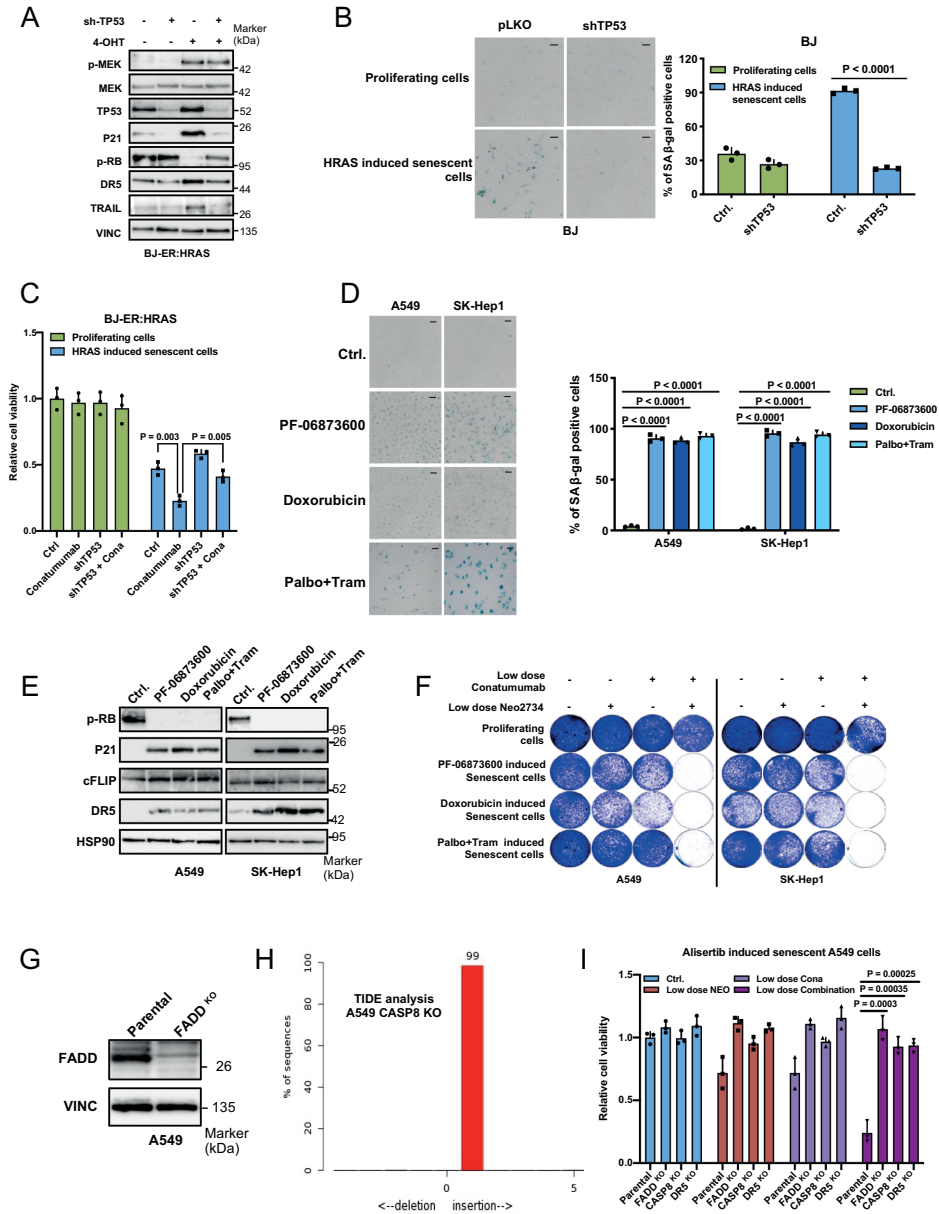
6

Figure S8. Examination of senolytic potentials with BRD2 inhibition and/or death receptor 5 activation on additional senescent models. (**A**) Western blot analysis on tamoxifen (4-OHT)-inducible mutant HRAS^{V12} vector infected BJ cells. (**B**) Senescence associated beta-galactosidase staining in proliferating and HRAS^{V12} induced senescent BJ cells transduced with an shRNA against TP53. The black scale bars represent 100 μm. (**C**) Cell viability accessed by colony formation assay on TP53 knockdown senescent BJ cells treated with 10 μg/ml conatumumab, representing an extremely high dose. (**D**) Senescence associated beta-galactosidase staining in A549 and SK-Hep1 cells treated with senescence inducers for one week (0.5 μM PF-06873600, 100nM doxorubicin and the combination of 5 nM trametinib plus 0.5 μM palbociclib). The black scale bars represent 100

µm. **(E)** Western blot analysis of senescence and death receptor signaling markers on A549 and SK-Hep1 treated with different senescence inducers. **(F)** Colony formation using low dose 0.25 µM of NEO2734 and 0.125 µg/ml conatumumab on SK-Hep1, 0.25 µM of NEO2734 and 1 µg/ml conatumumab on A549 cells made senescent by one-week treatment of different senescence inducers. **(G)** Western blot analysis for FADD on A549 FADD knock-out cells. **(H)** TIDE analysis of Caspase 8 knockout cells. **(I)** Colony formation using low dose 0.25 µM of NEO2734 and 1 µg/ml conatumumab on FADD, CASP8, or DR5 null A549 senescent cells. Error bars in this figure represent the mean ± standard deviations from biological triplicates (*P≤0.05, ** P≤0.01, *** P≤0.001, two-tailed t-test).
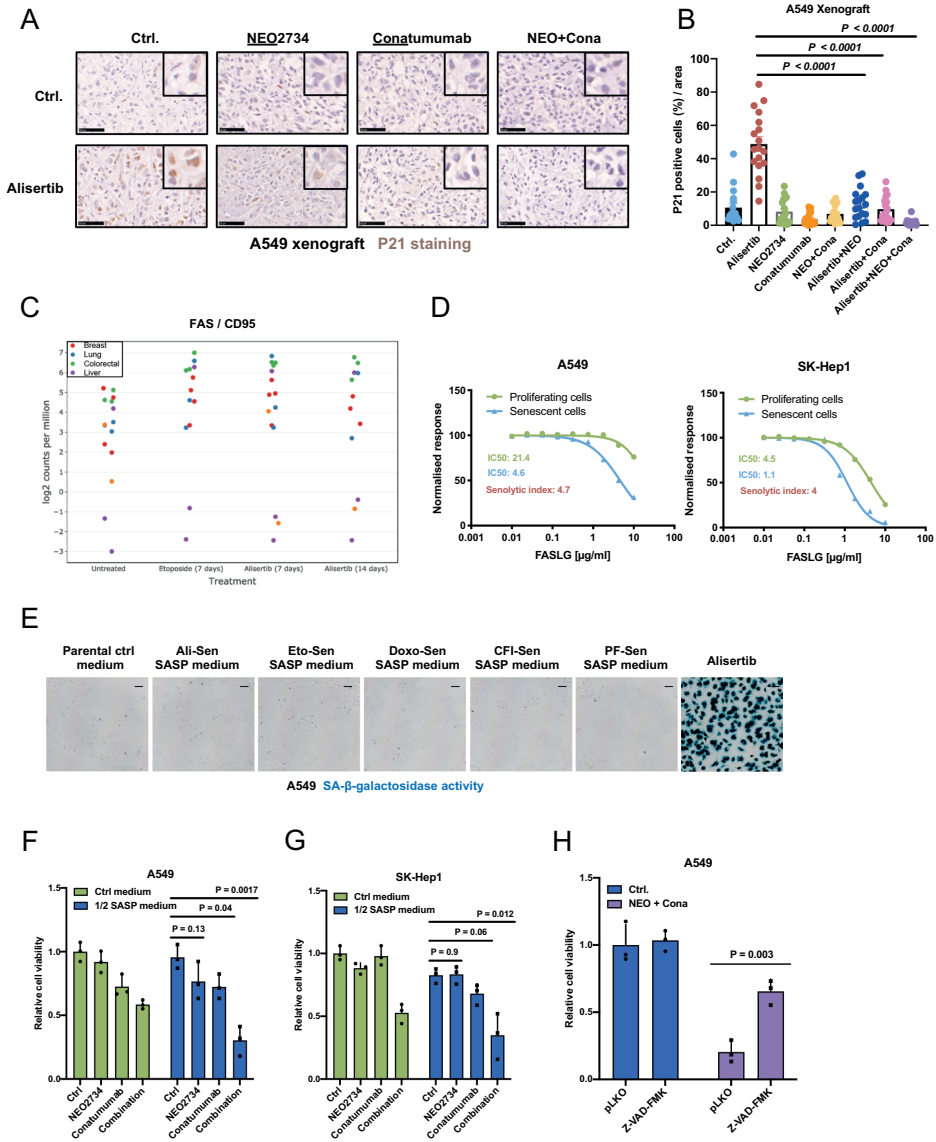
Figure S9. Death receptor activation mediated immune surveillance and evidence of a SASP-mediated bystander effect. (A) Fixed tissues were dehydrated and embedded in paraffin. Sections of 2-4 µm were prepared and immunostained with P21 to indicate senescent cells in the tumors of A549. The black scale bars represent 50 µm. **(B)** Quantification of P21 immunostaining. **(C)** Transcriptomic analysis of CD95 (FAS) in A549 cells treated for 1 week with 0.5 µM alisertib. **(D)** Dose-response curves in 0.5 µM alisertib-induced senescent A549 and SK-Hep1 cells treated with CD95 ligand (FASLG). **(E)** Senescence associated beta-galactosidase staining on A549 cells cultured in the presence of conditioned medium from senescent or proliferating control cells for one week. 0.5 µM Alisertib-induced senescent cells were used as staining control. The black scale bars represent 100 µm. **(F-G)** SASP medium was collected from the alisertib-induced senescent cells and mixed with an equal volume fresh medium. Ctrl medium was collected from proliferating cells and mixed with an equal volume fresh medium. Afterwards, The SASP medium or Ctrl medium were added to

new proliferating A549 (**F**) and SK-Hep (**G**) cells and treated with NEO2734 and Conatumumab. (**H**) Cell viability accessed by colony formation of SASP medium cultured A549 cells treated with the combination of 0.25 μM NEO2734 plus 4 μg/ml conatumumab and 10 μM Z-VAD-FMK. Error bars in this figure represent the mean ± standard deviations from biological triplicates ($*$ P≤0.05, $**$ P≤0.01, $***$ P≤0.001, two-tailed t-test).
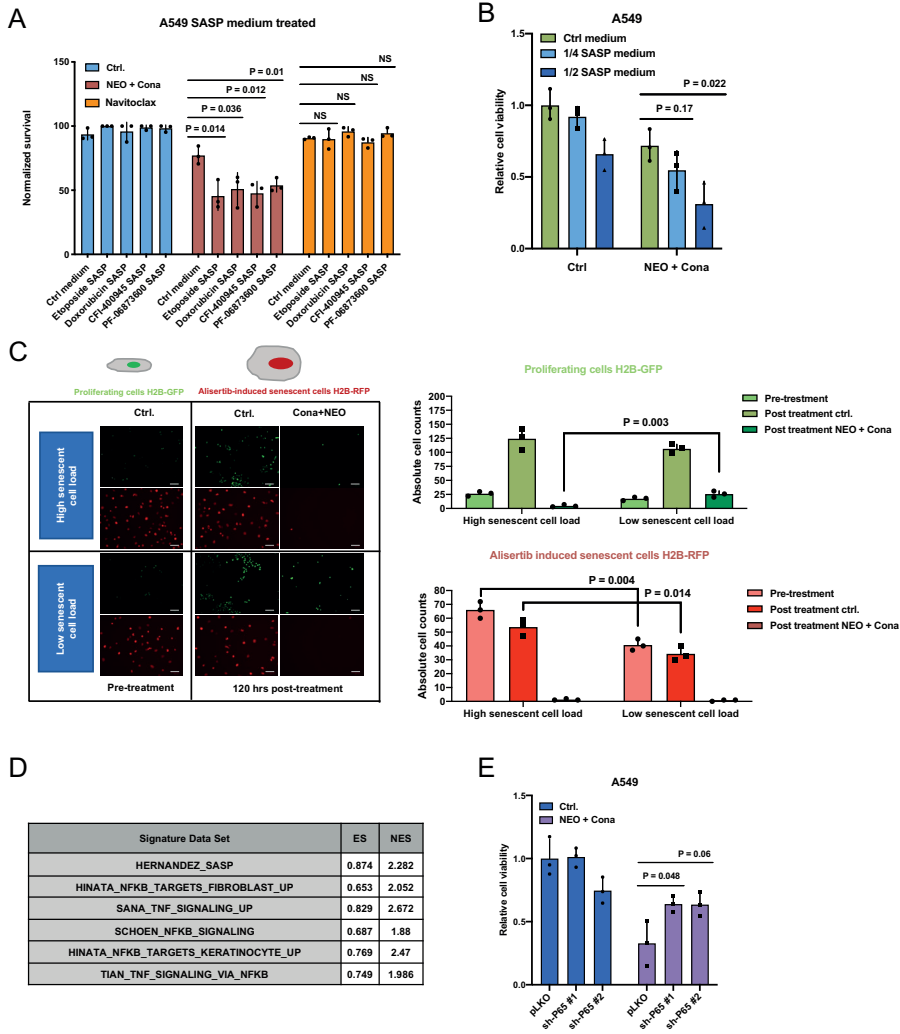
Figure S10. SASP-mediated bystander effect with BRD inhibitor and DR5 agonist combination is regulated by NF-kB signaling. **(A)** The proliferating A549 cells were cultured with SASP medium from different treatment-induced senescent A549 cells and treated with a combination of 0.25 μM NEO2734 plus 4 μg/ml conatumumab or 1 μM navitoclax. **(B)** A549 cells were cultured with different concentrations of SASP media and treated with the combination of 0.25 μM NEO2734 plus 4 μg/ml conatumumab. **(C)** *in vitro* competition assay, to study the bystander effect of conatumumab plus NEO2734 in a heterogeneous population containing proliferating and senescent cells. GFP and RFP cells were generated through infection with a lentiviral vector encoding H2B-GFP and H2B-RFP. RFP labelled cells were induced to senescence by one week of 0.5 μM alisertib treatment. GFP labelled cells were used as proliferating cells. Different ratios of GFP and RFP cells were initially mixed and treated with the drug combination. The grey scale bars represent 100 μm. **(D)** RNA sequencing was performed on A549 cells cultured with SASP medium for 1 week and followed by gene set enrichment analysis (GSEA) of SASP medium cultured cells versus ctrl medium cultured cells for multiple independent NF-KB signalling gene sets. **(E)** P65 knockdown A549 cells were cultured with SASP medium and treated with 0.25 μM NEO2734 plus 4 μg/ml conatumumab. Error bars in this figure represent the mean ± standard deviations from biological triplicates (* P≤0.05, ** P≤0.01, *** P≤0.001, two-tailed t-test).

Supplemetary table

Table s1. shRNA sequences for shRNAs against P65, TRAIL, DR5, DR4, FADD, BRD2, BRD4, and cFLIP.

Name	Full Sequence	Oligo ID
sh-P65 #2	CCGGCGGATTGAGGAGAAACGTAAACTCGAGTTTACGTTTCTCCTCAATC-CGTTTTT	TRCN0000014684
sh-P65 #3	CCGGGCAGGCTATCAGTCAGCGCATCTCGAGATGCGCTGACTGATAGCCT-GCTTTTT	TRCN0000014685
shTRAIL #29	CCGGGCAGTCTCATTTGCACCCATACTCGAGTATGGGTGCAAATGAGACT-GCTTTTT	TRCN0000005929
shTRAIL #30	CCGGCCACAAAGAATCAGGTACAAACTCGAGTTTGTACCTGATTCTTTGTG-GTTTTT	TRCN0000005930
shDR5 #1	CCGGGCAGTCTCATTTGCACCCATACTCGAGTATGGGTGCAAATGAGACT-GCTTTTT	TRCN0000005929
shDR5 #2	CCGGCCACAAAGAATCAGGTACAAACTCGAGTTTGTACCTGATTCTTTGTG-GTTTTT	TRCN0000005930
shDR4 #1	CCGGCTTAGGTGTTAGGAGTTAATACTCGAGTATTAACTCCTAACACCTAAGT-TTTT	TRCN0000005934
shDR4 #2	CCGGGCACACAGCAATGGGAACATACTCGAGTATGTTCCCATTGCTGTGT-GCTTTTT	TRCN0000005935
shFADD #1	CCGGGCTGACCTGGTACAAGAGGTTCTCGAGAACCTCTTGTACCAGGT-CAGCTTTTTG	TRCN0000332993
shFADD #3	CCGGCATGGAACTCAGACGCATCTACTCGAGTAGATGCGTCTGAGTTCCAT-GTTTTTG	TRCN0000332994
shFADD #4	CCGGGTGCAGCATTTAACGTCATATCTCGAGATATGACGTTAAATGCTGCACT-TTTTG	TRCN0000332992
shBRD2 #1	CCGGGCCCTCTTTACGTGATTCAAACTCGAGTTTGAATCACGTAAAGAGG-GCTTTTT	TRCN0000006309
shBRD2 #2	CCGGCCCTGCCTACAGGTTATGATTCTCGAGAATCATAACCTGTAGGCAGG-GTTTTT	TRCN0000006310
shBRD4 #1	CCGGCCTGGAGATGACATAGTCTTACTCGAGTAAGACTATGTCATCTCCAG-GTTTTTG	TRCN0000318771
shBRD4 #2	CCGGCCCTTTGCTGTGACACTTCTTCTCGAGAAGAAGTGTCACAGCAAAGG-GTTTTT	TRCN0000006308
sh-CFLIP#1	CCGGCCTCACCTTGTTTCGGACTATCTCGAGATAGTCCGAAACAAGGTGAG-GTTTTT	TRCN0000007229
sh-CFLIP#1	CCGGCACTCTGAGAAAGAAACTTATCTCGAGATAAGTTTCTTTCTCAGAGT-GTTTTT	TRCN0000007232

6

CHAPTER 7

General Discussion

General discussion

Cellular senescence and apoptosis are considered protective mechanisms against cancer transformation. Cancer develops in a multi-step process in which cells evade senescence and apoptosis through the accumulation of DNA mutations. However, even after this evasion, cancer cells can still be tricked back into senescence and apoptosis by chemo or targeted therapies. The senescent state is characterized by alterations in morphology, metabolism, gene expression, and anti-apoptotic dependency. The latter can be exploited by senolytic agents, which can activate apoptosis in senescent cells specifically. Most studies have focused on the characterization and elimination of normal senescent cells since these are associated with various age-related diseases and their removal increases longevity in mice. Still, the heterogeneity of the senescent phenotype forms a major challenge for its unequivocal detection, and not a standalone marker, but rather a constellation of features is required to define senescence. As cancer cells harbor mutations in cell cycle and apoptosis pathways, it is likely that senescence-induction, senescence hallmarks, as well as vulnerabilities of senescent cancer cells differ from that of normal cells.

   This thesis focused on how senescence can be induced in tumor cells, finding common hallmarks and vulnerabilities of senescent cancer cells, and ways to eliminate them. This with the overall aim to treat cancer cells using a one-two punch strategy: by first inducing senescence in tumor cells with potent senescence-inducers or (chemotherapeutic) anti-cancer treatment, followed by a senolytic treatment that removes the (remaining) senescent cancer cells.

Unmasking the senescence phenotype in senescent cancer cells

Most senescence triggers and hallmarks of senescence discussed in **chapter 1** derive from studies performed in non-cancer cells. An important aspect in the development of one-two punch treatment strategies is the efficiency and selectivity of the first punch to induce senescence in tumor cells. Moreover, upon treatment with senescence-inducing therapies, it will be essential to monitor senescence-induction in tumors to determine the timing and efficacy of senolytic therapies. Other aspects that influence one-two punch therapy are the features of senescent cancer cells, their diversity across cancer types and senescence triggers, and their effect on the tumor microenvironment.

The role of autophagy in cancer cell senescence

The aim of **chapter 2** was to find ways to induce senescence specifically in cancer but not in normal cells. Earlier work from our laboratory showed that it was possible to find senescence inducers through screening with focused CRISPR libraries, using FACS-based screening with a miR-146a senescence reporter (Wang et al., 2017). However, as senescent cells are depleted from the cell population over time, it would be cumbersome to sort enough cells to cover a genome-wide CRISPR library. Therefore, a suicide switch was engineered **in chapter 2** that depletes proliferating cells through the expression of an inducible caspase 9 (Straathof et al., 2005) under the Ki-67 promoter. This screen identified various macroautophagy-related genes. These hits could have been unrelated to senescence because inhibition of macroautophagy causes the stabilization of GATA4 and subsequent expression of miR-146a (Kang et al., 2015). Nevertheless, the genetic and pharmacological inhibition of macroautophagy through ULK-1 inhibitors efficiently induced senescence in lung, liver, pancreatic, and colon cancer cells, while leaving untransformed fibroblasts unaffected.

The process of autophagy is essential for the turnover of cellular components, and consists of three different types: macroautophagy, which degrades organelles and proteins, hereafter referred to as autophagy; microautophagy, which involves the direct engulfment of cytosolic material into the lysosomes; and chaperone-mediated autophagy. In this process, targets are enclosed by double membranes derived from ER, mitochondria, or Golgi, to form the autophagosome. After that, the autophagosome is fused with lysosomes and its content is degraded and molecules are recycled (Feng et al., 2014). Autophagy can be activated upon various stress conditions, like lack of nutrition, reactive oxygen species, or hypoxia (Poillet-Perez et al., 2015). The initiation of autophagy is regulated through the activation of AMPK or the inhibition of mTOR, which activates the ULK complex, consisting of ULK-1, ATG13, ATG101, and FIP200. This complex regulates autophagosome formation.

The role of autophagy in senescence and cancer has been heavily debated (Kang and Elledge, 2016; Kwon et al., 2017; Patel et al., 2021). On the one hand, autophagy has been described to mediate senescence. For instance, the knock-down of key autophagy genes delays the onset of oncogene-induced senescence, and overexpression of ULK3 induces autophagy and senescence (Young et al., 2009). Especially the 'TOR-autophagy spatial coupling compartment (TASCC)' seemed to be important for recycling components for IL-6 and IL-8 production (Narita et al., 2011), and knock-down of ATG5 prevented OIS in melanoma cells (Liu et al., 2013). Furthermore, the senolytics Ouabain and chloroquine have been described to kill BRAF-senescent cells through the inhibition of autophagy (L'Hôte et al., 2021). Additionally, it has been suggested that autophagy plays a role in the nucleus-to-cytoplasm transport of lamin B1, resulting in lysosomal degradation and loss of

7

lamin-associated-domains (LADs) containing damaged DNA (Dou et al., 2015).

On the other hand, pharmacological or genetic inhibition of autophagy did not influence senescence-induction in combination with DNA-damaging agents in lung, breast, and colorectal cancer cell lines (Saleh et al., 2020a). This indicates that autophagy is not required for senescent cancer cells. This is in line with the idea that senescent cells have dysfunctional lysosomes and impaired autophagy, leading to accumulation of components like SA-ß-gal (Wiley and Campisi, 2021). In fact, the pharmacological inhibition of autophagy in cancer cells can lead to the accumulation of dysfunctional proteins and organelles, like depolarized mitochondria, leading to the induction of senescence. This is also seen in stellate cells (García-Prat et al., 2016) and primary fibroblasts (Kang et al., 2015, 2011). Moreover, restoring the autophagic flux by AMPK activation or mTOR inhibition can prevent oxidative-stress induced senescence (Han et al., 2016; Nopparat et al., 2017; Tai et al., 2017), BET family degraders senolyse senescent HCT116 and fibroblast cells through the upregulation of autophagy (Wakita et al., 2020), and the suppression of mTOR by Sertraline or AZD8055 had a senolytic effect in *TP53* mutant liver cancer cells induced to senescence with a CDC7 inhibitor (Wang et al., 2019).

Overall, discrepancies regarding the role of autophagy in senescent cells probably result from the use of different cell and senescence models. There seems to be a particular difference between normal and cancer cells, as autophagy is considered a survival mechanism to sustain high proliferation rates and increased energy demands of cancer cells (Bhutia et al., 2015). Oncogenic signaling often results in increased autophagy in cancer, and inhibiting this process likely affects cancer cells more than normal cells. This corroborates the findings reported in **chapter 2** that inhibition of autophagy with ULK-1 inhibitors elicits senescence in cancer cells specifically. Moreover, the suicide switch system used here can also be a valuable tool for enriching any growth-arrested phenotypes, like quiescence, drug-tolerant persister phenotypes, dormancy, or terminal differentiation.

The search for biomarkers of cancer cell senescence

The opposing roles of autophagy in senescent cells form an example of the variation in senescence features. Common characteristics of senescent cancer cells were sought in **chapter 3** to identify universal vulnerabilities and allow the unambiguous detection of cancer cell senescence. An important observation was that the SASP expression and the response to ABT-263 were more dependent on the intrinsic features of the cell line rather than the senescence trigger. Where the qualitative SASP mixture seems to be dependent on the epigenetic ability of cells to express specific cytokines, the quantitative SASP composition can still significantly differ between different senescence triggers. Nevertheless, other studies indicated both qualitative as well as quantitative differences between cells induced via different senescence

triggers (Basisty et al., 2020; Coppé et al., 2011; Hernandez-Segura et al., 2017; Hoare et al., 2016; Wang et al., 2022a). As SASP expression evolves over time (**chapter 3;** (Hernandez-Segura et al., 2017; Martínez-Zamudio et al., 2020)), quantitative and qualitative differences might arise from the fact that the onset of senescence for different triggers is not synchronized. Alternatively, the senescence-inducers used in **chapter 3** - alisertib, etoposide, doxorubicin and CDK2/4/6 inhibitor PF-06873600 - might trigger very similar (DNA-damage) responses that lead to qualitatively similar SASP in a particular cell line. Complicating these cell line-based studies is the finding that expression changes seen at a cell population level can be attributed to the elevated SASP expression of only a few cells in the population (Wiley et al., 2017). This raises the question whether these 'outperformer' cells are epigenetically pre-existing or rather stochastically formed during the senescence process. In light of therapeutically-induced senescence, it will be crucial to dissect what determines the SASP composition of senescent tumor cells and how this affects the tumor environment in each tumorous context. This is a challenging endeavor as the nature of the tumor cells, immune cells, senescence trigger, vasculature, and cell-to-cell heterogeneity influence these effects. With this knowledge, the use of so-called senomorphic drugs could be applied to modify SASP expression and counteract the pro-tumorigenic effects of senescent tumor cells (Schmitt et al., 2022).

Besides the variation in SASP expression, **chapter 3** shows that protein markers of senescence (RB phosphorylation, P53, P53 phosphorylation, P21, P16, γH2AX, and lamin B1) strongly varied between different cell lines. Notably, after SA-β-gal positivity, growth arrest, and morphology change, a reduction of lamin B1 on protein and RNA level was observed in multiple senescent cancer cells. Even though the regulation of lamin B1 in senescence has been attributed to elevated autophagy of the senescent state (Dou et al., 2015), senescence-induction through knock-out of genes involved in autophagosome formation still reduced lamin B1 protein levels (**chapter 2**). This indicates that the loss of lamin B1 in senescent cells might be regulated through an alternative mechanism.

Intriguingly, a recent study showed that nuclear proteins, including HMGB1 and lamin B1, sub-scale with cell size and were diluted in larger non-senescent cells, while lysosomal proteins, like ß-galactosidase, super-scaled (Lanz et al., 2022). As the presence of SA-ß-galactosidase and the loss of lamin B1 are not required for the senescence phenotype (Dreesen et al., 2013; Lee et al., 2006), it is possible that various markers of senescence are the result of the enlarged morphology of senescent cells. This can be caused by an inconsistent change in protein/RNA concentration of specific proteins compared to the total protein/RNA concentrations. This phenomenon is especially important in mechanistic studies that compare senescent versus non-senescent cells in which total protein/RNA levels are used for normalization. For qPCR studies, the use of stable senescence-associated reference

7

genes has already been recognized (Hernandez-Segura et al., 2019). The increased cell size of senescent cells also influences the read-out of other cellular assays measuring protein abundance, like fluorescence microscopy and flowcytometry. In **chapter 4** for instance is shown that the mitochondrial load measured by flowcytometry is increased in senescent cells, but it will remain challenging to understand the biological consequence of having more mitochondrial proteins per cell (Lanz et al., 2022), as the relative abundance of proteins per mitochondrial unit might still be constant.

Nevertheless, to find unambiguous markers of senescence of cancer cells in **chapter 3**, transcriptome data from 13 cell lines derived from breast, colon, lung, and liver cancer in parental, alisertib-induced and etoposide-induced senescent state were subjected to machine learning. In this way, the SENCAN classifier was established, which indicates the probability that a specific sample is senescent through a 'senescence score'. The classifier as well as the transcriptome data is available on the interactive interface at https://ccb.nki.nl/publications/cancer-senescence/. Even though the classifier has been validated for *in vitro* use only, Salmerón-Bárcenas *et al.* used SENCAN to measure the difference in senescence score of patient samples from cervical cancer with low versus high EZH2 expression (Salmerón-Bárcenas et al., 2022). Another study combined the SENCAN gene set together with 16 other aging-associated expression patterns to establish a list of 1535 genes associated with aging, used for single-cell RNA-seq analysis. They revealed that this aging-associated gene set was enriched in samples from colon, liver, lung, pancreas, and blood cancers compared to healthy tissues (Saul and Kosinsky, 2021). After that, this research group built the SenMayo gene set, which encompasses 125 genes curated from literature. They describe that SenMayo identifies senescence in various tissues from aged mouse and human, and can detect the clearance of senescent cells in mice (Saul et al., 2022). They claim that this gene set outperforms gene sets from R-HSA-2559582 (National Center for Biotechnology Information, 2004), Casella (Casella et al., 2019), Hernandez (Hernandez-Segura et al., 2019), Purcell (Purcell et al., 2014), Fridman (Fridman and Tainsky, 2008), and SENCAN. Nevertheless, as the gene coefficient effects in the SENCAN classifier are lost when the gene set is used in a gene set enrichment analysis (GSEA), it is problematic to directly compare gene sets from classifiers with GSEA gene sets.

In conclusion, the hallmarks of senescent cancer cells seem to be influenced by the cell origin and less by the (DNA-damage) inducing trigger. The Cancer SENESCopedia webtool and the SENCAN classifier will contribute to future studies in understanding and detecting cancer cell senescence.

Activating intrinsic and extrinsic apoptosis in senescent cancer cells

The second step in the one-two punch approach is killing of senescent cancer cells that arise from the first punch. Where **chapter 3, 4,** and **5** studied the activation of intrinsic apoptosis with ABT-263, **chapter 6** focused on stimulating extrinsic apoptosis with DR5 agonists. In depth understanding why cells respond differently to both senolytic strategies will help in the design of better treatments, as well as the discovery of biomarkers for response.

Response and resistance to intrinsic apoptosis activator ABT-263
The variable senolytic response to ABT-263 shown in **chapter 3** was not readily explained by protein levels of BCL-2 family members, nor the gene expression in parental or senescent cells. This can be attributed to the post-translational regulation of BCL-2 proteins, which not only depends on protein abundance but also on the variability in protein binding affinity, localization, and post-translational modifications (Kale et al., 2017). For this reason, BH3 profiling was applied in **chapter 4** to measure the apoptotic priming and anti-apoptotic dependencies of senescent and parental cells. This functional assay showed that the overall apoptotic priming, measured by BIM, and the overall apoptotic dependency, measured by PUMA, correlated to ABT-263 sensitivity of senescent cells. Interestingly, cells that were resistant to ABT-263 in parental state and only sensitize upon senescence induction, responded to BIM and PUMA already in the parental state. This was in line with the observation in **chapter 3** that the (SASP) gene expression and ABT-263 response of senescent cells was dictated by the parental cells. Nevertheless, another -rather counterintuitive- result from this chapter was that (ABT-263 sensitive) senescent cells showed a lower apoptotic priming than their (ABT-263 resistant) parental counterparts. This was also observed in cells that remained refractory in senescence.

   This finding that (ABT-263 sensitive) senescent cells were less primed than their parental (ABT-263 resistant) counterparts was counterintuitive because various studies showed that increased BIM priming was predictive for the response to ABT-263 and other BH3 mimetics (Deng et al., 2007; Letai, 2022). Another observation that was difficult to explain was that the mitochondrial response to ABT-263 and BAD peptide, both targeting BCL-XL, BCL-2, and BCL-W, did not correlate to their cellular response to ABT-263. This mismatch between the mitochondrial and cellular response was only seen in senescent but not in parental cells. Some technical reasons have been explored in chapter 4, but other insights in the regulation of apoptosis and BH3 profiling might explain why senescent cells are less primed to BIM compared to their parental counterparts.

   Various studies indicated that the sensitivity to ABT-263 of senescent cells is

7

mainly attributed to the activity of BCL-XL (Gayle et al., 2019; Saleh et al., 2020b; Shahbandi et al., 2020). BCL-XL is a protein that executes its function through its binding with activator and effector proteins via two modes: 'MODE 1' is active in cells with low stress levels, in which BCL-XL predominantly sequesters activator proteins BIM and BID. 'MODE 2' occurs in cells with elevated stress levels, in which BCL-XL binds with effector proteins BAK and BAX, preventing mitochondrial fusion (Llambi et al., 2011). MODE 1 is more easily disturbed than MODE 2, partly because BAX is sequestered by BCL-XL from the mitochondrial membrane to the cytosol, preventing the activation of MOMP (Edlich et al., 2011; Todt et al., 2015). Another way in which BAX can be inhibited is via Ser184 phosphorylation by AKT, which also results in the translocation to the cytosol and enhanced interaction with anti-apoptotic proteins (Gardai et al., 2004).

Recently, it has been shown that the ability of BH3 profiling to assess the inactive phosphorylated form of BAX is hindered by the loss of post-translational modifications (PTMs) during profiling (Kale et al., 2018). Moreover, as the cellular membrane is permeabilized, cytosolic components that are not anchored in the mitochondrial membrane are lost upon BH3 profiling. The loss of PTMs and cytosolic components might explain mismatches between cellular and mitochondrial (BH3 profiling) assays. It is likely that MODE 2 is active in senescent cells, as they endure severe stress. This interaction is predominantly driven by BCL-XL binding to BAX, since BAX but not BAK seems to be essential for ABT-263 killing. This is based on resistance screen hits in **chapter 5** and work of others (Saleh et al., 2020b).

Taken together, the following model could explain the BH3 profiling results and the underlying biological process (**Figure 1**): in the cellular setting, senescent cells activate MODE 2 in which BCL-XL translocates BAX to the cytosol. BCL-XL can be displaced by ABT-263, leading to activation of BAX to induce MOMP. This is different in the mitochondrial setting, as BCL-XL:BAX complexes will exit the cell through the permeabilized cellular membrane. This subsequently reduces the number of active BAX available on the mitochondrial membrane, which decreases the response to BIM peptide in senescent cells. Moreover, ABT-263 cannot act on BCL-XL:BAX complexes anymore in the mitochondrial setting, reducing the ability of this BH3 mimetic to induce MOMP. This explains the reduced priming to all peptides and BH3 mimetics in senescent cells.

However, another additional mechanism might play a role in the parental cells that explains why parental cells show high responses to ABT-263 in the mitochondrial but not the cellular setting. It might be possible that in the parental state, BAX is rendered inactive through phosphorylation, leading to sequestration to the cytosol. When this PTM is lost during profiling, BAX has the natural tendency to reside at the mitochondrial membrane. This results in an increased mitochondrial abundance of BAX protein, which can be readily activated by BIM peptides. Moreover, as parental

cells are not considered highly stressed, BCL-XL predominantly binds to BIM and BID, leading to a high response to ABT-263 in the mitochondrial setting. At the same time, these cells show a low response to ABT-263 in the cellular setting because of BAX phosphorylation.
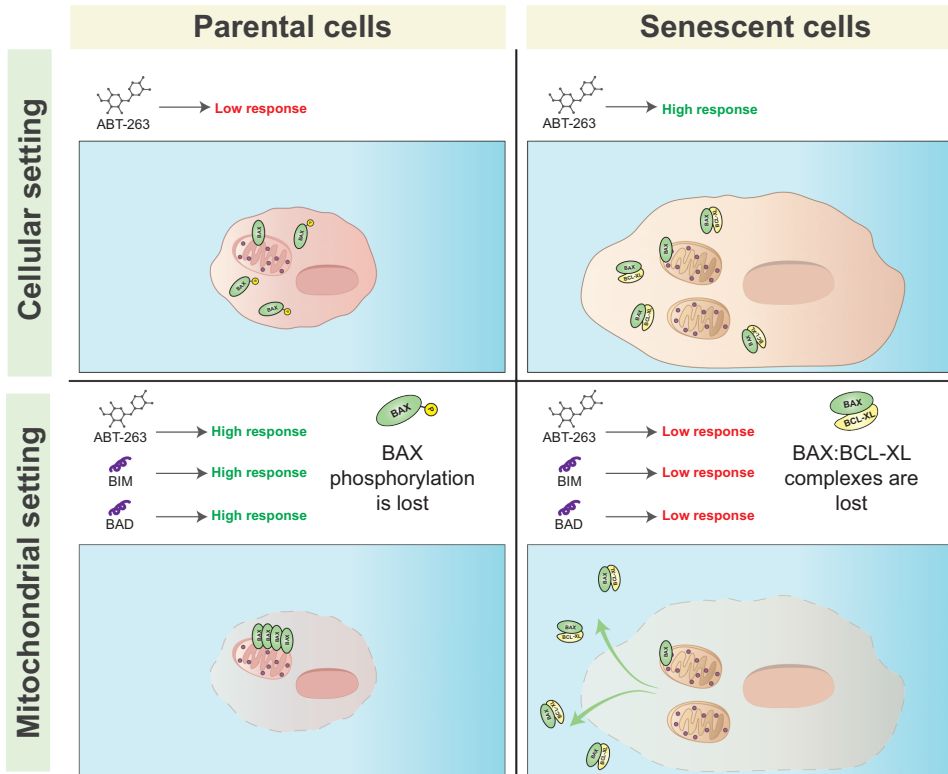

Figure 1. Model explaining the BH3 profiling results in senescent cells. In the cellular setting, parental cells show a low response to ABT-263, while ABT-263 sensitive cells show a high response. In the mitochondrial setting, cells are permeabilized and challenged with BH3 peptides and mimetics. As a result, post-translational modifications are lost and cytoplasmic content is released to the external environment because of cellular membrane permeabilization with digitonin. Surprisingly, the mitochondrial and cellular responses were contradicting each other. In the mitochondrial setting, ABT-263, BAD, and BIM triggered a high response in the parental cells and a low response in the senescent cells, while in the cellular setting this was the opposite. Two explanations could explain this mismatch: (i) BAX is phosphorylated in the parental cells and BAX phosphorylation is lost upon BH3 profiling. The loss of phosphorylation allows BAX to reside at the mitochondrial membrane and form pores upon stimulation with BIM, BAD, and ABT-263. (ii) BCL-XL binds to BAX in the senescent state and sequesters BAX to the cytosol. Upon membrane permeabilization, BCL-XL:BAX complexes diffuse out of the cell. This results in the loss of BAX, and cell remain unresponsive to ABT-263, BIM, and BAD.

7

Future research is required to determine whether ABT-263 indeed predominantly disturbs BAX:BCL-XL complexes in senescent cells and whether the loss of these complexes encumbers the functioning of BH3 profiling. Moreover, it is yet to be observed whether BAX phosphorylation plays a role in the parental state and how this phosphorylation occurs and is lost in the senescent state. Multiple observations from this thesis support the role of BAX phosphorylation by AKT in parental cells: (i) senescence-induction with etoposide and alisertib leads to reduction of the mTORC1 signaling signature in **chapter 3**. As mTORC1 is downstream of AKT, it might be possible that AKT signaling is lower in senescent than in parental cells; (ii) alisertib is known to inhibit the AKT/mTOR pathway (Fu et al., 2016), which might explain the loss of AKT signaling in alisertib-induced senescent cells; (iii) the ABT-263 resistance screen in senescent cells from **chapter 5** yielded multiple hits involved in inhibiting AKT/mTOR signaling. And besides BAX phosphorylation, AKT/mTOR signaling can also increase the expression of MCL-1.

Interestingly, both in **chapter 4** and **chapter 5,** MCL-1 came out as the main determinant of resistance to ABT-263. In **chapter 4,** dynamic BH3 profiling showed that ABT-263 semi-sensitive senescent cells were less responsive to MCL-1 antagonism, probably caused by the upregulation of MCL-1 protein seen in semi-sensitive cell lines. In **chapter 5,** hits from the ABT-263 resistance screen in senescent cells negatively regulate MCL-1 expression: RACK1, VHL and ARID2A, which negatively regulate the AKT/mTOR pathway, and NOXA/MULE, involved in the degradation of MCL-1. Together these results suggest that the main contributor to ABT-263 resistance in senescent cells is MCL-1 activity, and that inhibition of all anti-apoptotic proteins is required to induce apoptosis.

This idea that you need to neutralize all the (key) anti-apoptotic protein components of a cell in order to induce apoptosis corroborates other recent studies that contradict 'the direct activation model' for BAX and BAK activation. This model states that BH3-only proteins can be divided into sensitizer and activator proteins (Letai et al., 2002). However, studies form the Luo lab show that cells lacking all BH3-only proteins were resistant to apoptotic stimuli, but sensitive to BCL-XL and MCL-1 inhibition. They also showed that exogenous BAX/BAK could autoactivate themselves in the absence of anti-apoptotic proteins and their endogenous counterparts (O'neill et al., 2016). In a follow-up study, they showed that reconstitution of BH3-only proteins could not accelerate BAX/BAK activation after deletion of all the anti-apoptotic proteins. This suggests that BH3-only proteins, including BIM and BID, only have a sensitizer rather than an activator role, in which they displace anti-apoptotic BCL-2 proteins from BAX/BAK, leading to apoptosis (Huang et al., 2019). Nevertheless, it will be important to study this biological principle in other (non-cancer) cells as well, as these studies were performed in HCT116 only.

To exploit this knowledge therapeutically, it will be important to find drug

combinations that disrupt the activity of anti-apoptotic proteins in senescent cancer cells. The challenging part will be to find a therapeutic window, as normal cells are also sensitive to the neutralization of anti-apoptotic signaling. The lack of or inhibition of both MCL-1 and BCL-XL has shown to cause severe normal (liver) tissue toxicities and lethality in mice (Hikita et al., 2009; Khan et al., 2023; Weeden et al., 2018). Recently, a study in small-cell lung cancer cells circumvented the on-target toxicity of MCL-1 and platelet toxicity of ABT-263 through the combination of AZD8055 and DT2216 (Khan et al., 2023). AZD8055 downregulates MCL-1 by the inhibition of mTOR, and DT2216 is a platelet-sparing PROTAC targeting specifically BCL-XL for degradation. In this case, modulating upstream pathways that cause the activation of anti-apoptotic proteins can circumvent adverse effects and provide treatment opportunities for senescent cancer cells. When targeting anti-apoptotic proteins is not sufficient for the elimination of senescent cells through BAX inactivation, specific BAX activators exist that even showed synergy with ABT-263 in various cancer models resistant to ABT-263 (Lopez et al., 2022).

Activating extrinsic apoptosis to eliminate senescent cancer cells
As the utility of ABT-263 as a senolytic was context dependent (**chapter 3**), the search for a superior senolytic treatment strategy was performed in **chapter 6** through functional genetic drop-out screens in senescent cells. These identified that senescent cancer cells were vulnerable to the loss of c-FLIP, an anti-apoptotic protein inhibiting extrinsic apoptosis signaling. Activation of extrinsic apoptosis with a DR5 agonist or TRAIL could induce apoptosis in senescent cells at lower doses than proliferating cells. This selective sensitivity is readily explained by the increased expression of DR5 receptor and TRAIL, concomitant with increased cFLIP levels. This also creates a bystander effect, in which TRAIL produced by senescent cells also induced killing of non-senescent cancer cells upon DR5 agonist treatment.

The senolytic effect of DR5 agonist Conatumumab is even seen in cell lines that are resistant to ABT-263. For instance, *BAX* mutant HCT116 and LoVo cells are sensitive to DR5 stimulation (**chapter 6**), while cells are resistant to ABT-263 (**chapter 3**). The advantage of stimulating DR5 signaling is that in BAX-deficient cells, BAK or even tBID can permeabilize the mitochondrial outer membrane (Flores-romero et al., 2022; Gillissen et al., 2010). Nevertheless, BCL-XL activity has been described as a resistance mechanism against TRAIL-induced apoptosis (Kim et al., 2003; Manzari et al., 2019). It is therefore interesting that senescent cells are more sensitive to DR5 stimulation, as BCL-XL activity is described to be upregulated in senescent cells (Gayle et al., 2019; Saleh et al., 2020b; Shahbandi et al., 2020). This might be related to the model described above, where BCL-XL might predominantly inhibit BAX rather than BAK. Moreover, the findings in **chapter 6** corroborates a study in alisertib-induced senescent melanoma models that are sensitive to TRAIL and DR5 agonistic

7

antibodies (Liu et al., 2015). This further highlights that DR5 agonists have broad specificity potential for one-two punch therapies in various cancer types.

Nevertheless, another paper showed that TRAIL had a variable senolytic activity, as doxorubicin-induced senescent MDA-MB-231 and MCF7 cells did not show senolytic killing by TRAIL. The authors attribute the lack of response to the *CASP3* mutation in MCF7 and the expression of decoy receptors DcR1, DcR2, and OPG in MDA-MB-231. Yet, the senolytic effect was restored by the use of a DR5-selective TRAIL variant (Soto-gamez et al., 2019). In **chapter 6** is shown that alisertib-induced senescent MCF7 and MDA-MB-231 respond to DR5 agonist conatumumab, which is line with the observation that DR5 specific agonists circumvent the inhibitory effects of decoy receptors.

Multiple agents are currently in clinical development that target DR5 signaling. Examples of TRAIL ligands are SCB-313 (NCT-3443674), AMG 951 (NCT00508625), dulanermin (NCT00400764, NCT00873756), ABBV-621 (NCT03082209), recombinant human Apo-2 ligand (NCT03083743), and TRAIL-expressing mesenchymal stem cells (NCT03298763). Examples of DR5 agonists are conatumumab/AMG 655 (NCT01940172, NCT00630786, NCT01327612, NCT00630552, NCT00626704), DS-8273a (NCT02991196), and CS-1008 (NCT01033240, NCT00945191). The well-tolerated and safe toxicity profile enables the usage of DR5 activating agents in various drug combination clinical trials, but all with limited treatment efficacy (Deng and Shah, 2020). Conatumumab was also used in combination with various chemotherapies without signs of toxicity, but largely lacking improved therapeutic potential. Conatumumab has been combined with: doxorubicin (Demetri et al., 2012) (NCT00626704), paclitaxel plus carboplatin (Paz-Ares et al., 2013) (NCT00534027), a cocktail of mFOLFOX6 (oxaliplatin, folinic acid, 5-FU, and 5-FU 2) plus bevacizumab (Fuchs et al., 2013) (NCT00625651), FOLFIRI (folinic acid, fluorouracil and irinotecan) (Cohn et al., 2013) (NCT00813605). The only study that showed some evidence of increased survival was the combinatory treatment with the IGF1R antibody ganitumab. This was also the only study that showed (well-tolerated) neutropenia, anemia and thrombocytopenia. (Kindler et al., 2012) (NCT00630552). Moreover, a case-study of a relapsed Hodgkin lymphoma patient showed complete regression of disease after treatment with conatumumab combined with vorinostat (Skelton et al., 2020) (NCT00791011).

Resistance to TRAIL therapies have mostly been attributed to the short half-life of TRAIL (30-60 min) in the circulatory system, and various delivery methods have been adopted to prolong its half-life (Stuckey and Shah, 2013). Interestingly, the half-life of therapeutic antibodies is generally higher, with 13-19 days for conatumumab (Herbst et al., 2010). Other reasons for treatment resistance to TRAIL-based therapies are the overexpression of anti-apoptotic proteins XIAP, cFLIP, BCL-XL, BCL-2, and MCL-1, the lack of apoptosis core proteins FADD and caspase-8, lack of TRAIL expression in immune cells, and the hypoxic environment in tumors (Knoll et al., 2016; Lee et al.,

2014; Stuckey and Shah, 2013; Zhang and Fang, 2005). As senescent cells upregulate apoptosis signaling through activation of the DDR and NF-κB, the expression of anti-apoptotic protein cFLIP indicates that these cells survive through anti-apoptotic signaling and are more sensitive to apoptosis stimulation than non-senescent cells. Moreover, senescent cells express TRAIL in the tumor microenvironment that could compensate for the lack of TRAIL expression in immune cells, and SASP-induced vasculature might prevent hypoxia-induced TRAIL resistance. Future studies will be required to understand if the resistance mechanisms of cancer cells to TRAIL are circumvented by senescence-induction in the context of conatumumab treatment.

Conclusions and future perspectives

This thesis shows that the features of senescent cancer cells are unique and divergent between tissues. Consequently, the aftermath of senescent cancer cells in the tumor environment will be highly context dependent, which emphasizes the need of ablating these cells with a senolytic agent. This thesis demonstrates that senescent cells live on the edge of dying, and that neutralization of anti-apoptotic members in the intrinsic and extrinsic apoptosis pathway selectively kill senescent over non-senescent cancer cells. This therapeutic window can be exploited in future one-two-punch therapies.

The most challenging part of the first punch is to homogenously induce senescence in tumor but not in normal cells. As a senescence-inducing therapy generally induces lower cellular stress than an apoptosis-inducing trigger, this might increase the chance that therapy resistant cells arise. Perhaps, a first punch that predominantly induces apoptosis but leaves some senescent cells behind might be a better strategy. However, the paracrine reinforcement of the senescent phenotype could enhance senescence-induction in cells that did not respond to the senescence-inducing therapy. Moreover, recent studies from the Lowe and Serrano lab highlight the advantage of having senescent cells in the tumor environment. These studies show that alarmins, interferon signaling, and neoantigens produced by senescent cells can activate dendritic cells and antigen specific tumor-infiltrating CD8 T-cells. This creates a strong immunogenic environment that even provides protection against non-senescent tumor cells (Chen et al., 2023; Marin et al., 2022). As interferon signaling is generally increased in almost all senescent cancer cell lines tested in **chapter 3** (Chen et al., 2023), the senescence-induction of the first punch might be an important step in tumor control. And the question remains how many senescent cells are minimally needed to provoke these immunogenic effects.

This thesis also shows that the use of senolytics as a second punch increases treatment efficacy in preclinical models. Besides senolytics, treatments that boost

7

the immune system can also be considered. For instance, treatment with immune checkpoint inhibitors has been shown to eliminate senescent cancer cells (Brenner et al., 2020; Deng et al., 2018; Goel et al., 2017; Jerby-Arnon et al., 2018; Knudsen et al., 2021; Zhang et al., 2018). Alternatively, CAR-T cells engineered against uPAR induced senolytic killing in lung adenocarcinoma (Amor et al., 2020). And PD-L2 blockade in senescent cancer cells enhances its immune-mediated killing (Chaib et al., 2022). Nevertheless, it is important to emphasize here that the publication bias towards positive results fails to highlight the context-dependent efficacy of immune checkpoint inhibitors (Wang et al., 2022b). Similarly, the SENESCopedia data shows that uPAR and PD-L2 expression are only elevated in a few cell lines upon senescence. Therefore, senolytic agents targeting survival pathways may have broader utility compared to (targeted) immune therapies. Another important consideration is that most studies are performed in young mice, and it will be imperative to test one-two punch therapies in older mice as well. As the senolytics might have a rejuvenating effect on older patients, the combination with a pro-senescence therapy might cause higher toxicities in patients with compromised immunity and repair machineries.

Taken together, in the path forward it will be essential to better define senescent cancer cells in every tumor context at a single cell resolution. Novel techniques like single-cell spatial transcriptomics and proteomics are promising methods to elucidate the behavior of senescent cells and trace the effect of one-two punch therapies. Now that the scientific community has been woken up by senescent tumor cells, the coming decades will tell us how senescence can be exploited as a stepstone for the treatment of cancer.

7

References

Amor, C., Feucht, J., Leibold, J., Ho, Y.J., Zhu, C., Alonso-Curbelo, D., Mansilla-Soto, J., Boyer, J.A., Li, X., Giavridis, T., et al. (2020). Senolytic CAR T cells reverse senescence-associated pathologies. Nature https://doi.org/10.1038/s41586-020-2403-9.

Basisty, N., Kale, A., Jeon, O.H., Kuehnemann, C., Payne, T., Rao, C., Holtz, A., Shah, S., Sharma, V., Ferrucci, L., et al. (2020). A proteomic atlas of senescence-associated secretomes for aging biomarker development. PLoS Biol. *18*, e3000599. https://doi.org/10.1371/journal.pbio.3000599.

Bhutia, S.K., Mukhopadhyay, S., Sinha, N., Das, D.N., Panda, P.K., Patra, S.K., Maiti, T.K., Mandal, M., Paul, D., Wang, X.-Y., et al. (2015). Autophagy: Cancer's friend or foe? *118*, 61–95. https://doi.org/10.1016/B978-0-12-407173-5.00003-0.Autophagy.

Brenner, E., Schörg, B.F., Ahmetlić, F., Wieder, T., Hilke, F.J., Simon, N., Schroeder, C., Demidov, G., Riedel, T., Fehrenbacher, B., et al. (2020). Cancer immune control needs senescence induction by interferon-dependent cell cycle regulator pathways in tumours. Nat. Commun. https://doi.org/10.1038/s41467-020-14987-6.

Casella, G., Munk, R., Kim, K.M., Piao, Y., De, S., Abdelmohsen, K., and Gorospe, M. (2019). Transcriptome signature of cellular senescence. Nucleic Acids Res. *47*, 7294–7305. https://doi.org/10.1093/nar/gkz555.

Chaib, S., López-domínguez, J.A., Lalinde, M., Prats, N., Marin, I., Meyer, K., Muñoz, M.I., Aguilera, M., Attolini, C.S., Llanos, S., et al. (2022). The efficacy of chemotherapy is limited by intratumoural senescent cells that persist through the upregulation of PD-L2. BioRchiv https://doi.org/: https://doi.org/10.1101/2022.11.04.501681.

Chen, H.-A., Ho, Y.-J., Mezzadra, R., Adrover, J.M., Smolkin, R., Zhu, C., Woess, K., Bernstein, N., Schmitt, G., Fong, L., et al. (2023). Senescence Rewires Microenvironment Sensing to Facilitate Antitumor Immunity. Cancer Discov. *13*, 433–453. https://doi.org/10.1158/2159-8290.cd-22-0528.

Cohn, A.L., Tabernero, J., Maurel, J., Nowara, E., Sastre, J., Chuah, B.Y.S., Kopp, M. V., Sakaeva, D.D., Mitchell, E.P., Dubey, S., et al. (2013). A randomized, placebo-controlled phase 2 study of ganitumab or conatumumab in combination with FOLFIRI for second-line treatment of mutant KRAS metastatic colorectal cancer. Ann. Oncol. *24*, 1777–1785. https://doi.org/10.1093/annonc/mdt057.

Coppé, J.P., Rodier, F., Patil, C.K., Freund, A., Desprez, P.Y., and Campisi, J. (2011). Tumor suppressor and aging biomarker p16 INK4a induces cellular senescence without the associated inflammatory secretory phenotype. J. Biol. Chem. https://doi.org/10.1074/jbc.M111.257071.

Demetri, G.D., Le Cesne, A., Chawla, S.P., Brodowicz, T., Maki, R.G., Bach, B.A., Smethurst, D.P., Bray, S., Hei, Y.J., and Blay, J.Y. (2012). First-line treatment of metastatic or locally advanced unresectable soft tissue sarcomas with conatumumab in combination with doxorubicin or doxorubicin alone: A Phase I/II open-label and double-blind study. Eur. J. Cancer *48*, 547–563. https://doi.org/10.1016/j.ejca.2011.12.008.

Deng, D., and Shah, K. (2020). TRAIL of Hope Meeting Resistance in Cancer. Trends in Cancer *6*, 989–1001. https://doi.org/10.1016/j.trecan.2020.06.006.

Deng, J., Carlson, N., Takeyama, K., Dal Cin, P., Shipp, M., and Letai, A. (2007). BH3 Profiling Identifies Three Distinct Classes of Apoptotic Blocks to Predict Response to ABT-737 and Conventional Chemotherapeutic Agents. Cancer Cell *12*, 171–185. https://doi.org/10.1016/j.ccr.2007.07.001.

Deng, J., Wang, E.S., Jenkins, R.W., Li, S., Dries, R., Yates, K., Chhabra, S., Huang, W., Liu, H., Aref, A.R., et al. (2018). CDK4/6 inhibition augments antitumor immunity by enhancing T-cell activation. Cancer Discov. https://doi.org/10.1158/2159-8290.CD-17-0915.

Dou, Z., Xu, C., Donahue, G., Shimi, T., Pan, J.A., Zhu, J., Ivanov, A., Capell, B.C., Drake, A.M., Shah, P.P., et al. (2015). Autophagy mediates degradation of nuclear lamina. Nature *527*, 105–109. https://doi.org/10.1038/nature15548.

Dreesen, O., Ong, P.F., Chojnowski, A., and Colman, A. (2013). The contrasting roles of lamin B1 in cellular aging and human disease. Nucleus *4*, 283–290. https://doi.org/10.4161/nucl.25808.

Edlich, F., Banerjee, S., Suzuki, M., Cleland M, M., Arnoult, D., Wang, C., Neutzner, A., Tjandra, N., and Youle, R.J. (2011). BCL-XL retrotranslocates BAX from the mitochondria into the cytosol. Cell *145*, 104–116. https://doi.org/10.1016/j.cell.2011.02.034.Bcl-x.

Feng, Y., He, D., Yao, Z., and Klionsky, D.J. (2014). The machinery of macroautophagy. Cell Res. *24*, 24–41. https://doi.org/10.1038/cr.2013.168.

Flores-romero, H., Hohorst, L., John, M., Albert, M., King, L.E., Beckmann, L., Szabo, T., Hertlein, V., Luo, X., Villunger, A., et al. (2022). BCL- 2 -family

7

protein tBID can act as a BAX-like effector of apoptosis. 1–17. https://doi.org/10.15252/embj.2021108690.

Fridman, A.L., and Tainsky, M.A. (2008). Critical pathways in cellular senescence and immortalization revealed by gene expression profiling. Oncogene 27, 5975–5987. https://doi.org/10.1038/onc.2008.213.

Fu, Y., Zhang, Y., Gao, M., Quan, L., Gui, R., and Liu, J. (2016). Alisertib induces apoptosis and autophagy through targeting the AKT/mTOR/AMPK/p38 pathway in leukemic cells. Mol. Med. Rep. 14, 394–398. https://doi.org/10.3892/mmr.2016.5249.

Fuchs, C.S., Fakih, M., Schwartzberg, L., Cohn, A.L., Yee, L., Dreisbach, L., Kozloff, M.F., Hei, Y.J., Galimi, F., Pan, Y., et al. (2013). TRAIL receptor agonist conatumumab with modified FOLFOX6 plus bevacizumab for first-line treatment of metastatic colorectal cancer: A randomized phase 1b/2 trial. Cancer 119, 4290–4298. https://doi.org/10.1002/cncr.28353.

García-Prat, L., Martínez-Vicente, M., Perdiguero, E., Ortet, L., Rodríguez-Ubreva, J., Rebollo, E., Ruiz-Bonilla, V., Gutarra, S., Ballestar, E., Serrano, A.L., et al. (2016). Autophagy maintains stemness by preventing senescence. Nature 529, 37–42. https://doi.org/10.1038/nature16187.

Gardai, S.J., Hildeman, D.A., Frankel, S.K., Whitlock, B.B., Frasch, S.C., Borregaard, N., Marrack, P., Bratton, D.L., and Henson, P.M. (2004). Phosphorylation of Bax ser184 by Akt regulates its activity and apoptosis in neutrophils. J. Biol. Chem. 279, 21085–21095. https://doi.org/10.1074/jbc.M400063200.

Gayle, S.S., Sahni, J.M., Webb, B.M., Weber-Bonk, K.L., Shively, M.S., Spina, R., Bar, E.E., Summers, M.K., and Keri, R.A. (2019). Targeting BCL-xL improves the efficacy of bromodomain and extra-terminal protein inhibitors in triple-negative breast cancer by eliciting the death of senescent cells. J. Biol. Chem. 294, 875–886. https://doi.org/10.1074/jbc.RA118.004712.

Gillissen, B., Wendt, J., Richter, A., Richter, A., Müer, A., Overkamp, T., Gebhardt, N., Preissner, R., Belka, C., Dörken, B., et al. (2010). Endogenous Bak inhibitors Mcl-1 and Bcl-xL: Differential impact on TRAIL resistance in Bax-deficient carcinoma. J. Cell Biol. 188, 851–862. https://doi.org/10.1083/jcb.200912070.

Goel, S., DeCristo, M.J., Watt, A.C., BrinJones, H., Sceneay, J., Li, B.B., Khan, N., Ubellacker, J.M., Xie, S., Metzger-Filho, O., et al. (2017). CDK4/6 inhibition triggers anti-tumour immunity. Nature 548, 471–475. https://doi.org/10.1038/nature23465.

Han, X., Tai, H., Wang, X., Wang, Z., Zhou, J., Wei, X., Ding, Y., Gong, H., Mo, C., Zhang, J., et al. (2016). AMPK activation protects cells from oxidative stress-induced senescence via autophagic flux restoration and intracellular NAD+ elevation. Aging Cell 15, 416–427. https://doi.org/10.1111/acel.12446.

Herbst, R.S., Kurzrock, R., Hong, D.S., Valdivieso, M., Hsu, C.P., Goyal, L., Juan, G., Hwang, Y.C., Wong, S., Hill, J.S., et al. (2010). A first-in-human study of conatumumab in adult patients with advanced solid tumors. Clin. Cancer Res. 16, 5883–5891. https://doi.org/10.1158/1078-0432.CCR-10-0631.

Hernandez-Segura, A., de Jong, T. V., Melov, S., Guryev, V., Campisi, J., and Demaria, M. (2017). Unmasking Transcriptional Heterogeneity in Senescent Cells. Curr. Biol. 27, 2652–2660. https://doi.org/10.1016/j.cub.2017.07.033.

Hernandez-Segura, A., Rubingh, R., and Demaria, M. (2019). Identification of stable senescence-associated reference genes. Aging Cell 18, 1–6. https://doi.org/10.1111/acel.12911.

Hikita, H., Takehara, T., Shimizu, S., Kodama, T., Li, W., Miyagi, T., Hosui, A., Ishida, H., Ohkawa, K., Kanto, T., et al. (2009). MCL-1 and BCL-XL cooperatively maintain integrity of hepatocytes in developing and adult murine liver. Hepatology 50, 1217–1226. https://doi.org/10.1002/hep.23126.Mcl-1.

Hoare, M., Ito, Y., Kang, T.W., Weekes, M.P., Matheson, N.J., Patten, D.A., Shetty, S., Parry, A.J., Menon, S., Salama, R., et al. (2016). NOTCH1 mediates a switch between two distinct secretomes during senescence. Nat. Cell Biol. 18, 979–992. https://doi.org/10.1038/ncb3397.

Huang, K., O'Neill, K.L., Li, J., Zhou, W., Han, N., Pang, X., Wu, W., Struble, L., Borgstahl, G., Liu, Z., et al. (2019). BH3-only proteins target BCL-xL/MCL-1, not BAX/BAK, to initiate apoptosis. Cell Res. 29, 942–952. https://doi.org/10.1038/s41422-019-0231-y.

Jerby-Arnon, L., Shah, P., Cuoco, M.S., Rodman, C., Su, M.J., Melms, J.C., Leeson, R., Kanodia, A., Mei, S., Lin, J.R., et al. (2018). A Cancer Cell Program Promotes T Cell Exclusion and Resistance to Checkpoint Blockade. Cell https://doi.org/10.1016/j.cell.2018.09.006.

Kale, J., Osterlund, E.J., and Andrews, D.W. (2017). BCL-2 family proteins: changing partners in the dance towards death. Cell Death Differ. 25, 65–80. https://doi.org/10.1038/cdd.2017.186.

Kale, J., Kutuk, O., Brito, G.C., Andrews, T.S., Leber, B., Letai, A., and Andrews, D.W. (2018). Phosphorylation switches Bax from promoting to inhibiting apoptosis thereby increasing

drug resistance. EMBO Rep. *19*, 1–21. https://doi.org/10.15252/embr.201745235.

Kang, C., and Elledge, S.J. (2016). How autophagy both activates and inhibits cellular senescence. Autophagy *12*. https://doi.org/10.1080/15548627.2015.1121361.

Kang, C., Xu, Q., Martin, T.D., Li, M.Z., Demaria, M., Aron, L., Lu, T., Yankner, B.A., Campisi, J., and Elledge, S.J. (2015). The DNA damage response induces inflammation and senescence by inhibiting autophagy of GATA4. Science *349*, aaa5612. https://doi.org/10.1126/science.aaa5612.

Kang, H.T., Lee, K.B., Kim, S.Y., Choi, H.R., and Park, S.C. (2011). Autophagy impairment induces premature senescence in primary human fibroblasts. PLoS One *6*. https://doi.org/10.1371/journal.pone.0023367.

Khan, S., Kellish, P., Connis, N., Thummuri, D., Wiegand, J., Zhang, P., Zhang, X., Budamagunta, V., Hua, N., Yang, Y., et al. (2023). Co-targeting BCL-XL and MCL-1 with DT2216 and AZD8055 synergistically inhibit small-cell lung cancer growth without causing on-target toxicities in mice. Cell Death Discov. *9*, 1–10. https://doi.org/10.1038/s41420-022-01296-8.

Kim, I., Jung, Y., Noh, D., Song, Y., Choi, C., Oh, B., Masuda, E.S., and Jung, Y. (2003). Functional screening of genes suppressing TRAIL-induced apoptosis : distinct inhibitory activities of Bcl-X L and Bcl-2. 910–917. https://doi.org/10.1038/sj.bjc.6600795.

Kindler, H.L., Richards, D.A., Garbo, L.E., Garon, E.B., Stephenson, J.J., Rocha-Lima, C.M., Safran, H., Chan, D., Kocs, D.M., Galimi, F., et al. (2012). A randomized, placebo-controlled phase 2 study of ganitumab (AMG 479) or conatumumab (AMG 655) in combination with gemcitabine in patients with metastatic pancreatic cancer. Ann. Oncol. *23*, 2834–2842. https://doi.org/10.1093/annonc/mds142.

Knoll, G., Bittner, S., Kurz, M., Jantsch, J., and Ehrenschwender, M. (2016). Hypoxia regulates TRAIL sensitivity of colorectal cancer cells through mitochondrial autophagy. Oncotarget *7*, 41488–41504. https://doi.org/10.18632/oncotarget.9206.

Knudsen, E.S., Kumarasamy, V., Chung, S., Ruiz, A., Vail, P., Tzetzo, S., Wu, J., Nambiar, R., Sivinski, J., Chauhan, S.S., et al. (2021). Targeting dual signalling pathways in concert with immune checkpoints for the treatment of pancreatic cancer. Gut https://doi.org/10.1136/gutjnl-2020-321000.

Kwon, Y., Kim, J.W., Jeoung, J.A., Kim, M.S., and Kang, C. (2017). Autophagy is pro-senescence when seen in close-up, but anti-senescence in long-shot.

Mol. Cells *40*, 607–612. https://doi.org/10.14348/molcells.2017.0151.

L'Hôte, V., Courbeyrette, R., Pinna, G., Cintrat, J.C., Le Pavec, G., Delaunay-Moisan, A., Mann, C., and Thuret, J.Y. (2021). Ouabain and chloroquine trigger senolysis of BRAF-V600E-induced senescent cells by targeting autophagy. Aging Cell *20*, 1–14. https://doi.org/10.1111/acel.13447.

Lanz, M.C., Zatulovskiy, E., Swaffer, M.P., Zhang, L., Ilerten, I., Zhang, S., You, D.S., Marinov, G., McAlpine, P., Elias, J.E., et al. (2022). Increasing cell size remodels the proteome and promotes senescence. Mol. Cell *82*, 1–15. https://doi.org/10.1016/j.molcel.2022.07.017.

Lee, B.Y., Han, J.A., Im, J.S., Morrone, A., Johung, K., Goodwin, E.C., Kleijer, W.J., DiMaio, D., and Hwang, E.S. (2006). Senescence-associated β-galactosidase is lysosomal β-galactosidase. Aging Cell *5*, 187–195. https://doi.org/10.1111/j.1474-9726.2006.00199.x.

Lee, Y.J., Lee, J.H., Moon, J.H., and Park, S.Y. (2014). Overcoming hypoxic-resistance of tumor cells to TRAIL-induced apoptosis through melatonin. Int. J. Mol. Sci. *15*, 11941–11956. https://doi.org/10.3390/ijms150711941.

Letai, A. (2022). Apoptosis: Directly Targeted at Last. J. Clin. Oncol. *40*, 1693–1695. https://doi.org/10.1200/JCO.22.00304.

Letai, A., Bassik, M.C., Walensky, L.D., Sorcinelli, M.D., Weiler, S., and Korsmeyer, S.J. (2002). Distinct BH3 domains either sensitize or activate mitochondrial apoptosis, serving as prototype cancer therapeutics. Cancer Cell *2*, 183–192. https://doi.org/10.1016/S1535-6108(02)00127-7.

Liu, H., He, Z., Von Rütte, T., Yousefi, S., Hunger, R.E., and Simon, H.U. (2013). Down-regulation of autophagy-related protein 5 (ATG5) contributes to the pathogenesis of early-stage cutaneous melanoma. Sci. Transl. Med. *5*. https://doi.org/10.1126/scitranslmed.3005864.

Liu, Y., Hawkins, O.E., Vilgelm, A.E., Pawlikowski, J.S., Ecsedy, J.A., Sosman, J.A., Kelley, M.C., and Richmond, A. (2015). Combining an Aurora Kinase Inhibitor and a Death Receptor Ligand/Agonist Antibody Triggers Apoptosis in Melanoma Cells and Prevents Tumor Growth in Preclinical Mouse Models. Clin. Cancer Res. *21*, 5338–5348. https://doi.org/10.1016/j.gde.2016.03.011.

Llambi, F., Moldoveanu, T., Tait, S.W.G., Bouchier-Hayes, L., Temirov, J., McCormick, L.L., Dillon, C.P., and Green, D.R. (2011). A Unified Model of Mammalian BCL-2 Protein Family Interactions at the Mitochondria. Mol. Cell *44*, 517–531. https://doi.org/10.1016/j.molcel.2011.10.001.

Lopez, A., Reyna, D.E., Gitego, N., Kopp, F., Zhou,

7

H., Miranda-Roman, M.A., Nordstrøm, L.U., Narayanagari, S.R., Chi, P., Vilar, E., et al. (2022). Co-targeting of BAX and BCL-XL proteins broadly overcomes resistance to apoptosis in cancer. Nat. Commun. *13*. https://doi.org/10.1038/s41467-022-28741-7.

Manzari, M.T., Anderson, G.R., Lin, K.H., Soderquist, R.S., Çakir, M., Zhang, M., Moore, C.E., Skelton, R.N., Fèvre, M., Li, X., et al. (2019). Genomically informed small-molecule drugs overcome resistance to a sustained-release formulation of an engineered death receptor agonist in patient-derived tumor models. Sci. Adv. *5*. https://doi.org/10.1126/sciadv.aaw9162.

Marin, I., Boix, O., Garcia-Garijo, A., Sirois, I., Caballe, A., Zarzuela, E., Ruano, I., Stephan-Otto Attolini, C., Prats, N., Lopez-Dominguez, J.A., et al. (2022). Cellular senescence is immunogenic and promotes anti-tumor immunity. Cancer Discov. *148*. https://doi.org/10.1158/2159-8290.cd-22-0523.

Martínez-Zamudio, R.I., Roux, P.F., de Freitas, J.A.N.L.F., Robinson, L., Doré, G., Sun, B., Belenki, D., Milanovic, M., Herbig, U., Schmitt, C.A., et al. (2020). AP-1 imprints a reversible transcriptional programme of senescent cells. Nat. Cell Biol. *22*, 842–855. https://doi.org/10.1038/s41556-020-0529-5.

Narita, M., Young, A.R.J., Arakawa, S., Samarajiwa, S.A., Nakashima, T., Yoshida, S., Hong, S., Berry, L.S., Reichelt, S., Ferreira, M., et al. (2011). Spatial coupling of mTOR and autophagy augments secretory phenotypes. Science (80-.). *332*, 966–970. https://doi.org/10.1126/science.1205407.

National Center for Biotechnology Information, P. (2004). National Center for Biotechnology Information.PubChem Pathway Summary for Pathway R-HSA-2559582, Senescence-Associated Secretory Phenotype (SASP), Source: Reactome.

Nopparat, C., Sinjanakhom, P., and Govitrapong, P. (2017). Melatonin reverses H2O2-induced senescence in SH-SY5Y cells by enhancing autophagy via sirtuin 1 deacetylation of the RelA/p65 subunit of NF-κB. J. Pineal Res. *63*, 1–13. https://doi.org/10.1111/jpi.12407.

O'neill, K.L., Huang, K., Zhang, J., Chen, Y., and Luo, X. (2016). Inactivation of prosurvival Bcl-2 proteins activates Bax/Bak through the outer mitochondrial membrane. Genes Dev. *30*, 973–988. https://doi.org/10.1101/gad.276725.115.

Patel, N.H., Bloukh, S., Alwohosh, E., Alhesa, A., Saleh, T., and Gewirtz, D.A. (2021). Autophagy and senescence in cancer therapy (Elsevier Inc.).

Paz-Ares, L., Bálint, B., De Boer, R.H., Van Meerbeeck, J.P., Wierzbicki, R., De Souza, P., Galimi, F., Haddad, V., Sabin, T., Hei, Y.J., et al. (2013). A randomized phase 2 study of paclitaxel and carboplatin with or without conatumumab for first-line treatment of advanced non-small-cell lung cancer. J. Thorac. Oncol. *8*, 329–337. https://doi.org/10.1097/JTO.0b013e31827ce554.

Poillet-Perez, L., Despouy, G., Delage-Mourroux, R., and Boyer-Guittaut, M. (2015). Interplay between ROS and autophagy in cancer cells, from tumor initiation to cancer therapy. Redox Biol. *4*, 184–192. https://doi.org/10.1016/j.redox.2014.12.003.

Purcell, M., Kruger, A., Tainsky, M.A., Purcell, M., Kruger, A., Gene, M.A.T., Purcell, M., Kruger, A., and Tainsky, M.A. (2014). Gene expression profiling of replicative and induced senescence. Cell Cycle *13*, 3927–3937. https://doi.org/10.4161/15384101.2014.973327.

Saleh, T., Tyutyunyk-Massey, L., Patel, N.H., Cudjoe, E.K., Alotaibi, M., and Gewirtz, D.A. (2020a). Studies of non-protective autophagy provide evidence that recovery from therapy-induced senescence is independent of early autophagy. Int. J. Mol. Sci. *21*. https://doi.org/10.3390/ijms21041427.

Saleh, T., Carpenter, V.J., Tyutyunyk-Massey, L., Murray, G., Leverson, J.D., Souers, A.J., Alotaibi, M.R., Faber, A.C., Reed, J., Harada, H., et al. (2020b). Clearance of therapy-induced senescent tumor cells by the senolytic ABT-263 via interference with BCL-XL–BAX interaction. Mol. Oncol. *14*, 2504–2519. https://doi.org/10.1002/1878-0261.12761.

Salmerón-Bárcenas, E.G., Zacapala-Gómez, A.E., Ortiz-Ortiz, J., Torres-Rojas, F.I., and Ávila-López, P.A. (2022). Integrated Bioinformatics Analysis Reveals That Ezh2-Rich Domains Promote Transcriptional Repression in Cervical Cancer. EXCLI J. *21*, 852–868. https://doi.org/10.17179/excli2022-5029.

Saul, D., and Kosinsky, R.L. (2021). Single-cell transcriptomics reveals the expression of aging-and senescence-associated genes in distinct cancer cell populations. Cells *10*. https://doi.org/10.3390/cells10113126.

Saul, D., Kosinsky, R.L., Atkinson, E.J., Doolittle, M.L., Zhang, X., LeBrasseur, N.K., Pignolo, R.J., Robbins, P.D., Niedernhofer, L.J., Ikeno, Y., et al. (2022). A new gene set identifies senescent cells and predicts senescence-associated pathways across tissues. Nat. Commun. *13*. https://doi.org/10.1038/s41467-022-32552-1.

Schmitt, C.A., Wang, B., and Demaria, M. (2022). Senescence and cancer — role and therapeutic opportunities. Nat. Rev. Clin. Oncol. *19*, 619–636. https://doi.org/10.1038/s41571-022-00668-4.

Shahbandi, A., Rao, S.G., Anderson, A.Y., Frey, W.D., Olayiwola, J.O., Ungerleider, N.A., and Jackson,

7

J.G. (2020). BH3 mimetics selectively eliminate chemotherapy-induced senescent cells and improve response in TP53 wild-type breast cancer. Cell Death Differ. https://doi.org/10.1038/s41418-020-0564-6.

Skelton, W.P., Turba, E., and Sokol, L. (2020). Durable Complete Response to AMG 655 (Conatumumab) and Vorinostat in a Patient With Relapsed Classical Hodgkin Lymphoma: Extraordinary Response from a Phase 1b Clinical Protocol. Clin. Lymphoma, Myeloma Leuk. 20, e944–e946. https://doi.org/10.1016/j.clml.2020.07.012.

Soto-gamez, A., Quax, W.J., and Demaria, M. (2019). Regulation of Survival Networks in Senescent Cells: From Mechanisms to Interventions. J. Mol. Biol. 431, 2629–2643. https://doi.org/10.1016/j.jmb.2019.05.036.

Straathof, K.C., Pulè, M.A., Yotnda, P., Dotti, G., Vanin, E.F., Brenner, M.K., Heslop, H.E., Spencer, D.M., and Rooney, C.M. (2005). An inducible caspase 9 safety switch for T-cell therapy. Blood 105. https://doi.org/10.1182/blood-2004-11-4564.

Stuckey, D.W., and Shah, K. (2013). TRAIL on Trial: Preclinical advances for cancer therapy. Trends Mol Med 19, 1–7. https://doi.org/10.1016/j.molmed.2013.08.007.TRAIL.

Tai, H., Wang, Z., Gong, H., Han, X., Zhou, J., Wang, X., Wei, X., Ding, Y., Huang, N., Qin, J., et al. (2017). Autophagy impairment with lysosomal and mitochondrial dysfunction is an important characteristic of oxidative stress-induced senescence. Autophagy 13, 99–113. https://doi.org/10.1080/15548627.2016.1247143.

Todt, F., Cakir, Z., Reichenbach, F., Emschermann, F., Lauterwasser, J., Kaiser, A., Ichim, G., Tait, S.W., Frank, S., Langer, H.F., et al. (2015). Differential retrotranslocation of mitochondrial Bax and Bak. EMBO J. 34, 67–80. https://doi.org/10.15252/embj.201488806.

Wakita, M., Takahashi, A., Sano, O., Loo, T.M., Imai, Y., Narukawa, M., Iwata, H., Matsudaira, T., Kawamoto, S., Ohtani, N., et al. (2020). A BET family protein degrader provokes senolysis by targeting NHEJ and autophagy in senescent cells. Nat. Commun. 11, 1–13. https://doi.org/10.1038/s41467-020-15719-6.

Wang, B., Varela-Eirin, M., Brandenburg, S.M., Hernandez-Segura, A., van Vliet, T., Jongbloed, E.M., Wilting, S.M., Ohtani, N., Jager, A., and Demaria, M. (2022a). Pharmacological CDK4/6 inhibition reveals a p53-dependent senescent state with restricted toxicity. EMBO J. 41, 1–16. https://doi.org/10.15252/embj.2021108946.

Wang, C., Vegna, S., Jin, H., Benedict, B., Lieftink, C., Ramirez, C., de Oliveira, R.L., Morris, B., Gadiot, J., Wang, W., et al. (2019). Inducing and exploiting vulnerabilities for the treatment of liver cancer. Nature 574, 268–272. https://doi.org/10.1038/s41586-019-1607-3.

Wang, L., Leite de Oliveira, R., Wang, C., Fernandes Neto, J.M., Mainardi, S., Evers, B., Lieftink, C., Morris, B., Jochems, F., Willemsen, L., et al. (2017). High-Throughput Functional Genetic and Compound Screens Identify Targets for Senescence Induction in Cancer. Cell Rep. 21, 773–783. https://doi.org/10.1016/j.celrep.2017.09.085.

Wang, L., Lankhorst, L., and Bernards, R. (2022b). Exploiting senescence for the treatment of cancer. Nat. Rev. Cancer 22, 340–355. https://doi.org/10.1038/s41568-022-00450-9.

Weeden, C.E., Ah-Cann, C., Holik, A.Z., Pasquet, J., Garnier, J.M., Merino, D., Lessene, G., and Asselin-Labat, M.L. (2018). Dual inhibition of BCL-XL and MCL-1 is required to induce tumour regression in lung squamous cell carcinomas sensitive to FGFR inhibition. Oncogene 37, 4475–4488. https://doi.org/10.1038/s41388-018-0268-2.

Wiley, C.D., and Campisi, J. (2021). The metabolic roots of senescence: mechanisms and opportunities for intervention. Nat. Metab. 3, 1290–1301. https://doi.org/10.1038/s42255-021-00483-8.

Wiley, C.D., Flynn, J.M., Morrissey, C., Lebofsky, R., Shuga, J., Dong, X., Unger, M.A., Vijg, J., Melov, S., and Campisi, J. (2017). Analysis of individual cells identifies cell-to-cell variability following induction of cellular senescence. Aging Cell 16, 1043–1050. https://doi.org/10.1111/acel.12632.

Young, A.R.J., Narita, M., Ferreira, M., Kirschner, K., Sadaie, M., Darot, J.F.J., Tavaré, S., Arakawa, S., Shimizu, S., Watt, F.M., et al. (2009). Autophagy mediates the mitotic senescence transition. Genes Dev. 23. https://doi.org/10.1101/gad.519709.

Zhang, L., and Fang, B. (2005). Mechanisms of resistance to TRAIL-induced apoptosis in cancer. Cancer Gene Ther. 12, 228–237. https://doi.org/10.1038/sj.cgt.7700792.

Zhang, J., Bu, X., Wang, H., Zhu, Y., Geng, Y., Nihira, N.T., Tan, Y., Ci, Y., Wu, F., Dai, X., et al. (2018). Cyclin D-CDK4 kinase destabilizes PD-L1 via cullin 3-SPOP to control cancer immune surveillance. Nature https://doi.org/10.1038/nature25015.

7

APPENDIX &

Nederlandse samenvatting
Curriculum Vitae
Publication list
Acknowledgements

Nederlandse samenvatting

Het menselijk lichaam omvat ongeveer 10^{13} cellen die een sterk gereguleerd systeem vormen dat cruciaal is voor het goed functioneren van een individu. Gezonde cellen delen zich door groeisignalen van hun omgeving wanneer de omstandigheden gunstig zijn. Tijdens een mensenleven ervaren cellen voortdurend interne en externe dreigingen van stressoren. Voorbeelden van stressoren zijn een tekort aan voedingsstoffen, mechanische celstructuurschade, overmatige productie van celsignalen (signaaltransductie), fouten in DNA-replicatie en UV-straling. Verscheidene stressoren resulteren in DNA-schade, wat de integriteit van het genoom in gevaar brengt en kan resulteren in DNA-veranderingen (mutaties) als deze niet worden hersteld. Om deze reden hebben cellen 'sensor- en reparatiemachines' die bewaken tegen genetische transformatie en afwijkend gedrag van cellen. Desalniettemin, wanneer cellen ernstige schade oplopen en reparatie bemoeilijkt is, kunnen cellen een vorm van suïcide ondergaan. Dit wordt 'apoptose' genoemd. Een alternatief is dat de cel verder leeft in een slaapstand die 'senescence' heet - afkomstig van het latijnse woord 'veroudering' - waarin cellen (tijdelijk) gestopt zijn met delen en minder goed functioneren. Dit is het onderliggende principe van veroudering van lichaamsweefsels. Wanneer de sensor- en reparatiemachines niet goed werken, kan het zijn dat een cel toch voortleeft met mutaties in het DNA. Dit kan ervoor zorgen dat cellen zich kunnen delen zonder externe signalen, wat tot ongecontroleerde celdeling kan leiden en transformatie tot kankercellen en tumorgroei.

In dit proefschrift

In dit proefschrift is onderzocht hoe kankercellen in senescence kunnen worden gebracht met een eerste medicatie – waardoor ze tijdelijk niet meer delen – en hoe vervolgens deze senescente kankercellen geëlimineerd kunnen worden met een medicatie die apoptose in senescente cellen activeert. In **hoofdstuk 1**, de introductie van het proefschrift, staat beschreven wat senescente cellen typeert, wat hun relatie is tot kanker, hoe apoptose zich voltrekt en welke kwetsbaarheden in senescente kankercellen bestaan.

In **hoofdstuk 2** wordt een genetische screen (een experiment waarin bijna 20.000 genen in het DNA tegelijk worden getest via genetische modificatie met CRISPR-Cas9) ontwikkeld waardoor niet-delende cellen kunnen worden geselecteerd. Dit heeft als doel genen te vinden waarvan het verlies zorgt voor senescence in niet-kleincellige longkankercellen. Deze screen identificeerde genen die betrokken zijn bij autofagie, een proces waarbij beschadigde onderdelen van de cel worden afgebroken. Wanneer de genproducten van deze genen geremd worden, brengt dit longkanker cellen in senescence, wat leidde tot de ontdekking dat ULK1-remmers

SBI02169565 en MRT68921 niet alleen in longkanker maar ook in leverkanker, darmkanker en alvleesklierkankercellen senescence induceren. Vervolgens konden deze senescente kankercellen worden gedood met ABT-263, een medicatie specifiek voor senescente cellen doordat het zich richt op het mechanisme van de cel dat apoptose tegengaat. Dit onderzoek laat dus een nieuw ontworpen techniek zien die mechanistisch inzicht geeft hoe senescence kan worden geïnduceerd in tumorcellen en dat via een twee-staps-behandeling verschillende typen tumorcellen kunnen worden gedood.

In **hoofdstuk 3** wordt de vraag gesteld in hoeverre senescente tumorcellijnen afkomstig van verschillende kankertypes (darm, lever, long en borst) op elkaar lijken in hun gevoeligheid voor ABT-263, de signaalmoleculen die ze uitscheiden (SASP; senescence-associated secretory phenotype), de genen die (in)actief zijn (genexpressie) en of er universele eigenschappen of kwetsbaarheden te vinden zijn om senescente tumorcellen te detecteren en om te brengen. Uit dit onderzoek bleek dat er een grote variatie in ABT-263-gevoeligheid was tussen tumor cellijnen. Dit betekent dat niet iedere patiënt zou reageren op een twee-staps-behandeling waarin ABT-263 als tweede medicatie zou worden gebruikt en dat meer kennis over het resistentie-mechanisme nodig is om de medicatie te verbeteren en te kunnen voorspellen of patiënten wel of niet reageren. Daarnaast bracht dit onderzoek aan het licht dat de genexpressie en de SASP van senescente tumorcellen vooral bepaald worden door het kankertype en de eigenschappen van de cel voordat deze senescent wordt gemaakt. Dit betekent dat senescente kankercellen verschillende effecten kunnen hebben in de tumoromgeving: van het stimuleren van een ontstekingsreactie tot de aantrekking van immuuncellen. Om binnen de heterogeniteit van senescente cellen toch overeenkomsten te vinden in genexpressie is artificiële intelligentie (AI) gebruikt om een 'classifier model' te bouwen die de genexpressie van senescente en niet-senescente tumorcellen kan onderscheiden. Om de resultaten van deze studie toegankelijk te maken voor andere onderzoekers is er een website gebouwd waarin genexpressie resultaten kunnen worden geüpload in het classifier model om te analyseren of kankercellen senescent zijn of niet.

In **hoofdstuk 4** wordt gezocht naar een verklaring voor het verschil in gevoeligheid voor ABT-263. Deze medicatie stimuleert apoptose doordat het anti-apoptotische eiwitten remt. Eiwitten zijn verantwoordelijk voor alle reacties binnen een cel doordat ze met elkaar een interactie aangaan en signalen doorgeven. Dit kan leiden tot (in)activatie van transductiesignaalroutes. De transductiesignaalroute van apoptose bestaat uit een complexe choreografie van apoptose eiwitten die elkaar op verschillende manieren vasthouden en weer loslaten, en hierdoor voorkomen dat andere 'danspartners' zich kunnen binden. Anti-apoptotische eiwitten spelen hierdoor een belangrijke rol in het voorkomen van apoptose. Zo kan een cel veel stress signaalroutes hebben aangezet en pro-apoptotische eiwitten hebben

geactiveerd, maar overleeft de cel doordat anti-apoptotische eiwitten de functie van pro-apoptotische eiwitten inhiberen. Wanneer anti-apoptotische eiwitten geremd worden door een medicatie als ABT-263, dan kunnen die pro-apoptotische signalen alsnog apoptose veroorzaken. Een cel die dichtbij apoptose zit en afhankelijk is van anti-apoptotische eiwitten voor overleving heeft een hogere 'apoptotische priming'. De onderzoeksgroep van Prof.dr.Anthony Letai, gelieerd aan Harvard/ Dana-Farber Cancer Instituut, heeft een techniek ontworpen die deze apoptotische priming kan meten. In het onderzoek van hoofdstuk 4 is deze techniek toepast op tumorcellen met verschillende gevoeligheden voor ABT263, in senescente en niet-senescente staat. Hieruit werd gevonden dat senescente cellen die gevoelig zijn voor ABT-263 al een hogere 'apoptotische priming' hebben vóórdat ze senescent werden. Daarbij werd er, naast de anti-apoptotische eiwitten die ABT-263 remt, nog een ander anti-apoptotisch eiwit gevonden die belangrijk is voor de overleving van de cel: genaamd MCL-1. Het bleek dat MCL-1 tijdens behandeling in hoeveelheid toeneemt in cellen die resistent zijn tegen ABT-263. Aangezien het remmen van te veel anti-apoptotische eiwitten tegelijkertijd ook toxiciteit kan veroorzaken in niet-kanker cellen, zal nader onderzoek moeten uitwijzen of een combinatiebehandeling met MCL-1 remmers en ABT-263 een effectieve therapie tegen kanker zou kunnen zijn. Dit onderzoek laat zien dat de gevoeligheid voor een twee-staps-therapie met ABT-263 vooraf bepaald is in kankercellen, wat een mogelijkheid biedt te voorspellen welke patiënten baat hebben bij therapie.

In **hoofdstuk 5** wordt met een genetische screen gezocht naar alle genen die mogelijk betrokken zijn bij de onderliggende resistentiemechanismen tegen ABT-263 in senescente kankercellen. Dit onderzoek beschrijft hoe een resistentie screen in senescente cellen het beste kan worden uitgevoerd, waarbij een belangrijk verschil met andere resistentie screens is dat senescente cellen niet delen. Normaal gesproken is er een sterke positieve selectie van resistente cellen vergeleken met cellen die doodgaan door de behandeling, omdat resistente cellen doordelen en zich vermenigvuldigen. Uit deze cellen kan dan worden bepaald welk gen geïnactiveerd was. Een belangrijk aspect voor de screen in senescente cellen is dat het langer duurt voordat CRISPR/Cas9 de genen kapot knipt en dat er een hogere concentratie van de medicatie moet worden gebruikt om te voorkomen dat cellen achterblijven die niet volledig resistent zijn (vals positieve hits). De resistentie screen voor ABT-263 in longkankercellen identificeerde verschillende signaaltransductieroutes: (i) eiwitten die de PI3K/AKT/mTOR signaaltransductie route negatief reguleren, (ii) eiwitten die de anti-apoptotische eiwitten BFL-1 en MCL-1 negatief reguleren, en (iii) eiwitten die niet gerelateerd lijken aan apoptose. Veel eiwitten, wanneer uitgeschakeld, hadden als overeenkomst dat ze de hoeveelheid MCL-1 lieten toenemen, wat overeenkomt met de bevindingen in hoofdstuk 4. Vervolgonderzoek is nodig om te bevestigen dat de hits uit deze screen inderdaad betrokken zijn bij ABT-263 resistentie en of het

beïnvloeden van deze signaalroutes met medicatie een minder toxische combinatie is dan wanneer MCL-1-remmers worden gebruikt in combinatie met ABT-263.

In **hoofdstuk 6** wordt verkend of er een betere behandeling bestaat die senescente kankercellen efficiënter kan doden dan ABT-263. Hiervoor wordt een genetische screen in senescente cellen gedaan om genen te vinden die - wanneer afwezig - tot celdood leiden in senescente cellen. Uit deze screen kwam cFLIP, een eiwit dat apoptosis getriggerd door cel externe signalen remt. Hieruit bleek dat senescente kankercellen niet alleen gevoeliger zijn voor apoptose geactiveerd door interne signalen (geactiveerd door ABT-263), maar dat deze cellen ook gevoeliger zijn voor apoptose geactiveerd door externe signalen. En inderdaad, als senescente kankercellen worden behandeld met zo'n extern signaal in de vorm van TRAIL of DR5 agonist leidde dit apoptose. Deze medicatie bleek effectief in senescente tumorcellen van verscheidene tumortypes en liet remming van tumorgroei zien in muizen die behandeld werden met een therapie waarin senescence geïnduceerd werd met Aurora kinase A/B remmers gecombineerd met een activerend antilichaam voor DR5, een eiwit die externe apoptosis signalen ontvangt. De effectiviteit van deze behandeling lijkt verklaard te worden doordat senescente tumorcellen NF-κB activeren, wat leidt tot een toename van zowel cFLIP als DR5. Daarbij lijkt er ook een omstandereffect te zijn, waarbij senescente cellen signaalmoleculen uitstoten die niet-senescente cellen gevoelig kunnen maken voor behandeling met activerende antilichamen voor DR5. Deze therapie gecombineerd met een senescence-opwekkende behandeling laat hoopgevende resultaten zien in muizen met lever en longkanker, en toekomstig onderzoek is nodig om erachter te komen of deze behandelmethode een betere behandeling zou kunnen bieden aan kankerpatiënten.

In **hoofdstuk 7** worden de bevindingen van dit proefschrift bediscussieerd aan de hand van recent onderzoek. Hieruit wordt geconcludeerd dat de heterogeniteit van senescente tumorcellen een uitdaging vormt voor het ontwikkelen van een twee-staps-therapie in de kliniek, maar dat er ook steeds meer aanwijzingen zijn dat senescente kankercellen een belangrijke bijdrage kunnen leveren aan het activeren van verschillende componenten van het immuunsysteem. Recente successen met immuuntherapie, een behandeling die het eigen afweersysteem van patiënten helpt tumorcellen te verwijderen, blijken vooral succesvol wanneer immuuncellen in de tumor infiltreren. Omdat senescente tumorcellen dit effect hebben, lijken behandelingen waarbij senescente tumorcellen ontstaan een interessant onderzoeksgebied voor de toekomst te bieden.

&

Curriculum vitae

Fleur Jochems was born on the 16th of December 1991 in Haarlem, The Netherlands. In 2012, she received her Gymnasium (pre-university) degree from Murmellius Gymnasium Alkmaar. She pursued her undergraduate studies in Biomedical Sciences at the University of Amsterdam. During her bachelor's degree, she conducted research on the temporal and spatial dynamics of DNA double-strand break repair after local irradiation, under the supervision of Dr. Krawczyk at the Amsterdam Medical Center (AMC). After obtaining her BSc degree in 2015, she joined the Oncology track of the Biomedical Sciences MSc program. For her first Master's internship, Fleur worked in the lab of Prof. Dr. te Riele at the Netherlands Cancer Institute (NKI), focusing on homology-directed gene editing strategies to create intronic and exonic point mutations for evaluating the pathogenicity of gene variants in Lynch syndrome. Following this, she moved to the lab of Prof. Dr. Bernards at the NKI for her second internship. In this role, she utilized high-throughput compound screens and FACS-assisted functional genetic screens to identify targets to induce senescence in cancer cells. Subsequently, she wrote her literature thesis on the tumor-inducing capacity of episomal versus integrated HPV in cervical carcinoma. In 2017, Fleur graduated cum laude with her MSc degree and embarked on a PhD in the lab of Prof. Dr. Bernards. During her doctoral research, she investigated the characteristics and vulnerabilities of senescent cancer cells. Additionally, she took on the responsibility of conference event manager at the International Cell Senescence Association. In 2020, she had the opportunity to exchange to the lab of Dr. Anthony Letai at the Dana-Farber Cancer Institute/ Harvard Medical School in Boston, where she acquired expertise in the BH3 profiling technique. Subsequently, she returned to the NKI to make this technique accessible to other researchers. The findings of her PhD work are presented in this thesis.

&

Publication list

*shared first authors

Jochems, F.*, Thijssen, B.*, De Conti, G., Jansen, R., Pogacar, Z., Groot, K., Wang, L., Schepers, A., Wang, C., Jin, H., Beijersbergen, R.L., Leite de Oliveira, R., Wessels, L.F.A., and Bernards, R. (2021). The Cancer SENESCopedia: A delineation of cancer cell senescence. *Cell Reports*, 36, 109441. https://doi.org/10.1016/j.celrep.2021.109441.

Wang, L.*, Jin, H.*, **Jochems, F.**, Wang, S., Lieftink, C., Martinez, I.M., De Conti, G., Edwards, F., de Oliveira, R.L., Schepers, A., Zhou, Y., Zheng, J., Wu, W., Zheng, X., Yuan, S., Ling, J., Jastrzebski, K., Dos Santos Dias, M., Song, J., Celie, P.N.H., Yagita, H., Yao, M., Zhou, W., Beijersbergen, R.L., Qin, W., and Bernards, R. (2022). cFLIP suppression and DR5 activation sensitize senescent cancer cells to senolysis. *Nature Cancer,* 3, 1284–1299. https://doi.org/10.1038/s43018-022-00462-2.

Schepers, A., **Jochems, F.**, Lieftink, C., Wang, L., Pogacar, Z., Leite de Oliveira, R., De Conti, G., Beijersbergen, R.L., and Bernards, R. (2021). Identification of Autophagy-Related Genes as Targets for Senescence Induction Using a Customizable CRISPR-Based Suicide Switch Screen. *Molecular Cancer Reseach*, 1–10. https://doi.org/10.1158/1541-7786.mcr-21-0146.

Pogacar, Z.*, Groot, K.*, **Jochems, F.**, Dos Santos Dias, M., Mulero-Sánchez, A., Morris, B., Roosen, M., Wardak, L., De Conti, G., Velds, A., Lieftink, C., Thijssen, B., Beijersbergen, R.L., Bernards, R., and Leite de Oliveira, R. (2022). Genetic and compound screens uncover factors modulating cancer cell response to indisulam. *Life Science Alliance,* 5, 1–13. https://doi.org/10.26508/lsa.202101348.

Pogacar, Z., Johnson, J.L., Krenning, L., De Conti, G., **Jochems, F.**, Lieftink, C., Velds, A., Wardak, L., Groot, K., Schepers, A., Wang, L., Song, J.Y., van de Ven, M., van Tellingen, O., Medema, R.H., Beijersbergen, R.L., Bernards, R., and Leite de Oliveira, R. (2022). Indisulam synergizes with palbociclib to induce senescence through inhibition of CDK2 kinase activity. *PLoS One*, 17, 1–23. https://doi.org/10.1371/journal.pone.0273182.

Wang, C.*, Vegna, S.*, Jin, H.*, Benedict, B.*, Lieftink, C., Ramirez, C., de Oliveira, R.L., Morris, B., Gadiot, J., Wang, W., du Chatinier, A., Wang, L., Gao, D., Evers, B., Jin, G., Xue, Z., Schepers, A., **Jochems, F.**, Mulero Sanchez, A., Mainardi, S., Te Riele, H., Beijersbergen, R.L., Qin, W., Akkari, L., and Bernards, R. (2019). Inducing and exploiting vulnerabilities for the treatment of liver cancer. *Nature,* 574, 268–272. https://doi.org/10.1038/s41586-019-1607-3.

&

Wang, L.*, Leite de Oliveira, R.*, Wang, C., Fernandes Neto, J.M., Mainardi, S., Evers, B., Lieftink, C., Morris, B., **Jochems, F.**, Willemsen, L., Beijersbergen, R.L., and Bernards, R. (2017). High-Throughput Functional Genetic and Compound Screens Identify Targets for Senescence Induction in Cancer. *Cell Reports*, 21, 773–783. https://doi.org/10.1016/j.celrep.2017.09.085.

Jin, H.*, Wang, S.*, Zaal, E.A., Wang, C., Wu, H., Bosma, A., **Jochems, F.**, Isima, N., Jin, G., Lieftink, C., Beijersbergen, R., Berkers, C.R., Qin, W., and Bernards, R. A powerful drug combination strategy targeting glutamine addiction for the treatment of human liver cancer. *Elife*, 9, 1-20. https://doi.org/10.7554/eLife.56749.

Jin, H.*, Shi, Y.*, Lv, Y.*, Yuan, S.*, Ramirez, C.F.A., Lieftink, C., Wang, L., Wang, S., Wang, C., Henrique Dias, M., **Jochems, F.**, Yang, Y., Bosma, A., Hijmans, E.M., de Groot, M. H. P., Vegna, S., Cui, D., Zhou, Y., Ling, J., Wang, H., Guo, Y., Zheng, X., Isimia, N., Wu, H., Sun, C., Beijersbergen, R.L., Akkari, L., Zhou, W., Zhai, B., Qin, W., and Bernards, R. (2021). EGFR activation limits the response to liver cancer to Lenvatinib. *Nature*, 595, 730-734. https://doi.org/10.1038/s41586-021-03741-7.

&

Acknowledgements

&

Julie, our troubleshooting sessions have been extremely helpful, and you are such a pleasant person to work with. **Veerle**, bedankt dat je mij onder jouw hoede nam tijdens de drukke laatste maanden van jouw postdoc! Ook zijn onze gesprekken over vervolgstappen heel waardevol geweest.

My dear paranimfs, I am blessed to have you. **Ziva**, you cannot imagine how happy I was that you said 'YES'! Not only because you are an expert paranimf by now, but because your support has been the most empowering of all! You have been by my side from the very start of my PhD and never left. You pushed my scientific skills to the next level, and gave me the most honest, thoughtful, and valuable feedback. You cheered me up when times were rough, you visited me in Boston, you offered me a helping hand when I was overwhelmed, and best of all this: you have been a caring friend. I am excited for the future, and curious to see what lies ahead. One thing I know for certain: your bright mind and emotional intelligence bring greatness into this world, and I am grateful to be part of it.

Robin, wat was het leuk en leerzaam om jou te begeleiden tijdens je master stage. Ik ben trots en onder de indruk hoe jij nu floreert als PhD student én designer. Jouw enthousiasme, spontaniteit en interesse naar mensen om je heen maken van jou een dierbare collega. Het is zo fijn dat ik met jou over werkelijk ALLES kan praten. Jouw hulp en steun tijdens mijn PhD hebben mij naar de eindstreep geholpen, en ik weet zeker dat deze voor jou ook nabij is. Het betekent veel voor me dat jij mijn paranimf bent!

Rodrigo, my sestra! I believe we have the same SASP profile, secreting fabulousness into our microenvironments. From the very start of my PhD, you have been an incredible mentor in science and life in general. Your empathy and desire to help others is your number one superpower and makes you an inspirational leader. I really value our connection and miss your days in office 37. Especially when I was shedding tears about your jokes like there was no tomorrow.

Liqin, my PhD journey started with and thanks to you! As my internship supervisor, you taught me how to do science in a fast and efficient manner. I admire your ability to navigate projects towards high-impact publications, to identify the 'key experiments', and your goal-oriented attitude. It is amazing to see that you are a PI in China now. You have been a very important mentor to me. Thank you so much, because without you this thesis was not as great as it is now!

Bram, wat een geluk heb ik gehad met onze samenwerking. Ik waardeer je consciëntieuze manier van werken, wetenschappelijke nieuwsgierigheid en

fantastische uitleg over bioinformatica. En ik leefde op van onze wetenschappelijke discussies die onze projecten soms ver overstegen. Als partner in crime gaf je mij steun bij het overwinnen van de vele hobbels op mijn weg. Ik hoop ook na mijn PhD nog vele verhalen te horen over Diva & QT, mooie reizen, het leven en jouw weg naar een PI positie!

Arnout, waar anderen tien zinnen nodig hebben om complexe materie te begrijpen, heb jij aan twee woorden genoeg. Je daagde me uit om mijn wetenschappelijk denken te ontwikkelen en was een belangrijke vraagbaak voor mij. Ook werkten we - soms - heel goed samen als er weer iets georganiseerd moest worden met one-two punch cocktails, speurtochten, ice-breakers en Sinterklaas. De conferenties naar Montreal en Athene waren onvergetelijk. Zonder jou was dit proefschrift er zeker (nog) niet geweest! Dank je wel voor al je (ongepaste) grappen en creatieve ideeën, want deze gaven mijn PhD sjeu!

Giulia, it is such a blessing that our paths crossed during my PhD! I am very grateful to have worked with such a broadly-developed scientist who is also well-organized, social, and fun to be with. We shared many good and bad scientific moments together. Thank you for being an amazing person to work with, and for sharing our love for food and wine.

Marlou, het was geweldig om met jou samen te werken! Je bent zo leergierig, gedreven, georganiseerd en zorgvuldig dat jouw werk een compleet hoofdstuk in dit proefschrift vormt. Dank je wel voor alle steun die jij in het project geboden hebt en hoe jij me leerde een goede begeleider te zijn. Ik ben benieuwd naar je volgende stappen, waar die ook zullen zijn. Ik weet zeker dat je het fantastisch zult doen.

Chrysiida, our collaboration brought me so much joy and valuable input on the BH3 profiling project! I love how we connected also outside the lab and that we equally enjoy salsa dancing. You are an incredible scientist, and I am looking forward to publishing our story.

Gabriele, it has been so much fun having you as my new colleague ánd dancing partner in my final year. You bring a lot of positive energy and enthusiasm, and I admire your endless drive and your connective mind. I am certain that you will rock this PhD!

Patty, jij staat altijd klaar om een helpende hand te bieden als er iets geregeld moet worden. En dikwijls neem jij ons werk uit handen, zodat wij ons kunnen focussen op het onderzoek. Ook zorg je altijd voor attenties of een kaartje bij momenten van

&

lief en leed. Het is prachtig om te zien hoe zorgzaam jij bent voor de mensen om jou heen!

Jeroen, wat was het fijn om de leuke en minder leuke momenten van mijn PhD met jou te kunnen delen. Jouw relativeringsvermogen en sociale karakter maken je een fantastische arts én onderzoeker! **Antonio**, you are a man of many talents! Your happiness and kindness spreads through the department and bring borrels to life. I am happy we shared good and bad moments in our PhD journey together. **Matheus**, the visionary of our department! I love your endless passion for science. You have a unique and unconventional view on projects, and you are a talented relationship builder. The way you find the best side in every person always cheers me up. **João**, what a nice surprise that you came back! I admire your flexibility and courage to chase your dreams. **Sara**, I am impressed by how many responsibilities you can juggle! I enjoyed working with you on the Girona retreat.

Astrid en **Marielle**, jullie brengen niet alleen veel gezelligheid, maar zijn ook fantastisch in het organiseren van het lab! Jullie vliegensvlugge bestellingen en punctuele myco-plasma testen zorgden er altijd voor dat ik mijn experimenten snel en efficiënt kon uitvoeren. **Annemieke**, dank je wel voor al die noodzakelijke herinneringen aan mijn lab taken! Dankzij jou is het lab een stuk opgeruimder én gezelliger. **Katrien**, jij bent het geheugen van de groep. Jouw input en expertise tijdens werkbesprekingen heb ik altijd als waardevol ervaren. Ik vind het leuk te merken dat we dezelfde ideeën hebben over het welzijn van PhD studenten en waardeer je inzet voor anderen bij de OR.

Haojie, thank you for trusting me with your *in vivo* experiments. It is great to see how you have climbed the ladder towards a PI position! **Mengnuo**, your hard work is clearly paying off! You have bravely navigated into the unknown research area of DTPs. **Mani**, wat een prachtige aanwinst ben jij voor onze groep! Petje af hoe jij jezelf bioinformatica hebt aangeleerd. **Koen**, wat is het fijn om jouw klinische reflectie op projecten te horen en om zo'n sociale collega erbij te hebben.

Kathy, you always have been friendly and helpful in tangible ways! You are always happy to share your technical expertise, and have provided me with essential tips on how to optimally design experiments. I also value that you think along with other people's projects and are always happy to share articles, reagents, and ideas. One day, I wish I could be as well-organized as you are! **Silvana**, jouw aanstekelijke lach is overal te horen. Jij hebt een fantastisch gevoel voor orde en uitgebreide kennis over lab veiligheid, twee talenten waar de rest van ons lab (inclusief ikzelf) nog een puntje aan kan zuigen. Ik heb met veel plezier met je samengewerkt in het COVID-19

team, waar je plichtsgevoel en gedrevenheid de motor van onze samenwerking vormden. Wat was het fijn om jou als collega te hebben!

Cor, ik kijk met dankbaarheid terug hoe jij al tijdens mijn master de tijd nam om mij alle details van jouw analyses uit te leggen en hoe je mij hielp bij mijn eerste presentatie. Bedankt dat jij zo begaan was met mij en mijn projecten! **Johan**, jij staat altijd klaar om screeningadvies te geven aan iedereen. Met jouw eindeloze bron aan kennis heeft onze groep geluk gehad dat jij weer bent teruggekomen. Ik wil je bedanken voor alle waardevolle feedback op mijn projecten. **Elke**, it is beautiful that after your postdoc you decided to contribute to other people's projects and the organization of the lab. You have always been extremely helpful and friendly. **Marieke**, jouw komst heeft een frisse wind door ons lab doen waaien. Je sociale karakter en vrolijke persoonlijkheid maken het een fijn om jou als collega te hebben.

Michiel, jouw klinische inbreng tijdens de werkbesprekingen heeft ons dichter bij de patiënt gebracht. **Alberto**, I got to know you better during our career as film actors. I love to talk with you about looks, art, parties, and more.

I also would like to thank my former colleagues **Diede**, **Bastiaan**, **Kristan**, **Wouter**, **Sander**, **Ben**, **Tonci**, **Begoña**, **Jeroen**, **Martin**, **Cun**, **Lorenzo**, **Josephine**, **Isabel,** and **Finn** for the scientific discussions, inspiring conversations, and daily laughter. A special thanks to **Diede**, **Bastiaan**, **Josephine**, **Wouter**, and **Lorenzo** for sharing your experiences and useful connections outside academia. **Ben**, I am excited you are coming back!

Tim, ik wil jou bedanken voor de fantastische voorbereiding die ik van je heb gekregen om bij René lab te kunnen starten. Je leerde me (*in silico*) kloneren in 'the old school way' en bracht me kennis bij door vragen te stellen. Deze manier van kennis overdragen is zeker iets wat ik van je heb overgenomen. Ik denk met veel plezier terug aan mijn stage bij jou. De fijne werkomgeving die **Hein**, **Bente**, **Thomas**, **Marleen** en **Wietske** creëerden heeft mij enthousiast gemaakt over de wetenschap en de keuze voor een PhD! Hier ben ik jullie nog steeds dankbaar voor.

The NKI has been an amazing place to work, and colleagues from other departments have been equally fantastic. **Mark** and **Olaf,** it has been a great pleasure to receive your thoughts on my project, and I highly value your eye for detail. Thank you for collaborating with me.
Serena, your expertise in immunology and mouse models has been invaluable in our department. Having you in our STF meetings has been extremely helpful. **Aldo**, wat was het fijn om met jou te praten over de wetenschap, het PhD leven en onze

&

carrièredromen. Ik hoop dat onze paden elkaar in de toekomst zullen kruisen in de industrie! **Ronak**, we did our masters together and now we are defending just one day apart. It has been great to be able to share our PhD experiences and our time in Spetses.

Daarnaast waren de **NKI corefacilities** van onschatbare waarde. Ik wil graag mijn dank uitspreken aan **Marjolijn**, **Lenny**, **Frank**, **Martijn**, **Natalie**, en alle mensen van de **Intervention Unit**.

Naast collega's hebben mijn vrienden voor veel plezier, ontspanning en steun gezorgd tijdens mijn PhD. Ik voel me enorm rijk met de mooie en lieve mensen die ik om mij heen heb.

Bas, jij was al bijna klaar met je PhD toen ik je via Wieger leerde kennen. Alle open gesprekken over het promoveren hebben mij zeker voorbereid én gesterkt. Ook wil ik je bedanken voor het delen van je kennis over verschillende carrièremogelijkheden.

Jackie, when I was still deciding whether or not to do a PhD, Wieger introduced me to you. And I have been so glad he did. As a natural networker, you have always inspired me, and I admire how amazing you are as a freelance medical writer.

Anne-Mieke, wat een geschenk dat ik jou als coach voor onze retreats leerde kennen en je gaandeweg een dierbare geworden bent! Wat hebben we grandioze retreats mogen neerzetten, mede dankzij jouw creativiteit, humor, overtuigingskracht, organisatievermogen en gevoel voor menselijke verhoudingen. Ik vind het heerlijk om samen veel tentjes in Amsterdam af te struinen voor lekkere wijn en culinaire versnaperingen. Daarbij is het prachtig om te zien hoe attent en betrokken jij bent naar de mensen om je heen.

Jente, jij begrijpt als geen ander wat de uitdagingen van een PhD inhouden. Ik geniet ervan om met je te sparren over het verbeteren van het academische systeem, nieuwe wetenschappelijke inzichten en hoe wij zelf een impact kunnen hebben op de wereld. Ik ben onder de indruk van hoe jij jezelf hebt leren programmeren en een succesvolle carrière hebt opgebouwd in dat vakgebied. Als vriendin waardeer ik jouw openheid en eerlijkheid. Het lijkt mij fantastisch als onze wetenschappelijke paden zich ooit zouden kruisen.

Laura, jij bent een ware weldoener! Zorgde iedereen maar zo goed voor de mensen, dieren en natuur om zich heen als jij. Jouw vermogen om mensen goed te doorzien maakt dat gesprekken met jou vaak verhelderend zijn. Waar ik regelmatig meer

&

van mijzelf verwacht, laat jij mij inzien dat 'goed' ook goed genoeg kan zijn. Als ik in jullie fijne huis ben word ik gelukkig van jullie mooie gezin en de tijd die we samen doorbrengen.

Anna, jij hebt gewoon mijn eerste grote presentatie op een congres bijgewoond! Onze reis naar San Diego en LA heeft een speciaal plekje in mijn hart. Tijdens je verblijf in Amsterdam heb ik genoten van onze spontane etentjes en onze openhartige gesprekken. Ik heb veel respect en bewondering voor hoe jij je met positiviteit, humor en creativiteit door het leven navigeert. Je bent een powervrouw! **Wouter**, jij bent loyaal naar alle vrienden en familie om je heen. Je verliest niemand uit het oog, zelfs als je daarvoor heel Nederland moet afreizen. Het is fantastisch om te zien dat je zo'n mooi gezin hebt gevormd en je volledig op je plek bent als vader. Onze gedeelde liefde voor escape rooms heeft voor plezier en ontspanning gezorgd tijdens mijn PhD.

Lavinia, dankzij jou heb ik een swingend laatste jaar van mijn PhD gehad. Ik vind het geweldig dat we beste vriendinnetjes waren op de basisschool en door de jaren heen elkaar altijd weer weten te vinden. Jij bent een echte gangmaker op feestjes en ik kan altijd enorm met je lachen. Ik bewonder hoe jij je eigen bedrijf bent begonnen en je je altijd inzet voor anderen. **Sanne**, hoe heerlijk is het dat onze vriendschap een nieuw leven heeft gekregen in Amsterdam. Ik vind het prachtig om te zien hoeveel jij je in al die jaren hebt ontwikkeld. Die avondjes eten en dansen gaan we erin houden, ook als jij naar je nieuwe huis in Schoorl verhuisd bent!

Kim, **Chantal** en **Lisa**, wat ben ik blij dat wij onze krachten hadden bundelden in een online tentamen. Dit leidde niet alleen tot vier keer een tien, maar ook vele etentjes en uitjes vol gezelligheid, waar onze mannen ook vaak onderdeel van uitmaken. Het is leuk om te zien dat we alle vier een ander carrière pad zijn ingeslagen na onze biomedische avonturen. Tijdens mijn PhD waren jullie een belangrijk klankbord voor mij. **Kim**, jouw bruisende persoonlijkheid en aanstekelijke lach zorgen er regelmatig voor dat we in de slappe lach schieten. Dank je wel dat je altijd zo attent bent met lieve berichtjes als het leven tegen zit en jij vaak iedereen oproept weer wat leuks af te spreken. Geen wonder dat jij zoveel lieve mensen om je heen hebt die om je geven! **Chantal**, als jij ergens voor gaat, zet je je voor tweehonderd procent in! Ik vind het prachtig hoe jij je kan bekwamen in de meest uiteenlopende vaardigheden: van pianospelen, honden trimmen, schilderen en triatlons tot het maken van de perfecte koffie. Ik ben blij dat onze PhDs nog hebben overlapt en vind het geweldig dat je traject zo goed verloopt. **Lisa**, het was echt uniek dat wij onze stage op dezelfde plek konden doen. Ik bewonder hoe je je hebt ontwikkeld sinds die tijd! Mijn taak als paranimf bij je verdediging en mijn bezoek in San Diego waren fantastische

&

ervaringen. Hopelijk komen onze banen in de toekomst dichter bij elkaar.

Rosalie, ik ken weinig mensen zo gedreven als jij. Je bruist altijd van de grootste plannen en maakt ze dikwijls waarheid. Ik bewonder je creativiteit, hoeveel je om dierenwelzijn geeft en hoe je gedijt in zo'n competitieve sector. Tijdens onze etentjes geven jouw ideeën mij altijd een nieuwe kijk op de wereld. Bedankt dat je al sinds de basisschool zo'n waardevolle vriendin voor me bent! **Emma**, ik ben ontzettend blij dat ik jou via Rosalie als een lieve en fijne vriendin heb leren kennen. Ik kijk met een warme gevoelens terug op onze tijd in Casa400 en alle avondjes die we met z'n drieën hebben doorgebracht, kletsend en/of dansend. Hoe jij andere mensen feilloos aanvoelt en je je altijd voor anderen inzet, zowel in je werk als privé, maakt jou een prachtige vrouw. Je aanmoediging om goed voor mezelf te zorgen is tijdens mijn PhD zeker belangrijk geweest.

Karin, met jou kan ik zo vreselijk hard lachen! Jouw gevoel voor humor en taal maken je verhalen altijd vermakelijk om naar te luisteren. Tegelijkertijd bied jij altijd een luisterend oor waar ik de afgelopen jaren veelvuldig gebruik van mocht maken. Onze vele studie-uren samen hebben mijn scriptiedagen veel aangenamer en gezelliger gemaakt. Ik heb hier vaak aan teruggedacht tijdens het schrijven van dit proefschrift. Het is prachtig om te zien hoe jij het moederschap combineert met een succesvolle baan, sport en een sociaal leven. Je bent een dierbare vriendin waar ik nog velen jaren lief en leed mee wil delen.

Margot, vanaf die eerste rijlessen bij de Schildknapen tot nu: wat ben ik blij met onze 23 jaar hechte vriendschap! Ik ben dol op jouw spontane ideeën en ondernemende geest. Jouw openheid en doortastendheid maakt dat je altijd de juiste vragen stelt. Onze vele gesprekken over het leven, waarvan mijn PhD de afgelopen jaren een belangrijk deel was, hebben mij naar de finish geholpen. Zoals een waarzegster ooit voorspelde, hoop ik dat we als bejaarden samen lachend zullen terugkijken op ons leven. Maar dan wel op de Antillen, met veel cocktails graag!

Ze zeggen wel eens dat je je familie niet voor het kiezen hebt. Wat heb ik dan een enorm geluk gehad!

Allereerst met mijn schoonfamilie **Jan**, **Willemies**, **Froukje**, **Reijer**, **Margot**, **Faber** en **Doris**. Het is genieten om samen met jullie liefdevolle gezin te zijn. Ik koester warme herinneringen aan jullie familie-uitjes, dinertjes en feestdagen, waar er hopelijk nog veel van zullen volgen. Veel dank dat jullie zo mee hebben meegeleefd met alle ontwikkelingen tijdens mijn PhD! **Willemies**, ik sta versteld van jouw energie en fitheid. Met jouw supergeheugen en verbindende karakter ben jij enorm

attent naar de mensen om je heen. Jouw lieve berichtjes doen me altijd goed en ik geniet van onze één-op-één tijd samen! **Jan**, met jou in de buurt is er altijd iets nieuws te leren. Zo ook over mijn voorouders; ik koester de kwartierstaat die jij voor mij hebt uitgezocht. **Froukje**, dat wij tijdens de lockdowns een 'huishouden deelden' had de fijne bijkomstigheid dat ik jou nog beter heb leren kennen. Wat is het fijn om jou als mijn slimme, lieve en betrokken schoonzus te hebben! **Reijer**, je staat altijd klaar voor anderen met wijze adviezen. Ik verwonder mij over hoe jij al jouw rollen als directeur, basketballer, verbouwer, vader, zoon en broer allemaal tegelijkertijd vol houdt. **Margot**, waar mijn werk in dit proefschrift wellicht ooit een bijdrage gaat leveren aan nieuwe kankermedicatie, ben jij degene die nu een verschil maakt in het leven van kankerpatiënten. Daarbij toon je altijd interesse en heb je een ontwapenende werking op de mensen om je heen!

Oma, er zijn maar weinig mensen die zo positief en dankbaar in het leven staan als jij! Het is geweldig om te zien hoe stralend en verzorgd jij er altijd bij loopt. Onze lunches samen zijn altijd genieten. Dankzij jouw kinderen, kleinkinderen en achterkleinkinderen word ik omringd door een bruisende en liefdevolle familie: **Jeanette**, **Ruud**, **Percy**, **Fabian**, **Sharon**, **Remon**, **Charlenne**, **Priscilla**, en **Charissa**. Ook al zien we elkaar niet heel vaak, als we samenkomen voelt het altijd vertrouwd. **Jeanette**, jouw kleurrijke karakter én verschijning maakt elke ontmoeting met jou een feest. **Sharon**, je bent een krachtige en sociale vrouw waar ik bewondering voor heb. **Fabian**, jouw computervaardigheden hebben mij door mijn studie geholpen. **Percy**, ik ben onder de indruk van jouw persoonlijke groei in de afgelopen jaren.

Opa, jouw bijlessen in statistiek van vroeger hebben tijdens mijn PhD hun vruchten afgeworpen. Mijn affiniteit voor berekeningen komt zeker bij jou vandaan. Ik ben dankbaar voor de tijd die we samen doorbrengen en word blij van onze uitjes. **Oom Jan,** ik wil u bedanken voor mijn introductie aan René, wat een belangrijke start van mijn wetenschappelijke carrière is geweest. Vanaf dat moment heeft u altijd betrokkenheid getoond bij mijn promotietraject. U bent een groot voorbeeld voor mij. **Nicolette,** over voorbeelden gesproken, ook jij hebt mij enorm geïnspireerd om te promoveren. Jouw steun in mindere tijden van mijn PhD heeft mij veel goed gedaan. Daarbij zijn de familie-uitjes en feestjes met **Dolf**, **Ninette** en **Jorden** altijd leuk en gezellig!

Mijn lieve, sterke broertjes **Jofel** en **Flynn,** jullie bevlogenheid, ongekende discipline en doorzettingsvermogen zijn een constante bron van inspiratie en motivatie geweest tijdens mijn PhD. **Jofel,** wat hebben we samen hard gebikkeld tijdens dat eerste jaar van mijn promotie. Je ging vaak in de weekenden mee naar het lab om aan je scriptie te werken. Ik kijk met blijdschap terug op de tijd dat we samenwoonden

&

en ben enorm trots op hoe jij je de afgelopen jaren hebt ontwikkeld. **Noa,** ik geniet van jouw aanwezigheid in ons gezin! De empathie voor de mensen om je heen en jouw passie om anderen te helpen is prachtig. **Flynn,** jouw creativiteit en precisie kent geen grenzen. Jij inspireerde mij om te leren werken met Adobe Illustrator en hoewel je tekenvaardigheden niet te evenaren zijn, zijn mijn getekende figuren in dit proefschrift speciaal voor jou! **Katie,** bij het lezen van deze uitspraak dacht ik aan jou: 'When life gives you lemons, bake chocolate cake and leave everyone wondering how in the world you did it'. Je veerkracht en talent voor bakken doen mij versteld staan! Bedankt dat je ons zo vaak verwent met heerlijke lekkernijen.

Enorme dank gaat uit naar jullie, **papa** en **mama**. Jullie hebben mij een leven gegeven dat verre van 'gewoontjes' is, en hebben me laten zien hoe dromen waarheid kunnen worden en je van het leven een feestje maakt. Dankzij jullie ben ik gekomen waar ik nu ben. Ik voel me bevoorrecht met jullie als mijn ouders! **Papa**, jouw positieve en enthousiaste blik op de wereld breng je over op de mensen om je heen. Niemand is zo moedig en vrijgevig als jij! Ik geniet van de spectaculaire familie-uitjes die jij met liefde organiseert en de fijne tijd die we samen in Nederland en Spanje doorbrengen. **Mama**, waar jij ook bent, creëer jij sfeer en gezelligheid. Hoewel jij zelf niet graag in het middelpunt van de belangstelling staat, zorg jij ervoor dat anderen stralen. Je aanpassingsvermogen, creativiteit en zorgzaamheid maken jou een krachtvrouw! Onze band is bijzonder openhartig en hecht, hier ben ik dankbaar voor.

Wieger, EINDELIJK heb je het proefschrift vast waar zoveel van mijn tijd, energie en liefde heen is gegaan. Dit boek ademt jouw onvoorwaardelijke steun. Ik leunde op jou wanneer er maar geen licht aan het einde van de tunnel leek te komen en wanneer het lab werk op avonden en weekenden doorging. Waar ik beweeg in extremen, ben jij stabiel en robuust. Aan jouw zijde voel ik me gelukkig en geliefd. Onze relatie kenmerkt zich door een onbegrensd vertrouwen en het gunnen van elkaars geluk. Zelfs wanneer dit betekent dat we niet dicht bij elkaar kunnen zijn. Zoals in oude psalmen zo mooi omschreven staat: 'aan u gebonden ben ik vrij'.

With love,
Fleur